



The innovations and applications toward establishing low-carbon emission steel making

Steven P Woolass

A thesis submitted to The University of Sheffield for the degree of Doctor of Philosophy

Supervisor: Professor William B J Zimmerman

The University of Sheffield

Faculty of Engineering

Department of Chemical and Biological Engineering

December 2021



Abstract

The consensus that global CO₂ emissions must be controlled to prevent a catastrophic change to the climate has dominated a significant proportion of global research and technology development.

The IPCC Synthesis Report on climate change (2014) calls for urgent action to minimise an increase in global temperatures to prevent irreversible harm to the planet's ecosystem and its inhabitants. The more recent IPCC Special Report (Global Warming of 1.5°C) places specific culpability on human actions. Whilst economical technologies have emerged for power generation, and to a certain extent transport and heating, cost competitive solutions to industrial CO₂ emissions continue to elude these businesses. As demand for steel is expected to rise with growing populations, quality of life and new low-carbon infrastructure, this carbon intensive manufacturing process must be addressed. Globally, the steel industry accounts for 4.3Gton, about 8% of anthropogenic CO₂ emissions. To reach the Paris Agreement of a maximum 2°C increase in global temperature, we must find viable, cost-effective solutions to lower not only domestic but global steel industry emissions. Steel is a globally traded commodity and CO₂ is not patriotic.

At present, there is no cost-effective method for significant decarbonisation of the steelmaking process. The following thesis documents this journey of research, identifying gaps within the field of knowledge and producing three world-firsts. It focuses upon two propriety technologies (CO₂ plasma dissociation and microbubbles) and places these into the context of an integrated steel plant, along with a complimentary, detailed techno-economic strategic model.

Through experiential design and testing, we find that the integration of microbubbles to the CO₂-NH₃-H₂O system can lead to rapidly improved kinetics, achieving high CO₂ loadings within a remarkable 8 minutes. This discovery would be directly applicable to low-energy aqueous ammonia carbon capture systems, whereby reaction kinetics are a limiting factor on commercial deployment, cost and scale.

Current CO₂ plasma chemistry devices are unable to achieve both high conversion and high efficiency simultaneously. A new reactor design has been invented, which compliments the two stages of CO₂ dissociation in two plasma regions that operate within a single reactor. It was proven that a single reactor can operate with two distinct plasma regions, a primary region with a high-power input to initiate the reaction and a subsequent low-power

region to continue the reaction, without compounding energy losses. This resulted in a 40% increase in efficiency.

A first-of-a-kind, detailed techno-economic model for the transition to a future low-carbon steel production system has been developed, to compliment the analysis of the two low-carbon technologies and to understand their deployment in a future steel plant scenario. Simulation of multiple scenarios has been conducted on a year-by-year assessment to demonstrate if cost-effective low-carbon steel production will be possible prior to 2050.

Following the detailed assessment of potential future steelmaking operations, we find that the application of CO₂ micro-plasma dissociation may have a limited role within a future steel making operation for deep (>80%) decarbonisation. Nevertheless, we have shown that a revolutionary new multi-staged plasma invention has superior benefits over the current plasma reactors as it is more aligned to the CO₂ dissociation mechanisms, and that the first application of microbubbles to an aqueous ammonia capture system is highly applicable to steel plant decarbonisation and could yield annual saving in excess of £68m.

The techno-economic simulation has shown, for the first time within literature, that acting quickly with currently available technologies will critically have an equal, if not greater, effect on the cumulative carbon emissions to atmosphere, in contrast to waiting for the ‘ideal solution’, which maybe at a lower technology readiness level or currently uneconomical. If hydrogen is to be used as the steelmaking technology of the future, greater emphasis must be taken into accelerating the deployment of this technology, in particular making sufficient, affordable zero-carbon hydrogen available.

Keywords: *Steel, Climate Change, Plasma CO₂ Dissociation, Microbubbles, Aqueous Ammonia, Carbon Capture, Carbon Capture and Storage*

Acknowledgements

Access to an education in any form is a privilege not all of us can participate in. I consider myself very fortunate to have had the opportunity to study for this doctoral thesis to feed my precondition to ask questions and to continually learn. I hope that this research will make a difference.

A special thank you to my Supervisor, Professor William B. J. Zimmerman, for his unequivocal world leading knowledge and of course his patience as the years passed. I would also like to thank Bruce, for his knowledge and his encouragement. To my many colleagues at Tata Steel who have provided information and perspective, especially Jean-Pierre for his techno-economic modelling expertise. To Lawrie Campbell, for his time and dedication working in the laboratory and to Dr Desai for sharing his thoughts and ideas. Finally, I cannot have achieved this without the love and support from Jen.

Publications and notable appointments of relevance

Conference papers and presentations

1. Presenter - The Opportunities for Carbon Dioxide Utilisation (16/06/2014), European Steel Environmental & Energy Congress 2014 (ESEC), Teesside University, UK.
2. Presenter - The Application of Carbon Dioxide Capture and Utilisation Technologies within the Steel Industry (14/09/2016), 14th International Conference on Carbon Dioxide Utilization (ICCDU XIV), Sheffield, UK.
3. Presenter - Steel Plant CCS, UK Carbon Capture and Storage Research Centre (UKCCSRC), Short Course on CCS (11/12/2019), Sheffield, UK.

Conference Panel Member

1. Panel Member - C1Net, Special Conference “Circular Economy Now” (11/07/2018), The Royal Society, London, UK.
2. Panel Member - Ofgem, Sustainability Energy Conference (23/01/2020), Port Talbot, UK.

Publication contributions

1. Techno-economic survey and design of a pilot test rig for a trilateral flash cycle system in a steel production plant (McGinty, et al., 2017).
2. Delivering clean growth, CCUS Cost Challenge Taskforce Report (CCUS Cost Challenge Taskforce, 2019).
3. Investment Frameworks for Development of CCUS in the UK, Final Report, The CCUS Advisory Group (The CCUS Advisory Group (CAG), 2019).
4. Sustainable synthetic carbon based fuels for transport, Policy Briefing, The Royal Society (The Royal Society, 2019).
5. Analytical Review of Life-Cycle Environmental Impacts of Carbon Capture and Utilization Technologies (Garcia-Garcia, et al., 2020).

Contents

| | |
|--|------|
| Abstract | i |
| Acknowledgements | iii |
| Publications and notable appointments of relevance | iv |
| Abbreviations | x |
| Nomenclature | xii |
| List of Figures | xiii |
| List of Tables..... | xvi |
| Chapter 1 | 1 |
| Introduction..... | 1 |
| 1.1 General Introduction – the challenge | 1 |
| 1.2 Rational for research – identifying the opportunity | 3 |
| 1.3 Research aims and objectives..... | 5 |
| 1.3 Thesis structure | 6 |
| Chapter 2..... | 7 |
| Theoretical background and literature review..... | 7 |
| 2.1 Introduction | 7 |
| 2.2 Technology pathways to achieve low-carbon iron and steel production..... | 8 |
| 2.3 Research Programmes and Low-Carbon Steel Technologies..... | 14 |
| 2.3.1 Breakthrough steelmaking technologies..... | 16 |
| 2.3.2 CCU and CCS..... | 18 |
| 2.3.3 Hydrogen for steel production | 22 |
| 2.3.4 Biomass as a coke/coal substitute..... | 24 |
| 2.4 CO ₂ capture within aqueous ammonia solutions..... | 26 |
| 2.4.1 Ammonia – manufacture and uses..... | 26 |
| 2.4.2 Conventional Urea production..... | 28 |
| 2.4.3 Reaction pathways involving CO ₂ , NH ₃ and H ₂ O | 30 |
| 2.4.4 CO ₂ capture methods in ammonia solutions..... | 34 |
| 2.4.5 Kinetics of the CO ₂ -NH ₃ -H ₂ O system..... | 40 |

| | |
|---|----|
| 2.5 Microbubbles | 42 |
| 2.5.1 Microbubble Generation..... | 43 |
| 2.5.2 Characteristic features relevant to bubble size | 45 |
| 2.5.3 Bubble size | 45 |
| 2.5.4 Gas phase surface area | 46 |
| 2.5.5 Bubble rise velocity..... | 47 |
| 2.5.6 Benefits from the reduction in gas bubble size within a gas-liquid system..... | 48 |
| 2.5.7 Mass transfer flux..... | 48 |
| 2.5.8 Improved mixing | 49 |
| 2.5.9 Extraction of inhibitants | 49 |
| 2.6 The conversion of CO ₂ using plasma chemistry | 50 |
| 2.6.1 Introduction to CO ₂ plasma chemistry | 50 |
| 2.6.2 Plasma fundamentals..... | 51 |
| 2.7 Critical analysis of literature and assessment of knowledge gaps..... | 58 |
| 2.8 Formulation of hypothesis..... | 61 |
| 2.8.1 Hypothesis A..... | 61 |
| 2.8.2 Hypothesis B | 62 |
| 2.8.3 Hypothesis C | 62 |
| 2.9 Chapter summary | 62 |
| Chapter 3..... | 64 |
| Investigations toward achieving higher kinetic rates for CO ₂ uptake within aqueous ammonia, using plasma-assisted micro-bubbles | 64 |
| 3.1 Introduction to chapter 3 | 64 |
| 3.2 Experimental design..... | 65 |
| 3.2.1 Reaction vessel..... | 68 |
| 3.2.2 Plasma reactor characteristics and cooling system..... | 71 |
| 3.2.3 Influence of pH..... | 73 |
| 3.2.4 Analysis methods | 73 |
| 3.3 Results | 75 |

| | |
|--|-----|
| 3.4 Analysis..... | 81 |
| 3.4.1 Introduction | 81 |
| 3.4.2 Influence of NH ₃ concentration | 82 |
| 3.4.3 Effect of CO ₂ flow rate | 84 |
| 3.4.4 Effect of non-thermal plasma CO ₂ activation..... | 87 |
| 3.4.5 Influence of micro-bubbles..... | 90 |
| 3.4.6 Changes in reaction pH..... | 91 |
| 3.4.7 Yields of carbamate to carbonates..... | 91 |
| 3.4.8 Reaction kinetics | 92 |
| 3.4.9 NH ₃ loss..... | 95 |
| 3.4.10 Experimental Errors..... | 97 |
| 3.5 Chapter 3 summary | 100 |
| Chapter 4..... | 101 |
| The development of a breakthrough concept to high conversion efficiency plasma CO ₂ dissociation..... | 101 |
| 4.1 Introduction to chapter 4 | 101 |
| 4.1.1 CO ₂ plasma dissociation pathways..... | 102 |
| 4.1.2 Most efficient mechanisms to CO ₂ dissociation..... | 104 |
| 4.1.3 A comparison of current reactor efficiencies..... | 108 |
| 4.1.4 Invention of a new plasma reactor concept | 112 |
| 4.2 Experimental Design – A new plasma reactor invention | 114 |
| 4.3 Results & analysis | 118 |
| 4.3.1 Power consumption and reactor operation results | 118 |
| 4.3.2 Conversion rate and efficiency results..... | 120 |
| 4.3.3 Analysis and discussion..... | 121 |
| 4.3.4 Errors | 123 |
| 4.3.5 Conclusions | 124 |
| 4.4 Areas for further investigation | 124 |
| 4.5 Chapter summary | 125 |

| | |
|--|-----|
| Chapter 5..... | 126 |
| Detailed techno-economic simulation of a future low-carbon steel making facility for 2050 | 126 |
| 5.1 Introduction to research chapter 5..... | 126 |
| 5.2 Technology Roadmapping | 126 |
| 5.3 Construction of the techno-economic model | 127 |
| 5.3.1 Technology selection process..... | 127 |
| 5.3.2 Key asset replacement decision points | 128 |
| 5.3.3 Energy balance model | 129 |
| 5.3.4 Basic modelling principles | 131 |
| 5.3.5 Limitations of the model | 133 |
| 5.3.6 Commercial model | 133 |
| 5.3.7 Establishing a base case model (Blast Furnace route)..... | 135 |
| 5.3.8 Base case energy balance model | 137 |
| 5.3.9 EAF model | 139 |
| 5.3.10 DRI model | 140 |
| 5.3.11 State-of-the-art (SoftA) iron production model..... | 142 |
| 5.3.12 CCS model | 143 |
| 5.3.13 CCU model (the conversion of CO ₂ into a product of greater value) | 144 |
| 5.3.14 Risks | 146 |
| 5.4 Simulation results and discussion. | 147 |
| 5.4.1 Introduction to section..... | 147 |
| 5.4.2 Carbon reduction potential | 147 |
| 5.4.3 Cash flow (profitability)..... | 154 |
| 5.4.4 Error analysis..... | 159 |
| 5.5 Conclusions from techno-economic simulation | 160 |
| 5.6 Chapter summary | 162 |
| Chapter 6..... | 164 |
| The application of novel ammonia-based CO ₂ capture and micro-plasma systems to future steel plant operations..... | 164 |

| | |
|--|-----|
| 6.1 Introduction to chapter 6 | 164 |
| 6.2 Technology application of aqueous ammonia CO ₂ capture | 164 |
| 6.3 Technology application of CO ₂ dissociation by DBD plasma | 170 |
| 6.4 Chapter Summary | 175 |
| Chapter 7 | 176 |
| Final summary and future recommendations, | 176 |
| 7.1 Final summary | 176 |
| 7.2 Recommendations for further work | 177 |
| References | 180 |

Abbreviations

| | |
|--------|---|
| GHG | Greenhouse Gases |
| IPCC | Intergovernmental Panel on Climate Change |
| ULCOS | Ultra-Low Carbon Dioxide Steelmaking project |
| CCS | Carbon Capture and Storage |
| CCU | Carbon Capture and Utilisation |
| TEA | Techno-economic Appraisal |
| CO | Carbon Monoxide |
| BF | Blast Furnace |
| BF-BOF | Blast Furnace and Basic Oxygen Furnace Technology |
| EAF | Electric Arc Furnaces |
| BOF | Basic Oxygen Furnace |
| DRI | Direct Reduced Iron |
| NG | Natural Gas |
| SMR | Steam Methane Reforming |
| WAGs | Works Arising Gases |
| COG | Coke Oven Gas |
| BFG | Blast Furnace Gas |
| BOFG | Basic Oxygen Furnace Gas |
| AAIST | American Association for Iron & Steel Technology |
| BECCS | Bio-energy with Carbon Capture and Storage |
| LCA | Life Cycle Assessment |
| TGRBF | Top Gas Recycling Blast Furnace |
| ASU | Air Separation Units |
| CAPEX | Capital Expenditure |
| thm | Tonne of Hot Metal |
| OPEX | Operating Expense |
| CCC | UK's Committee on Climate Change |
| CCUS | Carbon Capture, Utilisation and Storage |
| IEA | International Energy Agency |
| CDU | Carbon Dioxide Utilisation |
| ATR | Autothermal Reformation |
| AN | Ammonium Nitrate |
| CAN | Calcium Ammonium Nitrate |

| | |
|----------|--|
| ABC | Ammonium Bicarbonate |
| UAN | Urea Ammonia Nitrate |
| EOS | Equation of State |
| MEA | Monoethanolamine |
| TEA | Triethanolamine |
| TZFO | Tesař-Zimmerman Fluidic Oscillator |
| DZFO | Desai-Zimmerman Fluidic Oscillator |
| EDPM | Ethylene Propylene Diene Monomer |
| EEDF | Electron Energy Distribution Function |
| DBD | Dielectric Barrier Discharge |
| FO | Fluidic Oscillation |
| SEI | Specific Energy Inputs |
| C-13 NMR | C ¹³ Nuclear Magnetic Resonance |
| ISE | Ion Specific Electrode |
| HRC | Hot Rolled Coil |
| BCG | Boston Consulting Group |
| BAT | Best Available Technology |
| ETS | Emissions Trading Scheme |
| SofTA | State-of-the-art |
| TA | Turbine Alternator |
| T&S | Transport and Storage |
| FEED | Front End Engineering Design |
| WGS | Water Gas Shift |
| tcs | Tonne of Crude Steel |
| EOR | Enhanced Oil Recovery |
| SPECCA | Specific Primary Energy Consumption for Carbon Avoided |

Nomenclature

| | |
|-----------------------|--|
| c_l | Concentration of the dissolved gas within the liquid phase |
| $c^*(T)I$ | Saturated concentration at equilibrium with the gas phase, at the temperature of the liquid |
| J | Net mass transfer flux, proportional to the driving force (between the phase transition) |
| $k_L a$ | Combined constant of proportionality |
| k_L | Mass transfer coefficient |
| a | Surface area per unit volume of the gas phase |
| T_g | Temperature of the plasma gas |
| T_g | Plasma electron temperature |
| V_b | Plasma breakdown voltage |
| A & B | Constants determined experimentally for each plasma gas composition |
| p | Plasma pressure |
| d | Electrode spacing |
| γ_{sec} | Secondary electron emission coefficient of cathode |
| λ_{De} | The Debye length |
| L | The plasmas 'characteristic length' |
| ϵ_0 | Vacuum permittivity |
| e | Plasma electronic charge and |
| n_0 | Number density of particles within a plasma |
| n_e | Electron density |
| n_i | Ion density |
| n | Plasma density |
| eV | Electron Volt |
| E/n | Reducing electric field. Where E is the electric field and n is concentration of neutral particles |
| Td | Townsend, unit of E/n |
| x_{CO_2} | The % conversion rate of CO_2 |
| E_{CO} | Energy required to produce 1 mol of CO |
| η | Plasma reactor energy efficiency |

List of Figures

| | |
|--|----|
| Figure 1.1: Global steel demand trajectory..... | 3 |
| Figure 2.1: A & B Projected steel demand and the estimated split of future production route, based upon arising scrap availability..... | 9 |
| Figure 2.2: Extraction from McKinsey and Company, depicting global steel production..... | 10 |
| Figure 2.3: Steel making process routes..... | 12 |
| Figure 2.4: Total CO ₂ emissions from key sources at the case study steel plant (tonnes/annum assuming complete combustion) | 13 |
| Figure 2.5: An introduction to State-of-the-art steelmaking technology from Tata Steel, Hlsarna | 17 |
| Figure 2.6: Process configuration of the Top Gas Recycling Blast Furnace Concept..... | 18 |
| Figure 2.7: Hierarchy of waste reduction strategies | 20 |
| Figure 2.8: Potential pathways for valorisation of steel plant gases, CORSYM project | 21 |
| Figure 2.9: Locations of locally sourced biomass availability, beyond existing market demand | 25 |
| Figure 2.10: Nitrogen fertiliser application by region and product..... | 28 |
| Figure 2.11: Depiction of the CO ₂ -NH ₃ -H ₂ O system, as described within the UNIQUAC Equation of State (EOS) | 32 |
| Figure 2.12: Schematic of sour gas sweetening (carbon capture) process | 35 |
| Figure 2.13: Literature values (MEA) and Aspen HYSYS simulation (Ammonia) reboiler comparison | 37 |
| Figure 2.14: Gas vapour pressure vs CO ₂ absorbed at 283K and NH ₃ concentration of 4.5 wt. %.. | 38 |
| Figure 2.15: A comparison of CO ₂ kinetics at increasing temperature for MEA and NH ₃ by various authors..... | 42 |
| Figure 2.16: Two dimensional representation of the Tesař-Zimmerman Fluidic Oscillator (TZFO). | 44 |
| Figure 2.17: Size distribution of bubbles in both steady and oscillatory flow regimes for an MD 500 diffuser. | 44 |
| Figure 2.18: Bubble generation, in the air-lift loop bioreactor at Tata Steel UK (previously Corus) power station prior to algae introduction..... | 46 |
| Figure 2.19: FO microbubbles (Left) and non-oscillatory fine bubbles (Right) | 46 |
| Figure 2.20: Bubble size and transfer rate relationship | 47 |
| Figure 2.21: A typical DBD (coaxial) configuration, as used with experiments by Bogaerts et al. (2015)..... | 55 |
| Figure 2.22: Distribution of energy lost by electrons In CO ₂ among excitation channels..... | 57 |
| Figure 3.1: Schematic of CO ₂ -NH ₃ -H ₂ O reactor configuration..... | 66 |
| Figure 3.2: Reaction vessel dimensions..... | 69 |
| Figure 3.3: Complete experimental set-up..... | 70 |
| Figure 3.4: Exposed (out case removed) plasma reactor core with spiral wire electrode design shown operating on the right, with a characteristic, violet plasma glow. | 72 |
| Figure 3.5: Thermal Imaging of reactor with and without copper coil cooling system..... | 72 |

| | |
|--|-----|
| Figure 3.6: Reaction vessel temperature (average of the triplicate tests) over time for the 8 test configurations..... | 79 |
| Figure 3.7: Reaction pH (average of the triplicate tests) over time for the 8 test configurations .. | 80 |
| Figure 3.8: Reactor exit gas NH ₃ concentrations over time (Test variations 1 to 4) | 81 |
| Figure 3.9: Reactor exit gas NH ₃ concentrations over time (Test variations 5 to 8) | 81 |
| Figure 3.10: Flow rate influence on bubble generation at high NH ₃ concentrations, test case number 7..... | 86 |
| Figure 3.11: Temperature increase with respect to NH ₃ weight% at 2 l/min (16% CO ₂ concentration) | 88 |
| Figure 3.12: The removal efficiency and absorption capacity for increasing NH ₃ concentrations.. | 95 |
| Figure 4.1: Operational, twin-plasma reactor design with visibly high and low SEI regions | 101 |
| Figure 4.2: Chemical reactions within DBD plasma CO ₂ dissociation | 103 |
| Figure 4.3: The fraction of electron energy transferred to different channels of excitation as well as ionization and dissociation of CO ₂ for MW plasma and DBD plasma | 105 |
| Figure 4.4: CO ₂ electronic and vibrational levels for dissociation | 105 |
| Figure 4.5: Densities of vibrationally excited CO ₂ species (left axis) and the ground state CO ₂ (right axis) as a function of time..... | 106 |
| Figure 4.6: CO ₂ conversion as a function of input power: CO ₂ /He = 1/1 AC power supply | 108 |
| Figure 4.7: The Relationship between CO ₂ Conversion and Efficiency..... | 108 |
| Figure 4.8: Streamer evolution (left to right)..... | 109 |
| Figure 4.9: Low streamer (Electron/plasma) density..... | 110 |
| Figure 4.10: High streamer (Electron/plasma) density..... | 110 |
| Figure 4.11: Twin electrode DBD plasma concept | 114 |
| Figure 4.12: Plasma power supply A continuous waveform | 115 |
| Figure 4.13: Plasma power supply B decaying waveform | 115 |
| Figure 4.14: Twin electrode DBD plasma circuit | 116 |
| Figure 4.15: First-of-a-kind two-stage plasma reactor concept in operation..... | 120 |
| Figure 5.1: UK steel plant energy Sankey diagram..... | 130 |
| Figure 5.2: Breakdown of site energy balance in to upstream (heavy end) and downstream processes | 138 |
| Figure 5.3: Definition of emissions scope 1, 2 and 3..... | 140 |
| Figure 5.4: Forecast of CO ₂ grid intensity | 140 |
| Figure 5.5: Example of DRI data input into the model..... | 142 |
| Figure 5.6: Site annual carbon intensity, as simulated in the year 2050, under the different technology scenarios | 149 |
| Figure 5.7: The cumulative summation of all the carbon emitted between 2020 and 2050 | 151 |
| Figure 5.8: Annual carbon emission intensity of the chosen scenarios and contribution of technologies, within the year 2040..... | 151 |

| | |
|---|------------|
| <i>Figure 5.9: Annual carbon emission intensity of the chosen scenarios and contribution of technologies, within the year 2040.....</i> | <i>152</i> |
| <i>Figure 5.10: The percentage shift (increase) in the sites operational costs as a results of decarbonisation methods in the year 2050</i> | <i>155</i> |
| <i>Figure 5.11: The cost per ton of steel from 2020, up to 2050 within each scenario. Actual values have been concealed, due to the commercial sensitivity of the scenario outputs.....</i> | <i>156</i> |
| <i>Figure 5.12: The estimated net cash flow, between 2020 and 2050 for the chosen scenarios.....</i> | <i>157</i> |
| <i>Figure 5.13: The volatility of iron ore prices over time.....</i> | <i>159</i> |
| <i>Figure 6.1: Breakdown of blast furnace MEA capture costs</i> | <i>169</i> |
| <i>Figure 6.2: Configuration, energy balance and carbon savings of the top gas recycling blast furnace process.....</i> | <i>171</i> |
| <i>Figure 6.3: Energy density for fuel options including tank weight.....</i> | <i>174</i> |
| <i>Figure 6.4: Current examples of synthetic fuel production</i> | <i>174</i> |

List of Tables

| | |
|--|------------|
| <i>Table 2-1: Typical compositions of steel plant works arising gases.....</i> | <i>13</i> |
| <i>Table 2-2: A breakdown of Steel Company Low-carbon research projects and technology focus..</i> | <i>15</i> |
| <i>Table 2-3: Pros and Cons of the most common types of carbon capture technology.....</i> | <i>36</i> |
| <i>Table 2-4: A comparison of key characteristics of CO₂ capture solvents</i> | <i>40</i> |
| <i>Table 2-5 A comparisons of capture system kinetics at 25°C</i> | <i>42</i> |
| <i>Table 3-1 Control test parameters.....</i> | <i>67</i> |
| <i>Table 3-2 Upper and lower process variable limits.....</i> | <i>67</i> |
| <i>Table 3-3 Process variations</i> | <i>68</i> |
| <i>Table 3-4 DBD Reactor Critical Dimensions</i> | <i>71</i> |
| <i>Table 3-5 SEI and residence time at high and low flow rates</i> | <i>72</i> |
| <i>Table 3-6 Reactor Measurement Equipment.....</i> | <i>74</i> |
| <i>Table 3-7 Control experiments, with and without plasma and microbubbles.....</i> | <i>75</i> |
| <i>Table 3-8 Process variations</i> | <i>76</i> |
| <i>Table 3-9 Total Precipitate Mass, Carbamate and Carbonate Production</i> | <i>76</i> |
| <i>Table 3-10 Results and estimated errors for the 8 test configurations.....</i> | <i>77</i> |
| <i>Table 3-11 Mass conversion, CO₂ excess, CO₂ per gram and plasma energy</i> | <i>78</i> |
| <i>Table 3-12 Comparison between best and worst tests configurations.....</i> | <i>79</i> |
| <i>Table 3-13 Corresponding peak temperatures and CO₂ uptake</i> | <i>83</i> |
| <i>Table 3-14 Peak concentrations of NH₃ gas measured in the reactor flue off-gases.....</i> | <i>96</i> |
| <i>Table 3-15 Error estimate for precipitate mass calculation.....</i> | <i>99</i> |
| <i>Table 3-16 Error estimate for reactor vessel conditions monitoring</i> | <i>99</i> |
| <i>Table 4-1 Most relevant CO₂ dissociation pathways within atmospheric, non-thermal plasma regime.....</i> | <i>104</i> |
| <i>Table 4-2 A comparison of plasma reactors and their conversion and efficiency using pure CO₂ only</i> | <i>112</i> |
| <i>Table 4-3 Reactor geometry</i> | <i>117</i> |
| <i>Table 4-4 ADC MGA 3000 series, multi-gas analyser specification.....</i> | <i>117</i> |
| <i>Table 4-5 Power consumption for the 3 operation modes of the twin-plasma concept.....</i> | <i>118</i> |
| <i>Table 4-6 SEI at 0.5 and 1 litres per minute (l/min).....</i> | <i>119</i> |
| <i>Table 4-7 Gas residence time comparison at 0.5 to 2 litres per minute (l/min) for a 50mm electrode, plus 13mm electrode gap</i> | <i>120</i> |
| <i>Table 4-8 Max conversion rate and max efficiency achieved</i> | <i>121</i> |
| <i>Table 5-1 Inputs to the modelling base case calculations (values used with the model are deliberately hidden for confidentiality of processes conditions)</i> | <i>136</i> |
| <i>Table 5-2 Carbon intensity of the blast furnace (base case) processes</i> | <i>148</i> |
| <i>Table 5-3 Carbon intensity of processes, as determined by the model and World Steel data.....</i> | <i>148</i> |
| <i>Table 5-4 Cumulative emission of selected pathways</i> | <i>152</i> |

Table 5-5 % reduction of process compared to base case 2016 emissions 153

Table 5-6 The percentage of the total sites operational costs, per ton of steel for the EAF route 158

*Table 5-7 The percentage of the total sites operational costs, per ton of steel for the BF-BOS route
..... 158*

Chapter 1

Introduction

1.1 General Introduction – the challenge

The gradual change in the earth's climate, dominated by an accelerated increase in global temperature post-industrialisation, has generated significant concern. The Kyoto Protocol in 1997 was the first point in history that developed nations committed themselves to legally binding targets to address this challenge (UNFCCC, 1997). The 2015 Paris Agreement set ambitious targets to limit the rise in global temperature to well below 2°C by the end of the century and to also pursue a course for temperature rise of no greater than 1°C (UNFCCC, 2015).

Back in 2013, the Intergovernmental Panel on Climate Change (IPCC) published their working group report, which confirmed that human activities are the primary cause for climate change (Alexander, et al., 2013). A possible increase in average global temperature can be linked to the growing concentration of gases within the atmosphere that cause a warming effect, referred to as greenhouse gases (GHG) (Estrada, et al., 2013). Of primary concern has been the increased concentration of CO₂, as this can be linked to human activities, particularly the combustion and use of energy dense fossil fuels. Multiple studies have shown apparent links between the rise in atmospheric GHG concentrations and climate change (Pycroft, et al., 2014). The 2018 IPCC Special Report on Global Warming of 1.5°C (SR15) highlighted that a 2°C temperature rise scenario would have devastating consequences for life on our planet, and that the aiming for the 1.5°C is essential.

As the need to lower our impact and move towards a circular economy grows, the recyclability of materials such as steel will mean that steel will secure its place in our future (Wortler, et al., 2013). Its relatively high value means that steel is rarely discarded (88% recycled), instead it is collected and melted down to form an infinite possibility of products. It is expected that demand for steel will continue to grow as steel products find their way into the technologies of the future; wind turbines for new renewable energy, lightweight components or the electric motors in a new generation of low emission vehicles. No other material shares this versatility, abundance and recyclability. Its downfall, however, is that the primary steel production needed to satisfy demand is currently a very carbon intensive process. The conversion of iron ore requires large amounts of fossil carbon for both the reduction of the iron ore and the heat for the iron and steel to flow and be forged into new shapes, which ultimately results in the emissions of CO₂ to atmosphere.

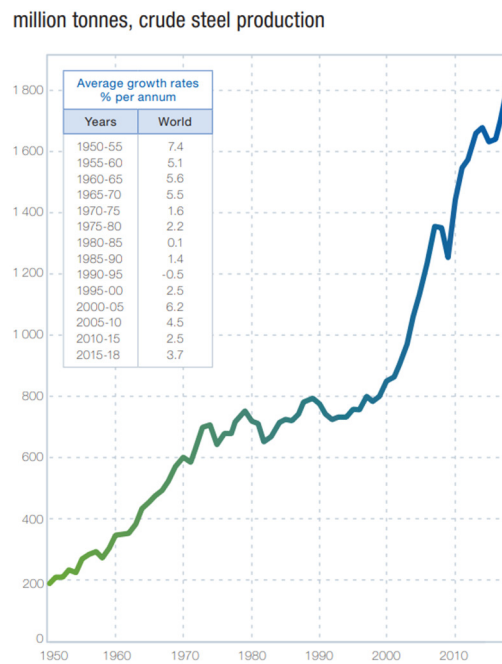
Although there have been significant improvements in the efficiency of steel making over the past 50 years and the collaboration of many steel manufacturers to find a low carbon manufacturing processes, the solution to a low-carbon and cost-effective alternative still eludes steel manufacturers today. Clearly this presents a challenge, and one which demands the attention of further research. The steel industry today emits 4.3 Gt of CO₂ equivalent per year, which represents 8% of global anthropogenic emissions. As the power and transport sector, backed by Governments and large corporations, receives the attention of major research and investment, competitive solutions are now emerging to enable the carbon emission from these sectors to reduce, however large industry still represents a major challenge. Unfortunately, the steel industry is an energy intensive process and is reliant upon fossil carbon to process the raw materials.

Steel is made from abundant naturally occurring raw materials and is very versatile and recyclable, therefore we do not anticipate finding an alternative material with superior properties as demand continues to grow at a steady rate to match population growth. It is also essential to support the low-carbon transition, with the material being used for wind energy, batteries, solar arrays and lighter weight components.

The threat to business as usual due to climate change and the challenge of CO₂ reduction during steel production, owing to the industries reliance upon fossil carbon, has been known for some time. 2004 saw the formation of the multi-partner European collaboration project, Ultra-Low Carbon Dioxide Steelmaking project (ULCOS). With 47 partners over 15 European Countries, the aim of the ULCOS consortium of steel producers and research institutions was to reduce the emissions from steel production by an ambitious 50%. The 50% ULCOS target now falls short of the 80% reduction targets set by the European Governments and subsequent ambitious targets set out to achieve net-zero. The research program and supporting demonstrations concluded that to reach greater than 20% CO₂ emissions reduction carbon capture and storage (CCS) must be deployed.

Further efforts to find solutions have seen the development of hydrogen based steel making solutions. Yet the process of producing large volumes of hydrogen at present still demand high fossil energy inputs and subsequent CO₂ emissions. It seems that the pathway to decarbonisation for the sector is still unclear and that the transition is still likely to see large volumes of CO₂ produced and released over the coming decades in order to meet demands for this product. This challenge represents an opportunity to identify novel solutions to abate the carbon emissions and develop greater clarity on pathways that could meet the global climate ambition in the necessary timescales.

Figure 1.1: Global steel demand trajectory



Source: (World Steel Association , 2019)

1.2 Rational for research – identifying the opportunity

The steel sector represents a major global source of problematic anthropogenic emissions. The output of previous research, such as ULCOS suggests that carbon capture will be needed to go beyond a 50% carbon reduction, generating large volumes of CO₂ that will need storage. This may be challenging for those sites with limited access to carbon storage, or at a great distance from a nearby store, such as inland European steel making facilities. Capture and storage is also considered an expensive process, which has prevented full scale deployment of this process on existing integrated blast furnace steel sites.

An alternative to storage could be utilisation of CO₂ for products, although it is recognised this would be challenging to convert all steel plant emissions, the process could improve the economics of carbon capture, or provide an initial pathway to its commercialisation. At the start of the studies, the concept of steel plant carbon capture and utilisation (CCU) was in its infancy, with only conceptual ideas being proposed. However, during the past few years it has bloomed into a worldwide, multi-partner research area, with ongoing research programmes and new research institutions. The Carbon2Chem and Carbalyst being the most significant steel linked projects of this type. It was recognised at the start of this research thesis that it would not be possible to operate in the same field as these large multi-million euro projects, therefore this project must compliment the ideas and solutions being proposed to yield step change carbon reduction in the industry.

Multiple products could be produced from CO₂, however fertiliser is currently a large consumer of CO₂ and has large global demands needed to meet high yields of food production. It is thought that ongoing demand for fertiliser and urea will be needed in ever greater quantities. Yet the process is energy intensive and a whole systems approach is not carbon neutral (Styring & Jansen, 2011). Applications to enhance this process and limit energy input could provide new pathways to carbon dioxide utilisation. Also recent research at The University of Sheffield has presented a potential method to liberate ammonia from waste water. Ammonia being the primary feedstock to fertiliser and it's production a major consumer of energy within urea production (Desai, et al., 2020). Previous work within the Faculty of Engineering at The University of Sheffield has demonstrated some of the unique characteristics and benefits offered by the proprietary microbubble technology, and the team is continually searching for new applications of this technology (Gilmour & Zimmerman, 2020). The principles have been successfully applied to research fields such as: enhanced algal growth, wastewater treatment and oil emulsion separation, but have yet to find suitable application in either the steel sector or to address CO₂ processes emissions. It would seem that the unique benefits of microbubbles had yet to be applied to the field of CO₂ and ammonia interactions.

The concept arose, whereby microbubbles could be used to enhance the CO₂-NH₃-H₂O system to, hypothetically, generate fertiliser. Secondly, it was estimated that a phantom catalyst could be introduced via a plasma reactor to further enhance the reaction process as shown to be viable within other CO₂ systems (Zimmerman & Kokoo, 2018). The same micro plasma devices could also be applied to the dissociation of CO₂ to produce CO and O₂, both products of high value. The CO could in principle be reinjected into the Blast Furnace to increase carbon recycling and reduce total fossil carbon input, as demonstrated in the ULCOS Top Gas Recycling Furnace. The O₂ may substitute production at the air separation units that supply the Basic Oxygen Furnace. This, it was thought, would be preferential to storage for those sites, who as mentioned have limited options for CO₂ storage.

A supporting area of development became evident as the research progressed. With the emergence of hydrogen-based steelmaking as a viable concept, the future pathway of the global steel industry had become uncertain. It became ever more challenging to evaluate how the CCU concepts being developed, as well as current and emerging technologies, could be applied to achieve significant decarbonisation of the steelmaking process. A solution to this uncertainty could be achieved through a detailed, techno-economic model, forecasting the potential configurations and rate of technology deployment of a future low-carbon steel plant, up to 2050. This would provide a basis for technology comparisons and look specifically at carbon and financial implications of transitioning to a low-carbon alternative. Whilst the two technologies described above have significant research value, a lack of detailed understanding of their impact

and application would leave this research incomplete. The model development and simulation allows the evaluation of the two CCU techniques within the context of greater decarbonisation strategy and a look at their overall impact on the steelmaking process, rather than just the individual technological advances.

1.3 Research aims and objectives

The aims of this research are to enhance the knowledge and understanding surrounding the pathways to steel decarbonisation and the application of CCU within the sector. With particular emphasis in exploring new applications for microbubble technology and plasma activation and dissociation of CO₂.

Following the identified challenge and opportunities, three objects have been set.

The objectives are:

1. Demonstrate the application of microbubbles and plasma reactors to the CO₂-NH₃-H₂O system.

Here, a system will be designed, developed and tested. This will present a first of a kind application of microbubbles, and plasma active CO₂ to this type of reaction.

2. Enhance the knowledge within the application of micro-plasma devices to CO₂ dissociation.

The pathways and barriers to CO₂ dissociation via plasma suggest further development in this area is possible. After a thorough investigation into the dissociation processes and existing systems, it is proposed that a new reactor design will be developed and demonstrated at laboratory scale.

3. Develop a detailed techno-economic model of a future low-carbon steel plant.
 - a. To understand the possible carbon reduction pathways, up to 2050
 - b. Establish which of the possible pathways could be economically viable
 - c. Evaluate which of the pathways provides the greatest cumulative emissions reduction, assisting the climate target of a 1.5°C temperature increase.
 - d. To determine if the two carbon reduction technologies under development, could lead to significant carbon reduction within the most viable pathways

The aim of this objective is to address the outstanding uncertainty surrounding the potential pathways and future application of the CCU technologies. Following the successful delivery of this objective, it will be possible to carry out an appraisal CCU concepts within a future, low-carbon steel making environment.

1.3 Thesis structure

The thesis is organised into 7 chapters in total. These chapters will guide the reader through the logical process carried out within this research to address the challenge identified and objectives that have been set. The structure outline below will help the reader navigate the relevant sections. The conclusion from the research performed in chapters 3, 4 and 5, feed into the evaluation carried out in chapter 6.

The two proprietary technologies being investigated in detail are subsequently underpinned by the techno-economic modelling section and evaluation, which then takes a high-level view of the implementation of the new discoveries and technologies into a future low-carbon industrial scenario.

Chapter 1: An introduction to the research and the rationale. The project aims and objectives and also the scope of work.

Chapter 2: A detailed review of the currently available literature. Followed by an analysis of the technology challenges and remaining knowledge gaps. Concluding with the establishment of the research hypothesis.

Chapter 3: Presents the experimental methods, procedures, results and analysis, for the application of microbubbles and plasma activated CO₂ into the CO₂-NH₃-H₂O system.

Chapter 4: Details the issues and barriers to the successful, high-efficient dissociation of CO₂. With the design and operation, results and analysis of a new reactor invention.

Chapter 5: Establishes a first-of-a-kind detailed techno-economic model to describe the transition of a steel plant up to 2050 under different scenarios. The construction and details of the model are introduced, with the subsequent presentation of the model outputs and analysis of the models results.

Chapter 6: Utilising the knowledge established within research chapters 3, 4 and 5, the data is used to analyse the applicability of the two technologies developed with Research Chapters 3 and 4, at full-scale, within a future, low-carbon steelmaking facility.

Chapter 7: Provides a discussion and conclusion of the thesis results, the significance of the findings, the potential impact as a result from the three novel and first-of-a kind discoveries, along with recommendation for future work to enhance the knowledge with the field.

Chapter 2

Theoretical background and literature review

2.1 Introduction

Given the identified challenge and the project aims, we look toward the literature to identify answers to the following questions:

- 1) Are there clearly defined solutions available to the existing steel industry decarbonisation challenge and does it warrant a complex steel plant techno-economics model and future simulation?
- 2) How have microbubbles previously been applied?
 - a. Have microbubbles and plasma-activated microbubbles been applied to the injection of CO₂ into aqueous ammonia solutions?
 - b. What is the potential application of this technology and the influence on the CO₂-NH₃-H₂O system?
 - c. Can this technology be applied within a steel industry context?
- 3) What is the current status of knowledge with regard to the dissociation of CO₂ with micro-plasma devices and can they be applied in a steel industry context to achieve decarbonisation?

To answer these questions, naturally this literature review covers quite a broad range of topics, as a result of the three research areas of interests and their diverse supporting subsections. A detailed knowledge of steel plant processes and decarbonisation pathways is needed to fully understand the potential application of the two technological solutions and in order to develop future strategic, technology pathways for the model and simulation exercise. The literature review is structured into the following three areas of interest that align with the questions identified above, in the following order:

- The production of iron and steel with low carbon emissions
- Processes involving the reactions between CO₂ and ammonia and the application of microbubbles
- The conversion of CO₂ using plasma chemistry

To provide context for the technology application as well as the techno-economic appraisal (TEA), the following review provides an overview of current and possible future iron making technologies. Given the identified challenge, the focus is upon technologies that can address this challenge and that could lead to deep (>80%) decarbonisation of the current industrial processes. The following is an extensive review of the literature relating to the challenges

identified; not an exhaustive list of all literature and possible methods within this field, which again is quite diverse, rather a directed overview for the reader so that they may understand the challenges facing this industry and the most likely pathways to decarbonisation, which are later evaluated in the techno-economic model. Emphasis is on the solutions viable within the UK. Whilst there is considerable literature available on the subject of steel plant decarbonisation, the research at the leading-edge of developments is part of large budget, multi-partner collaborative projects and is commercially sensitive with limited public access.

The review of literature within the field of CO₂ capture in aqueous ammonia explores the well-established production of urea as a common form of ammonia-based carbon utilisation, followed by the more recent expansion into carbon capture systems that can be used as part of full-chain CCS. The section is concluded with an introduction to the applied technology of microbubbles, with a focus on their role for improving the gas-to-liquid surface area and their influence on reactions at the bubbles surface, which is later applied to an innovative ammonia-based capture system.

The review is completed with an introduction into plasma, plasma reactors and more specifically the use of plasma reactors for the dissociation of CO₂. The use of plasma reactors will be incorporated into the aqueous ammonia capture system, to evaluate their influence, but also into a stand-alone technology to treat CO₂ process emissions from the steel sector.

To conclude, the literature is evaluated and gaps are recognised within the current knowledge.

2.2 Technology pathways to achieve low-carbon iron and steel production

The traditional method for the reduction of iron ore to produce iron (referred to as pig iron within the industry) can be summarised in the equation 2.1:



This very well-established reduction reaction is reliant upon a carbon source to produce the vast quantities of carbon monoxide (CO) needed and subsequently produces a significant amount of CO₂. CO₂ is produced in greater quantity than the iron itself. This reduction reaction is accountably for ~70% of associated steel production emissions. Approximately 780kgs of coal is required per ton of crude steel, resulting in the production and release of ~1.8 tons of CO₂ (depending upon the emissions scope, scrap input and processes efficiencies). This reaction process has been optimised over 100 years into the highly effective modern blast furnace (BF) and there are limited commercial alternatives to this dominating and highly optimised technology. The reliance on coal as a carbon source for the reductant (and also its mechanical properties within the burden) and the resulting production of CO₂ due to the oxidation of iron ore make decarbonisation of this processes rather challenging. Indeed, the sector has been termed

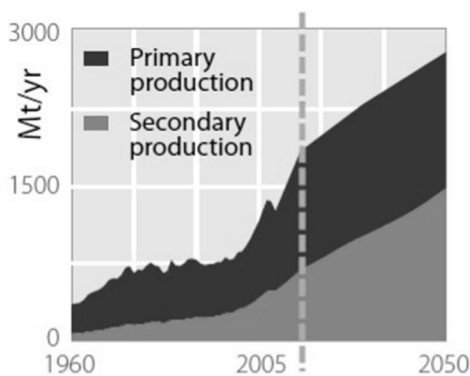
“difficult to decarbonise”, due to its current reliance on coal and limited alternatives to the well-established and cost competitive BF route.

Today, production is split between Blast Furnace and basic oxygen furnace technology (BF-BOF) and Electric Arc Furnaces (EAF). BF-BOF is known as the primary method, whereby new steel is generated from the earth’s raw materials; iron ore, fluxes (lime) and coal (coke). The BF produces iron, that is later converted into steel within a Basic Oxygen Furnace (BOF), so-called due to the basicity of the reaction, hence the process is known as the BF-BOF route. EAF technologies rely upon a high percentage of scrap feedstock, however, some furnaces still feed these furnaces with primary iron in order to reach, at a low cost and high volume, the higher qualities needed for some steel grades and markets. Whilst there are some alternative technologies, which use natural gas, known as Direct Reduced Iron (DRI), BF-BOF and EAF represent 99% of total steel production. BF-BOF accounts for around 72% of total steel production today, with the remaining 27% from an EAF route and 1% DRI (World Steel Association , 2019).

Scrap is a finite commodity and the amount of steel produced via the EAF route is limited by the global scrap availability. This is expected to increase as more previously used steel becomes available, whereby the steel making of the past, dictate the available of scrap in the future. The predicted increased global demand will ensure a continuous demand for primary iron as the arising new scrap, based on estimates from previous production of steel, is not enough to meet demand. Figure 2.1 A and B below shows the projected split between the two routes of primary iron (BF-BOF or a new low carbon alternative) and scrap based, secondary production (re-melting technologies, such as EAF) (Allwood & Cullen, 2012) (Pauliuk, et al., 2013). A very similar projection of arising scrap vs steel demand is presented in ArcelorMittal’s excellent Climate Action Report (ArcelorMittal, 2019).

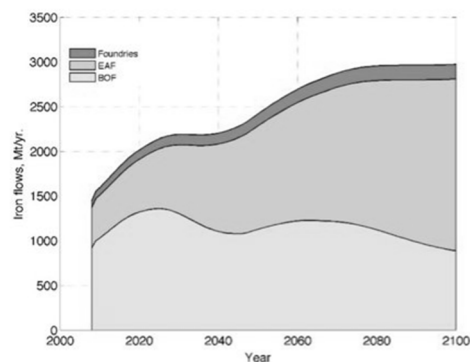
Figure 2.1: A & B Projected steel demand and the estimated split of future production route, based upon arising scrap availability

A



Source: (Allwood & Cullen, 2012)

B

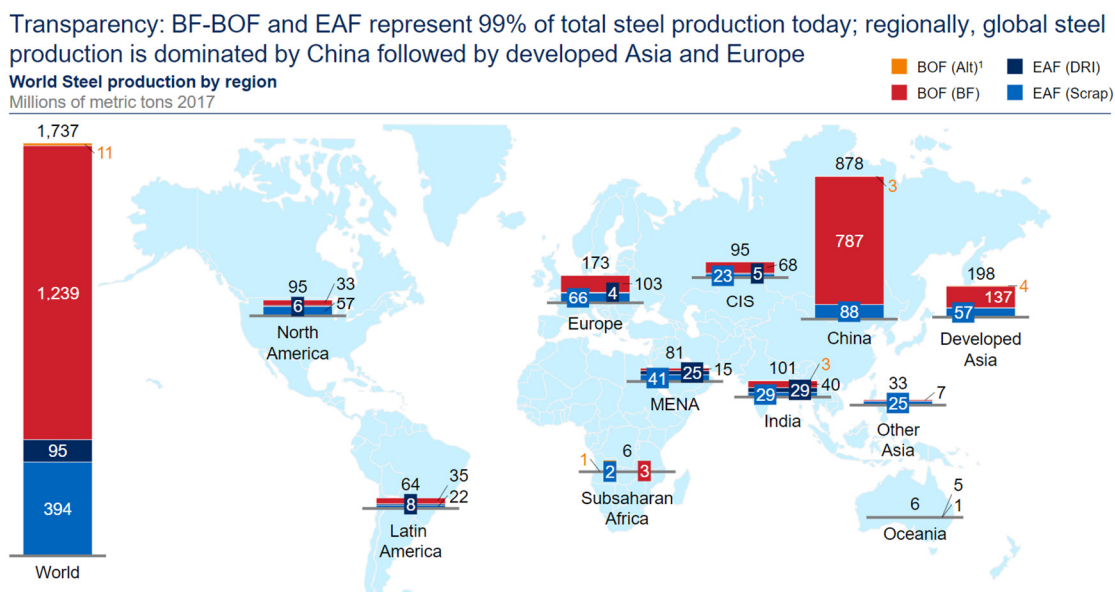


Source: (Pauliuk, et al., 2013)

The EAF process produces significantly less CO₂ emissions per ton of steel produced at around 0.37 tCO₂ per ton of crude steel (tCS) against ~1.8 tCO₂/tCS for BF-BOS (depending upon the source and carbon within the electricity). With greater volumes of used steel scrap becoming available within developing regions, especially China, a transition towards EAF in these regions is to be expected, with the global EAF share increasing from 27% of production, up to a maximum of between 55-60% by 2050 (Allwood & Cullen, 2012), (Pauliuk, et al., 2013), (Fickling, 2020).

Within a global context, the UK's contribution to the global steel supply chain and the relative CO₂ emissions are quite small. China is the most dominant steel producer with respect to total volume as demonstrated in figure 2.2. To place this in context, China produces more steel in one month than the UK will in 13 years. It is anticipated that future growth within the sector will come from developing regions, in particular India. Low-carbon steel making solutions will need to be transferable to these regions. (McKinsey and Company, 2017).

Figure 2.2: Extraction from McKinsey and Company, depicting global steel production



Source: Steel Institute VDEh, 2017, McKinsey metallics model 2017

It is possible to summarise the potential low-carbon production options for the steel sector into three basic categories, as shown below. The choice of future pathway would be determined by multiple factors, which the thesis will evaluate during the techno-economic modelling in chapter 6.

1. Replacement of carbon-based reductant with low-carbon alternative. This would include:
 - a. Hydrogen*, produced via a low carbon method, such as electrolysis (which also overlaps with option 2b, below) or conventional water gas shift of natural gas

(NG), but with the addition of carbon capture and storage (which overlaps with 3, below).

- b. Natural gas*. The presence of hydrogen within natural gas helps lower the total CO₂ emission.
- c. Biofuels

*Note that both a and b would require a switch from blast furnace technology to a direct reduced iron facility and that the use of NG would still contain a high proportion of carbon, limiting carbon reduction potential.

- 2. Electrification. Maximising the use of low-carbon electricity within the process raises many challenges. An increase in the use of renewable power, either within the steelmaking site or to decarbonise another fossil-based industry using steel plant gases, could see total carbon emission reductions. A simplified description of the options include:
 - a. Electrification of heating processes, including melting of scrap.
 - b. Supply of Hydrogen via electrolysis. This overlaps with 1a above.
 - c. Carbon conversion, such as CO₂ utilisation or conversion to new products using renewable energy as the primary energy source.
- 3. Carbon capture and storage (CCS). Certain steel production methods can improve the ability to capture or recycle the carbon from the steel plant process gases by reducing the nitrogen content and increasing CO₂ concentrations, but permanent sequestration of the CO₂ is needed to yield significant reductions in carbon emissions to atmosphere from these steelmaking approaches.

If hydrogen was used as a reductant and the source was blue hydrogen via steam methane reforming (SMR), this would also require CCS to reduce the carbon emissions to atmosphere. Fuel switch (option 1) in this case, would still require CCS (option 3), indicating that the 3 options are interdependent.

The two technology methods investigated within this thesis can be considered methods of electrification and CCS (options 2 and 3).

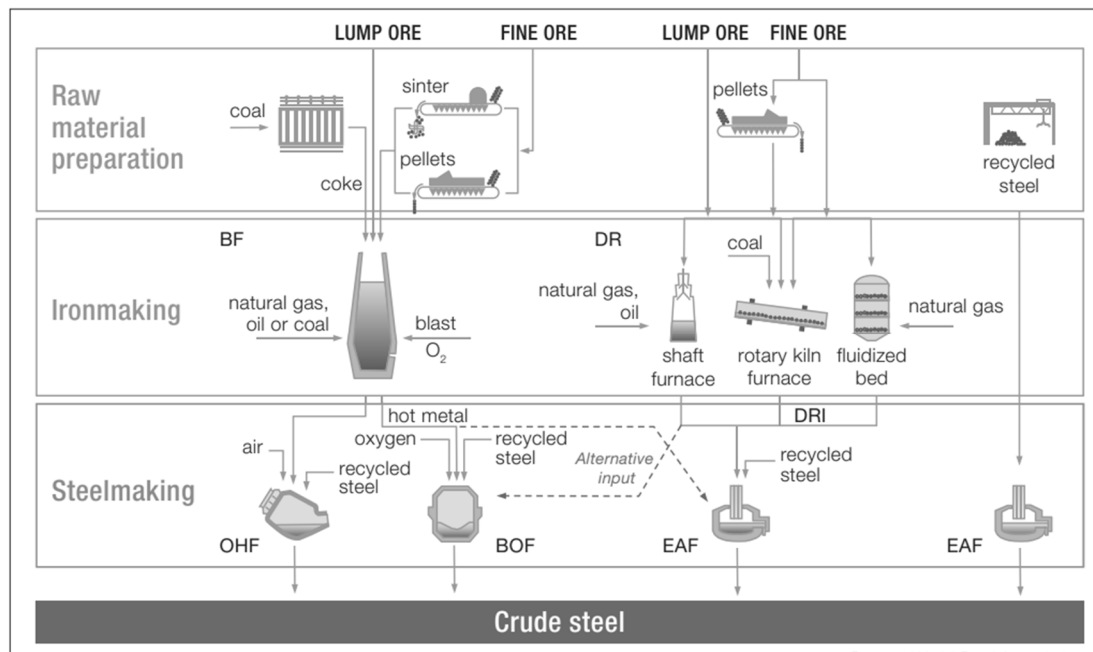
Steel in a typical integrated steel production site follows a series of production processes. These are:

- 1. Burden preparation; comprising of coking ovens (coke ovens) to produce metallurgical coke, a sinter plant and flux preparation.
- 2. The Blast Furnace (BF) whereby coke, sinter and fluxes are combined to produce iron.
- 3. The Basic Oxygen Furnace (BOF), where iron is transformed into steel via the injection of oxygen.

4. Secondary steelmaking; a selection of process steps chosen by the manufacturer to produce the desired steel properties.
5. Casting; typically in a continuous caster, but could be ingots.
6. Rolling and finishing; to turn the cast material into the final product (although cast material can be sold directly to customers, rolling and finishing is the typical route).

These process steps are shown in the diagram (Figure 2.3) below, alongside the Direct Reduction (DR) route and also the much simpler EAF route (although most steel facilities including EAFs will be accompanied by a secondary steelmaking step (step 4) to tune the metallurgical properties prior to casting as described above) (World Steel Association, 2019). It is important to note that scrap (termed ‘recycled steel’ in figure 2.3) is used within all three of the process routes, often for enhanced cooling purposes, and that primary iron is sometimes fed into the EAF route for quality purposes.

Figure 2.3: Steel making process routes



Source: (World Steel Association, 2019)

The pie chart in figure 2.4 highlights how the blast furnace is the predominant consumer of raw materials and carbon, resulting in the greatest volume of processes gases and source of CO₂ emissions. For this reason, research effort for decarbonisation has targeted the BF (primary iron) process. Whilst the BF is the primary carbon consumer, it worth noting that it is the result of the collection of these gases and subsequent use for energy and reheating that result in CO₂ emissions to atmosphere. The steel making process produces high volumes of gases. Their compositions can be seen in the accompanying table 2-1.

Figure 2.4: Total CO₂ emissions from key sources at the case study steel plant (tonnes/annum assuming complete combustion)

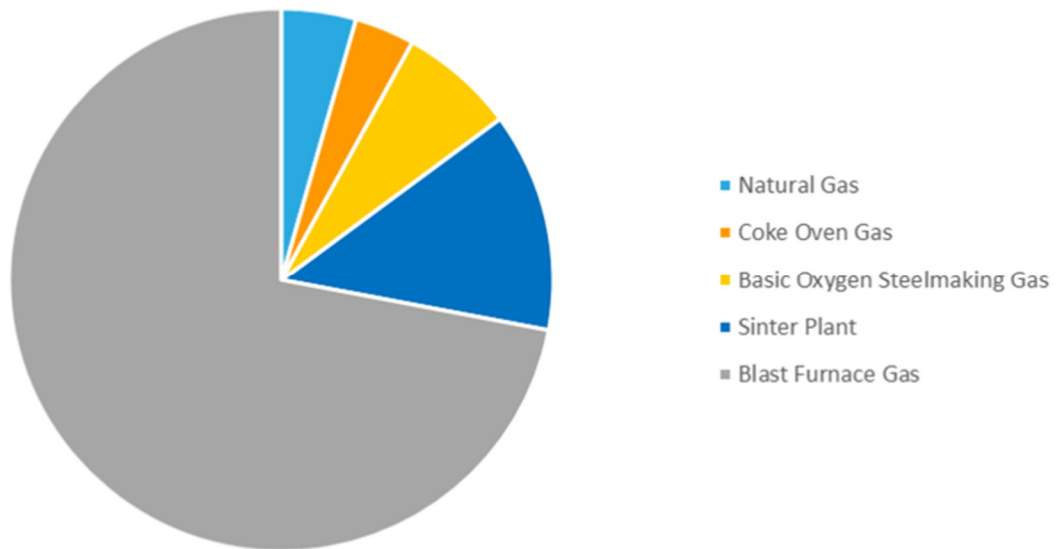


Table 2-1: Typical compositions of steel plant works arising gases

| Component | Coke Oven Gas (COG) | Blast Furnace Gas (BFG) | Basic Oxygen Furnace Gas (BOFG) | Mix |
|-----------------------|---------------------|-------------------------|---------------------------------|-------|
| | % | % | % | % |
| N₂ | 10 | 50-60 | 15-30 | 39-47 |
| H₂ | 58-65 | 2-4 | 1-2 | 15-18 |
| CO | 4.8-6.8 | 20-35 | 50-70 | 18-30 |
| CO₂ | 1.5-2.5 | 20-30 | 10-20 | 15-23 |
| CH₄ | 24-33 | - | - | 6-8 |

These gases contain significant quantities of useful constituents; CO, H₂ and CH₄, which are used on-site for further energy production. The most efficient use of these gases will result in the least carbon emission to atmosphere for a fossil fuel reliant integrated site. The result of utilising these gases on-site for heat generation is that the on-site power plant and the BF stoves are the primary single sources of CO₂ emissions from a site, even though the blast furnace is the greatest consumer of carbon, (Birat, 2010), (Carpenter, 2012).

2.3 Research Programmes and Low-Carbon Steel Technologies

The large multi-partner ULCOS project was the first major collaborative effort to identify potential low-carbon alternatives within the steel sector. Individual nations have similar projects, such as the Course50 project in Japan and the American Association for Iron & Steel Technology (AAIST) programme. The current environment is much less collaborative as the market and the opportunity becomes more competitive. Within Europe, individual organisations backed by National Government now dominate the research in this area. A breakdown of publicised steel research focus within Europe is presented below. A review of research efforts in iron and steel is provided by Quader M. et al., (2015), entitled ‘A comprehensive review...’ (Quader, et al., 2015). Unfortunately, such reviews lack sufficient detail to assess the technology deployment and are quickly out of date as a result of the pace and diversity of the research field. This review does provide a good overview of the range of technologies that could be deployed. The type of technologies that are considered are starting to converge into common themes: CCS, CCU, Electrification and Hydrogen. Rather than large, multi-technology research programmes, similar to ULCOS, the research is now fragmented into smaller research subjects, so the scene is much more fluid with projects coming and going or being re-branded. Within Europe, these projects typically align with the programme themes of Horizon 2020 funding, which is accessed by most of the projects. One of the best reviews of technology options is provided by the steel company ArcelorMittal (ArcelorMittal, 2019). This is a very good report, believed to comprise a strong research team, with access to a wide range of data and strong process knowledge, given the size and geographical diversity of the ArcelorMittal company, to rival any academic review. Given the diverse locations of ArcelorMittal’s operations, to paraphrase the report, it concludes that ‘*all options are on the table*’. A breakdown of the current research projects and technology focus for individual steel companies is provided in table 2-2.

Table 2-2: A breakdown of Steel Company Low-carbon research projects and technology focus

| Steel Company | Region | Low-carbon research focus (project names) |
|----------------------|---------------|--|
| Tata Steel | UK | Hisarna, CCU(S), DRI + EAF |
| Tata Steel | Netherlands | Hisarna, CCU(S), DRI + EAF (Everest, Athos) |
| ThyssenKrupp | Germany | CCU, (Carbon2Chem) |
| SSAB | Sweden | Hydrogen, DRI, (HYBRIT) |
| ArcelorMittal | Belgium | CCU, (Carbalys) |
| ArcelorMittal | Germany | Hydrogen, DRI, (H2BI) |
| ArcelorMittal | France | CCS, (3D, IGAR) |
| Salzgitter | Germany | Hydrogen, DRI, (SALCOS) |
| Voestalpine | Austria | Hydrogen, DRI, (H2Future, SuSteel) |

The focus of research is highly regionally specific. Reviewing the access to CCS stores, surplus renewable power, or political appetite for the technologies, this determines the type of technology focus for the individual companies. The choice of research direction for the steel companies is therefore highly influenced by geographical location, available resources (such as low-carbon energy), proximity to geological CO₂ sequestration sites and Government intervention, especially in their (the Governments') appetite for a hydrogen-based steel making process, as this is likely the most challenging and expensive route. This makes generic reviews of technologies, such as those described above, difficult to relate to real-world scenarios, as regional opportunities and politics play a much greater role in technology choice and economic viability.

At the start of this research there was little investment in CCU projects, with a handful of individuals promoting the concept on the global arena, primarily with a few algae, carbonisation and fermentation research projects (The Institute of Materials, Minerals and Mining (IOM3), 2014). The benefit of algae, carbonisation and fermentation was that expensive carbon dioxide capture and concentration systems were not required. Since then, the potential value has been recognised and this has become a highly competitive research area. In terms of advancement of knowledge and science, this thesis is unlikely to compete with such multi-million € projects, but using analysis of the available literature, we are able to identify some key opportunities to move developments in this field forward. The major research programmes within this CCU are Carbon2Chem (ThyssenKrupp), the renamed project Carbalyst (ArcelorMittal) and Everest (Tata Steel / ArcelorMittal).

The global research for steel decarbonisation can be split into two common themes: hydrogen-based iron production, or carbon capture (utilisation) and storage. Biomass, for the purpose of

this assessment, has been associated with CCS rather than as an independent technology. Including biomass with CCS can reduce emissions further (potentially net negative), which is discussed later. Given the need to meet the maximum 2°C scenario, all available biomass needs to be used in the most carbon negative way possible, i.e. Bio-energy with Carbon Capture and Storage (BECCS). It is worth recapping that carbon utilisation can be viewed as a method to incorporate more renewable electricity into the processes and further reduce fossil carbon extraction that would have been needed as the input carbon source to either reduce the impact from the steel industry, or that of another fossil-based industry (such as chemicals, plastics and fuels). To assess the viability of these processes, it's essential that a full, standardised Life Cycle Assessment (LCA) study is carried out (Garcia-Garcia, et al., 2020).

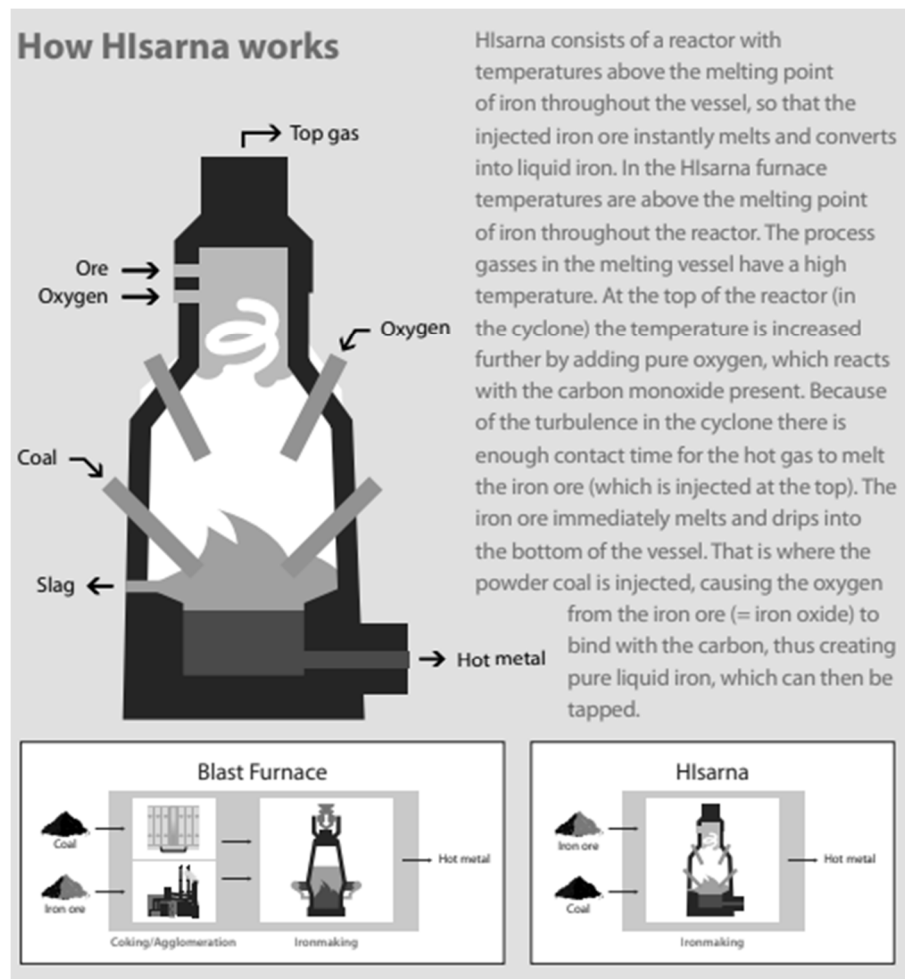
2.3.1 Breakthrough steelmaking technologies

From the ULCOS programme emerged two potential low-carbon production methods. HIsarna and the Top Gas Recycling Blast Furnace (TGRBF) (Hirsch, et al., 2013). HIsarna is the preferred option for Tata Steel, who now own the IP outright for this process, figure 2.5. The HIsarna method has numerous benefits, but essentially removes the need for coke and sinter production and uses a new furnace design. Through oxygen injection into the furnace, a purer CO₂ off-gas is produced, allowing easy CO₂ capture. This makes the process ideal for CCS. Without CCS the quoted CO₂ savings are 20%, but this will increase to 80% with the use of CCS.

The HIsarna technology is currently at technology readiness level (TRL) 6-7, with the demonstration now in its 5th campaign, which aims for continuous operation of the process. This unit is capable of 60,000 tonnes per annum. The next phase will look to scale up the technology to full production capacity of 1mt/annum per HIsarna unit. The IJmuiden site can produce 7mt of steel per annum from 2 BF. 1-1.5mt/annum is expected to be the limit for the HIsarna technology. Therefore, multiple units will be needed to reach a 7mt/annum (Tata Steel Europe, 2019).

To operate the furnace and ensure a high concentration of CO₂ ready for carbon capture, large volumes of oxygen injection are needed. This would be achieved using air separation units (ASU), which consume large volumes of electrical energy. This energy import needs to be considered when evaluating the overall impact of the technology. If co-located with hydrogen electrolyzers, the oxygen by-product could be used within the steel making processes. The value of oxygen from electrolyzers is often overlooked when evaluating the price of hydrogen, as industrial sectors such as steel and wastewater treatment require large amounts of oxygen, which is currently produced from air separation units.

Figure 2.5: An introduction to State-of-the-art steelmaking technology from Tata Steel, Hisarna



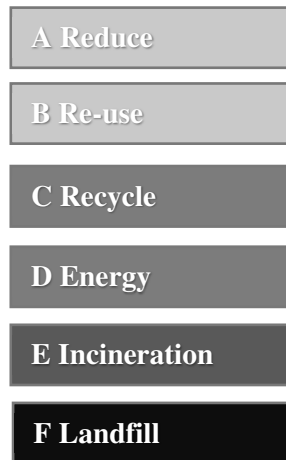
Source: Tata Steel Europe factsheet

The TGRBF method utilises a BF retrofit with carbon capture technology. (Hirsch, et al., 2013). This allows a potentially simpler transition to a new technology by utilisation of existing assets and may decrease overall capital expenditure (CAPEX). The CO₂ is separated from the off-gases using conventional carbon capture methods, likely pressure swing absorption, with cryogenics. The CO₂ could be sent to storage, and the remaining CO and H₂ is reinjected back into the furnace. These capture reagents are recycled once again into the furnace reducing the carbon input from fossil coke/coal. It was estimated that this process could lead to expected carbon savings between 21-25% depending on configurations and coal injections rates per ton of hot metal (thm) of 170 kg/thm – 150 kg/thm respectively. Reinjecting the gases without first removing CO₂ was found to have minimal impact on coal consumption (internal Tata reference). With both TGRBF and Hisarna, the energy balance for the site is disrupted and the power (steam and electricity) that would have been generated via the BF off-gases needs to be replaced. Ideally with low carbon grid electricity to yield the greatest carbon savings. As the power generated from a typical onsite steel power plant is no greater than around 30% efficient (due to the low calorific value gases),

negative technologies (BECCS or air capture with CCS) that will be needed to achieve a maximum of 1.5°C of global warming or ‘net-zero’ (Committee on Climate Change, 2019b)

If high concentration carbon dioxide is available in bulk quantities, separated from industrial gases, there could be a market to use this carbon dioxide directly or as a carbon substitute for other industries (Styring & Jansen, 2011). (Aresta , et al., 2013). Conversely, at present there is often a shortage of CO₂ on the market in the UK (Hotten, 2018). Whilst CO₂ is available in abundance in its atmospheric, low concentration form (0.04% atmospheric concentration), to provide CO₂ in high concentrations and purities (of critical concern for food grade CO₂), commercial CO₂ separation methods are required, which are energy intensive and costly. On the 21st November 2012, I presented the concept of applying the waste hierarchy, also known as Lansink’s Ladder (figure 2.7) at an industrial meeting of the UK CO₂Chem Network. If applied to CO₂, we should seek methods to reuse or recycle unavoidable carbon, before it is disposed of. Many industries, such as the chemical sector, are reliant upon carbon as an essential building block in much in the same way as the steel sector, to produce products. Some companies have committed to achieving non-fossil based carbon for their future products, such as Akzo Nobel. Obtaining this carbon from a recycled source, rather than fossil fuel extracted from the earth, should in principle prevent further emissions to atmosphere. This has created much debate over the potential impact and now LCA has become an essential tool in analysing the positive impact, if any, from recycling captured carbon (Garcia-Garcia, et al., 2020). Assessment of these various opinions and analysis, is that it depends on the scenario. What is being replaced, is there a better alternative, and what is the overall impact? Conducting a comprehensive LCA for each scenario is quite difficult and requires access to quality data sets. One of the challenges of reusing carbon dioxide is that carbon dioxide is very stable, and separating the carbon atoms can be energy intensive. This energy must come from a clean, carbon emissions-free source, or possibly waste heat, if we are to achieve a positive CO₂ reduction. The arguments for and against carbon dioxide recycling are an area of intense debate, therefore we must look at the pros and cons to ensure we are not creating a future problem. A comprehensive review was conducted by Armstrong and Styring (2015), with an estimated rise in CO₂ for carbon utilisation from 122 Mt (2015) up to 39 Gt/year in 2050 (Armstrong & Styring, 2015). To counteract the negative implication of a CCU industry, the technologies must demonstrate that they meet the energy trilemma; environmental impact, energy security and cost (World Energy Council, 2013). Indeed, all new technologies should align to these principles. Whilst current utilisation rates are low, a rise of this amount would see a significant contribution in the future as deep decarbonisation becomes more challenging.

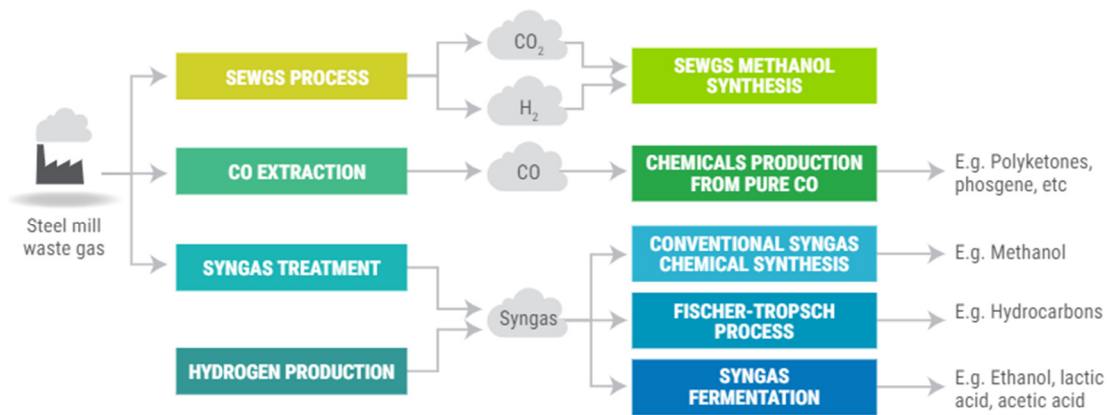
Figure 2.7: Hierarchy of waste reduction strategies



With regard to CCU in a steel plant context, due to the gas compositions available within a conventional integrated steel mill, there have emerged some leading opportunities for CCU.

The diagram in figure 2.8 from the CORSYM project, is a very good summary of potential process routes for alternative uses of steel mill derived gases (METABOLIC, 2017). Of all the industrial sectors, steel plants provide a potentially viable route to CCU commercialisation, due to the gas compositions. As previously mentioned, the works arising gases are most often used onsite to generate heat, steam and power, in a relatively inefficient power plant. The BFG is of low calorific value. ($CV = 3-4 \text{ MJ/Nm}^3$) following its high CO_2 and N_2 concentrations. The combustion of these gases results in the generation of large volumes of CO_2 , per MWh, these being much greater than those of a coal fired power station. Generating power from a cleaner source and then recycling this carbon could lead to a much lower emission to atmosphere. However, the reason steel mill gases have potential is the CO concentration, and these approaches maybe viewed as fossil carbon avoidance rather than conventional CO_2 based CCU. The CO is a more useful building block for carbon-based products than its more stable CO_2 counterpart and avoiding combustion of CO to CO_2 leads to possible emissions reduction. The CO is recycled rather than incinerated, which, as shown in the waste hierarchy, is more attractive. Increasing the value of this CO by conversion to a product and/or extracting more useful energy, typically by raising its calorific value, is the goal of these CCU projects. Additionally, if CCS is to be implemented, then this is a good opportunity to optimise the process, with a new configuration making best use of the available gases. This has generated a complicated scenario with many potential pathways and approaches.

Figure 2.8: Potential pathways for valorisation of steel plant gases, CORSYM project



Source: (Metabolic, 2017)

Worthy of note are the major CCU projects by European Steel makers. The first is the Carbon2Chem programme of ThyssenKrupp (ThyssenKrupp Steel, n.d.). Details are scarce, due to the commercially sensitive nature of the project, but it most certainly contains some form of syngas route to chemicals, exploiting the high CO content of the steel plant gases. Tata Steel also has a similar project, entitled project Everest, which again looks to exploit the value of CO and avoid generating further CO₂ emissions. Project partners involved in the pilot plant development are: DOW, Arcelor Mittal, ISPT, University of Gent, ECN and Tata Steel (Zutphen, 2018).

The Steelanol project is an initiative led by major steel producers ArcelorMittal and partly funded by the European Commission's H2020. It takes a different approach, utilising the syngas fermentation technology pioneered by the development company, LanzaTech (Steelanol Project,, n.d.). This is a successful near commercial method to produce fuels. Of particular interest is aviation fuel, as aviation is recognised as a hard to decarbonise sector, needing dense energy fuels. If the power that was otherwise generated by the steel plant in a low efficiency, high carbon emitting plant, is replaced by renewable power, the emissions occur at the aircraft as a new point source. No additional fossil fuel was extracted and added to the carbon cycle to power the aircraft. This results in a lower carbon emission overall, as more energy is extracted from the original coal input and the shortfall in demand is met by clean energy. The uptake of this technology is limited by the current steel sites' powerplant configurations (imported power will be needed to meet the new shortfall in onsite generation) combined with relatively low fossil fuel prices.

Assessing all forms of possible steel plant CCU and opportunities, it is clear that one major hurdle exists: the viability and availability of bulk volume, low-carbon hydrogen. Whilst some processes do not need hydrogen, their potential for significant decarbonisation is severely limited. These processes untimely need access to hydrogen to carry out stages of the conversion. Whilst

hydrogen is available within steel plant gases, it is in limited supply to convert all the carbon. About ~15% conversion of available CO₂ may be possible using existing available hydrogen. This is highly dependent upon coke production volume and the H₂ to CO₂ ratio of the chosen product. This hydrogen is almost always used as a valuable low carbon fuel gas on an integrated site, if the coke ovens are adjoined. Therefore, this hydrogen will have to be replaced with a suitable low emission source, if emissions are not to increase. The source of this hydrogen will determine the carbon reduction potential, and importantly the commercial viability. We will now investigate the implication of hydrogen in the steel sector.

2.3.3 Hydrogen for steel production

The use of hydrogen forms one of the two major research efforts for European steel makers (CCS / CCU being the second). Notably affluent research projects in this area are SALCOS (Salzgitter), H2FUTURE (Voestalpine), and HYBRIT (SSAB, LKAB and Vattenfall). Seemingly an elegant and clean solution, it is not without its challenges, which is reflected in the cost of the research programmes. First and foremost is the cost needed to develop and scale-up the concept, with major financial risks if it does not work. For this reason, the current research programmes are backed by National Governments to absorb this risk to industry. In principle, hydrogen can be used as a direct replacement for carbon as a reductant of iron ore within a DRI facility, but hydrogen will also be needed within the CCU concept to convert CO₂ to products. Therefore, both decarbonisation routes will require clean forms of hydrogen. Hydrogen may also be injected into a BF, but within limits to avoid instability of the furnace, therefore it can only replace a small part of the fuel input. The reactions describing the reduction of iron ore with hydrogen are shown in equations 2.2, 2.3 and 2.4.



Approximately 70-80kg of hydrogen is needed to produce 1 ton of steel, equivalent of ~10 GJ per tonne of steel, which means enormous quantities of hydrogen are required. Exact quantities of hydrogen needed vary depending on source, as no-one has adopted this technology at scale, following the hydrogen availability. Critical changes in steel production methods are also needed. Most integrated steel plants around the world use a blast furnace. The switch to a gas-based reductant, rather than a solid coke-based solution, would need a new type of furnace. These are affectively known as DRI units, which are currently operated using natural gas (gasification of coal can also be used). In addition to a DRI unit, an EAF is also needed. At present only 1 % of iron is made via the DRI route, in locations with access to abundant and cheap natural gas. Vogl et al., provide a recent assessment of hydrogen reduction and economics (Vogl, et al., 2018). Yet

their assessment only suggests 51kg of hydrogen is needed per ton of steel, which is much lower than the 10 GJ needed for a DRI furnace and considering the hydrogen reaction is endothermic, more energy will be needed to generate heat to keep the iron molten. The review highlights that there is little information available regarding the use of hydrogen DRI and, as already identified, most of the information is confidential.

A switch to new iron making technology is very expensive, needing 1 – 2 £billion to transition a steel plant, depending upon location and re-use of existing infrastructure. Cost per ton of steel capacity is approximately 30% higher than a greenfield BF-BOF and range from €574 per tonne capacity, (Mergel, et al., 2013) & (Wortler, et al., 2013), to €874 per tonne capacity (Fischedick, et al., 2014).

In the early stages, it would be possible and probably necessary, given the availability of low-carbon hydrogen, to operate the DRI unit on natural gas, with a gradual switch to hydrogen as more capacity comes online. This is not addressed by the literature. Whilst this reduces the transitional risk, it assumes that there is also sufficient gas distribution infrastructure nearby to supply the furnace, which is unlikely given the volume of gas needed and hence more gas capacity will need to be added, increasing the cost. In the case of the UK, this is would involve increased production within the North Sea, and likely imported from elsewhere.

The traditional method to produce bulk hydrogen is via the water gas shift reaction, using natural gas. In order to decarbonise this process, CCS would be needed. This raises the obvious question, why not apply CCS directly to a conventional blast furnace? The coveted solution is to produce hydrogen from renewable energy sources.

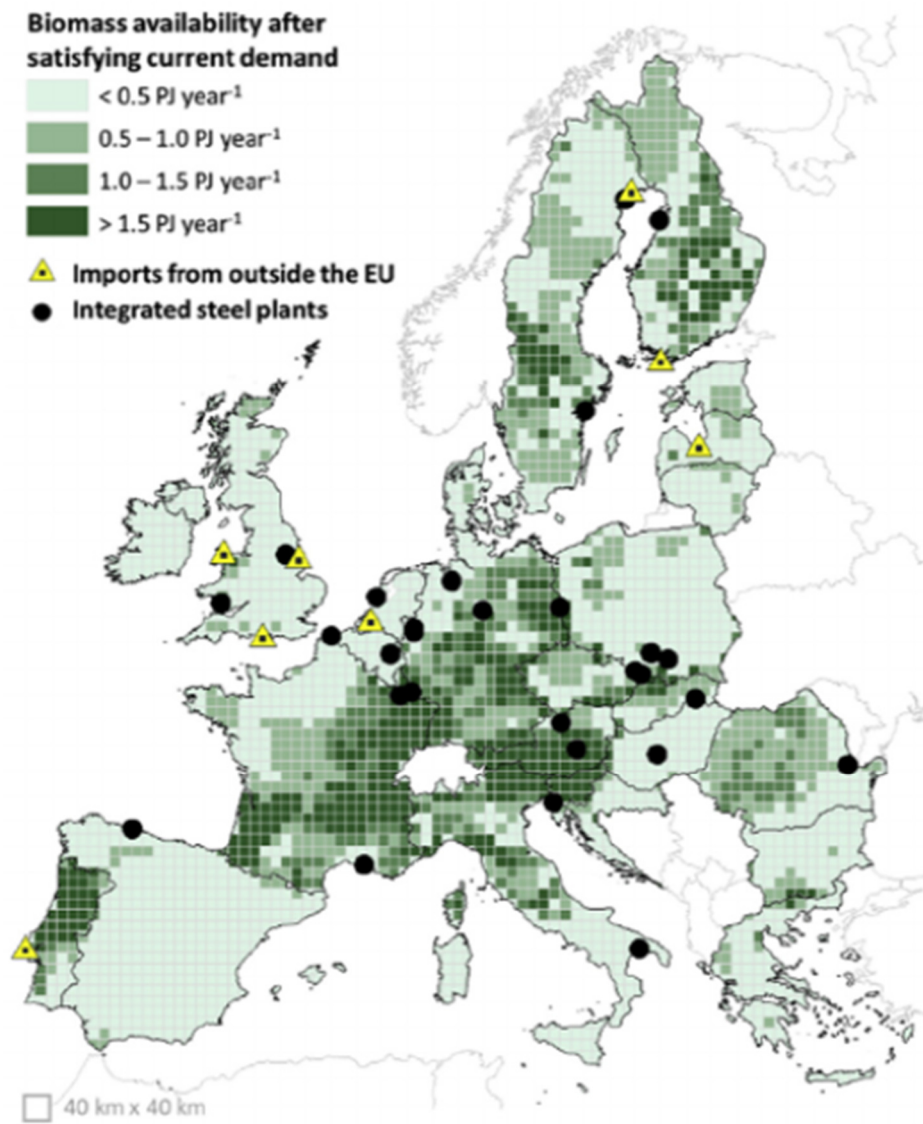
Ammonia is also proposed as an alternative energy storage vector for hydrogen. Whilst it is corrosive and potentially toxic, it is easier than hydrogen to store and transport and the energy density is also high, at around 3kWh/l. This may not be as high as fossil-based fuels, yet it is the highest energy density of the current possible low-carbon alternatives. The vaporisation temperature of ammonia is -33°C and it must be chilled or compressed for storage. Hydrogen must be cryogenically cooled to -253°C , making hydrogen much more difficult to store or transport. Using ammonia is a popular concept with Japan, who have teamed up with Australia, who are rapidly developing CCS facilities, where fossil carbon can be turned into ammonia and shipped to Japan as an energy source. The Royal Society provide an excellent overview of ammonia and its use as a potential energy vector in their Green Ammonia Policy Briefing (The Royal Society, 2020).

2.3.4 Biomass as a coke/coal substitute

Biomass could be used within steelmaking in vast quantities. According to Mandová, et al., biomass can result in up to a 40% reduction in onsite emissions. This figure is limited by process limitations associated with the conventional BF-BOF route (Mandová, et al., 2019). The HIsarna experimental blast furnace could be particularly well suited to the use of large volumes of biomass as it does not require a structural burden (that a BF does) and can manage the volatiles within the process off-gases and gas cleaning. This author will go on to participate in one of the most comprehensive examinations of global steel decarbonisation assessments, as an employee of the International Energy Agency (IEA). Within the HIsarna process an estimated 50% substitution of coal with biomass should be easily achievable.

Some issues arise over quality and consistency of the biomass product that will be used in the furnace, but for the UK, the most significant challenge is access to suitable quantities of biomass material, without the obvious implication on land use, competing food production and, ironically, solar farms. Figure 2.9 below demonstrates that the UK does not have the potential abundance of bioenergy crops available. If a steel plant were to be fitted with CCS, the availability of surplus biomass, especially if these are wastes, could lead to a negative emission technology (Mandova, H, 2019), (MacDowell & Fajardyab, 2017). Negative emissions technologies are essential to reach net-zero targets and the maximum 1.5°C target, certainly beyond 2050 (Committee on Climate Change, 2019a). Hence, the use of biomass should not be ruled out. Given the progressive closure of coal fired power stations, there may be few options remaining to combine large volumes of existing coal users with BECCS to achieve these negative emissions targets.

Figure 2.9: Locations of locally sourced biomass availability, beyond existing market demand



Source: (Mandová, et al., 2019)

2.4 CO₂ capture within aqueous ammonia solutions

Following the future low-carbon technology trends and limitation within the steel sector, gaps begin to emerge along with possible new opportunities. Many of the large, infrastructural changes must be addressed by multi-organisational partnerships, along with Government support. There are indeed some opportunities that these projects and partnerships have not addressed, and we seek to expand the knowledge in these areas.

Reviewing the available literature and with the knowledge acquired of the possible pathways to decarbonisation of the sector, it is apparent that one technology in particular is key to unlocking some of these potential pathways. To achieve deep decarbonisation (80%), the ability to separate CO₂ from the process gases in an efficient and cost-effective way is critical for the following technologies: BF-BOF, Hisarna, BECCS, carbon dioxide utilisation (CDU) and H₂-DRI, with hydrogen supplied via SMR or autothermal reformation (ATR). The only process pathways that do not require a form of carbon capture are conversion to full EAF or the use of H₂-DRI with hydrogen sourced from electrolyzers using renewable energy.

For this reason, carbon capture technologies are critical to the future low-carbon options for steel making processes. There is a complex array of possible configurations and capture technologies, but we will explore one highly promising capture technology in particular. That is the capture of CO₂ within ammonia.

The following review will assess:

- a) Current production and uses of ammonia
- b) Reaction pathways involving CO₂, NH₃ and H₂O
- c) The use of ammonia within a carbon capture system
- d) An introduction to microbubbles, their formation, benefits, properties and their potential application

2.4.1 Ammonia – manufacture and uses

Since the commercialisation of the Haber Bosch processes for the mass synthesis of ammonia, it has played an ever-increasing role as the feedstock to inorganic nitrogen fertilisers. The total global production of ammonia has reached 176 million tonnes per year and this process now supports food production for half the world's population (Smil, 2000). The synthesis of ammonia via the Haber-Bosch process requires the reaction of nitrogen and hydrogen over a catalyst. To generate the feedstocks for this reaction, nitrogen is supplied from air compression or air separation. Creating the necessary hydrogen represents 80% of the energy used and it is generated almost exclusively from SMR. The use of SMR results in the generation of hydrogen, but also large quantities of carbon dioxide. Whilst coal can be used instead of methane, this results in greater emissions as the hydrogen content of methane is much greater than coal. The production

of ammonia is therefore fossil fuel intensive and accounts 1.8% of total global carbon emissions (IEA (International Energy Agency), 2013). Following the synthesis process and its high production volume, ammonia production has the greatest emission within the chemical industrial sector. (McKinsey & Company, 2018).

80% of the ammonia produced is used as nitrogen release fertilisers. It is also used within resins and adhesives, pharmaceuticals, large scale refrigeration and cleaning. Many will also associate its use within modern diesel pollution abatement systems, such as BlueTec, and known as Adblue in the form of urea. (Yara, 2013) As a fertiliser the method of application varies between regions. Ammonia can be used on the soils directly, which is commonplace in America and resulted in a vast ammonia storage and disturbing system (The Royal Society, 2020). In the UK, ammonia is converted to nitrate fertilisers, such as Urea. Urea has a significant nitrogen content (~46.3 %wt), it is stable, has less of the toxic and corrosive issues that are associated with ammonia and is therefore better for storage and transport. Urea is synthesized using a two-step reaction of ammonia and carbon dioxide. Achieving a commercially viable route to CCU has proven challenging. While some niche applications show promise in utilising smaller volumes of CO₂, urea production accounts for the largest single use of CO₂ in organic chemical synthesis (Xiang, et al., 2012). The market for urea is currently saturated, but the demand for the product is growing slowly and expected to continue as populations and need for greater food yields increase (Meeseen, 2012). Whilst the process of urea synthesis utilises significant quantities of CO₂, it still accounts for a significant release of CO₂ emissions to atmosphere. (Styring & Jansen, 2011). Estimated to now be in the region of >130mt per annum (Hunt, et al., 2010), following associated CO₂ generated with the Haber-Bosch process. Whilst there is often integration of the CO₂ from the ammonia production into the urea formation, this is not always the case.

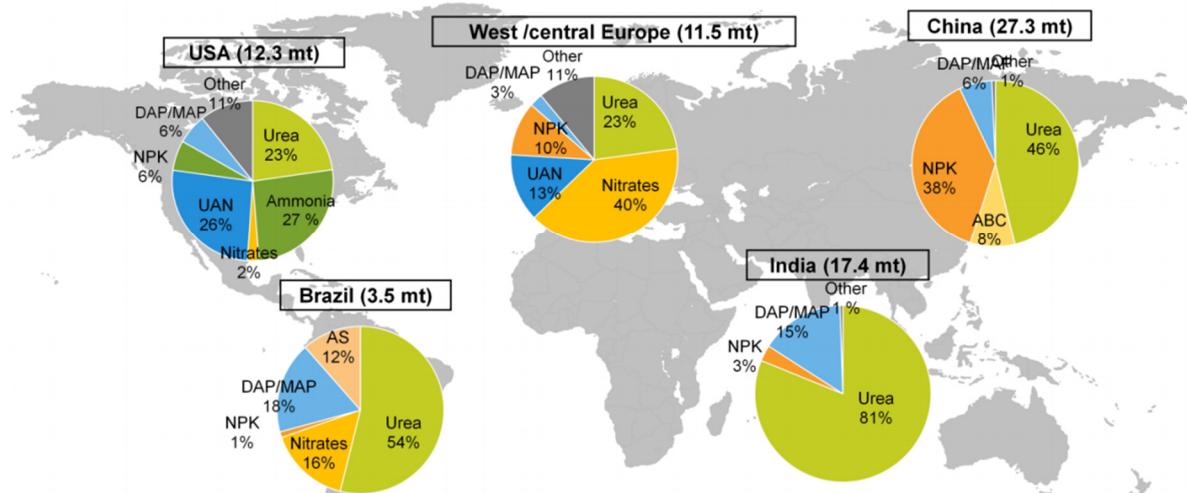
Whilst 80% of the ammonia is used for agriculture, only 17% of this nitrogen ends up in the food chain (Leach, et al., 2012). The remainder of this ammonia is lost to the ecosystem, causing biodiversity loss. It can also transform into nitrous oxide, a problematic greenhouse gas (Erisman, et al., 2013).

Global ammonia production is currently dominated by the Haber-Bosch process (Brown ammonia). However, it could be generated in a cleaner form (Green ammonia), using renewable energy and electrolyzers to generate the ammonia, and/or recovery from waste waters (Desai, et al., 2020). As previously mentioned, green ammonia could provide an attractive hydrogen energy vector, following its higher energy density and enhanced storage characteristics, significantly reducing transport costs (The Royal Society, 2020).

Urea is favoured as a fertiliser due to its greater stability, reducing degradation within storage and the low cost to transport (high nitrogen content), but it not the ideal form of fertiliser. Hence

nitrates dominate in Europe, as urea must first be converted to ammonium and then nitrate before it can be available to the plant. This process is highly dependent upon pH and temperature. Nitrates are directly absorbed by the plants, the release is easier to predict and results in much greater ammonia losses. Ammonium nitrate (AN), calcium ammonium nitrate (CAN) or ammonium bicarbonate (ABC) can also be used as nitrate release alternatives. Nitrate fertilisers have the advantage that the valorisation of ammonia is much less than urea, creating significantly less ammonia loss to atmosphere, however, ammonium nitrate is explosive. Much less AN need be used for the equivalent crop yields as liquid urea ammonia nitrate (UAN) or urea, again limiting the losses into the environment. ABC is still commonly used in China (8%), although it is now being replaced by urea (46%) (Yara, 2013). The distribution of nitrogen fertiliser application is shown in figure 2.10.

Figure 2.10: Nitrogen fertiliser application by region and product

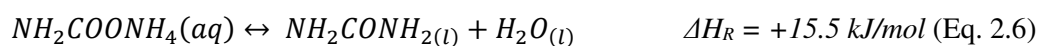
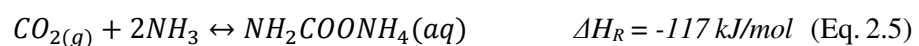


Source: (Yara, 2013)

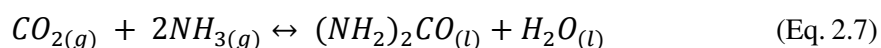
2.4.2 Conventional Urea production

The precursor to urea is the reaction of CO₂ and ammonia to produce ammonium carbamate (Bosch & Meiser, 1922).

Urea is commercially produced using the two-stage chemical reaction equation 2.5 and 2.6 (Zolotajkin, et al., 1984):



This, two stage reaction can be summarised as shown in equation 2.7.



An undesirable side reaction is the formation of biuret (Eq. 2.8). Biuret has a negative effect on crop growth, therefore its concentration must be kept to a minimum.



The concept underpinning the modern urea production process was originally developed by Bassarov in 1870 (Bassarov, 1870). His method synthesised urea from ammonia carbamate in a glass vessel, held at constant pressure and heated to 140°C. Today's industrial production method carries out the two-stage process in a single vessel using ammonia and CO₂ at elevated temperature and pressure. With only a 40-60% conversion on the first pass, subsequent recycling and purification steps are needed to reach a 99% purity. The off-gases cannot be recompressed, owing to the presence of carbamate solids and the risk of severe corrosion (Bosch & Meiser, 1922), (Agarwal, et al., 2007), (Meesen, 2012).

The current commercial process for producing urea is a compromise, however, this is clearly an acceptable compromise, following the global demand for the product and sustainable prices. Corrosion is the primary reason that the NH₃ and CO₂ reaction took a long time to reach full commercialisation, needing suitable corrosion resistant materials. Excess NH₃ is used, with minimum temperature and pressure conditions, so that stainless steel may be used, and corrosion is kept to an acceptable level.

The first stage of the reaction, to produce carbamate (Eq. 2.5) is a highly exothermic gaseous phase reaction. The process is operated at pressure (150atm) and at 180°. At these conditions the process is almost instantaneous. Below 155°C solids are formed that inhibit the flow within the reactors and at about 200°C corrosion becomes very aggressive. The second reaction (Eq. 2.6), is the dehydration of carbamate to urea. It is much slower than the carbamate formation, but thankfully favours higher temperatures in the range of 180 – 210°C. The heat generated from the former reaction is available to drive the second reaction and accordingly the reaction for the commercial process takes place in a single vessel (with subsequent recycling or refining stages).

An excess of ammonia is used to drive the reactions forwards as the reactions are reversible. Continuous removal of urea from the process ensures that carbamate to urea is also favoured and the process does not become saturated.

The need to carry out the two reactions in a single vessel leads to quite low generation of urea on a single pass at ~ 60%. This requires subsequent recycling of the ammonia, CO₂ and carbamate, whilst avoiding biuret formation and reverse reactions. The success of the process is determined by how effectively the carbamate may be recycled back to the reactor and the evolution of the

process and patents reflect different approaches to recycle the products back to the reaction vessel.

Whilst the energy efficiency of the ammonia process and urea & fertiliser production has improved over the century, it is clear that the environmental impact is still quite high, energy consumption is above the theoretical minimum and CO₂ emissions are considerable. According to the Yara Fertiliser Industry Handbook, 42GJ is required per ton of nitrogen for the ammonia production process, and a total 51GJ per ton of nitrogen is required in the production of urea (Yara, 2013). To provide perspective, around 20GJ is used on average per ton of steel produced (World Steel Association, 2019).

2.4.3 Reaction pathways involving CO₂, NH₃ and H₂O

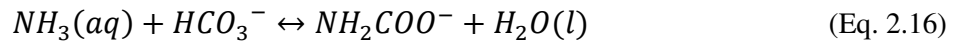
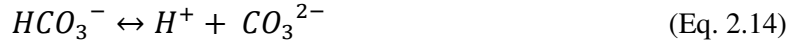
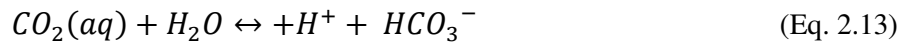
Whilst the urea production reactions are optimised for high temperature and pressure, the CO₂-NH₃-H₂O system at mild conditions can be used as an effective form of CO₂ capture. The application of aqueous ammonia in a more conventional chemical absorption carbon dioxide capture system has been recognised as highly applicable to the steel sector, producing a potential overlap of the two industrial sectors (Han, et al., 2014). If Green hydrogen is produced, the hydrogen for ammonia production is not generated from fossil fuels (such as SMR) and CO₂ is not produced. This CO₂ cannot be integrated into the fertiliser production and an alternative source of CO₂ is required for the conversion of ammonia to nitrogen release fertilisers. The source of CO₂ could be supplied by the foundation industries, such as steel and cement.

The CO₂-NH₃-H₂O reaction, even at mild conditions may be considered a volatile and complex electrolyte system, comprising of some rapid, yet also some slow and limiting reactions. The vapour, liquid and solid phase reactions have been studied extensively over the past ~100 years (Thomsen & Rasmussen, 1999). Interest in this system has once again increased, following the search for more sustainable fertiliser routes and carbon capture systems. The reactions pathways involving CO₂ and aqueous ammonia that are most dominant are still debated, as the equilibria are dependent upon the system conditions (concentrations, pH, pressure, temperature) and the species are difficult to detect using current methods within the changing system (Qin, et al., 2011). We find that the most likely pathways comprise of the following reactions of vapour-liquid-solid equilibrium, as presented in the UNIQUAC model (Thomsen & Rasmussen, 1999):

Vapor–liquid equilibria:



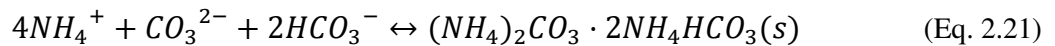
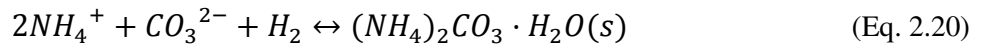
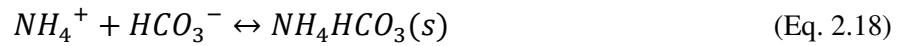
Liquid speciation:



Not included in Thomsen & Rasmussen (1999), but considered important by Valenti & Bonalumi, (Valenti & Bonalumi, 2018):



Liquid-solid equilibria:

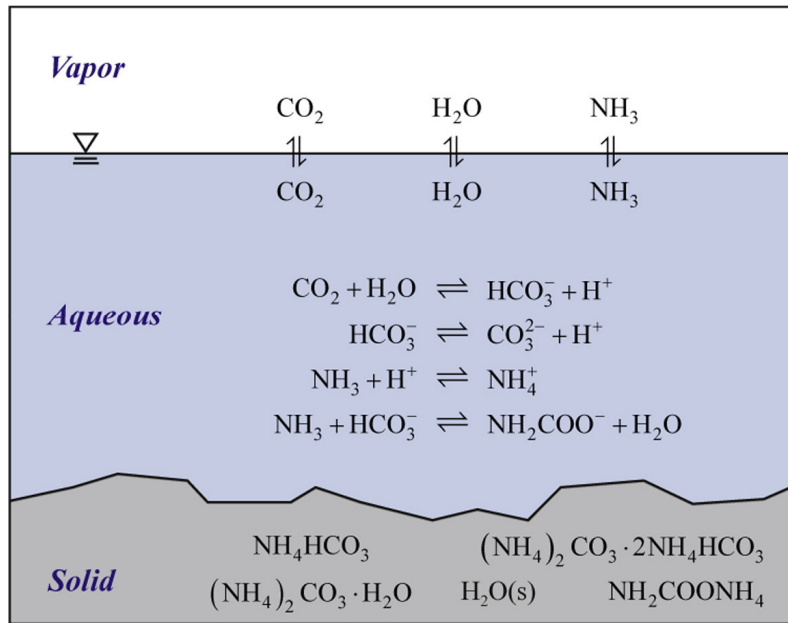


Within the system, the following solids are expected to form:

- | | |
|--|---------------------------------|
| 1. Ammonium bicarbonate (BC) | NH_4HCO_3 |
| 2. Ammonium carbamate (CM) | NH_2COONH_4 |
| 3. Ammonium carbonate monohydrate (CB) | $(NH_4)_2CO_3 \cdot H_2O$ |
| 4. Ammonium sesqui-carbonate (SC) | $(NH_4)_2CO_3 \cdot 2NH_4HCO_3$ |

The ammonium salts are expected to have a very high solubility of in water: 320 g/l Carbonate, 790 g/l carbamate and 220 g/l for bicarbonate (Mani, et al., 2006). Solids formation is expected, at lower temperatures, once concentrations of salts exceed a threshold within the aqueous phase. Below, figure 2.11, shows the various phases within the UNIQUAC Equation of State (EOS) model (Sutter, et al., 2015).

Figure 2.11: Depiction of the CO₂-NH₃-H₂O system, as described within the UNIQUAC Equation of State (EOS)



Source: (Sutter, et al., 2015)

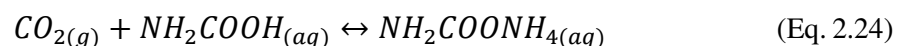
Some of the reaction pathways can be considered negligible following their small equilibrium constants (Mani, et al., 2006), which is supported by more recent assessments (Valenti & Bonalumi, 2018).

The recent expansion upon the UNIQUAC EOS model provides greater clarity on the possible pathways of the quite complex system, but there is still some uncertainty over which mechanisms dominate at the various concentrations, pH, pressures and temperatures (Lillia, et al., 2016), (Valenti & Bonalumi, 2018). It would seem that at the different system conditions (which can change over the course of the reaction experiments) different reaction mechanisms dominate and they are likely to follow a non-linear relationship. It has, so far, been difficult to accurately measure these mechanisms.

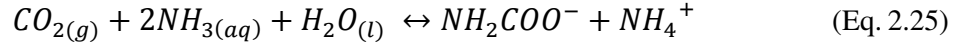
According to Liu et al. and also Shuangchen et al. the pathway is likely to follow the subsequent absorption steps (Liu, et al., 2011) (Shuangchen, et al., 2015). The total absorption reaction can be summarised by equation 2.22.



First, CO₂ and NH₃ react to form NH₂COONH₄, potentially in two stages, according Shuangchen et al. (2015), as described in equations 2.23 and 2.24.



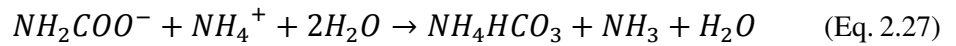
NH_2COONH_4 then hydrolyses (instantaneously in the opinions of Liu et al.,) defined in equation 2.25.



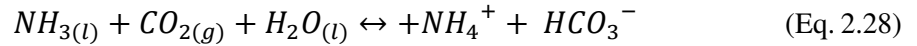
Or, according to Valenti & Donalumi (2018), the following reaction occurs to generate NH_2COO^- and H^+ :



Following the fast hydrolysis described by equation 2.25, the NH_4^+ and NH_2COO^- undergo a reaction (irreversible as stated by Liu et al.,) to form NH_4HCO_3 according to equation 2.27.

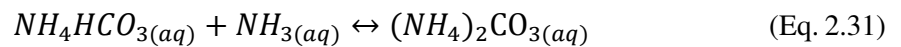


Previous authors show pathways involving the bicarbonate ion, carbonic acid (HCO_3^-), within the electrolyte system. This suggest a suitable, fast pathway to generate sufficient HCO_3^- within the same order of magnitude as the reactions described above, if it is to be of concern. Here, $CO_{2(aq)}$ is first reacted with H_2O , which is known to be quite slow and limiting. This could be described as in equations 2.28 (Mani, et al., 2006), 2.29 and 2.30 (Valenti & Bonalumi, 2018).

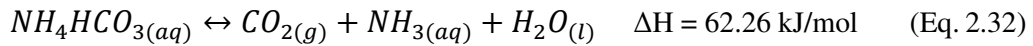


Whilst equation 2.30 presumes a prior formation of OH^- , this will be present within the electrolyte solution following the reaction of NH_3 and H_2O (the liquid speciation reaction 2.12 above), so this pathway is highly probable. Valenti & Donalumi, (2018) believe that the most important reaction limiting kinetics are those of equations 2.26 and 2.30, and they are anticipated to significantly influence the kinetics of the overall process as they are expected to be rather slow. (highlighted above in blue).

Whilst bicarbonate is anticipated to be the main product within the described pathway, ammonium carbonate can be formed following the further reaction of ammonium bicarbonate with available NH_3 , as shown in equation 2.31. This pathway maybe prevalent within systems of high NH_3 excess. The UNIQUAC EOS model above shows alternative pathways to carbonate formation, equations 2.31.



The desorption process (equation 2.32), relevant to the carbon capture process, sees the release of CO_2 gas when the CO_2 rich solution is heated.



2.4.4 CO₂ capture methods in ammonia solutions

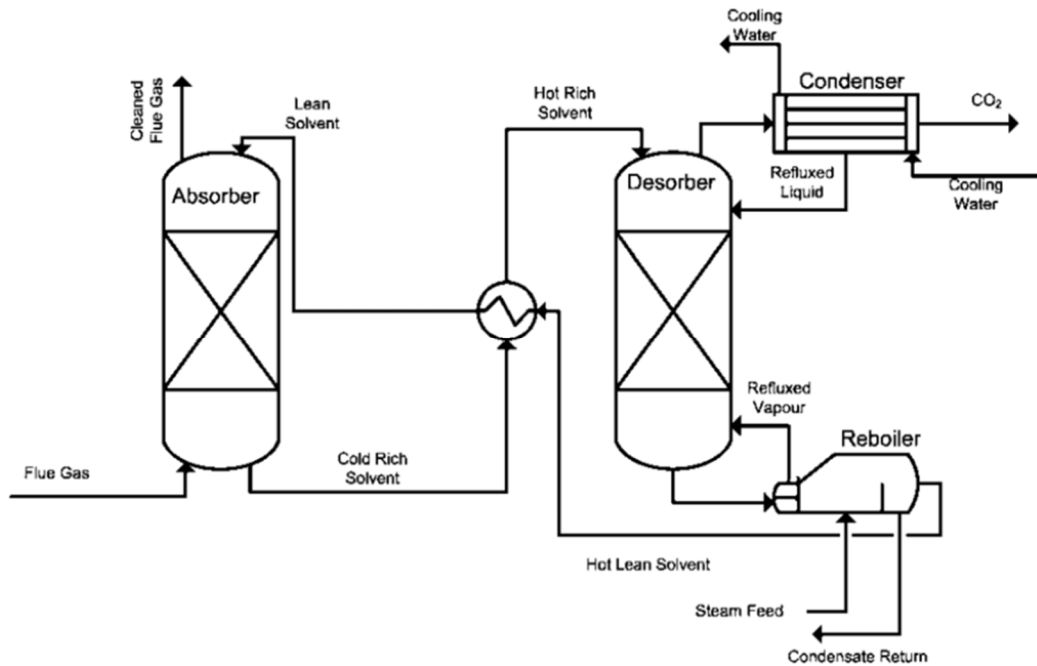
In most cases, to successfully deploy either CCU or CCS, CO₂ must be first separated from industrial waste process gases. There are some exceptions to this, whereby CO₂ is already produced in high concentrations (ammonia production) or the process does not require high concentrations of CO₂ (carbonation or biological transformations). Capture and concentration of CO₂ is achieved using carbon (CO₂) capture systems, which are well established technologies in the petrochemical and oil and gas sectors, to remove the undesirable CO₂. Previously the technology was known as sour gas sweetening, but recently, more often in the case for CO₂ removal, termed carbon capture.

The type of capture system varies depending upon each application, but all require significant energy input (typically for the regeneration of the solvent, or efforts to minimise this energy) leading to high costs, much greater than the current value of CO₂ within emissions trading schemes. This leads to great challenges in deploying CCS, as, whilst it is known to be the least costly route for industrial decarbonisation, it is still too expensive without some external financial incentive. The choice of capture system is dependent upon various operation factors, but primarily linked to the pressure requirement and the composition (including contaminants) and concentration requirements of the incoming and exiting gases. Capture (CO₂ separation) systems can be in a variety of forms: absorption (chemical and physical), adsorption (including pressure-swung absorption), membranes, cryogenics separation, and microbial (Badiei, et al., 2012).

The post-combustion capture processes are often suited to chemical absorption, due to the low partial pressure of the industrial waste gases. Ammonia based capture systems are a form of chemical absorption capture. A summary of the pros and cons of the various capture methods is provided in table 2-3.

The CO₂ capture process has changed very little from its design in the original sour gas sweetening patent. Similarities to modern capture processes can be seen with this initial design, consisting of a CO₂ absorption column and a solvent regeneration column, as shown in figure 2.12. (Florin, et al., 2010). A detailed explanation of the process capture process is provided by Kohl and Nielsen (Kohl & Nielsen, 1997).

Figure 2.12: Schematic of sour gas sweetening (carbon capture) process



Source: (Florin, et al., 2010)

To release the CO₂ from the chemical capture solvent, once the solvent is saturated (regeneration), a significant amount of heat (usually a steam supplied reboiler) is required to raise the temperature of the solvents; ~140°C in the case of monoethanolamine (MEA). The regeneration process also generates large volumes of CO₂ and can reduce the power station efficiencies, with a parasitic loss in the region of 10% - 37% for coal power stations. The range of parasitic loss varies significantly between the different authors (Goto, et al., 2013), (Badiei, et al., 2012).

Note that, as discussed above, applying CCS to the low-efficiency steel plant power station would lead to an unacceptably low power station efficiency. With only a typical max-efficiency of ~30%, even a 10% loss would be uneconomically high. Low temperature regeneration options, with the ability to use low temperature waste heat, would be very attractive and could reduce capture costs dramatically. Waste heat is typically available in abundance in the steel industry, however the exergy is low, and therefore its value is also very low, following the thermodynamic rules of Carnot.

Table 2-3: Pros and Cons of the most common types of carbon capture technology

| Separation Technology | Pros | Cons |
|-----------------------|---|---|
| Ammonia process | Lower heat of regeneration than MEA | Ammonium bicarbonate decomposes at 140°C, so, temp. in the absorber must be lower than 140C |
| | Higher net CO ₂ transfer capacity than MEA | Ammonia is more volatile than MEA and often provides an ammonia slip into the exit gas. |
| | Offers multi-pollutant control | |
| Amine scrubbing | Applicable to CO ₂ partial pressures. | Process consumes considerable energy |
| | Recovery rates of up to 95% and product purity >99% vol. can be achieved. | Solvent degradation and equipment corrosion occur in the presence of O ₂ |
| Physical absorption | Rectisol uses inexpensive, easily available methanol. | Hydrocarbons are coabsorbed in Selexol, resulting in reduced product revenue and often requiring recycle compression. |
| | Selexol has a higher capacity to absorb gases than amines. | Refrigeration is often required for the lean selexol solution. |
| | Selexol can remove H ₂ S and organic sulphur compounds. | More economical at high pressures. |
| Membrane technology | No regeneration energy is required. | Membranes can be plugged by impurities in the gas stream. |
| | Simple modular system. | Technology has not been proven industrially. |
| | No waste stream. | |

Source: (Badiei, et al., 2012)

Amines solvents are also expensive with an associated environmental impact and are degraded by the presence of NO_x, SO_x, particulate (all to be found in abundance in steel plant process gases) and oxygen. In comparison, it is proposed that ammonia-based capture solutions have much greater tolerance to such components, which is highly valuable to a steel plant operation as these contaminants are difficult to remove at low cost given the high gas volumes. Ammonia is also much cheaper, allowing acceptable solvent losses and energy consumption to be much lower. Ammonia was used extensively for coke-oven gas (town gas) purification, for the removal of CO₂ and H₂S in the earlier decades of 1900s, but this was prior to the commercialisation of the ammonia process and so ammonia was quite expensive. It was replaced with alkanolamines, with its superior capture properties, following the commercialisation in 1930 of triethanolamine (TEA), (Valenti & Bonalumi, 2018).

Novek et al. provides a clear introduction to aqueous ammonia capture systems, and also introduces the idea of the addition of organic solvents to enhance the regeneration process (Novek, et al., 2016). With the addition of an organic solvent (acetone, dimethoxymethane, or acetaldehyde), the ammonia solvent can be regenerated at much lower temperature. The organic

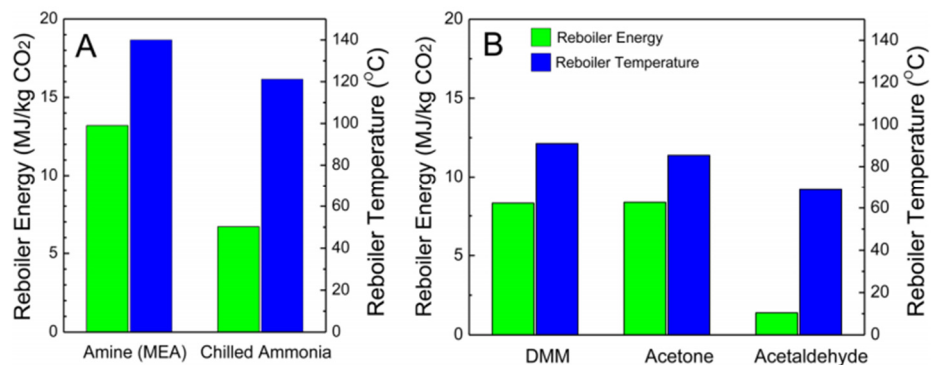
solvent is then recovered at much lower temperatures in a distillation process. The process described by Novek et al. (2016) involves three stages, They are:

- (1) flue gas CO₂ absorption in a CO₂ lean aqueous ammonia solution
- (2) pure CO₂ generation through mixing in an organic solvent
- (3) recovery of organic solvent via low-temperature distillation

Pure CO₂ was created from ammonium bicarbonate solutions at room-temperature and pressure (RTP). A 51% increase in CO₂ generation was achieved with the addition of acetone, with acetaldehyde showing the greatest recovery rates with very low recovery temperatures, owing the low boiling point of acetaldehyde.

The suggested reboiler energy consumptions shown in B, (MJ/kg CO₂), are significantly better than those of the conventional process (A) and could allow the use of low-grade waste heat recovery. This would represent a significant improvement in energy consumption and cost over the conventional amine process. Shown below in figure 2.13 (Novek, et al., 2016).

Figure 2.13: Literature values (MEA) and Aspen HYSYS simulation (Ammonia) reboiler comparison



Source: (Novek, et al., 2016)

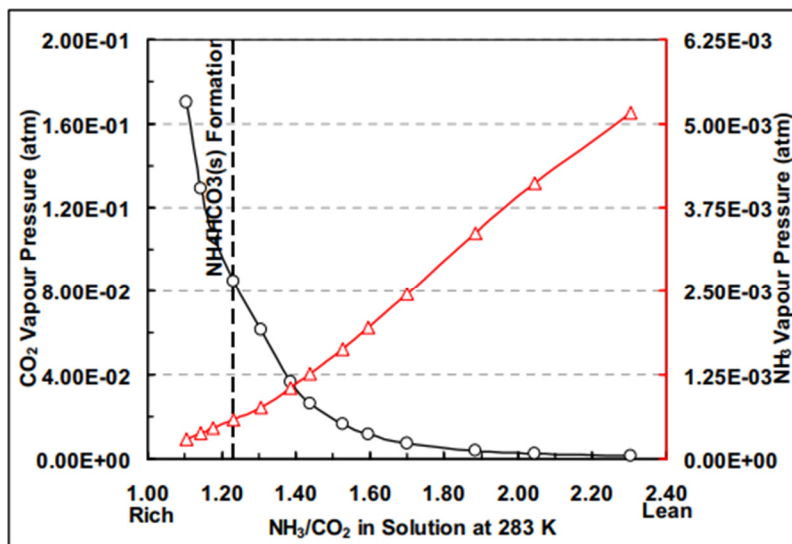
Although the regeneration of this novel capture solvent has been shown possible at low temperatures, carbon capture units are large, with a significant footprint needing large adjacent, low-value land. Given that the production of urea is typically carried out at high temperature and pressure, the uptake of CO₂ into the ammonia solution at mild conditions is likely to be the process limiting step, requiring large vessels and long residence times.

When CO₂ is presented to an ammonia solution, we expect CO₂ to be absorbed and the formation of ammonium bicarbonate, ammonium carbonate and ammonium carbamate. Once maximum solubility is reached, they will precipitate out of the solution, forming solid phase ammonium salts. Even at very low NH₃ concentrations (4.5%wt), ammonium bicarbonate solids still form (Zhuang, et al., 2011). Typical packed reactors would block with the solids, therefore modified

designs would be needed, with a wide packing structure to allow a wash down of the solids into a slurry at the bottom of the reaction vessels from the incoming CO₂ lean solvent.

The slurry is then passed into the regenerator and heated by the reboiler. Zhuang et al. proposed that this regeneration could be carried out at elevated pressure, to prevent unactable NH₃ from slipping back into the CO₂ stream (figure 2.14) (Zhuang, et al., 2011). CO₂ needs to be compressed post capture for storage and transport. The compression stage must occur at some point within the full-chain capture process. Compression requirements vary depending upon type of transportation, whether it be pipe or shipping, as shipping requires a liquefaction stage at the port, which is the vast majority of the transport and storage cost, so the point at which compression occurs is often location and process specific.

Figure 2.14: Gas vapour pressure vs CO₂ absorbed at 283K and NH₃ concentration of 4.5 wt. %



Source: (Zhuang, et al., 2011)

On first assessment of the ammonia capture system, it would seem that it is only practical to regenerate the solvent to a 50% CO₂ release, leaving half of the CO₂ still present in the returning CO₂ lean gas stream, to avoid significant NH₃ in the CO₂ rich gas. This CO₂ will mostly be present in the ammonium carbonate form. This would appear to be unacceptable, needing larger volumes of solvent. Yet previous research has shown that the capacity for CO₂ loading of aqueous ammonia can be very high, and indeed much higher than that of an MEA system. For an amine-based system at steel plant, CO₂ loading in the MEA solvent would be about 5%. In comparison the difference between the two CO₂ loadings of the rich and lean ammonia solvent would be 8.4% weight following the initial high CO₂ capacity in an NH₃ rich solution (21.6 wt. %). Maximising the initial CO₂ loading (>22%) via increased production of precipitate in the ammonia solution and slurry to the regenerator could, in principle, improve the process further.

So too would increasing the solvent regeneration and removal of CO₂ to return CO₂ lean (reduced carbonates) back into the absorber. (Zhuang, et al., 2011), (Han, et al., 2014).

Another approach to address NH₃ losses has been the patented chilled ammonia process from Alstom. Alstom was acquired by GE in 2015. The chilled ammonia approach prevents high rates of NH₃ slip, and yet allows a high concentrated ammonia solution to be used. This has resulting in a number of pilot studies and various modification, between 2005 up to 2014. It may be considered the world's leading ammonia capture approach. This process operates within a low temperature region of 5-15⁰C, with regeneration occurring at temperatures above 80⁰C, (Yu, 2018).

To summarise, the key challenges of the CO₂-NH₃-H₂O system with respect to industrial applications are:

1. Solid formation needs slurry transfer and is considered problematic in an industrial application (Yu, 2018). Solids can be avoided whilst operating at higher temperatures, pressures and/or low CO₂-NH₃ concentrations. Avoiding solid formation and process optimisation requires a detailed understanding of the reaction system. The published kinetic models are not in agreement, leading to uncertainty over the reaction mechanisms and pathways (Qin, et al., 2011) (Lillia, et al., 2016).
2. The uptake of CO₂ within the system is slower than alternative capture systems, (Han, et al., 2014), leading to a larger absorption column, or the use of packing materials or baffles to reduce the height by extending the pathway of the incoming gases. Solids formation is to be avoided in this case, unless a washdown is used to avoid blockages (Yu, 2018).
3. Losses of NH₃ can be high, leading to either a recycling (washing) system or the need for a chilled system, both adding cost and additional complexity. Whilst less toxic than alternatives (MEA), NH₃ is still an irritant and harmful to the environment (Yu, 2018).

A comparison of the merits of three capture solvents is shown in table 2-4 (Han, et al., 2014).

Table 2-4: A comparison of key characteristics of CO₂ capture solvents

| Characteristics | Amines | Ammonia | K ₂ CO ₃ |
|---|-------------|------------|--------------------------------|
| CO ₂ capture capacity [mol-CO ₂ /mol-solvent] | 0.5 for MEA | 1.0 | 1.0 |
| Regeneration energy [GJ/tCO ₂] | 4.0 (MEA) | <2.0 | 2.2–2.78 |
| Regeneration temp [°C] | ~120 | ~80 | ~115 |
| Absorption rate | Fast | Slow | Similar to MEA |
| Volatility | Low | High | Low |
| Thermal degradation | Severe | Negligible | Negligible |
| Corrosiveness | Severe | Mild | Mild |
| Absorbent cost | Expensive | Cheap | Expensive |

Source: (Han, et al., 2014)

Searching for ammonia capture applications within the steel industry, we find that, according to Han et al. this process is suited to BFG capture following an analysis of capture systems at various CO₂ concentrations vs pressure (Han, et al., 2014). However, this is an oversimplification, as the choice of CCS technology is also influenced by the fate of the CO₂ once captured (exiting delivery pressure), current plant configuration, energy balance, power generation, steam availability and available external energy supply. The prospect of a low-energy capture route, and tolerance to BFG contaminants, have resulted in the construction of a pilot aqueous ammonia CO₂ capture facility at the POSCO owned steel plant at the Pohang Works, with subsequent publication of some of the process performance data (Rhee, et al., 2011), (Han, et al., 2014). The process evidently works for steel plant processes gases, but it is unclear how the BFG gas composition affects performance from this review.

2.4.5 Kinetics of the CO₂-NH₃-H₂O system

A detailed understanding of the kinetics is essential in order to optimise the process conditions, tailor and maximise the product formation and understand the gas-liquid interface reaction mechanisms, to minimise the loss mechanisms and reach maximum efficiencies. Although the theoretical absorption, mass transfer and reactions continue to receive attention, the kinetics of the liquid-phase reaction have not been extensively studied, leading to contradictory opinions on the most dominant pathways and species formation (Valenti & Bonalumi, 2018).

As we have discussed, aqueous ammonia can be very effective at absorbing CO₂, with potentially low energy consumptions, resulting in the pilot facility at the POSCO steel plant. Impressive CO₂ capture efficiencies of >90% can be achieved, yet the rate of CO₂ uptake is low, leading to larger capital investment required for taller, baffled or multiple absorption towers to increase the gas

distance. This problem would appear to be compounded by the use of low NH_3 concentrations to avoid NH_3 vaporisation.

These reaction processes have been evaluated under various conditions, although, following the use of different calculation methods (Qin, et al., 2011), there is some debate over the pathways, which reactions dominate and the kinetics. The kinetic rates publicised range by orders of magnitudes, potentially from variations in the testing, analysis, calculation method and different ammonia concentrations. It is likely that the reactions follow a non-linear relationship which will lead to some of the discrepancies within the literature (Lillia, et al., 2016). For this reason, it is difficult to make accurate comparison between the performances of various systems given the variability within the results.

Of concern to industrial application is the comparison to alternative solutions and the potential to increase reaction kinetics. Liu et al. documented the lab-based experimental studies to determine mass transfer rates and kinetics and the analysis clearly showed that the kinetics of CO_2 uptake are a limiting factor in the ammonia capture concept, compared to conventional capture methods, as shown in the data (table 2-5), (Liu, et al., 2011). The NH_3 capture kinetics do not appear to improve significantly with an increase in temperature, as depicted in figure 2.15. NH_3 concentration, however, may be a contributing factor within this relationship, with the availability of NH_3 the limiting parameter, not temperature. Low concentration of NH_3 are used to avoid volatilisation and losses of NH_3 from the system.

Difficulty then arises when making comparisons to alternative capture solvent systems (the kinetics of the system change under various process parameters and it would appear are non-linear). The overall cost of capture per ton of CO_2 is possibly the most useful metric for comparing industrial capture processes. However, this does not allude to the issues and opportunities for process improvements, or current stage of process refinement.

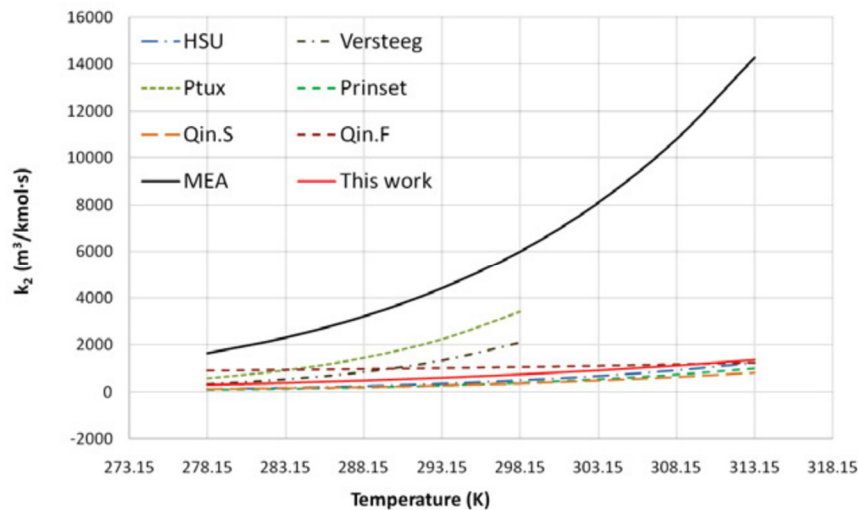
Evidence strongly suggests that ammonia capture systems are significantly limited compared to MEA in terms of CO_2 capture rate. The rate of CO_2 absorption within the ammonia solution could be increased by improving mass transfer at the gas-to-liquid interface, by considerably increasing the gas bubbles surface area. Hence, we next introduce the concept of micro-bubbles.

Table 2-5: A comparisons of capture system kinetics at 25°C

| Absorbent | $10^{-3} k_{\text{absorbent}}^T$ ($\text{m}^6 \text{ kmol}^{-2} \text{ s}^{-1}$) | $k_{\text{H}_2\text{O}}^T$ ($\text{m}^6 \text{ kmol}^{-2} \text{ s}^{-1}$) | Source |
|------------------|---|---|---------------------------------|
| NH ₃ | 0.139 | 10.79 | This work |
| NH ₃ | 0.13 | 17.10 | Qin, 2010 ^[32] |
| MEA | 1.7 | 73.7 | Aboudheir, 2003 ^[33] |
| AEEA | 2.35 | 161 | Ma'mun, 2007 ^[34] |
| EDA ^a | 2.79 | 17.72 | Li, 2007 ^[35] |
| DETA | 17.5 | 179.7 | Hartono, 2009 ^[36] |
| PZ | 70.1 | 550 | Cullinane, 2007 ^[37] |

Source: (Liu, et al., 2011)

Figure 2.15: A comparison of CO₂ kinetics at increasing temperature for MEA and NH₃ by various authors



Source: (Liu, et al., 2011)

2.5 Microbubbles

Microbubbles are characterised by their size. Their diameter lies within the within the μm range of 1-999 μm . The small bubbles with a gas-liquid interface provide a very high mass transfer rate, following their surface area to volume ratio. Bubble of a smaller diameter are considered nano-bubbles.

The capture of steel plant derived CO₂ within aqueous ammonia for CO₂ capture seems promising. However, as we have discussed, there is concern over the compromise in reaction kinetics for favoured reaction pathways, rate of CO₂ uptake, and NH₃ slip. In this section we will explore the generation and applications of microbubbles and their unique properties, which may address the issues described, in particular the rate of CO₂ uptake. For this reason, the review will

touch briefly upon the novel bubble generation technology, with subsequent emphasis on their unique properties, benefits and influence upon the gas-liquid interface.

Beyond their current application within cleaning, dissolved air flotation and medical imaging, microbubble have also been applied (but not limited) to:

- Theranostics (Mulvana, et al., 2012), (Cai, et al., 2012)
- Enhanced algal growth, (Ying, et al., 2013)
- Microalgal separation (Hanotu, et al., 2012), (Ekins-Coward, et al., 2015)
- Wastewater clean-up (Agarwal, et al., 2011), (Rehman, et al., 2014)
- Oil emulsion separation (Hanotu, et al., 2013)
- Finally, and considered most pertinent to this thesis, enhancement of heat and mass transfer (Abdulrazzaq, et al., 2015)

The expansion into new fields is due to the ability to recently create the bubbles in an energy efficient method, following the invention and deployment of an auspicious new fluidic oscillation microbubble generator (Zimmerman, et al., 2008).

2.5.1 Microbubble Generation

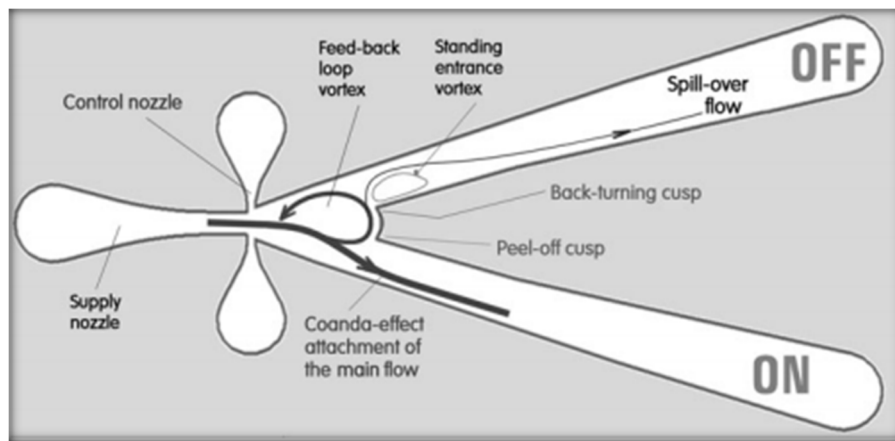
Previously the widely applied methods for the generation of these tiny bubbles would require large energy input, using either compression or ultrasonic waves (Lou, et al., 1998). The generation of tiny micro-bubbles with very low energy inputs has been revolutionised by the invention of the fluidic oscillator microbubble generator. Following the modification of a Warren type bistable diverter valve and its application to microbubble generation by Tesař and Zimmerman, it has been possible to produce microbubbles with very low energy input and minimal pressure loss (Tesař, et al., 2006). This earlier adaptation of the fluidic oscillator generator is known as the Tesař-Zimmerman Fluidic Oscillator (TZFO). Subsequent evolution has now led to the more tenable Desai-Zimmerman Fluidic Oscillator (DZFO) (Desai, et al., 2018), (Desai, et al., 2020).

The benefits of a fluidic oscillator approach, used in conjunction with a porous gas diffuser, are low energy, lack of mechanical or electrical inputs and absence of any moving parts. It is therefore very robust and reliable. It could be integrated into a production process, without the need for continuous regular servicing, if any. The CAPEX and ongoing OPEX of such a device would be considered very minimal. A 2D schematic of the device is shown in figure 2.16.

By supplying a continuous, steady flow of gas into the fluidic oscillator at the single supply nozzle, the device can be tuned to a correct frequency to provide uniform bubbles of similar diameter to that of the diffuser pore size. This occurs by pausing the flow of gas to the bubble, and due to the Coanda effect, the jet attaches the sidewall at one of the two outlets (Tesař, et al.,

2006). This draws fluid from the opposite outlet by a partial vacuum and, with the arrival of this flow, causes a switch of this effect to the opposite outlet. This continuous, repetitive switching cuts off from the gas supply to each outlet consecutively, creating an equal pulsed flow between the two outlets. The metered pulse of gas arrives at the diffusers and is detached from the diffuser before it has an opportunity to grow larger, as the flow is terminated. The fluidic oscillator frequency can be tuned by adjusting the length of the feedback loop (relative to flow rate) between the two exit terminals (identified with ON and OFF), along with the flow rate, to adjust the point at which the flow is cut and the amount of gas supplied to each bubble. Note that the pressure drop across both outlets needs to be equal so that the effect is maintained. Both gas outlets should be utilised in an industrial application and a restriction of equal value placed on the unused outlet if only one is used, such is the case in laboratory testing.

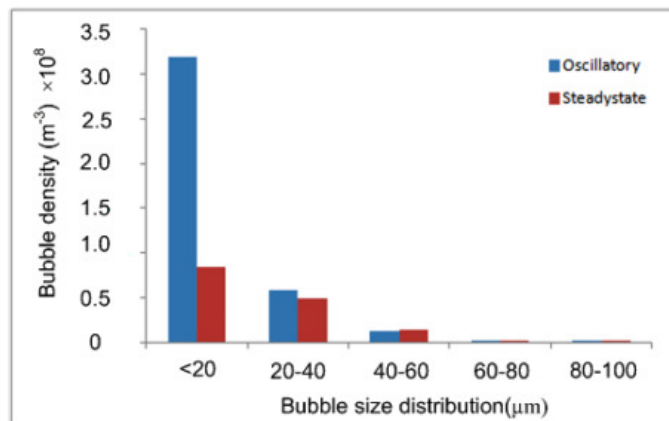
Figure 2.16: Two dimensional representation of the Tesař-Zimmerman Fluidic Oscillator (TZFO)



Source: (Tesař & Bandalusena, 2011)

The estimated distribution of bubble size, using optical methods is shown in comparison to steady state flow within figure 2.17 (Rehman, et al., 2014).

Figure 2.17: Size distribution of bubbles in both steady and oscillatory flow regimes for an MD 500 diffuser.



Source: (Rehman, et al., 2014)

2.5.2 Characteristic features relevant to bubble size

The features of a microbubble are not only defined by its size, but its existence and lifetime within a liquid and the influence this lifetime, from creation, absorption and (in some applications) the eventual release, has upon the gas-liquid system. These influences will be most relevant to the CO₂-NH₃-H₂O system.

Bubbles are not perfectly spherical throughout their lifetime, increasing drag forces and the probability of coalescence. Microbubbles propagate initially with a hemispherical cap, but form a spherical shape upon detachment (Zimmerman, et al., 2008). The smaller bubbles lends themselves to a more spherical profile owing to the associated forces, primarily surface tension, acting upon the bubble surface. (Tesař, 2014)

2.5.3 Bubble size

Typically, under non-oscillatory flow, bubbles from an ethylene propylene diene monomer (EPDM) diffuser produce fine bubbles of an average diameter 3-4mm. With FO bubbles, an average bubble size of 500µm can be achieved; a significant reduction in size. Whilst there are various factors influencing bubble formation, the liquid properties play a minor role, yet they have a greater influence on the rise velocity once the bubble is formed and detached. (Desai, et al., 2018) identified the primary factor for bubble size distribution as the frequency of oscillation, relative to the micropore size. Whilst, in general, higher frequencies are sought for smaller bubbles, there is an optimum, small frequency range to achieve the smallest bubbles (Desai, et al., 2018).

Bubble sizing can be achieved by optical techniques with reasonable accuracy (Wesley, et al., 2016). However, more recently bubble sizing by acoustic bubble spectroscopy has proven more accurate, demonstrating that smaller bubbles can be hiding out of sight from the optical method, behind the larger bubbles, accounting for some of the discrepancy in previous mass-transfer estimates (Desai, et al., 2019). A demonstration of bubble formation within an air-lift bio-reactor, prior to algal growth, is shown in figure 2.18.

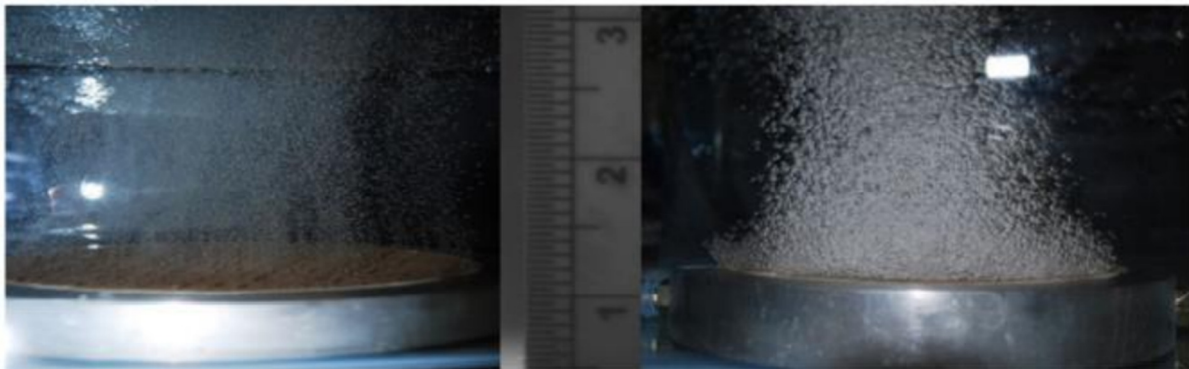
Figure 2.18: Bubble generation, in the air-lift loop bioreactor at Tata Steel UK (previously Corus) power station prior to algae introduction



Source: Personal archive

Also, in figure 2.19 is a direct comparison between FO microbubbles (left) and non-oscillatory flow fine bubbles (right).

Figure 2.19: FO microbubbles (Left) and non-oscillatory fine bubbles (Right)



Source: (Zimmerman, et al., 2011)

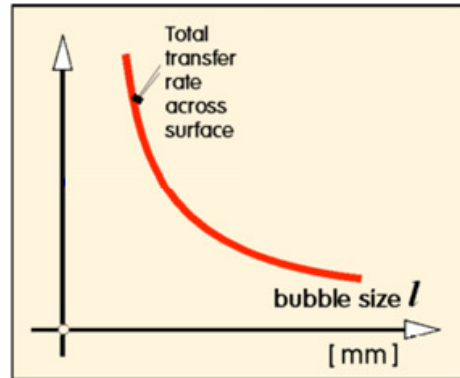
2.5.4 Gas phase surface area

The most immediately obvious advantageous feature of the microbubble, with respect to fine bubbles, is the significant increase in the surface area relative to gas volume.

The Tata Steel microalgal bio-reactor shown above in figure 2.18, has a volume of 2 m³. At a maximum flow rate of incoming gas into the reactor at 200l/m and an average bubble size of 7µm, the achievable bubble surface area flux is an astounding 0.15 hectare per second. Furthermore, with a gas phase fraction of only 1%, in a single cubic metre volume, the bubble surface area flux is an impressive 0.86 hectares (Gilmour & Zimmerman, 2020).

Overcoming gas transfer limitation can be achieved, with much smaller reactor volumes, following the exponentially inverse relationship between bubble diameter and total transfer rate, as demonstrated in figure 2.20.

Figure 2.20: Bubble size and transfer rate relationship



Source: (Zimmerman et al., 2008)

2.5.5 Bubble rise velocity

Large gas bubbles rise quickly and turbulently within a liquid, due to the buoyancy of the entrapped gases, often bursting and releasing their contents at the surface. In contrast, microbubbles rise very slowly. They are effectively non-buoyant and entrained within the liquid current. A bubble of 20 μm will take approximately 24 hours to rise only one meter (Gilmour & Zimmerman, 2020).

Critically, retaining the bubbles within the solution for longer reduces the need for tall columns or baffles to increase the residence time or pathway of the incoming gas, in order to address the slow CO_2 uptake expected within weak aqueous ammonia capture systems.

Beyond size, other factors that influence the velocity in a Newtonian liquid are: bubble shape, liquid density, viscosity, concentration, liquid purity, surface tension, direction of liquid motion, temperature, pressure, gravity, reactor walls and coalescence (Kulkarni & Joshi, 2005).

The uniform bubble size and slow rise velocity leads to steady laminar flow and, consequently, reduced coalescence. Beyond a column size of 10-15cm and heights above 1.3m the column dimensions have no influence on gas hold-up and it is increased, to a negative effect, with decreased viscosity, increased pressure and increased superficial gas velocity (Kantarci, et al., 2005). Gas hold-up causes greater coalescence, imperfect bubble conditions, turbulent or a slug like flow, depending upon the increased degree of hold-up, ultimately reducing the gas phase volume and increasing bubble size (Bouaifi, et al., 2001).

The generation of FO microbubbles also leads to a unique low kinetic energy density environment. The FO bubbles have been estimated to dissipate only $\sim 1/1000^{\text{th}}$ of the energy with

their release in to their environment of that of conventional bubble saturation (Hanotu, et al., 2012). This very low kinetic energy leads to long residence times (and slow bubble rise velocity) such that, when they reach the surface within a fermentation/H₂O vessel, they are completely saturated with water vapour.

2.5.6 Benefits from the reduction in gas bubble size within a gas-liquid system

The features of microbubbles previously described lead to some unique advantages that may be exploited. Reactive absorption processes, such as the CO₂-NH₃-H₂O system, are interfacial processes, which are strongly influenced by the reactivity of the species and the surface area available for either mass transfer or chemical reaction. Microbubbles are advantageous due to the inverse physical relationship of the surface area to volume on a reduction of bubble size. The most apparent advantage, therefore, of a reduction in bubble size is a significant increase in the available surface area, relative to gas volume, leading to much greater mass-transfer potential.

2.5.7 Mass transfer flux

As the bubble enters a reactive system, it instantly begins to attain chemical equilibrium with its environment at the bubbles surface. With a much greater gas surface area, the rate at which equilibrium can be achieved is increased dramatically and the mass transfer flux from gas to liquid phase will increase.

The physical chemistry can be, in general, described by pseudo-steady film theory, as described in equation 2.32 (Cussler, 1997).

$$J = k_L a (c_l^*(T) - c_l) \quad (\text{Eq. 2.32})$$

Within this definition, surface area plays an equal dominant role in the net mass transfer flux and can be exploited by reducing bubble size.

Although longer residence times (due to slow rise velocity) are expected, this may be irrelevant for microbubbles within typical rise heights. According to Zimmerman et al. (2013), bubbles of 100µm can exchange all their possible mass with the liquid boundary layer in just milliseconds of being released. The laminar boundary layer at the bubbles shell further opposes heat and mass transfer with the remaining liquid within the remaining rise time, making further gas phase reactions very slow. Internal mixing of the bubbles is expected to be rapid, given their small volume due to convection and molecular diffusion, especially over the initial milliseconds of formation, enhancing the speed at which the bubbles become capacity limited (Zimmerman, et al., 2013). It is known that 90% capture rates can be achieved with aqueous ammonia capture, therefore this shielding with large bubbles is a plausible cause for the 10% of CO₂ that is not captured.

When the first gas molecule enters the liquid, it could be possible that it sees an overwhelming excess of the receiving reagent. This concept is more pronounced if the bubbles are much smaller and surrounded by, what seems to the μm diameter bubble, a significant excess of the reagent in all directions. According to the principles of chemical affinity, introduced by de Donder (1936) and later established by Prigogine (1980), for the first molecule within the reaction system the Gibbs free energy is effectively infinite (de Donder, 1936), (Prigogine, 1980). This is such that at the microbubble interface this can be effectively catalytic (Gilmour & Zimmerman, 2020). This principle can help explain the particularly fast mass transfer flux. The strong non-equilibrium for the entering microbubbles, also as described by Le Chatelier's principle, will drive the reaction at the bubble's surface towards equilibrium.

2.5.8 Improved mixing

Conversely, in such a low kinetic environment an individual might not anticipate that the mixing would be enhanced. Particularly with such a slow rising bubble. Al-Mashhadani et al. (2015), demonstrated that with the assistance of an airlift loop reactor design, microbubbles improved mixing by 10 times that for 3mm fine bubbles (Al-Mashhadani, et al., 2015). Following the very slow rise velocity, the bubbles are able to transfer most, if not all their kinetic energy into the liquid, which they drag along within their wake. The Archimedes principle highlights that it is not the size of the bubble but the volume of gas that dictates the injected forces. With such small bubbles, it is possible to inject a high volume of gas within a small area without gas hold up and coalescence.

2.5.9 Extraction of inhibitors

Most often, reactions are opposed by the build-up of the products or inhibitors according to Le Chatelier's principle. Continual extraction of the product can be used to drive the reactions towards completion, or in the case of microalgal growth, the removal of inhibitory oxygen. During the demonstration of microbubble enhancement of microalgae growth at the Tata Steel power plant, it was shown that the oxygen produced by the microalgae (*D. Salina*), which acts as an inhibitor to growth, is stripped from the reactor at the liquid surface by the escaping microbubble, having deposited its useful contents for algal growth, CO_2 , SO_2 and NO_x (Zimmerman, et al., 2011), (Ying, et al., 2013).

Within the $\text{CO}_2\text{-NH}_3\text{-H}_2\text{O}$ system, given the high solubility of the products, extraction of the products in the vapour stage is not anticipated. But whilst extraction of unwanted products is desirable, equally extraction of useful components (NH_3) should be avoided and may prove problematic. This is certainly a significant problem with ammonia-based carbon capture systems, as discussed earlier.

2.6 The conversion of CO₂ using plasma chemistry

2.6.1 Introduction to CO₂ plasma chemistry

Carbon in its most oxidised state as carbon dioxide is very stable, but it can still form the building block for many products. Urea, as we have discussed, is one such commercially established example. Hence the emergence of a global interest in CCU. Over the period of study, we have seen the interest in CCU change dramatically as well as the terminology, knowledge, support and opinions. Fundamentally, there is a critical issue holding back large-scale deployment of CCU. That is, the current commercial processes gain their carbon from fossil fuels and this is still the cheapest way of producing these products, even in the face of a climate emergency. Incentives maybe needed, similar to those employed for renewable power, to kick-start a carbon recycling industry. Secondly, the high concentration CO₂, which is required for most of the CCU technologies, is not readily available in the quantities needed to start a global industry and in fact is often, ironically, in short supply (Hotten, 2018). If the large scale roll out of CCS across foundation industries becomes likely, as will be evaluated for the steel sector in the following research section, then an attributed CCU product may become more financially attractive than geological storage (Armstrong & Styring, 2015).

The component elements of carbon dioxide are valuable if separated in their gaseous form of carbon monoxide and oxygen. The dissociation of CO₂ with the potential to utilise periods of excess renewable power could lead to a viable and relatively simple solution. The utilisation of what is termed excess renewable power is a subject of debate and potential solutions. (Armstrong & Styring, 2015).

There are two leading fields of research for the electronic dislocation or conversion of CO₂, which are electrochemical conversion or plasma chemistry. Both areas show promise. This research will focus upon the later, plasma conversion, as there is an opportunity to push the knowledge within this field forward utilising the breakthroughs in micro-plasma knowledge developed within The University of Sheffield.

There was significant research effort undertaken in the 1980s to understand the processes of CO₂ decomposition, which forms the foundation of our understanding today. (Rusanov, et al., 1981), (Nigara & Cales, 1986), (Fridman, 2008). More recently, the focus of the research has been dominated by the availability of new analytical and computer modelling methods to better understand these subatomic processes (Aerts, et al., 2012), (Kozák & Bogaerts, 2014), (Aerts, et al., 2015). Naturally, within this literature review we will review the processes that lead to the most efficient dissociation routes, as studied by the early pioneers, and follow with more recent research, which looks to understand these mechanism in more detail and gain higher process

efficiencies within the experimental set-up. This will lead us to discuss the gaps in the current knowledge and where novel research can be targeted.

2.6.2 Plasma fundamentals

Plasma is possibly the most common state of matter within the galaxy. Recognised as the ‘fourth state’ of matter, it is gas that is ionised as a result of an electric field, with low-current and high voltage. It was Langmuir, in 1929, who was the first to use the term ‘plasma’ to describe an ionised gas. Naturally occurring examples we are familiar with would be the solar corona surface and the aurora borealis. The terms thermal and non-thermal plasma refer to the average plasma temperature profile. Within a thermal plasma, a homogenous temperature is present where the temperature of the gas (T_g) is approximately equal to the electron temperature ($T_e = T_g$). These plasmas operate with a gas temperature up to 30,000 °K. A non-thermal plasma is characterised by the low-gas temperature, yet the electrons, which are significantly smaller, approximately 10^{-5} than that of an ion, can be at a significantly elevated temperature >300 °K. Because of the electrons’ relatively small mass compared to that of the surrounding larger particles, it is more difficult to transfer this energy within collisions. Thermal plasmas are also known as plasmas in local thermodynamic equilibrium (LTE plasma), whereby the temperatures (excluding the radiation) are equal. In contrast, non-LTE plasmas are low-temperature or cold plasmas and they are defined by the low bulk gas temperature and their high electron temperature.

More specifically, plasmas are defined as a gas that is a quasi-neutral collection of both neutral and charged particles that exhibit a *collective behaviour*. Within a natural gas state, there are no forces acting between the molecules of the gases, which flow with random direction within a range of velocities. Their random motion is influenced by their container (walls) and collisions with themselves. They are said to exhibit a random Brownian motion. The average number of collisions between the molecules is determined by the gas temperature and pressure. Within a plasma, the charged particles exhibit a non-random direction, influenced by the applied electric field (E) with locally high concentrations of positive and negative charges. The resulting electromagnetic Coulombic fields from these charge concentrations have a relatively large spherical range and are able to influence the entire plasma. It is this influence that leads to the *collective behaviour*. The electric field is usually described in terms of the E/n ratio, whereby E is the applied electric field and n is gas number density.

A plasma is generated when the input energy exceeds the breakdown voltage (V_b), which is supplied to a neutral gas (in its most simplistic form, a high potential difference between two electrodes), to allow ionisation of the gas into the ions and electrons. As demonstrated by equation 2.33.



The breakdown voltage (V_b), is the minimum applied voltage that is needed to achieve plasma ignition. This critical voltage is a relationship dependent upon the electrode spacing, pressure and gas composition. It is defined by equation 2.34.

$$V_b = \frac{B(p \cdot d)}{\ln[A(p \cdot d)] - \ln\left[\ln\left(1 + \frac{1}{\gamma_{sec}}\right)\right]} \quad (\text{Eq. 2.34})$$

Constants A and B vary and are determined experimentally for each gas composition. p is the pressure, d is the electrode spacing and γ_{sec} is the secondary electron emission coefficient of cathode. This parameter becomes more important when the distance between the electrodes are reduced.

Another two important plasma parameters, which are also dominant at reduced electrode distances, are the Debye length and the plasma Sheath. The Debye length λ_{De} is the distance over which the local charge concentrations occur. For the plasma to exist, it must extend greater than the Debye length. This is the plasmas ‘characteristic length’ (L). Therefore $\lambda_{De} \ll L$, where L is the dimension of the plasma system. The Debye length is defined by equation 2.35.

$$\lambda_{De} = \left(\frac{\epsilon_0 T_e}{en_0}\right)^{1/2} \quad (\text{Eq. 2.35})$$

Within equation 2.35, ϵ_0 is the vacuum permittivity, T_e is the electron temperature, e is the electronic charge and n_0 is number density of particles. The Debye length decreases with increasing electron densities. Hence, at low electron densities, small plasma reactor systems cannot operate sustainably. The response of the charged particles to attempt to reduce the effects of the localised charge concentrations is called the Debye shielding.

The plasma sheath is the region closest to the plasma walls and is often only a few λ_{De} . The plasma sheath is a region of low electron density (n_e) compared to the bulk of the plasma. n_e starts to decrease in the pre-sheath region, with a rapid drop to negligible n_e within the sheath. At the plasma walls, ions and electrons recombine and represent losses from the plasma system. With a small L , the relative influence of the sheath region, with respect to the bulk of the plasma, increases. The mechanisms that influence the sheath region are not fully understood, but it is known to be influenced by the frequency of the electromagnetic field, applied voltage and the system pressure. Because the sheath region can extend to mm distances, it becomes important for small electrode gaps, as the bulk (quasi-neutral plasma) is no longer dominant (Bellan, 2006).

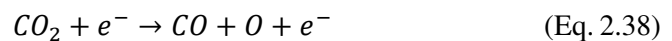
Beyond the characteristic length (L), the plasma is able to exist within a quasi-neutral state, following the influence of the Debye shielding. In a quasi-neutral plasma state, the densities of electrons (n_e) and ions are equal (n_i) and the plasma density (n) is equal to the densities of either n_e or n_i . $n = n_e = n_i$. The plasma density is highly influential in the energy efficiency and the reaction rates occurring within the plasma. The lightweight electrons are accelerated first by the

applied field and pass on their energy via collisions with the heavier, neutral or charge particles. A greater applied electric field will result in greater electron densities (n_e) and an increased probability of collisions. The rate of reactions occurring is therefore dependent upon the electron density, or electron energy distribution function (EEDF).

There are two types of collisions that are occurring between the electrons and the particles;

- a) Elastic collisions = do not result in an excitation of the collided particle as the electron energy is too small
- b) Inelastic collisions = result in the collided particle becoming excited as the electron has sufficient energy

Given the small mass of the electron, the transferred energy during a collision between an electron and particle is relatively small. In contrast, the energy transferred between two electron collisions is much greater. It is the inelastic collisions that form the ionisation and dissociations with the plasma, whereby an electron accelerated by the electric field, can transfer nearly all of its energy to the heavy particle, resulting in an energetic plasma species. The energy transfers within a plasma range from 0.1 eV to >10 eV, for excitation and ionization respectively. Sufficient electron energies (>10eV) and collisions also result in dissociations; the dissociation of CO₂ is specifically of interest to this study. Dissociation reactions are shown in equations 2.36, 2.37 and 2.38.



The electrons can collide with other electrons, natural atoms or positive or negative ions, which lead to various mechanisms for ionisation or plasma reactions. Similarly, the heavy particles can also be involved in collisions, which can lead to ionisation, recombination, or electron detachment.

Thermal plasmas exist when the heavier particles have high energies ($10^2 - 10^4$ eV). Increasing the plasma pressure results in greater collisions, leading to thermodynamic equilibrium, but their increase in temperature leads to greater energy losses, with the confining plasma walls. Continuous heating of the plasma reactor is needed and sputtering occurs, leading to erosion of the plasma vessel and unwanted arcing. Within the context of CO₂ dissociation the thermal plasma acts as a heater, driving the reaction in temperatures above 2500 – 3000 K (Nigara & Cales, 1986). Once the products of CO and O₂ exit the reactor at high temperature, they must be rapidly quenched, to avoid the recombination back into CO₂. Even if rapid quenching is possible, the maximum energy efficiency that can be achieved is estimated to be 43% (Fridman, 2008). In

contrast, the useful characteristics of non-thermal plasmas are the low bulk gas temperature, which results in a reduction of thermal energy losses to the reactor walls and high efficiencies can be achieved. It is these high-efficient processes that we are interested in for further study for high efficiency conversion of CO₂.

2.6.2.1 Types of non-thermal plasma reactors

Because of their ability to carry out chemical reactions at low temperatures and high efficiencies, the focus will be upon non-thermal plasmas. The properties of three of the most relevant reactor designs are now discussed. Their operations can be characterised by their electron densities and temperatures, which typically overlap, but most critical to their operation is their geometries and their power source/input.

2.6.2.2 Corona discharges

Corona discharges are the most simplistic reactor design. These types of reactors are of interest in the micro-plasma application of ozone generation (Lozano-Parada, & Zimmerman, 2010). They are often constructed with a needle (multiple pinpoint source electrodes may be used) and a perpendicular electrode, or two parallel plate electrodes. The electrical field is generated using a pulsed DC power source. These type of plasma reactors are successfully deployed within industrial waste gas cleaning equipment, for the removal of particulates. Indeed, the large electrostatic precipitators at the Sinter plants at Tata Steel, UK and British Steel, UK are of this design.

The plasma is initiated with high voltages, in the range of 2-5kV and small currents in the range of 10^{-10} - 10^{-5} A. The average electron energies of the total plasma are approximately 5 eV, but feature regions of high and low electron energy densities as a result of streamer formation across the electrodes, where the electrons are accelerated across the electrode gap due to the electric field. They feature a high concentration of radicals, yet it is difficult to operate the corona discharge at elevated electron densities without increasing the current and transitioning into plasma arcs, which limits their application. Arcs are achieved beyond a maximum voltage of 5×10^4 V (Schutze, et al., 1998). Arcs are limited by using periodic pulsed DC inputs, whereby the pulse duration is shorter than the arc formation. The plasma is extinguished before electron temperatures become too high. Alternatively, a dielectric layer can be used, which limits the localised current, such as in a dielectric barrier discharge (DBD), to create a DBD-corona hybrid.

2.6.2.3 Gliding arc plasma reactors

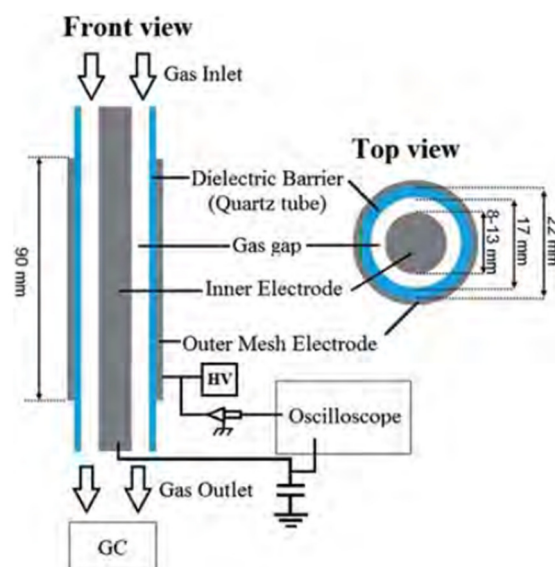
These plasma reactors are similar to that of a corona discharge, yet they are self-regulating to prevent high plasma arcing. They are of particular interest, as they yield surprisingly high (>40%)

conversion efficiencies of CO₂ dissociation can be achieved (Nunnally, et al., 2011), (Sun, et al., 2017). By using two diverging electrodes, the gas enters between the electrodes at the most constricted point. Here the gap is narrowest, leading to a high electric field and plasma initiation. The plasma may form in the thermal state, due to the high energy density. The flow of gas moves the plasma front into the ever-increasing electrode gap, until the field strength is no-longer able to sustain the plasma and it is extinguished. Once the plasma is extinguished, the plasma regenerates at the constriction and the process becomes self-perpetuating. The scale up of the technology has yet to be achieved (Fridman, 2008).

2.6.2.4 Dielectric barrier discharge plasma

Once of the most common types of plasma reactor used in CO₂ dissociation is the DBD. DBD reactors are also particularly successful in the commercial scale ozone generation, used in wastewater treatment. By incorporating a dielectric layer at a position between the two electrodes, high current densities can be avoided, removing the formation of arcs and a transition towards undesirable localised thermal plasma operations. The insulating dielectric is often constructed of glass, quartz or ceramic material. (Fridman, 2008). The reactors can operate over a range of pressures, including atmospheric. The breakdown voltage (V_d) at which plasma is generated is dependent upon the dielectric material and thickness, and also the electrode distance gap. With a reduction in the gap, following the inverse relationship of distance to electric field strength, the breakdown voltage can be reduced. A typical, coaxial DBD design, used by Bogaerts et al. (2015) is shown in figure 2.21.

Figure 2.21: A typical DBD (coaxial) configuration, as used with experiments by Bogaerts et al. (2015)



Source: (Bogaerts, et al., 2015)

Micro-plasma DBD systems, with a gap of less than 1mm can be used to significantly reduce the voltage requirement and increase efficiencies. These reactors take advantage of their high surface area to volume ratio. At pressures above a few Torr the small gap results in a low breakdown voltage that obeying Paschen's law. With a small electrode gap, high electron densities can be achieved of up to 10^{17} cm^{-3} , which is similar to that of a semiconductors. However, with smaller gaps, the relative effect of the plasma walls and losses from recombination increase. The % of the sheath region with the plasma bulk also increases, which is significantly important for CO_2 gas dissociation. Power input is usually supplied by a high voltage AC input between 1-100 kV, as the DC input is shielded by the dielectric layer. Frequencies inputs are typically $\sim 60 \text{ kHz}$ for micro-plasmas, but for DBDs can be within a relative wide range of a few Hz up to MHz, generating electron energies in the range of 1-10 eV (Fridman, 2008). Scale up of DBD system is relatively straightforward and can use multiple banks of parallel reactors, with quite a high degree of flexibility in geometric shapes and configurations.

2.6.2.5 Early advances and limitations of CO_2 plasma chemistry

The dissociation of CO_2 in an endothermic plasma-chemical process is set out by Friedman and can be summarised as the following formula (Fridman, 2008).



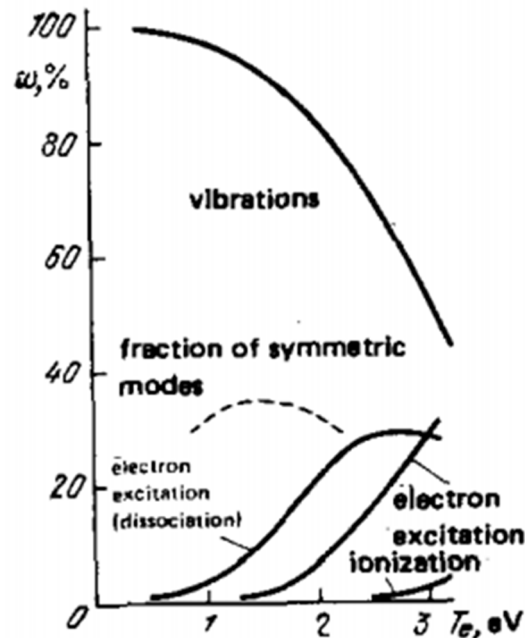
The equation 2.39 oversimplifies the process and causes some misunderstanding of the energy needed to first activate and conduct the dissociation process. The rate determining step is the C-O double bond breaking into $\text{CO}\cdot$ and atomic oxygen. This single oxygen atom can then either recombine with another single oxygen atom, or detach another oxygen atom from a passing carbon dioxide molecule.



The above formulas (Eq. 2.40, 2.41 and 2.42) do not provide all the mechanisms to CO_2 dissociation, but highlight that the minimum energy is $\geq 5.5 \text{ eV/mol}$ to initiate the dissociation. Often this leads to an excess of energy within the system, if electronic excitation is the primary discussions mechanism. This leads to low energy efficiencies. CO_2 plasma dissociation can be characterised by a compromise between high conversion rates and high conversion efficiencies. The two cannot exist simultaneously, given the current knowledge. The detailed study by Rusanov et al. (1981), identified vibrational excitation as the most energy efficient mechanism for CO_2 dissociation, as most of the energy can be transferred from the discharge energy without significant losses (Rusanov, et al., 1981). The theoretical maximum energy efficiency for CO_2

dissociation, within a quasi-equilibrium system, was determined as ~43%. Greater efficiencies can be achieved, by operation in a non-equilibrium condition that favours the most effective, vibrational excitation mechanisms. Vibrational excitation is the most dominant process below electron temperature of $T_e = 2$ eV, as described in figure 2.22.

Figure 2.22: Distribution of energy lost by electrons In CO₂ among excitation channels.



Source: (Rusanov, et al., 1981)

Whilst high energy efficiencies have been reached (80-90%) under supersonic flow rates, these are at very low conversion rates, too low for industrial application, and they have not been repeated (Fridman, 2008). Achieving a relatively high conversion rate within a DBD plasma of 35% corresponded to an efficiency of only 2% (Bogaerts, et al., 2015). Further detailed discussion on the mechanisms and the limitations of dissociation process of CO₂ will be evaluated in chapter 4, as well as investigations and experimentations, in attempt to overcome these barriers.

2.7 Critical analysis of literature and assessment of knowledge gaps

Following a full review of the available literature, it is possible to provide answers to the questions set out at the start of the review and to analyse the available literature for gaps within the knowledge. To recap:

1. Are there clearly defined solutions available to the existing steel industry decarbonisation challenge and does it warrant a complex steel plant techno-economics model and future simulation?
2. How have microbubbles previously been applied (specifically to the CO₂-NH₂-H₂O system)?
3. What is the current status of knowledge with regard to the dissociation of CO₂ with micro-plasma devices and can they be applied in a steel industry context to achieve decarbonisation?

Question 1: TEA of existing steel industry approaches

After following global developments within the area of steel production decarbonisation for more than a decade, clear research trends have emerged and the focus of the efforts have converged upon a narrowing field. The work can be categorised into either hydrogen-based steelmaking (H₂ DRI + EAF), or CCUS. There is still a large amount of research effort required to establish these technologies as common practice; to determine the correct technologies, configurations, products and to reach commercial scale.

Given the diversity and difficulty of decarbonising the steel sector there have appeared numerous projects, reports, roadmaps and demonstrations of new technologies, at various TRLs and budgets, and supported by individual businesses, consortiums and backed by respective Governments. Besides one DRI facility in Saudi Arabia using CCS for enhanced oil recovery (which, controversially, maybe classified as carbon sequestration) no other steel facility has yet managed to achieve deep decarbonisation. Whilst there exists a published techno-economic assessment, what we find missing in the available literature is any assessment of how a particular steel plant, from different global locations, may transition from their current operations to a low carbon position from now up to 2050 (Fishedick, et al., 2014). The most comprehensive attempt at a steel industry roadmap was carried out by EUROFER and the Boston Consulting Group (Eurofer The European Steel Association, 2013) (Schuler, et al., 2013). Both assessments utilised the same detailed techno-economic model, underpinned by the predicted availability of scrap. It assumed a generic ideal steel making facility for the whole of Europe. In practice, each steel facility in Europe will have different assets, geographical and regional political considerations, access to different low-carbon energy supplies and extremely varied product portfolios. This review, therefore, does not provide an effective roadmap that the industry can follow, identifying the

least-risk pathway, the potential to transition from one technology to the next, or addressing the current asset configuration or lifetime of the existing assets. A UK specific steel roadmap was produced, which does provide a more local view of the possible ideal steel facility, but again, this is not a regional approach and does not identify how a transition will be made (WSP, Parsons Brinckerhoff & DNV.GL (On behalf of DECC & BIS), 2015). A follow-up roadmap, available for all other UK industrial sectors, was never published.

Assessing gaps within the knowledge of decarbonisation options, it seems more work is needed for full chain LCAs. The COSRESYM project report provides a very good overview of the potential to deploy carbon utilisation technologies, with further work being carried out under current research activities (Metabolic, 2017). A successful LCA requires access to detailed and accurate data for the potential options and scenarios. Again, this is lacking, following only generic, road mapping exercises.

Ultimately, with the emergence of hydrogen featuring prominently in many steel companies low-carbon strategies, it is unclear how the industry will transition and weather fossil fuels (and CO₂) will still be present in future steel making. Having assessed the current publicly available knowledge, we find that to address the gap in the knowledge, the solution *is to develop a detailed steel plant technology roadmap and a techno-economic assessment*, using accurate steel plant data in order to evaluate the available decarbonisation options. This model will also provide a method of evaluating new technologies that could be applied to a future steel plant; one which aims to accurately compare the various transition pathways and technologies over time, up to 2050. At present, such a model does not exist. Without access to a single model it is not possible to evaluate the deployment of CCUS technologies to a future theoretical, low-carbon steelmaking facility. Therefore, a suitable model has been developed.

Question 2: Existing microbubble intensification approaches in the steel industry

Reviewing microbubble application, we find that there is ever increasing evidence of the benefits that microbubbles can bring to a variety of systems (Gilmour & Zimmerman, 2020), such as dramatically increasing the gas-liquid interface. At the time of testing, there had been no application of microbubbles to the CO₂-NH₃-H₂O system. Subsequently, the technology has been applied by The University of Sheffield, but specifically for NH₃ removal, within shallow liquid heights and low NH₃ concentrations (Desai, et al., 2020). Using the method described by Desai, et al. it would seem plausible the recovery of ammonia from waste waters is within reach. Microbubbles have not been applied for the purpose of CO₂ capture using NH₃ or enhanced ammonia salt production, which presents an opportunity to explore this area further.

Reviewing opportunities to decarbonise steel making, carbon capture features prominently in the literature, in past and current industrially driven research projects. Potentially liberating abundant

CO₂ which could be utilised for carbon derived products. The literature identifies fertiliser, specifically urea, as a key consumer of CO₂ and currently the greatest area for carbon utilisation (Aresta & Dibenedetto, 2007). Yet the urea production process is very energy intensive and corrosive. The work of Mani, et al. sets out an interesting pathway to fertilise routes at mild processes conditions (Mani, et al., 2006). Demonstrating that this low energy pathway could be possible if the system could be further enhanced. With both access to waste CO₂ and potentially recoverable ammonia from waste water as described by Desai et al, it seems the two maybe combined into a commercial process.

Within a steel plant context, there has been the application of aqueous ammonia capture at a steel facility (Han, et al., 2014). The technology seems well suited to the steel plant (BF) processes gas composition and provides an opportunity to reduce the overall capture cost. Yet, the system appears limited by the rate of CO₂ absorption and NH₃ losses. To reduce NH₃ losses, the systems have been operated at either low NH₃ concentration, which compounds the slow CO₂ absorption, or chilled conditions, which increases the energy demand and parasitic losses. Although trials of ammonia capture have been carried out at steel facilities, it would seem that some of the negative aspects of using ammonia as a capture solvent, which have been highlighted in the literature remain. Although the work in this area seems advanced, there is no indication that microbubbles have been applied to solve issues identified, which clearly represents an invitation to explore this further.

A combined microbubble-plasma system has been applied to upgrading of used oils, via bubble ozonolytic. Utilising the enhanced catalytic effect at the bubbles interface, (a so-called “phantom” catalyst or pseudo-catalyst) following the presence of plasma generated radicals, combined with an increase in interfacial area (Zimmerman & Kokoo, 2018). Plasma activation has also been applied to the concept of urea production at mild conditions, using a similar “phantom” catalyst approach, but not in conjunction with microbubbles. Xiang et al. (2012) applied a negative corona plasma discharge to synthesize urea at mild conditions. Using both gas phase CO₂ and NH₃, high (82%) conversion of CO₂ could be achieved without the presence of the usual metallic catalysis (Xiang, et al., 2012).

Given the review and analysis of the literature, it is therefore proposed *that highly efficient FO microbubble technology be applied to the CO₂-NH₃+H₂O system in conjunction with plasma activated CO₂*, to analyse the effect on the performance of CO₂ capture and potentially catalyse the ammonia salts production.

Question 3: Current status of plasma microreactor devices in steel industry decarbonisation

Within the literature it is clear that there remains significant challenges to the successful conversion of CO₂ via plasma chemistry. A review of DBD operations showed only an 8% energy

efficiency at very low conversion rates (Bogaerts, et al., 2015). Whilst high conversion rates of the CO₂ are not required for the CO₂ capture processes, such low energy efficiencies still represent a challenge for scale-up of this technology. Although there have been some innovative developments in fast quench microwave vortex approaches, the DBD design used within research has not changed significantly since the early work in the 80s (Bongers, et al., 2017). Theory suggests that a ~43% efficiency within a quasi-equilibrium system should be possible (Fridman, 2008). The gap between theory and experimental reality provides an opportunity for new innovation. By reviewing the dissociation mechanisms and potentially modifying the existing DBD reactor approaches, an improved reactor design should be possible. As the plasma devices are to be used with the application of the research posed in question 2, this might represent a considerable parasitic loss. Equally, splitting the CO₂ into CO and O₂ might represent an opportunity to further enhance the work carried out within the field of TGRBF, (Danloy, et al., 2009). Enhancing the system could potentially benefit both areas of research. The work carried out in the field of efficient, low energy plasma microreactor units with The University of Sheffield, suggests some innovation exists and that these concepts of plasma microreactor systems might be deployable to CO₂ dissociation (Lozano-Parada, & Zimmerman, 2010).

It is therefore proposed that to enhance the knowledge and application of CO₂ plasma chemistry, a detailed review of CO₂ plasma dissociation mechanisms is required to address the gap within low energy efficiencies and conversion rates, along with the proposal of a potential new plasma reactor design.

2.8 Formulation of hypothesis

The review of the publicly available literature has demonstrated three specific areas of research and knowledge gaps that can be addressed. To address these knowledge gaps requires three complementary hypotheses, which will be tested within the subsequent chapters: 3, 4 and 5. These seemingly independent hypotheses play an important role in moving each understanding forward, so that they may be successfully applied to determine a low-carbon steel making future: addressing capture, use or conversion of CO₂ and applying this to a future, hypothetical steel plant.

2.8.1 Hypothesis A

There is room for improvement within the energy intensive and commercial scale urea production process following high temperatures, pressures and corrosion. In addition, the aqueous ammonia capture systems, whilst promising, demonstrate two interconnected weaknesses: slow CO₂ absorption and NH₃ losses into the off-gas stream. Through the application of both microbubbles and plasma-assisted microbubbles, it should be possible to operate the first stage of the urea production process (carbamate production) at mild conditions (low temperature and pressure).

The enhanced gas-to-liquid interface, as a result of significant bubble surface area increase, will allow faster reaction kinetics. Also, the plasma excitation should amplify the pseudo-catalytic effect, so that greater carbamate yields at mild conditions are possible. Similarly, the microbubble properties will accelerate the absorption of CO₂ within the aqueous ammonia solution, overcoming one of the primary barriers to aqueous ammonia capture system, that is, the slow reaction kinetics.

2.8.2 Hypothesis B

There is an inverse relationship between CO₂ plasma conversion rate and efficiency and the current reactor designs do not lend themselves to the achievement of both simultaneously. Therefore, the mechanism to efficient CO₂ plasma dissociation will be studied in depth and a new reactor design will be developed, built and tested. The advantageous properties of the gliding arc plasma devices that lead to high efficiencies will be replicated within a more controlled DBD reactor concept. Separating the two reaction stages, into a high energy region followed by a subsequent low energy region, the two stages of CO₂ excitation will better align to the power input from the reactor, thereby limiting losses from over-energising the incoming CO₂ gas and increasing conversion efficiency.

2.8.3 Hypothesis C

To date, the analyses for a decarbonised steel plant focus upon the end point (2050) and utilise generic data sets for entire regions with multiple production sites. Because of this, they do not provide a clear view of how a steel plant may transition to a new technology, what the most significant considerations are, or how and where new technologies (such as those demonstrated within hypothesis A and B) could be applied within this transition. A new site-specific techno-economic model will be developed to facilitate the simulation of multiple future steel plant configurations. By simulating the transition of various technology pathways over time, the impact of the transition will be demonstrated. The correct pathway can be identified and the impact from each pathway, in relation to cash-flow and climate impact can be realised. This will mean the correct pathway, or actions to address this, will be visible.

2.9 Chapter summary

This chapter sets out the context of the research, by exploring the existing knowledge after identifying 3 research questions. The known steel making low carbon technologies and current research in this field are introduced. An introduction to fertiliser, as a potential for a CO₂ derived product is provided, as are the background and current application of two technologies, microbubbles and CO₂ plasma chemistry.

Analysis of the existing research identifies gaps in the knowledge that are both barriers to steel decarbonisation, yet present opportunities to enhance knowledge within the identified research areas. We find that whilst technologies for deep decarbonisation of the sector are known, the likely pathway to be taken is still unclear with many internal and external considerations still required. Although microbubbles have been applied to many areas of research, they have yet to be applied to a $\text{CO}_2\text{-NH}_3\text{+H}_2\text{O}$ system, as is the case for plasma active CO_2 . Also further development of CO_2 plasma reactors appears to be needed to overcome the trade-offs between conversion rate and efficiencies. Recognising these challenges and opportunities, three hypothesis are set.

Chapter 3

Investigations toward achieving higher kinetic rates for CO₂ uptake within aqueous ammonia, using plasma-assisted micro-bubbles

3.1 Introduction to chapter 3

From the literature analysis, it is clear that nitrogen containing fertilisers will still be needed in ever-greater quantities within a low-carbon future. Providing these essential products on a commercial scale with minimal impact on climate change will become increasingly important. An assessment of the literature identified a potential gap and opportunity to progress the knowledge within this research, by applying new technology. This research therefore aims to make a novel contribution towards the science and engineering fields, by utilising CO₂ that could be obtained from carbon intensive industry and operating an aqueous ammonia process at mild conditions, though the application of microbubbles and plasma assisted reactions.

Upon reviewing the literature, it also became evident that an aqueous ammonia-based CO₂ capture system would be highly applicable to the capture of industrial emissions. Given the focus of the research will be the application of these technologies within a steel plant and industrial context, the results will be evaluated for suitability of CO₂ capture performance, to demonstrate how the results could be used to determine success within carbon capture systems and application to industry. This will be analysed and discussed in this chapter (Chapter 3).

The follow experimental design will aim to test the influence from the application of the two technologies, microbubbles and plasma activation, whereby the focus is to generate maximum precipitate yields, exploiting maximum CO₂ capture, using two technologies for ultimate precipitate formation and CO₂ uptake. Thereby creating, for a given NH₃ concentration the maximum ammonia salts production and respective carbon captured.

3.2 Experimental design

Throughout this area of research I was fortunate to receive advice and assistance from both Dr Desai and Mr Campbell. Dr Desai assisted with the concept, for the application of microbubbles and plasma activation to carbon utilisation for ammonia production. Mr Campbell provided excellent assistance within the laboratory, setting up the experiments and analysis equipment as well partnering in the practical laboratory experiments. Both were helpful in the ongoing dialogue for reactor and experimental design considerations, improvements and fault analysis.

To test the two hypotheses expressed above, a laboratory scale reaction system was designed, constructed and experimental data obtained in a series of complimentary tests. The fertiliser production stages that were considered to be within scope are the initial reaction vessel whereby CO_2 is introduced into the aqueous ammonia solution and the following decomposition of ammonium carbamate and carbonate reaction. The subsequent recovery, recycling, concentration and prilling of a modern commercial scale urea production process were out of scope, as these stages would not be influenced by the presence of micro-bubbles or non-thermal plasma of the reaction vessel operated at mild conditions (Figure 3.1). The system therefore represents the more simplified once through urea production process, without recycling. This configuration, with precipitate formation stage, also closely mimics the CO_2 solvent capture stage in a CO_2 capture system, with the subsequent solvent regeneration and recycling also considered out of scope. Natural evolution of this work would be to expand the research to include a full chain integrated system, yet for the purpose of the research we focus our attention on the influence of the applied concepts on precipitate formation and upon CO_2 capture performance.

To test if either microbubbles or plasma assisted micro-bubbles have any influence upon the CO_2 - NH_3 reaction, a series of experiments to determine the effect of these variables were carried out. The 4 variations of the experiment relate to the introduction of CO_2 into the reaction vessel. These are:

1. CO_2 gas only (no external influence)
2. Generation of CO_2 gas microbubble using the fluidic oscillator (DZFO)
3. Activation of the CO_2 gas using a plasma reactor
4. Generation of microbubbles and activation of the CO_2 using both the DZFO and plasma reactor respectively

Essential features and components of the systems (as shown in diagram x) are:

- A. CO_2 gas supply – controlled by a mass flow controller
- B. Fluidic oscillator – to generate the pulsed flow needed for micro-bubble generation
- C. Plasma reactor and plasma reactor power supply

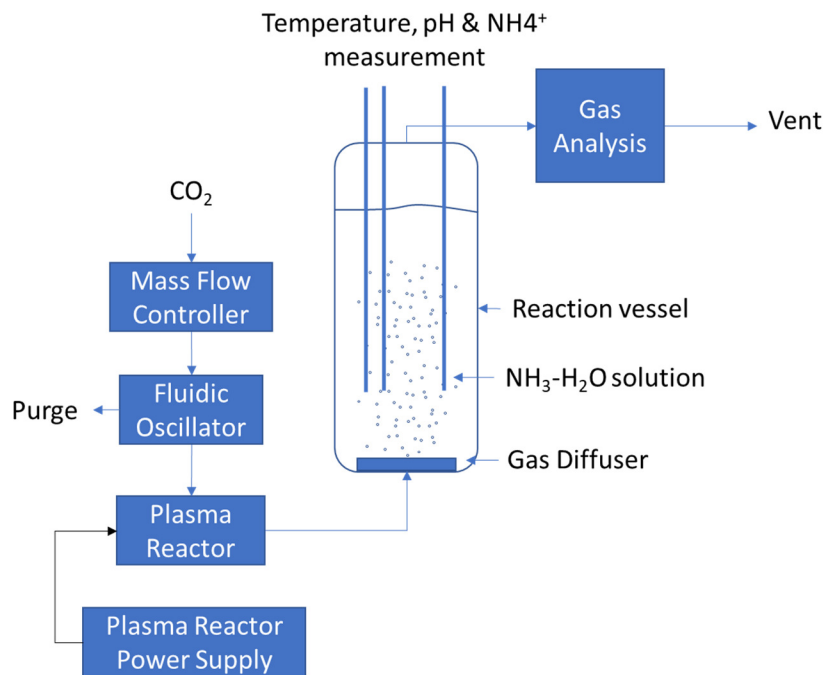
- D. Reaction vessel – constructed of glass with inlet at the base and outlet at the top, with vertical gas flow
- E. Gas diffuser – at the base of the reaction vessel
- F. Reactor exhaust gas analysis – monitoring of CO, and NH₃ gas concentration

The design of the CO₂ absorption reactor system is similar to the seminal CO₂-NH₃ study of Yeh and Bai (1999), Diao et al. (2004), Mani et al. (2006), and more recently, the work of Shuangchen et al. (2015), with complementary, additional real time analysis of the reaction vessel conditions to provide more information on the system performance.

The system incorporates the two technologies, DZFO and plasma reactor and is therefore very similar to the effective system used for biodiesel esterification, used by Zimmerman & Kokoo (2018).

An air-lift loop reactor design is not used for this system, but could be employed to improve mixing within the reactor.

Figure 3.1: Schematic of CO₂-NH₃-H₂O reactor configuration



To determine if microbubbles have an influence upon the system, an initial series of control tests were performed, with and without microbubbles. The parameters of these tests are shown in table 3-1. Following this series of tests, based upon initial process results, a factorial design testing schedule was implemented, to determine the influence of the 4 parameters. The upper and lower limits of the process variables are shown below in table 3-2, with the complete schedule shown in table 3-3.

Table 3-1: Control test parameters

| Variable | Value | Unit |
|--|-------|-------|
| CO ₂ Flow Rate | 1.2 | l/min |
| CO ₂ total volume | 40.5 | l |
| NH ₃ solution concentration | 13.3 | mol/l |
| NH ₃ solution volume | 0.25 | l |
| Experimental duration | 34 | min |

To represent the high NH₃ concentrations of a capture system for greatest CO₂ uptake and maximum production yield, a high concentration of 25% wt NH₃ is used. This is simply the concentration that the solution is supplied, with a specific gravity of 0.91 and a molarity of 13.3 mol/l. This is beyond the 20%wt expected to be used in a chilled ammonia process and above the 15% wt expected for unacceptable NH₃ loss in an un-cooled system. A second, low concentration is therefore also considered, at approximately ¼ the concentration of the supplied solution at a concentration of 3.3 mol/l to allow comparisons of both low and high NH₃ and the influence of NH₃ availability on CO₂ uptake and salts formation.

Each of the process variations run until completion, whereby maximum CO₂ uptake is achieved. An estimate of test duration, given the CO₂ and NH₃ molar ration, was determined to provide insight into the expected duration of each test. This method was chosen to maximise the production yield of ammonia salts and to stress the limitations of the system, to gain knowledge of the process boundaries and the point at which CO₂ uptake and the applied technologies are no longer effective.

Table 3-2: Upper and lower process variable limits

| Variable | Upper limit | Lower limit |
|--|--------------|-------------|
| Plasma Reactor | On (32 W) | Off (0 W) |
| CO ₂ Flow Rate | 0.8 (l/min) | 0.2 (l/min) |
| NH ₃ solution concentration | 13.3 (mol/l) | 3.2 (mol/l) |

Applying these upper and lower limits, we develop 8 potential variations of the process as shown in table 3-3. Each process variation is carried out in triplicate sets.

Table 3-3: Process variations

| Test Number | Plasma Reactor | DZFO Status | CO ₂ Flow Rate | NH ₃ concentration |
|-------------|----------------|-------------|---------------------------|-------------------------------|
| 1 | On | | Low | Low |
| 2 | On | | High | Low |
| 3 | On | | Low | High |
| 4 | On | | High | High |
| 5 | Off | | Low | Low |
| 6 | Off | | High | Low |
| 7 | Off | | Low | High |
| 8 | Off | | High | High |

3.2.1 Reaction vessel

The reaction vessel used for the aqueous ammonia reaction is shown below (figure 3.2). Adequate liquid height and headspace are needed for the full dissolution of the CO₂ gas within the bubble rise duration. Too short a height will result in ‘fizzing’ of the bubbles from the liquid surface as the bubbles burst, compounded by an increase in flow rate, bubble size, bubble kinetic energy and rise velocity. Bubbles bursting at the liquid surface and releasing their contents were discovered during microalgae-microbubble pilot trials at the Corus Steel plant, Scunthorpe power station (Zimmerman, et al., 2011). This process was discovered to be beneficial within this study, because the busting bubbles removed inhibitory oxygen. Short residence time and liquid height has also proven to be beneficial in the extraction of NH₃ from wastewater, utilising hot microbubbles (Desai, et al., 2020). This situation is to be avoided, so that excessive NH₃ slip into the off-gases does not occur (a recognised issue within aqueous ammonia CO₂ capture systems), therefore complete absorption of the bubble is favoured. A tall, thin (large height-to-diameter ratio) reaction vessel geometry is typical of urea and carbon capture systems.

A 100mm liquid volume was chosen for the reaction vessel. With an estimated rise velocity of 0.002 m/s, for a 100mm liquid height, a total rise time of 50 seconds is calculated. An L/d (length/diameter) ration in the range of $2 < L/d < 5$ is considered preferential within a bubble column reactor (Kantarci, et al., 2005). This liquid height provides an L/d of 2.12, within range. Gas holdup can also be present, below 100mm column diameters (Kantarci, et al., 2005). With a 47mm diameter, the influence of the reactor walls can be present, but gas holdup is not anticipated due to the use of microbubbles, with laminar flow.

The reaction vessel is sealed, along with the gas analysis, to avoid air ingress and interference with the system monitoring. It is operated at a slight positive pressure, following the steady injection of CO₂ into the system, so that no air ingress will occur.

The complete experimental set-up is shown in figure 3.3.

Figure 3.2: Reaction vessel dimensions

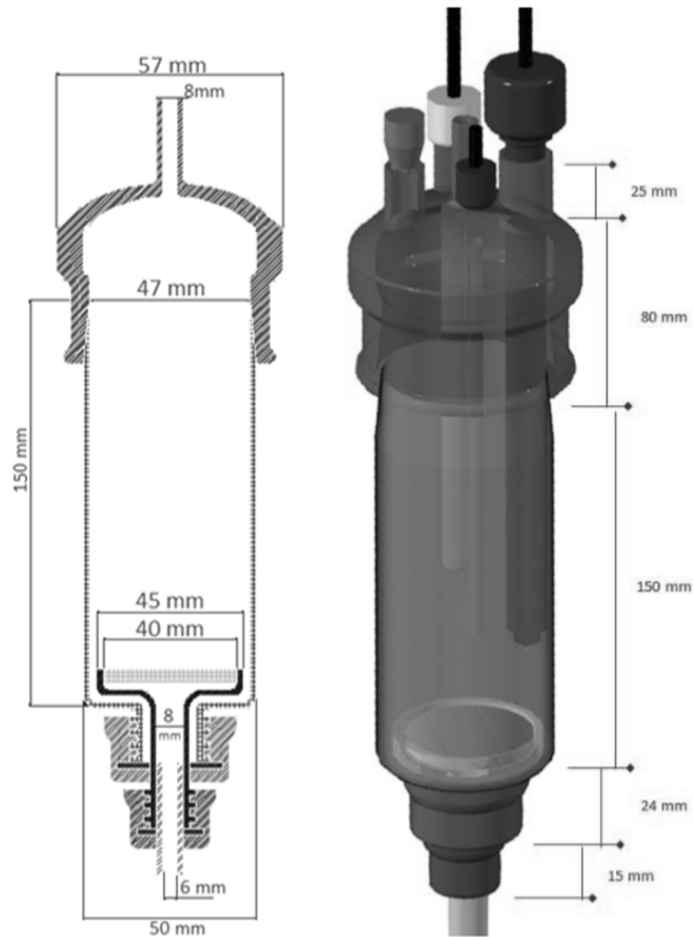
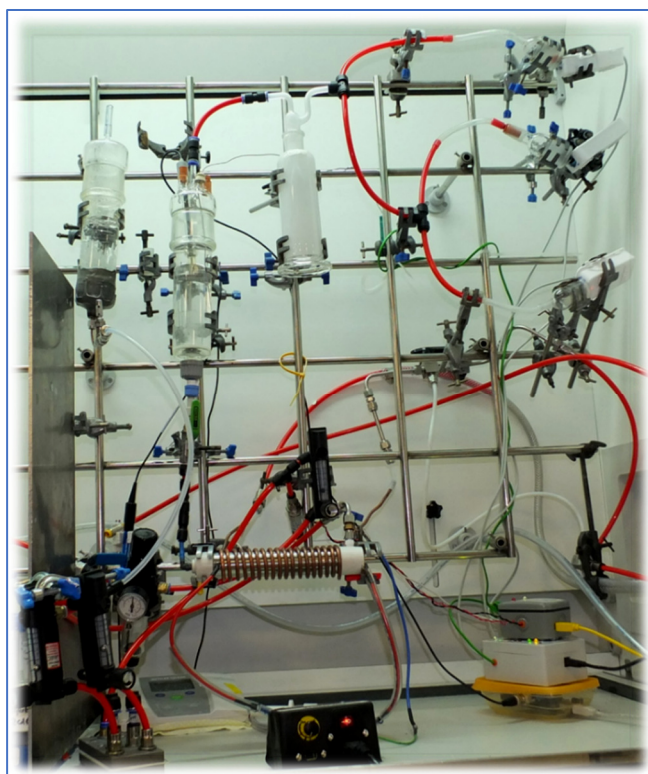


Figure 3.3: Complete experimental set-up



At the bottom of the reaction vessel, as shown in figure 3.2, is the gas diffuser. Along with the DZFO, this is an essential part of micro-bubble generation. A maximum off-the-shelf diffuser size of 40mm is allowed, due to the limited size of the reaction vessel. Maximising diffuser size to cover the floor of the vessel will produce the greatest density of bubbles and an even bubble distribution. The size of the pours of the diffuser has a twofold impact upon the bubble formation. First, depending upon the DZFO frequency, they ultimately limit the bubble size, and secondly the pressure drop increases across the diffuser with each respective reduction in pour size. Too high a pressure drop will limit flow rates and influence the DZFO operation, however too large a pour size, in order to reduce pressure drop, will increase the average size of the bubbles produced.

The maximum fluidic oscillation (FO) frequencies possible (when combined with the correct diffuser) have been shown to provide the smallest of bubbles, yet as this is the first application of this technology to the $\text{CO}_2\text{-NH}_3\text{-H}_2\text{O}$ system and proof of principle, pushing the boundaries of bubble size was not a priority. A previously proven resonance loop length was used (5 mm loop), providing a pulse frequency in the range of 100 to 150Hz. Following initial design experimentation, a gas diffuser with a pour diameter size range of 10-16 μm was chosen (Grade 4). This gives acceptable pressure drop for the expected flow rates and liquid volume height, with an estimated mean microbubble (Sauter) diameter of 52.5 μm and 9.0 μm for the high (0.8 l/min) and low CO_2 (0.2 l/min) flow rates respectively.

The gas flow from the DZFO is delivered in ‘plugs’ of consistent length and volume. The lower flow rates produce a smaller gas plug volume and plug length (0.02 cm³ and 0.11 cm), compared to the high flow rate (0.13 cm³ and 0.66 cm).

3.2.2 Plasma reactor characteristics and cooling system

The choice of plasma reactor and power supply are determined by the expected flow rate of the gas into the vessel. High flow rates lead to low residence times within the reactor, limiting the activation of the CO₂. Whilst various reactor designs are available, an ozone generator, DBD reactor was chosen as the borosilicate glass dielectric, had proven reliability and fitted the flow requirements. This design has a coiled electrode, which produces good results, without the high-streamer intensities of a mesh electrode design, which often produces hot-spots within the reactors and damages the glass. More detailed discussion of reactor properties will be discussed within research chapter 4. A variety of low-budget power supplies were obtained and tested for this purpose. All show remarkably good performance for the cost with good reliability, however the control of their output is limited, and the voltages and frequencies are fixed. A hybrid reactor was constructed, using an ozone specific power supply, from Dyden Aqua, which has power input control (but a high degree of reliability), combined with a longer reaction vessel, more suited to the longer residence times required for CO₂ activation. The geometry of the reactor is shown in table 3-4.

Table 3-4: DBD Reactor Critical Dimensions

| Effective Reactor Length | Gas Volume | Discharge Gap | Dielectric Thickness |
|---------------------------------|-----------------------|----------------------|-----------------------------|
| <i>Mm</i> | <i>cm³</i> | <i>mm</i> | <i>mm</i> |
| 209.97 | 35.2 | 1.89 | 1.11 |

The Specific Energy Inputs (SEI) and the residence time within the reactor are determined experimentally and are shown below in table 3-5. The Lissajous power figures are determined for each corresponding power settings for the chosen power supply and SEI are calculated at the flowrates for the chosen reactor. The plasma reactor is operated at 32W for the 24 variations, corresponding to an SEI of 2.39 J/cm³ and 23.89 J/cm³, for the high and low flow rates, respectively. This represents quite a significant difference between the activation levels.

SEI is defined using the following equation 3.1.

$$\text{Specific Energy Input (SEI), } (Jcm^{-3}) = \frac{\text{Plasma Power } (W \text{ or } Js^{-1})}{\text{Gas Flow Rate } (cm^3s^{-1})} \quad (\text{Eq. 3.1})$$

Table 3-5: SEI and residence time at high and low flow rates

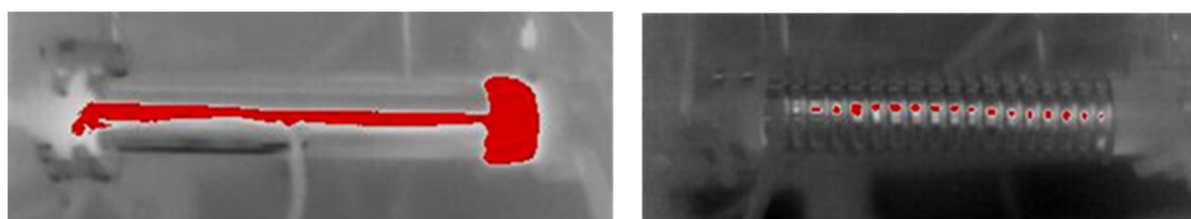
| Reactor Power | SEI High Flow Rate (0.8 l/min) | SEI Low Flow Rate (0.2 l/min) |
|----------------------|---|--|
| <i>W</i> | <i>J/cm³</i> | <i>J/cm³</i> |
| 10.01 | 0.75 | 30.03 |
| 31.85 | 2.39 | 23.89 |
| 54.20 | 4.07 | 162.60 |
| Residence Time (sec) | 3.1 | 12.4 |

Figure 3.4: Exposed (out case removed) plasma reactor core with spiral wire electrode design shown operating on the right, with a characteristic, violet plasma glow.



The plasma reactor produces heat during operation and will heat the incoming gases. Whilst this heat is advantageous to the kinetics of the reaction, it is not possible to compare the influence that the higher electron energies have, rather an increase in incoming gas temperature. It has also been demonstrated that hot microbubbles cause release of NH_3 from solution (Desai, et al., 2020). To limit the number of variables and to identify the possible effect of a “phantom” catalyst, a copper coiled reactor cooling system was designed, to limit the gas temperature increase. A once through coolant approach is used, by using adjacent potable water supply. The copper cooling coil can be seen in the reaction set up (figure 3.3). Commercial scale ozone generators are often operated within a water coolant jacket for increased reliability. Recovery of this heat may be desirable, so it might be that a full-scale system operates without cooling, if this does not impact reliability or increase NH_3 losses. A visual thermal analysis of the cooling system shows the influence of the cooling on the overall temperature distribution below in figure 3.5. Left image shows the uncooled reactor, compared to the cooled reactor on the right, showing only minimal heat from between the copper coils.

Figure 3.5: Thermal Imaging of reactor with and without copper coil cooling system



3.2.3 Influence of pH

With a transition towards greater acidity anticipated, following the absorption of CO₂, the pH of the aqueous ammonia solution will have a negative influence upon the total CO₂ uptake and the carbamate formation. Therefore, to maintain alkalinity, a sodium hydroxide (NaOH) solution is used for a selection of the tests (best and worst performing) to attempt to maintain a > 8 pH value. The NaOH should cause no influence on the CO₂ reaction, producing sodium cations and hydroxide anions. The initial 24 factorial experiments were operated without NaOH. The best and worst case experiments, were repeated with the addition of NaOH, to interoperate the influence of pH change on reaction performance.

3.2.4 Analysis methods

For the continuous, real time analysis of the reaction vessel, the temperature is measured for the vessel and the incoming and outgoing gases. Gases, NH₃ and CO will also be measured in the reactor off-gases. Continuous pH and ammonia measurement of the vessel are also recorded.

Data logging is performed by the use of custom Arduino hardware and programmed software.

Equipment used for the measurements are listed below (table 3-6). Measurement accuracy is not considered as critical as the ability to monitor the shift in trends between the variables. The monitors were considered to provide acceptable accuracy, with a fast response and with added benefits; that a customised analytical setup can be established, close to the outlet of the reactor, limiting losses and interference.

For the analysis of the precipitated solids and fractions, for the detection of ammonium carbamate, urea and carbonates generated within the reacted ammonia solution, post testing is analysed remotely, using C¹³ nuclear magnetic resonance (C-13 NMR).

Table 3-6: Reactor Measurement Equipment

| Parameter | Device (Source) | Method | Range |
|---|--|-----------------------------------|----------------------|
| Temperature (gas/liquid) | K-type with Max13855 amplifier | K-type | -200°C to 1,260°C |
| pH (liquid) | SG68 Seven Go Duo pro pH probe | | NA |
| CO (gas) | MQ7 (Winsen) | Heated conductivity element | 20-2000 ppm |
| NH ₃ (gas) | MQ135 (Winsen) | Heated conductivity element | 10-300 ppm |
| NH ₃ (gas) | TGS 826 (Figaro) | Electrochemical | 30-1000 ppm |
| NH ₄ ⁺ Ion (liquid) | Ion Specific Electrode (ISE) (Cole-Palmer) | | NA |
| NH ₂ COONH ₄ , (NH ₄) ₂ CO ₃ , NH ₄ HCO ₃ | Bruker AVANCE III HD spectrometer | C13 NRM | NA |

The expected products and intermediates all contain a single carbon atom, hence this is considered a reliable method and the spectrum will be easily defined, as there are not multiple carbon nuclei. This method is used by Mani et al., (2006) for the investigation into the effect of pH on the CO₂-NH₃ system and also Holmes et al., (1998). Whilst Mani et al. consider this method a reliable, tried and tested technique, Holmes et al., suggest a degree of caution and estimate the errors from such a method as 10.6% (ammonia carbonate), 7.5% (ammonia bicarbonate), 7% (ammonia carbamate). The fraction of production yields may therefore be treated with some consideration, but it is thought appropriate for comparison to previous work. The precipitated mass from each of the triplicate tests are combined and were sent for analysis. Between 175-250 mg of dried sample is required, which is later dissolved within 0.7 ml of D₂O.

3.3 Results

To establish the influence of fluidic oscillations, we first conducted experiments with and without the fluidic oscillator. The reactor vessel was operated with 250ml of NH₃ solution. Tests were operated at the high CO₂ flowrate of 1.2 l/min and high NH₃ concentration of 13.3 mol/l, so that the tests are neither CO₂ nor NH₃ limited.

An estimate of maximum precipitate mass production and duration to achieve maximum precipitated was determined, based upon the required CO₂ and flow rate. This determined the minimum estimated reaction duration. Reactions were run until maximum precipitate was formed and the vessel diffusers were no longer able to sustain gas flow, ensuring maximum CO₂ uptake and equilibrium was achieved and the limitations of the system were established.

Results for the initial control experiments are displayed within table 3-7.

The influence of the DZFO and reduced bubble size is clearly seen on the increase in total precipitate mass, but also a preference for increase carbamate production. Upon initial analysis, the use of plasma and DZFO provide preferential conditions for the production of carbamate. The quantity of precipitate produced, per litre of CO₂ supplied is also shown. With a significant difference between FO microbubbles and non-FO bubbles. These control tests appear to confirm the hypothesis, that microbubbles would increase salts formation and therefore CO₂ absorption. A further 24 experiments were conducted to conclude this theory.

Table 3-7:Control experiments, with and without plasma and microbubbles

| Test | Average Precipitate Mass | | | Carbonate/ Carbamate Ratio | CO ₂ (l) per gram of precipitate |
|-------------------------------|--------------------------|---------------|----------------|----------------------------------|---|
| | Total (g) | Carbamate (g) | Carbonates (g) | | |
| Grade 4 Diffuser only | 30.61 | 3.16 | 27.45 | 8.70 | 3.18 |
| DZFO only | 47.47 | 5.65 | 41.82 | 7.40 | 1.57 |
| Plasma activation only | 43.15 | 5.68 | 37.47 | 6.60 | 1.81 |
| DZFO and Plasma activation | 45.31 | 6.38 | 38.93 | 6.10 | 1.59 |

To narrow the operational parameters and optimise the carbamate and solids production, 8 test configurations are presented. We are reminded of the test number configuration again in table 3-8.

Table 3-8: Process variations

| Test Number | Plasma Reactor | CO ₂ Flow Rate | NH ₃ concentration |
|-------------|----------------|---------------------------|-------------------------------|
| 1 | On | Low | Low |
| 2 | On | High | Low |
| 3 | On | Low | High |
| 4 | On | High | High |
| 5 | Off | Low | Low |
| 6 | Off | High | Low |
| 7 | Off | Low | High |
| 8 | Off | High | High |

Following the completion of triplicate tests for each of the 8 configurations, the solids were sent for analysis. The total precipitate mass and the production of carbamate and carbonate as determined by C-13 NMR analysis is show in table 3-9. The C-13 NMR results analysis, confirmed that the final product is composed of mostly ammonium carbonate, with a smaller fraction of carbamate present, as demonstrated by the carbonate to carbamate ration.

Table 3-9: Total Precipitate Mass, Carbamate and Carbonate Production

| Test No. | Average Dry Precipitate Mass (g) | | | Standard Deviation | Carbonate/Carbamate Ratio |
|----------|----------------------------------|-------------|--------------|--------------------|---------------------------|
| | Total | Carbamate | Carbonates | | |
| 1 | 8.01 | 0.40 | 7.61 | 0.64 | 18.9 |
| 2 | 10.67 | 0.40 | 10.27 | 1.00 | 25.4 |
| 3 | 41.76 | 1.94 | 39.82 | 1.31 | 20.5 |
| 4 | 55.48 | 2.52 | 52.96 | 0.22 | 21 |
| 5 | 14.33 | 0.81 | 13.52 | 2.23 | 16.6 |
| 6 | 11.54 | 0.53 | 11.01 | 3.19 | 20.6 |
| 7 | 61.79 | 2.53 | 59.26 | 1.49 | 23.4 |
| 8 | 38.64 | 1.70 | 36.94 | 1.58 | 21.7 |

Test configuration 7, (plasma off/low CO₂ flow/high NH₃) produced the highest mass of total precipitate (61.8 g) and total carbamate formation (2.53 g) essential for the subsequent dehydration to urea. Configuration 5, again plasma off and low flowrate, but this time low NH₃ concentration, produced the highest % of carbamate with relation to total precipitate.

The critical parameters, % conversion of NH₃ to total mass precipitates, test duration (estimated duration) and standard deviations of the test durations (for the triplicate tests), peak reactor temperature and final reactor pH measurement are displayed below in table 3-10. As anticipated and predicted, the higher flow rates required significantly less reaction time to produce maximum precipitates. The total % precipitate is determined as a percentage of total precipitate that was produced, against the total mass of NH₃ within the reactor solution, if we assume all NH₃ is preferentially converted, within this system to ammonia carbamate. This yield would be lower if carbonate is formed, and lower still if bicarbonate is formed, due to their respective masses and utilisation of greater mols of CO₂ and H₂O. This result however, provides insight into how much of the NH₃ was utilised in product formation and how much is likely to remain unreacted. Due to reaction pathways and enthalpies, we expect carbamate to be formed first, prior to formation of bicarbonate and carbonate. The Error is determined as the % of the Standard Deviation between the triplicated tests as a function of the total precipitate mass produced. Most of the tests show good consistency, with only test 6 showing increased signs of deviation in mass precipitate produced.

Table 3-10: Results and estimated errors for the 8 test configurations

| Test No. | Total Precipitate | Error (St Dev as % of mass) | Final pH | Average Test Duration (estimate) | Test Duration St. Deviation | Maximum Temperature |
|-----------------|--------------------------|------------------------------------|-----------------|---|------------------------------------|----------------------------|
| | % | % | | <i>min</i> | <i>min</i> | <i>°C (min)</i> |
| 1 | 26 | 8 | 8.6 | 153 (49) | 7.64 | 33 |
| 2 | 34 | 9 | 8.4 | 55 (12) | 8.66 | 43 |
| 3 | 32 | 3 | 9.9 | 228 (203) | 12.58 | 37 |
| 4 | 43 | 0 | 9.6 | 86 (51) | 3.21 | 66 |
| 5 | 46 | 16 | 9.1 | 120 (49) | 5.00 | 38 |
| 6 | 37 | 28 | 9.1 | 29 (12) | 8.08 | 47 |
| 7 | 48 | 2 | 9.9 | 152 (203) | 7.64 | 59 |
| 8 | 30 | 4 | 9.7 | 58 (51) | 6.56 | 67 |

Whilst the higher concentration NH₃ solutions produced greater precipitate solids, this is to be expected from the increased NH₃ available in solution, therefore the percentage of the mass of NH₃ available, which has subsequently formed into precipitate, is presented. Test 7, once again, is clearly dominant in terms of effective CO₂ utilisation and precipitate formation. Also, test 7 was driven to completion, before the predicted end time, whereas the slower actual reaction durations were experienced for all other tests. Test duration standard deviation is calculated from the test termination time of the triplicate tests and are all within respectable limits. Of interest is also the variation from the stoichiometric assumptions and the quantity of CO₂ required to produce the precipitate. Presented in table 3-11 is the mass conversion of both carbamate and carbonate. The amount of CO₂ delivered to the reactor compared to stoichiometric calculations is provided, as well as the amount of CO₂ per gram of precipitate and plasma energy input. Once again, test 7 appears superior, in that the yields are dominant and the excess of CO₂ required is less than that calculated, determined from the estimated test duration, as a factor of CO₂ supplied per mass of NH₃. A summary is provided of the best and worst tests in table 3-12.

Table 3-11: Mass conversion, CO₂ excess, CO₂ per gram and plasma energy

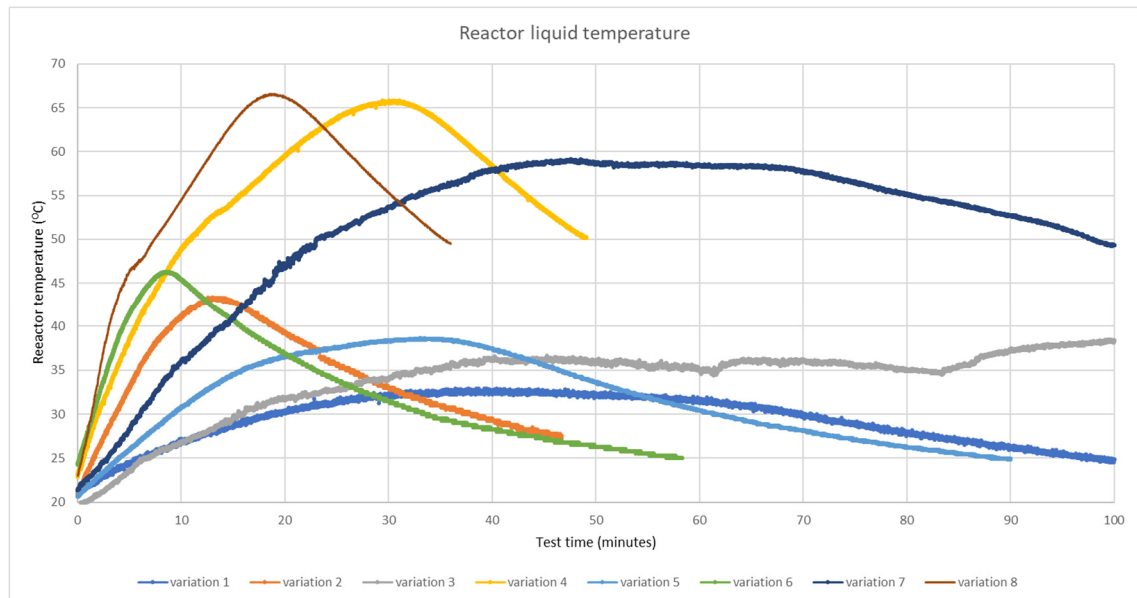
| Test No. | Mass Conversion | | CO ₂ Volume Excess | CO ₂ l/g of precipitate | Plasma Energy |
|----------|-----------------|--------------|----------------------------------|---------------------------------------|---------------|
| | Carbamate % | Carbonates % | | | |
| 1 | 26 | 21 | 215 | 3.83 | 588.8 |
| 2 | 34 | 28 | 352 | 4.12 | 211.2 |
| 3 | 32 | 26 | 13 | 1.09 | 876.8 |
| 4 | 43 | 35 | 71 | 1.24 | 331.5 |
| 5 | 46 | 37 | 146 | 1.67 | 0 |
| 6 | 37 | 30 | 135 | 1.99 | 0 |
| 7 | 48 | 39 | -25 | 0.46 | 0 |
| 8 | 30 | 24 | 15 | 1.20 | 0 |

Table 3-12: Comparison between best and worst tests configurations

| Test | Mass Conversion | | | CO ₂ l/g of precipitate |
|-----------------------|-----------------|-------------|--------------|------------------------------------|
| | Total (g) | Carbamate % | Carbonates % | l/g |
| Grade 4 Diffuser only | 30.61 | 24 | 19 | 3.18 |
| Test No 7 | 61.79 | 48 | 39 | 0.46 |

The rate of temperature increase within the vessel provides interesting insight into the reaction variations and the kinetics, shown in the chart in figure 3.6. Data for all of the real-time parameters are logged in 0.5 second intervals, providing very high resolution. The test with the highest flow rates shows the most rapid increase in temperature (2, 4, 6 and 8). Tests 4 and 8, both high flow rate and high NH₃ concentration, provide a rapid initial increase in temperatures and activity. Test 6 produces a high peak temperature very early in the process, reaching peak just after 8 minutes of operation, showing a rapid uptake of CO₂ given the very low NH₃ concentration. This soon drops, at a similar rate to test 2. Tests 1, 3, 5 and 7, all low flow rates, produce a steady increase in the reactor temperature.

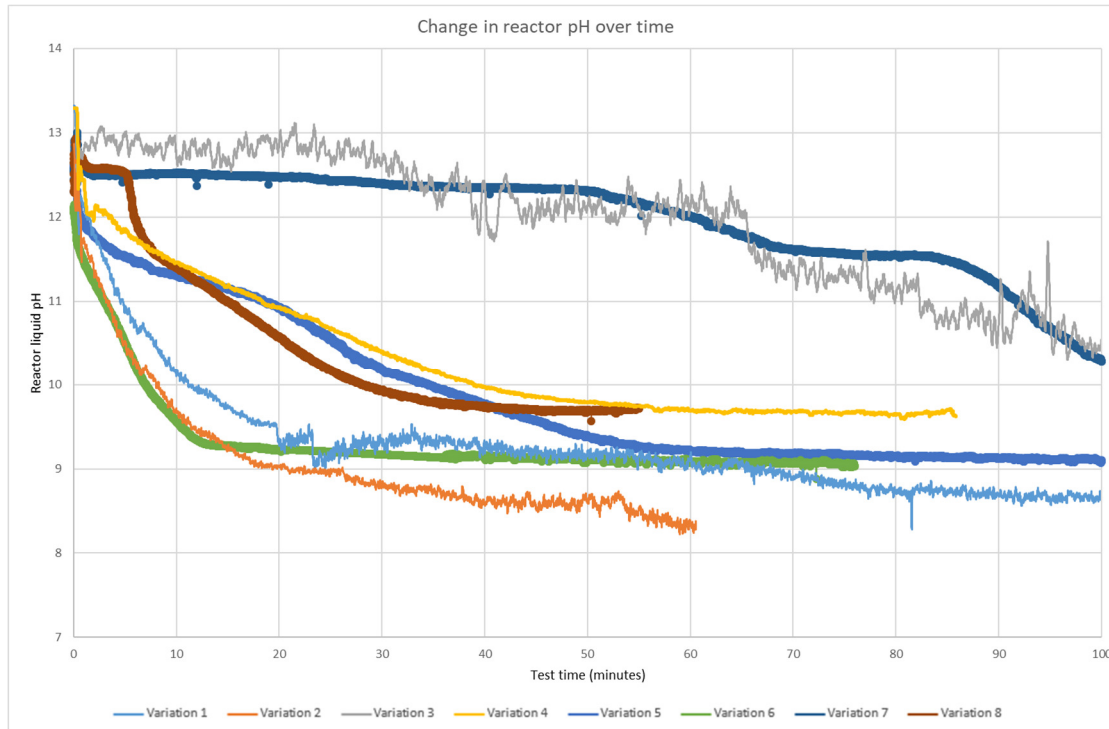
Figure 3.6: Reaction vessel temperature (average of the triplicate tests) over time for the 8 test configurations



The solution pH is well known to influence the CO₂ and NH₃ reaction. The continuous pH measurements, taken from within the vessel are shown in figure 3.7. We find that variation 3 and 7, both low CO₂ flow and high NH₃ concentration, produce remarkably better stability of pH over the test duration. Although the variability of the data points over this range is much greater for

test 3. This is believed to have been caused by the interference from the operating plasma reactor. We find that all the data for test variations 1 to 4 display a high degree of variability as a result of plasma reactor interference of the pH probe signal.

Figure 3.7: Reaction pH (average of the triplicate tests) over time for the 8 test configurations



Figures 3.8 and 3.9 shows the NH_3 concentrations within the off-gases from the reactor vessel, presented in ppm. The data is split into two charts (Tests 1, 2, 3 & 4 and Tests 5, 6, 7 & 8) for greater clarity of data and cut at 60 minutes, as there is no further significant variation within concentration, up to termination. It should be noted that, for the gas detection system design, a zero function was not available. Uncorrected logged data is presented. A zero figure is not acquired at the start of the testing, therefore a zero error of between 10-30ppm may be present, or as a result of interference. For the high flow rates and high concentrations (Tests 4 and 8), the NH_3 in the off-gases, following the peak in the reactor temperature, rises rapidly; up to ~140ppm. This signifies the limit of CO_2 uptake at these flow rates and saturation of the NH_3 solution and coincides with the peak temperature of the reaction vessel in figure 3.6. All other test cases show a more continuous trend throughout the test duration within the ~20-60 ppm range. Such a significant and consistent increase in NH_3 for these test cases provides greater confidence in the result and the ability to detect NH_3 presence in the off-gases, noting that it is more likely to under report the presence of NH_3 , especially due to its high solubility, if moisture is present.

Figure 3.8: Reactor exit gas NH₃ concentrations over time (Test variations 1 to 4)

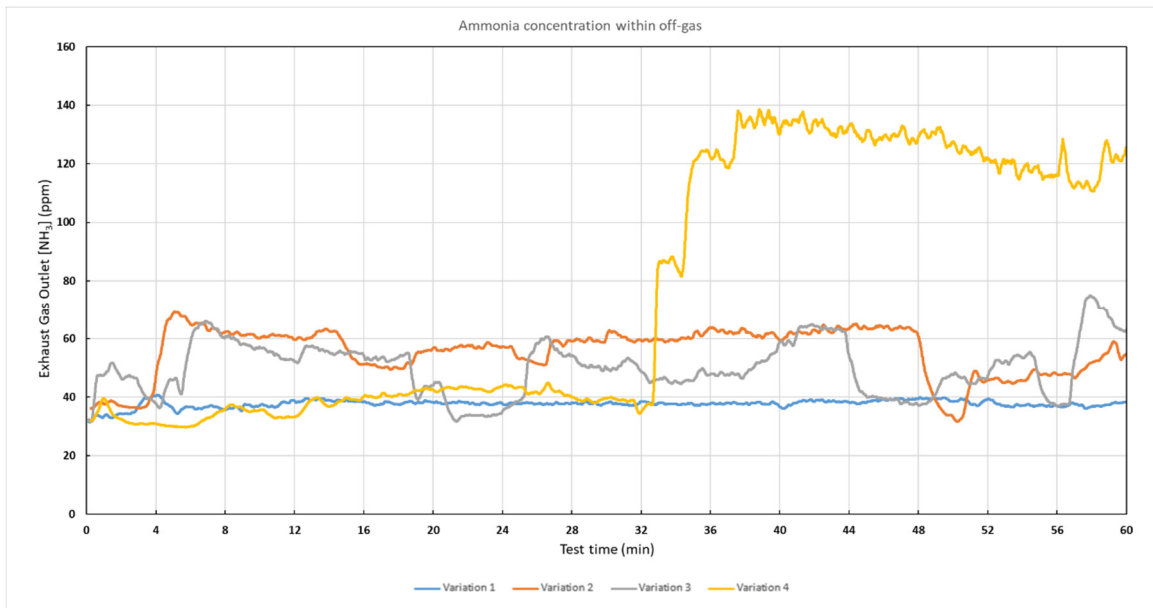
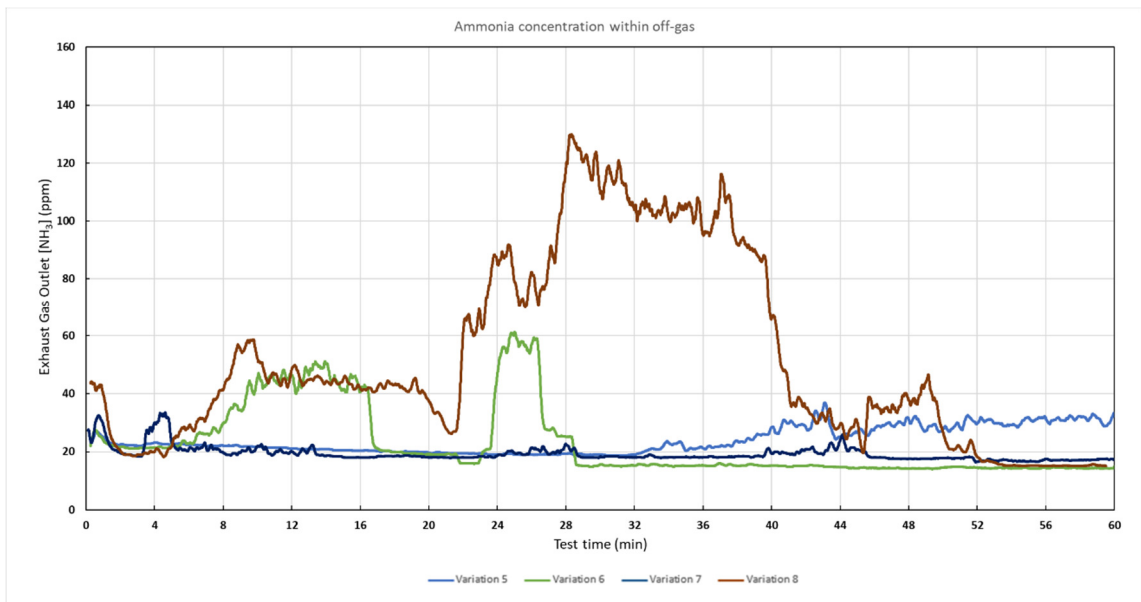


Figure 3.9: Reactor exit gas NH₃ concentrations over time (Test variations 5 to 8)



3.4 Analysis

3.4.1 Introduction

This chapter of research was carried out with the laboratory assistance of MEng student Lawrie Campbell. This work was conducted before the completion of the simulation results presented in research chapter 5. As such, the application of these discoveries to industry could not be fully evaluated and Campbell's interpretation of the results focuses upon the application of the findings to fertiliser production only (Campbell, 2016). Following this seminal work on the application of micro-bubbles to CO₂-NH₃-H₂O system, the University department has engaged in further work,

exploring these relationships and micro-bubble properties, which has confirmed some of the unique properties (Desai, et al., 2020). In the following section, we analyse the work of this pioneering study and the new discoveries made. Within this section we discuss the results that have been presented and consider how the applied technologies have influenced the reaction mechanisms. The implications and application of these discoveries are further assessed following the outcome of the techno-economic evaluation and are discussed within chapter 6.

3.4.2 Influence of NH₃ concentration

The tests were carried out at two molar concentrations, determined to cause either a lack of molecular NH₃, and thereby a restriction to the formation of precipitate, or high levels of NH₃ where we expect the availability of CO₂ and its uptake to cause the restriction.

The increase in molar NH₃ concentration in solution resulted in greater solids formation, but surprisingly no discernible increase in the stoichiometric conversion yields that were achieved, with test 5 operated at a low concentration, producing almost as high yields as the high concentration case, test 7. (46% and 48% carbamate conversion respectively). This would indicate that, in the lower concentration solutions, the availability of free ammonia is not the limiting factor in the total precipitated mass as similar yields are achieved for those with greater NH₃ available. The higher concentrations resulted in a more rapid increase in reactor temperature when at higher flow rates compared to the low flow conditions of similar concentrations. We can determine that the reactions are clearly CO₂ limited, not NH₃ limited at the higher concentration, as the low CO₂ flow rates all produce a very gradual temperature increase, with respect to the higher flow counterparts, even at the higher NH₃ concentrations. The lack of CO₂ molecules available within the higher concentrations is preventing a faster reaction response and it is not limited by the gas-to-liquid surface area, which has been maximised following the use of micro-bubbles. Given the data, there is no apparent advantage to operating with lean NH₃ solutions, in either the low or high flow rate scenarios for the maximum precipitate formation and therefore maximum uptake of CO₂.

Peak temperatures and the volume of CO₂ uptake at the peak time are displayed within table 3-13. Beyond the peak temperature, it is expected that the rate of CO₂ uptake is reduced, especially for the high flow rate tests. The maximum effective CO₂ uptake within the system has been reached. The precipitate formation turns the solution into a slurry after peak temperature is reached and at this point the effectiveness of the microbubbles is reduced and CO₂ uptake is limited by the solids within the solution. Test 7 contradicts the general trend, with a gradual temperature rise, and peak temperature is reached with relatively small volumes of CO₂, demonstrating the efficient use of CO₂. It should be noted that after the peak, temperature is does

not drop off rapidly for the low flow rates tests, demonstrating that the reactions are still taking place.

We find all experiments produced less precipitate than the stoichiometric value would suggest for total conversion of the available NH_3 , which would effectively be a 100% mass conversion. However, we must also note that industrial fertiliser processes do not produce high yields, even at optimised temperature and pressure, in the presence of a catalyst. A 60% mass conversion is expected to be the maximum urea formation for the single-pass process.

Table 3-13: Corresponding peak temperatures and CO_2 uptake

| Test No. | 1 | 2 | 3 | 4 | 5 | 6 | 7 | 8 |
|--|------|-------|-------|-------|------|------|------|------|
| Peak Temperature (°C) | 32.9 | 43.4 | 44.3 | 65.8 | 38.7 | 46.3 | 59.1 | 66.6 |
| Peak Time (min) | 36.5 | 12.6 | 139.8 | 30.1 | 33.0 | 8.3 | 47.6 | 14.8 |
| CO₂ Volume (l) | 7.29 | 10.08 | 27.96 | 24.07 | 6.61 | 6.63 | 9.51 | 18.5 |
| CO₂ per NH₃ (l/mol) | 2.28 | 3.15 | 2.10 | 1.81 | 2.06 | 2.07 | 0.72 | 1.11 |

All tests performed consistently between the triplicates, following a very similar temperature profile, except for test 3, which varied significantly. Temperatures for test 3 peaked at 75, 100 and 145 minutes, with all three demonstrating an early false peak of varying degree with a subsequent dip before the actual temperature peak. Test 3 has the same conditions as the dominating test case 7 (low flow, high NH_3), but with the additional plasma input. Whilst the temperature profile of test 3 varied considerably, the variation in the final mass of precipitates were within ~3 grams (3% error). A source of the variation has not yet been established, however, the dip within reaction vessel temperature resembles the work of Yeh and Bei (1999) for similar high concentrations (figure 3.11), which was not observed at the low concentrations. In these experiments, except for test 3 a second peak was not present when using only microbubbles under similar conditions to Yeh and Bei (1999), which could be attributed to the microbubbles favouring certain reaction pathways.

For CO_2 capture systems, it is widely considered that there is value in operating in the lean NH_3 conditions, to reduce NH_3 slip. A low NH_3 solution may, therefore, be a way forward, although this is not necessarily the case within this system, as will be discussed later, with regard to NH_3 slip. In Test 6, the temperature peaked at a respectable 8 minutes, so whilst the CO_2 residence time of a capture system would be high (resulting in larger reaction columns), a reduced NH_3 concentration may be applicable. Although, we should note that the higher NH_3 concentration, achieves the same temperature increase in half the time. The limit of NH_3 concentration was not determined, but as mentioned the reaction is likely CO_2 limited given the temperature trends.

Reviewing the literature for CO₂ capture systems, we find that with concentrations above 15%, the ammonia is said to volatilise from the solution (Liu, et al., 2009). At the higher test concentration (25%), we are likely to experience a loss of NH₃ gas from the experiments. Whilst NH₃ within the off-gases of these tests did not cause an issue, this would be a problem for scale-up and commercialisation as greater recovery of the NH₃ would be needed. Generating NH₃ on a commercial scale is carbon intensive, so losses would need to be minimised and recovery would add additional cost.

3.4.3 Effect of CO₂ flow rate

As discussed above, flow rate had a significant impact on the speed and temperature increase of the reaction. The high flow rate and high concentration scenarios tested in variation 6 produced the most rapid and highest peak temperatures. The rate of temperature loss from the vessel to the surrounding environment was not determined. The volume of CO₂ per mol (l/mol) at peak temperature ranges from 1.11 l/mol up to 3.15 l/mol. for the high flow rates. The limit of CO₂ flow rate was not determined experimentally. It could be that increased flow of CO₂ results in even greater CO₂ uptake within the initial reaction stage, however an excess of CO₂ could equally result in greater CO₂ slip and the need for subsequent reaction vessels upon scale up. Greater flow could also lead to increased NH₃ slip, certainly at the higher concentrations, as we will discuss later. Significant increase in flow, would result in escape of the bubbles from the vessel surface, before complete CO₂ absorption could be achieved. The experiments did not result in the excessive gas ‘fizzing’ from the reactor surface at the chosen flow rates, which were appropriate for the reactor height. A taller reaction vessel could be used to test the maximum CO₂ flow rates possible. Whilst the initial experiments, at an elevated flow rate of 1.2 l/min produced a better carbamate to carbonate ratio, the overall production of solids was not as high as the lower flow rates.

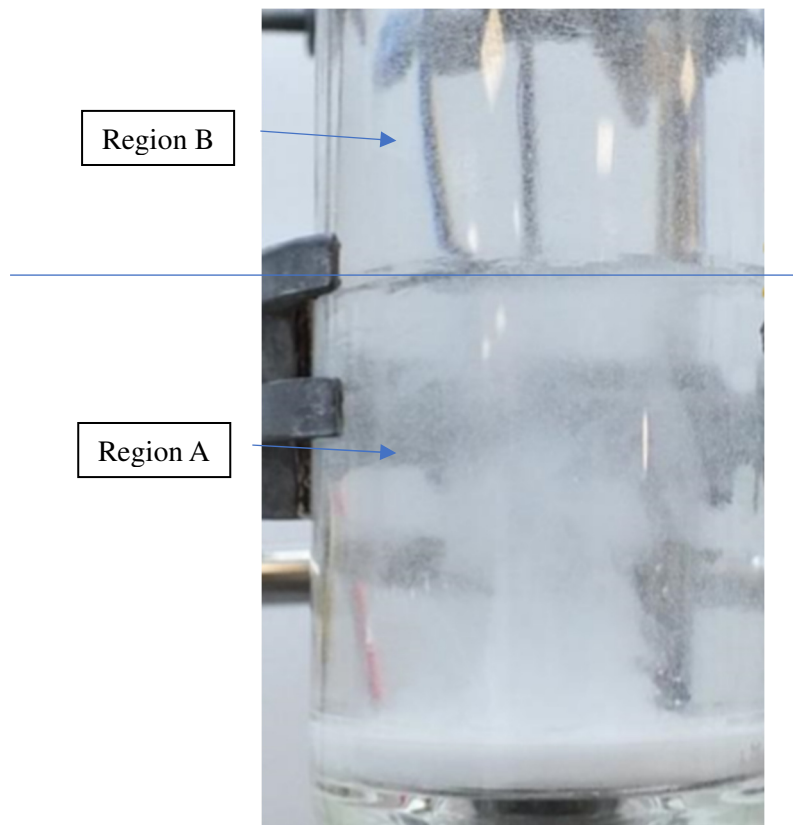
The low flow rate, combined with the higher NH₃ concentration demonstrated the greatest precipitate formation. The precipitate solids appear to form quickly at the diffuser surface, reaching saturation, with the precipitate solid high gradually rising as more CO₂ is injected and more NH₂ is reacted. Whilst the total speed of the reaction is CO₂ limited, this is not the case for total weight of precipitate and indeed carbamate formation. Therefore, a lower gas injection rate, combined with the increased residence time that this creates, is preferential for maximum carbamate and total solids formation. The fast flow rate could also produce the solid precipitate quicker, increasing the viscosity of the solution and solids in the earlier phase of the reaction, thus reducing the overall effectiveness of the reaction vessel and its current design as the diffuser becomes blocked from the solids formation preventing flow and bubble formation.

Bubble flow rate is also known to influence the bubble size and the rise rate. The bubble's Sauter diameter was calculated at 52.5 μm for the high flow rate of 0.8 l/min and 9.0 μm for the low CO_2 flow rate of 0.2 l/min. Therefore, decreasing the flow rate provides a greater gas-to-liquid surface area, potentially helping to promote greater solid formation. The smaller bubbles generated from the lower flow rate also caused product density separation during the course of the experiments for the low flow and high concentrations, 3 and 7. Taking note of the figure 3.10, an air-lift circulation was established within region A, with a central column of bubbles and returning wall flow was generated at the lower flow rates, upon hitting the change in fluid density in region B. The bubbles, upon contact with region B, either dropped at the walls or spread evenly across the separation and rose uniformly. The bubbles rose slowly within region B until they were completely absorbed within the solution. The size of region A increases, until B is no longer visible over the course of the ~2 hour experiments.

The separation of the fluid densities and two flow regimes indicate that the lower flow rates, at high concentrations, were not sufficient to cause complete mixing of the solution with the rising bubbles. Either a central column could be employed over a central diffuser to generate an air-lift reactor, or the reactor geometry could be changed so that it is wider and shorter, yet the shorter vessels could result in bubbles breaking the surface and loss of gas. It may be that the results could be improved further if better mixing was established in the low flow, high concentration experiments as the separation in layers will likely inhibit the product formation as region A is expected to have a greater concentration of precipitate.

Interestingly, we did not observe the laminar flow regime after the diffuser as expected within test 7, but we do experience laminar flow within the top region B.

Figure 3.10: Flow rate influence on bubble generation at high NH_3 concentrations, test case number 7.



Data from the control experiment, operated at an elevated flow of 1.2 and following calculation of the efficiency of CO_2 uptake, based upon the stoichiometric estimates, indicate that further increase in CO_2 flow rate would result in greater CO_2 loss and result in no greater uptake of CO_2 . For the NH_3 concentrations, we can say that the limit of CO_2 flow is reached, without resulting in greater system losses for this reactor design. The amount of excess CO_2 molecules supplied to the system that did not result in precipitate formation are greater at the low NH_3 concentrations, such that they are not absorbed within the solutions. At a high flow rate and low concentration, a CO_2 excess of 352% and 135% are calculated, against an excess of 13% and -25% for the other extreme, low flow rate and high concentration. At both high flow and high concentrations (tests 4 and 8), a CO_2 excess of 71% and 15% are required to reach CO_2 saturation, with 215% and 146% excess (tests 1 and 5) for the low flow rate and low concentration (table 3-11).

The greater excess of CO_2 required to drive the reaction to completion suggests that the CO_2 will be escaping from the reactor surface before complete absorption can take place, which would not be ideal for a capture process and require recycling of the CO_2 gas. In contrast, the separation seen in test 7 (figure 3.10) showed that the bubbles were fully absorbed before they exited the surface of the solutions. Increasing flow rate, without increasing the reactor volume and residence

time, would only allow greater quantities of CO₂ to escape from the solution surface, therefore we can assume that maximum CO₂ uptake has been achieved for this reactor design.

At the low flow rate, test 7 demonstrated remarkable CO₂ efficiency, producing significantly more precipitate per l of CO₂. Only **0.46 l of CO₂ per gram (l/g)** of solid precipitate was required, compared to the **3.18 l/g** without FO bubbles. This demonstrates that the use of microbubbles at the lower flow rates results in maximum CO₂ efficiency, with very little CO₂ escaping the system.

3.4.4 Effect of non-thermal plasma CO₂ activation

The operational plasma reactor system resulted in a maximum 5°C increase in input gas temperature, with the plasma reactor cooling system operational. The data showed that the influence of the plasma-activated CO₂ on the precipitate formation was limited and, in general, reduced the precipitate mass. The average precipitate mass produced was reduced by 10%. There was no clear correlation with the rapid decrease in pH with the plasma reactor operational. With all plasma-activated cases a delay in the peak temperature occurred, demonstrating that potentially the speed of reaction kinetics was influenced and reduced, or different pathways were favoured. It is worth noting that the exact pathways to CO₂ uptake is still under debate.

The plasma reactor SEI at the fixed power input changes significantly for the high and low flow rates (an SEI of 2.39 J/cm³ and 23.89 J/cm³, for the high and low flow rates, respectively). The activation level, therefore, for the low flow rates is anticipated to be much higher, however, given competing mechanisms, it is not clear how this influences the reactions from the data that was obtained. This is likely due to competing mechanisms at play.

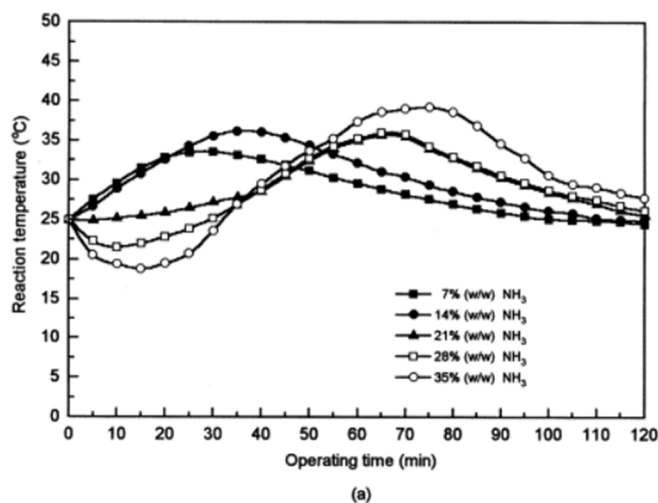
It was anticipated that the plasma activation of the gas would further catalyse the CO₂ absorption and salts formation. Equally charged gas bubbles could repel one another, preventing coalescences and maintaining bubble size. CO₂ as a polar molecule with two exposed electron pairs at the microbubble-liquid interface, the electronegativity of the charged surface of the microbubble could catalyse the reaction upon entering the fluid environment. While these mechanisms may or may not have been at play, they did not result in increased yields, suggesting that a stronger, counteractive mechanism is also present.

It is possible that there are a number of mechanisms at play that would cause the decrease in precipitate and delay in temperature peak. Within the higher CO₂ flow rates, where we do not expect to be CO₂ limited, there was also a reduction in precipitate formation with the plasma reactors on. To explain the decreased reaction kinetics, we could conclude that the presence of additional CO and O₂ within the activated gas as a result of CO₂ dissociation could hinder the reaction kinetics. The additional vibrational electron energy present in the bubble, expected from the plasma activation, did not materialise as an increase in reaction kinetics or precipitate formation. It could not be determined if this may have been as a result of the presence of CO and

O₂, not necessarily reacting themselves with the NH₃, but following their creation, reducing the amount of CO₂ present. Analysis of the post-reactor gas data showed no significant variation in the CO content of gas exiting the reactor with or without the plasma-activation. An excess of CO does not look to be the cause of the variance, although the CO could be consumed within the solution, yet at a slower rate. O₂ was not measured and could be the reason for the variance with plasma reactor on versus off. Yet, the literature suggests O₂ should not cause the degradation of aqueous ammonia, hence these systems would be preferable to conventional Amine capture when O₂ is present.

At the lower concentrations, Yeh and Bai (1999) demonstrated that the reactions are dominated by exothermal reactions, whereas at the higher concentrations, the reactions comprise a series of endothermal–exothermal reactions (Yeh & Bai, 1999). These pathways are not well understood and indeed, in the literature analysis only exothermic pathways are expected to be dominant. It maybe that, under the influence of plasma activation, the endothermal reactions become more dominant, and resist the temperature increase.

Figure 3.11: Temperate increase with respect to NH₃ weight% at 2 l/min (16% CO₂ concentration)



Source: (Yeh & Bai, 1999)

The activation of CO₂ from plasma electrons is known to decrease rapidly and could likely have returned back to ground state, having lost its energy to its environment within one second (Aerts, et al., 2015). Placing the plasma reactor directly at the base of the diffuser would be needed to test this theory, however, for practical design considerations and also safety reasons, this was not possible. A stop valve was needed to prevent fluid flowing back into the plasma reactor and great care was taken to ensure positive pressure remained at all times during operation, to prevent a reverse flow into the plasma reactor. Incorporation of the plasma reactor into the reaction vessel may be feasible, but will need a redesign and some ingenuity, as it was not thought possible to

operate this safely. As the bubbles need to flow upwards, naturally the reactor is placed below the vessel, and so ingress (reverse flow) of the NH_3 solution can occur if gas flow is not present, so start up and shut down of the system is difficult without a form of isolation. This leads to a longer than ideal pipework between the plasma reactor and the diffuser and a higher chance that the activated CO_2 will decay back to ground state. Under these conditions, it is likely that only the dissociated CO , O_2 and bulk CO_2 will be present within the reactor.

If the CO and O_2 within the bubble is not fixed to the NH_3 within the solutions, it is plausible that they attach to the free ammonia (particularly at an elevated temperature and under some slight activation / energetic and pseudo-catalytic bubble surface) and remove the NH_3 from the solution within the exhaust gases. If the molecules have not yet decayed back to ground state, their energies could cause the NH_3 within the solution to be more readily vaporised and result in the increased NH_3 loss from the reactor. This would likely be the case for a hot gas bubble, so an energetic (high electron temperature) CO_2 microbubble may have the same result. The benefits of the microbubble, discussed next, are therefore reduced, as the NH_3 is more likely to gain energy from the plasma activated gas bubble, to isolate the NH_3 within the solutions and raise the temperature beyond the vapourisation point, which is very low for NH_3 (-33°C), leading to greater losses. It could be that under these assumptions, a combination of a hot and plasma activated CO_2 bubble could lead to effective NH_3 stripping for water treatment, but for these conditions (greater CO_2 uptake) we wish to reduce NH_3 vaporisation as much as possible.

The NH_3 exhaust data appears to confirm this hypothesis, with test 1 to 4 all demonstrating greater ppm of NH_3 detected in the gas outlets. Typically $\geq 40\text{ppm}$, compared to below 40ppm for the non-activated tests 5 to 8.

Under the current process configuration, the additional 3-33 kJ expended per gram of precipitate when using a plasma device does not seem justifiable. The exact reasons why the addition of a plasma reactor prior to the NH_3 reactor would, in these experiments, hinder the precipitate formation is not fully clear from these results and certainly warrants further investigation.

3.4.5 Influence of micro-bubbles

Incorporation of the DZFO was shown, during the initial experiments, to have a significant increase in precipitate formation, increasing precipitate mass by 55%. Clearly the influence of the smaller bubbles and increased available liquid-to-gas interaction allowed the maximum uptake of CO₂ within the available ammonia solution. Even greater is the effectiveness of CO₂ utilisation. Only 0.46l of CO₂ per gram of solid precipitate was required for test case 7, compared to the 3.18 l/g without FO bubbles.

Further optimisation of the processes identified that, whilst the plasma activation had no discernible influence, reducing flow caused a significant increase in precipitate mass yields. A significant increase in over 60% (an increase from 30% to 48%) is experienced with a reduction in flow rate from 0.8 l/min to 0.2 l/min at the higher NH₃ concentrations.

Whilst the kinetics of the reaction in the early reaction stages are CO₂ limited at the lower flow rates (as shown by the slow temperature increases), an excess of CO₂ is used within all (except for test case 7) experiments and the test are run for longer at the lower flow rates to ensure that a maximum CO₂ uptake limit is achieved. It is understood that the decrease in flow rate coincides with a reduction in bubble diameter, from 52.5µm to 9.0µm for the lower flow rate. This reduction in bubble size, and relative bubble surface area, could be attributed to the increase in precipitate formation.

It is known that at the higher concentrations of NH₃, greater than 15%, it's likely that the NH₃ will volatilise and result in losses, but at the lower flows and smaller bubble sizes it was observed that all the CO₂ gas was absorbed into the solution and no bubbles are escaping the surface. The micro-bubbles are therefore likely to reduce the volatilisation and loss of NH₃ as the rising bubbles are not carrying the NH₃ into the reactor exit gases when they break the surface. It is possible that the increase in precipitate formation as a result of the smaller micro-bubble diameter, achieved at a reduced flow rate, is because more of the NH₃ is still present in the reactor vessel and has not been lost in the off-gases, so is viable for the precipitate reaction. Reducing NH₃ losses to maximise CO₂ uptake and precipitate formation is likely the key to the micro-bubbles success and essential for scale-up of a CO₂ capture system.

Analysing the NH₃ concentration in the reactor exit gases, we see that there is a significant increase in ppm for the high concentration and high flow rates, which also correlates with passing the peak in temperature. Once peak temperature is achieved, maximum CO₂ uptake is expected to no longer be sustained within the solution and the CO₂ starts to pick up NH₃ within the exiting gases. This results in a loss of usable NH₃ from the system.

To summarise, the influence of reducing bubble size are:

- a) Slow bubble rise velocity, leading longer residence times
- b) Increased bubble surface area, increasing the gas to liquid interface
- c) Reduction of NH_3 loss processes from NH_3 vaporisation
- d) Greater precipitate formation, in comparison to non-FO fine bubbles
- e) Much greater effective use of CO_2 per gram of product
- f) Unusual separation characteristic of the fluid at low flow and high concentrations

It would be possible to decrease the bubble size further, with an increase in FO operational frequency optimisation, combined with a smaller pore size diffuser and a removing of FO dampening to prevent back flow. The benefits of such a diameter reduction, could yield greater performance.

The significance of this discovery and its application to carbon capture systems in the steel sector will be discussed in detail in Chapter 6.

3.4.6 Changes in reaction pH

The changes in pH align well with the literature and allow confidence in the results obtained and the rate and quantities of CO_2 uptake. The pH decreases proportionally due to the rate of CO_2 absorption, which is the major contributing factor to the pH decline (figure 3.7).

An addition of NaOH (30ml of 8.5 mol/l to the 205ml of NH_3 solution) was made to the reaction vessels for the best and worst-case variations, 7 and 6. Little change in reaction performance could be attributed to the addition of NaOH. The best case, test 7, and also similar parameter test 3, both with high NH_3 concentrations and low flow rates, showed the most gradual change in pH from the initial ~13pH to 10pH. Whilst variation 3 had a similar rate of pH decline, it did not exhibit the same precipitate yields. We can therefore conclude from these results that the influence of the plasma reactor has a much greater negative effect on performance than the rate of pH change. The interference to the signal of the pH meter corresponds to the power on of the plasma reactor, causing interference with the signal of the pH meter. It is also likely that the NH_3 loss from the vessel, as a result of vessel temperature increase, again has a more profound impact upon total precipitate formation and the effective total CO_2 capture capacity than the pH in these test cases. Under a continuous operation, controlling the pH is likely to become a more significant factor in the system performance.

3.4.7 Yields of carbamate to carbonates

Whilst there are some discrepancies in the literature over the reaction pathways and dominating mechanisms, we might have expected a higher ratio of carbamate to carbonates than achieved. It is unclear if the reaction system causes a preferential reaction pathway to occur. It is possible to

attribute discrepancies in carbamate production to the analytical method, rather than the reaction system, or interpretation of the C_{13} - NMR spectra. Following preparation of the precipitate samples with dilution into deuterated water, this action is likely to promote the reverse formation of carbamate into carbonate to maintain equilibrium.

Within a urea production process, this parameter is critical, as carbamate is the precursor to the urea formation. With a CO_2 capture system, the mechanisms for carbamate formation are less of a concern and the primary objective is effective capture, regeneration and limited solvent loss. Given the potential issues surrounding carbamate losses from the C-13 NMR analysis method, it was chosen not to draw too much conclusions from the yield analysis within this study, due to potential errors. This does not detract from the conclusion on system performance and significantly, we do find much greater yield obtained compared to the literature (Mani, et al., 2006) within microbubble ammonia salt formation, both within these experiments, and subsequent experiments conducted by MSc students, used to validate these results.

3.4.8 Reaction kinetics

The experiments were not designed to specifically determine the reaction kinetics, following the use of a batch reactor system without a controlled temperature and/or consistent pH. Even so, the temperature profile (rate of temperature increase), the NH_4^+ ion ratio and change in pH all give insight into the reaction kinetics and the speed of CO_2 uptake in the solution.

Although the Cole-Parmer ammonium ISE probe used to determine NH_4^+ within the solutions demonstrated good response within the calibrations tests (13.2 and 3.2 mol/l were determined from electrical conductivity responses of 10.54 and 20.96 mV respectively), it did not perform as anticipated during the series of tests. Results of NH_4^+ ion are not in line with those of the calibration and electrical conductivity is limited to a range of 1.6 to 4.3 mV.

The potential reasons for this discrepancy could be:

1. A probe fault
2. External interference, either to the signal or the probe detection
3. The reaction mechanisms generating NH_4^+ does not dominate and so little is detected
4. The rate of NH_4^+ uptake is fast and results in little free NH_4^+ within the solution

Whilst the ion ratio data obtained during the experiments was evaluated, we find that the ISE probe within these tests did not function as expected, nor with the liner trend as it did within the calibration experiments, potentially following some interference or malfunction. Repeating the experiments, but with a focus on the kinetic regime and species formation, would be advantageous. The data was considered unreliable and therefore such calculations were not presented. The presence of NH_4^+ is, expected to increase, with an equal ratio of decreasing NH_3 ,

with a reduction in pH. Whilst this may be the case, only a small increase in electrical conductivity was noted with decreasing pH, as a result of the absorbed CO₂. Presumably this is again due to the presence of precipitate salts interfering with the ISE probe.

We may also find that some other microbubble phenomena are at play, with the generation of the bubbles influencing the charge at the bubbles' surface. Given the sensitivity of the probe to very small deviations in electrical conductivity (10.54 and 20.96 mV was the expected range), it might be that the presence of the bubbles prevented accurate measurement, certainly if surrounding or attracted to the ion probe, possibly changing the homogenous nature of the solution at the probe surface.

Looking towards the literature for a previous assessment of the kinetics, we find a large discrepancy in the consensus for reaction pathways. This is likely following the idealised systems that are considered, to simplify the determination of the parameters. It would appear that the influence of NH₃ concentration, temperature, pressure and pH all play a part in changing the pathways and mechanisms, which vary over the course of the reaction as temperature. We find that the temperature increases and the pH decreases as more CO₂ is input into the system, as expected, but this yields a change in kinetics that is most likely non-linear.

If we look toward the results obtained, at the lower flow rates, as we have discussed, the temperature increase was much lower, showing that the availability of CO₂ was the limiting factor in the reaction rate. Limiting the available CO₂ prevented an early temperature peak and also resulted in the overall increase in precipitate formation. Limiting the reaction in this way had a positive impact on precipitate formation, potentially by a reduction in the bubble size and the NH₃ losses in the off-gas. What is not clear is why the lower flow rate produced a preferential formation of carbamate to carbonate, by limiting the availability of CO₂ and the temperature increase.

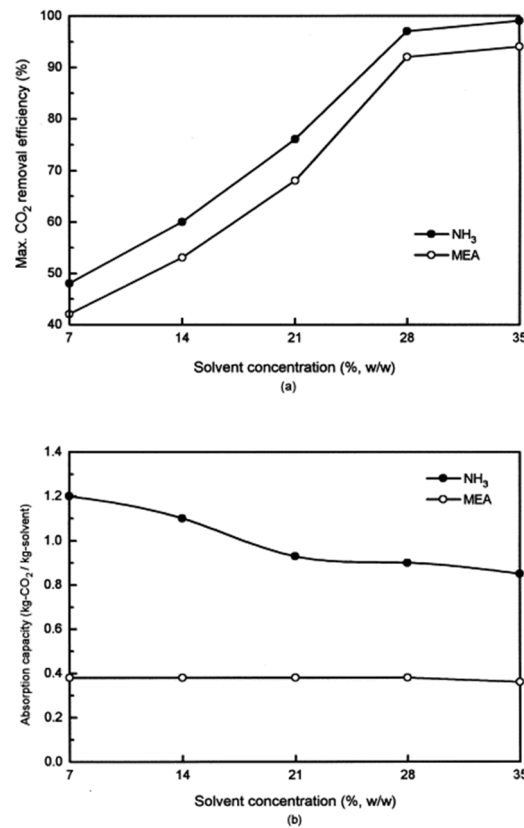
By increasing the gas-to-liquid surface area from the incorporation of a smaller bubble diameter, we would expect the kinetics of the reaction to be quicker for a given volume of CO₂ gas. The speed of the reaction was not a focus of the tests, however, fast CO₂ uptake is advantageous for scale-up and would reduce the reactor vessel size for a given volume of gas. CO₂ capture systems are known to be very large at an industrial scale, so minimising the footprint would be valuable. The work of Yeh and Bei (1999) concludes that a CO₂ loading of between 1.2 kg CO₂/kg NH₃ (lean NH₃ solvent concentration of 7% w/w) and 0.85 kg CO₂/kg NH₃ (rich NH₃ solvent concentration of 35% w/w) can be achieved. This is significantly higher than for an MEA solvent, typically 0.38–0.36 kg CO₂/kg MEA in either rich or lean solvent concentrations. Greater than NH₃ 28% (w/w) was required for >95% capture efficiency. Only <50% capture efficiency was observed for the lean 7% NH₃ concentrations in their work. With CO₂ breakthrough (the point at

which CO₂ is no longer effectively captured) ranging from 20 minutes up to 3 hours. Although specific breakthrough times are not presented within the work of Yeh and Bei (1999), test case 6 presented in this study showed that similar CO₂ loading for a lean solvent (0.89 kg CO₂/kg NH₃ for ~6% w/w) can be achieved within only 8 minutes. This corresponds to the peak temperature being reached, a reduction in CO₂ uptake resulting in higher NH₃ losses into the off-gases. We can therefore conclude that the slow CO₂ uptake that is considered prohibitive for capture processes at the lower NH₃ concentrations, can easily be overcome with the incorporations of microbubbles and that high CO₂ loadings can be achieved within <10 minutes of reaction time. It was concluded, by Yeh and Bei (1999) that CO₂ concentration did not influence CO₂ uptake and therefore the results were not presented. It is possible, that their reaction system is limited, not by CO₂ concentration, but the gas-to-liquid surface area, which is overcome using the microbubble, hence high CO₂ loadings can be achieved within short durations. Under test case 3 and 6, a CO₂ loading of 1.2 kg CO₂/kg NH₃, is achieved within 11.1 minutes, with little increase in NH₃ loss, up to termination. The absorption capacity, and removal efficiency, for increasing NH₃ concentrations, as determined by Yeh and Bei (1999) are displayed for comparison in figure 3.12.

Whilst the smaller bubble will increase the rate of CO₂ uptake, it is not considered possible to exceed the maximum CO₂ loading much above 1.2 kg CO₂/kg NH₃, demonstrated in the literature, due to physical stoichiometric limitation and the formation of solids preventing effective bubble formation. Greater CO₂ loadings would not be considered advantageous for the solvent regeneration processes within a capture facility.

For the lower flow rate used in the test, the surface area of the bubble did not limit the reaction only the availability of the CO₂ molecule, as previously described, hence the bubble dimensions had limited influence on the rate of CO₂ uptake within the low flow regime. These dimensions did play a significant influence on product yield and effective CO₂ utilisation. Noting the significance of this discovery, an optimisation process is needed to determine the CO₂ breakthrough point, for various NH₃ concentrations and flowrates, to optimise the capture performance under the influence of microbubbles, whereby CO₂ availability is no longer the limiting factor.

Figure 3.12: The removal efficiency and absorption capacity for increasing NH₃ concentrations



Source: (Yeh & Bai, 1999)

3.4.9 NH₃ loss

Increasing the concentration of NH₃ within the solution will lead to faster absorption of CO₂ (at high flow rates), as shown by the more rapid temperature increases and reduced residence times and reactor size. Yet, above 15% NH₃ concentration the NH₃ slip increases rapidly following NH₃ vaporisation. Ammonia boils at a very low temperature of $-33.3\text{ }^{\circ}\text{C}$ ($-27.94\text{ }^{\circ}\text{F}$) STP, yet its high solubility ensures that it is equilibrate in water and that increases in temperature of the bulk liquid do not yield high NH₃ removal.

Instead the bubbles released from the liquid surface, containing unreacted components, will strip the NH₃ from the solution. This has been shown to be a highly effective technique when using a hot microbubble and very small liquid depths (Desai, et al., 2020). At the suggested 15% weight concentration, this corresponds to 8.4 mol/l. Under the experimental test conditions, CO₂ capture was performed under a low and high concentration, corresponding to 25% (13.3 mol/l) and 5.4% (3.2 mol/l).

For the test conducted at the high ammonia concentration (tests 3, 4, 7 & 8), pH is high, ~13.0 pH, with few ammonium ions expected to be present. The maximum recorded concentrations in

the gas are displayed in table 3-14 in ppm and mg/m³. At >140ppm for high flow rates tests 4 and 8, this represents significant loss of NH₃ from the reactor vessel. The NH₃ monitors were not zeroed with NH₃ gas, which could represent a significant uncertainty in the measurement. The trends however, do show the point at when concentrations start to increase.

Table 3-14: Peak concentrations of NH₃ gas measured in the reactor flue off-gases

| Test Number | 1 | 2 | 3 | 4 | 5 | 6 | 7 | 8 |
|--|-------|-------|-------|---------------|-------|-------|-------|---------------|
| ppm NH₃ | 41.00 | 70.50 | 75.67 | 149.00 | 39.33 | 67.50 | 36.67 | 143.00 |
| mg/m³ NH₃ | 28.56 | 49.11 | 52.71 | 103.79 | 27.40 | 47.02 | 25.54 | 99.61 |

At the higher concentration and higher flow, a greater response in temperature increase was witnessed, with an earlier peak indicating the fast uptake of CO₂ that is desirable. Unfortunately, once the peak temperature is reached under these conditions, and the solutions moves towards CO₂ saturation, NH₃ slip into the reactor exit gases is witnessed for the higher flow rates. Within the tests, this resulted in an overall reduction in precipitate formation, following the losses of NH₃. As a result, the high concentration and high flow rates results in NH₃ stripping before maximum CO₂ loadings can be achieved. We can conclude that, if the residence times are kept to ~20minutes, no significant increase in NH₃ slip will occur for the high flow and high NH₃ concentrations, which corresponds to a respectable 0.52 kg CO₂/kg NH₃ loading without plasma activation. Within a continuous system, the solvent would be recycled once saturated and regenerated solvent will be continuously fed into the system avoiding saturation and the peak witnessed at >20 minutes. By employing micro-bubbles into the capture system, we have effectively increased the available surface area of the reactants, allowing greater uptake of CO₂ into the solution. This reduces the volume of CO₂ breaking the solvent surface and carrying vaporised NH₃ with it.

With low flow rates, and still high concentrations in test case 7, no temperature peak was established and there was no discernible NH₃ slip, even considering the high NH₃ concentration. However, given the low flow rates, high CO₂ loadings are not achieved. Average ppm for the full test duration for test 7 is 18.5 ppm and at its peak only reached 37ppm. This resulted in the best precipitate yields, following maximum CO₂ uptake and minimal loss of NH₃. The tests ran until completion, testing the limitation of the system, whereby precipitate blocked the diffusers and therefore no-more CO₂ could be captured. The combination of low flow and microbubbles allows all the CO₂ to be captured, without resulting in major NH₃ loss.

Reviewing the temperature profiles and the influence of microbubbles, we know that keeping the temperature low (0-20°C) to reduce vaporisation of the aqueous ammonia into ammonia gas is the method employed by Alstom/GE. However, by using micro-bubbles, the temperature peaked

at 66°C for the high flow rates and afterwards this led to a loss of NH₃. Prior to the peak, even though the temperature of the reactor was high, no significant slip (greater than average 60ppm) was apparent, even though the temperature was well above 20°C. The slip occurred as the temperature dropped and CO₂ was no longer being captured by the solutions due to saturation, showing the influence of CO₂ saturation is much greater than the vessel temperature for NH₃ loss when micro-bubbles are used. Within test case 7, a peak temperature of 58°C was achieved, without significant loss of NH₃ as evident from the gas data and solids formation based upon stoichiometric yield estimates. From this assessment we can say that, so long as the solution does not become CO₂ saturated, the microbubbles do not cause significant vaporisation of the NH₃ within the solution, even at temperatures up to 58°C. By replacing the CO₂ rich capture solvent with a constant regenerated lean solvent, saturation should not occur and the system, by employing microbubbles, can operate effectively beyond 20°C without significant NH₃ slip. Operating at reactor temperatures up to 50°C would also allow significant heat retention to drive the solvent regenerations stage and lower overall energy usage.

We can conclude that under the correct flow conditions and residence times prior to saturation (<20 mins) microbubbles can be used to increase CO₂ uptake, whilst reducing NH₃ losses for higher NH₃ solvent concentrations, greater than 15%. For a CO₂ capture system, low concentrations are desirable to prevent NH₃ loss, but this limits the capture performance following slow reaction rates and removal efficiency. Utilising the microbubbles, we can achieve high rates of CO₂ uptake, whilst using low NH₃ concentrations, preventing NH₃ losses as the NH₃ remains within the solution. Also, high reactor temperatures do not result in an increase in NH₃ losses when utilising microbubbles, contradictory to the chilled ammonia process. Only CO₂ loading and NH₃ concentration influence the loss of NH₃ from the system.

3.4.10 Experimental Errors

A great deal of the experimental output is highly reliant upon the accuracy of the detection methods. Personal experience with a wide range of analytic methods, techniques and equipment, often operated in hostile steel process environments, has provided an appreciation of the difficulties in acquiring accurate data, without loss or interference. General consensus is to over-estimate the accuracy of a measurement technique. Care must be taken when interpreting results, so not to jump to conclusions.

There are clearly some anomalies with the data acquired, and we certainly cannot assume any research data is 100% accurate. The main conclusions and analysis of the results are drawn from the most reliable of measurements, that is, the gas flow rate, the NH₃ concentration, the temperatures profiles and total precipitate mass measurements. Losses and overestimates

(creation of more heat and precipitate) within these two measurements are unlikely. With a good degree of certainty, we can conclude the maximum precipitate mass.

With the speciation of the products and expected yields, the results do not correlate well with the literature, but that is to say, the literature is also somewhat contradictory. The use of C-13 NMR was chosen due to the availability of the equipment and apparent suitability for the species of interest. It is understood that future work will target more accurate measurements of this parameter, hence we have not drawn too many conclusions upon the ability to produce commercial scale urea from this process, which is reliant upon the high yields of carbamate. In the preparation of the samples for C₁₃-NMR, a 250 mg of dehydrated precipitate sample is than dissolved in 0.7 ml of deuterated water. It is likely that this action will cause the loss of carbamate, given the high solid to solvent ratio. In order to maintain equilibrium, the carbonates fraction must increase.

The calibration of the equipment showed an acceptable level of response to a change in environment, yet under the process operations, we find that the NH₄⁺ ion probe did not provide an accurate response in line with the expected results, either due to salts present, unexpected reaction pathways or interference. Similarly, the pH probe demonstrates obvious interference with the plasma reactor operational, yet this does not detract from the overall trend, showing the risk in taking spot samples. This has led to some issues with the kinetics estimates as described.

Acquiring a homogenous or representative sample for the entire system is also a potentially large source of error, not accounted for in the instrumental or analytical equipment specification error, resolution or response. Ensuring a homogenous (or representative if homogeneity is not feasible) point is measured within the reactor is a source of error, as we find for the low flow experiments. As the total reactor solution is dried and weighed, we can assume this is not an issue for the total precipitate mass, rather losses of precipitate are much more likely. Hence greater confidence can be applied to these mass results.

A rather inexpensive and customisable form of gas detection is used, so that the detection is placed as close to the outlet as possible for fast response and to cause limited interference with the vessel and operating pressures. The electrochemical cell used (TGS 826 Figaro) according to specification is considered very sensitive to NH₃ with a fast response time. This type of analysis is also known for interference with other species and can deteriorate at high exposures over prolonged periods, so should be regularly replaced, given their low cost. NO_x, for example, is commonly known to cause interference with NH₃ detection. Within the pure CO₂ experiments from the literature review, we do not expect NO_x formation, yet this could be possible under the correct conditions. Detection systems were modified to provide a hermetically sealed system. We can be reasonably confident with this result as the sealed vessel is at a slight positive pressure

and therefore unlikely to have ingress, and the inputs (NH₃-H₂O-CO₂) are carefully controlled. In any case, the likelihood with all gas detection is that the species of interest are lost and a reduced value is reported rather than over-reported, especially in the case of soluble gases, hence some analysis equipment is heated to beyond the dew point. No moisture vapour was seen collecting in the off-gases tubing, but this does not rule out NH₃ present within the vapour phase due to its high solubility. In this instance, a loss of NH₃ would provide a false positive and underreport of NH₃ slip, with the influence of the microbubble enhanced.

Given these errors, we can be confident in the variation of the data sets between testing scenarios, but we must maintain caution when comparing the data with literature, in which case every effort should be made to produce the most accurate data possible.

An estimate of the analytic errors is made below (tables 3-15 and 3-16). Note that for the precipitate mass, temperature profile, pH and NH₃ concentration, from which we are able to determine the most significant findings, we find acceptable errors. Further work is needed to improve the NH₄⁺ sensitivity and the speciation of the precipitate.

Table 3-15: Error estimate for precipitate mass calculation

| Mass Measurement | Measurement technique graduation | Estimated error range (+/-) | Average measurement value | % error estimate (+/-) |
|-------------------------------|----------------------------------|-----------------------------|---------------------------|------------------------|
| Reactor volume | 2 ml | 2 ml | 250 | 0.80% |
| Flow rate | 0.05 l | 0.05 l | 0.8 | 6.25% |
| Mass filtration losses | - | 2 g | 60 | 3.33% |
| Weight | 0.0001 g | 0.001 g | 60 | 0.002% |
| C13-NMR speciation | 20 | 20 | 250 | 8.00% |
| Total % Error Estimate | | | | 18.4% |

Table 3-16: Error estimate for reactor vessel conditions monitoring

| Mass Measurement | Measurement technique graduation | Estimated error range (+/-) | Average measurement value | % error estimate (+/-) |
|------------------------------|----------------------------------|-----------------------------|---------------------------|------------------------|
| Temperature | 0.01 °C | 0.01 °C | 50 | 0.02% |
| Gas analysis | 0.01 ppm | 0.1 ppm | 50 | 0.02% |
| pH | 0.01 pH | 0.1 pH | 12 | 0.83% |
| NH ₄ ⁺ | 0.01 mV | 0.1 mol | 4.5 | 2.22% |

3.5 Chapter 3 summary

In a series of test configurations, plasma activated CO₂ microbubbles were applied to an aqueous ammonia system. The aim, *that highly efficient FO microbubble technology be applied to the CO₂-NH₃+H₂O system in conjunction with plasma activated CO₂* has been achieved. In doing so, the discoveries made have confirmed most of Hypothesis A. That the application of microbubbles, will lead to enhanced kinetics and rate of CO₂ uptake. It did not however, confirm that the addition of the plasma reactor further catalysed the reaction, possibly due to the enhancement of competing mechanisms.

In test case 7, under a low flow rate (0.2 l/min) and high NH₃ concentration (13.3 mol/l), high product yields were achieved. A 50% increase in precipitate yield was achieved, compared to tests without FO bubbles. (61.76 g and 30.61 g respectively). It is believed that high yields were obtained, as the NH₃ losses from the process were minimised, under the influence of microbubbles and a very high percentage of the incoming CO₂ was absorbed within the solution. A remarkable CO₂ utilisation efficiency was achieved under the same test scenario, consuming only 0.46 l CO₂/g, compared to 3.18 l CO₂/g for the non-FO bubbles. This demonstrates that the CO₂ entering the system was effectively absorbed within the NH₃ solution when utilising microbubbles.

A high CO₂ loading of 0.9 kg CO₂ / kg NH₃, (MEA solvent is typically 0.4 kg CO₂ / kg MEA) can be achieved within a period of 8 minutes for a relatively lean capture solvent (test case 6). This corresponds to the vessel temperature peak and results in no significant increase in NH₃ losses. Also, the vessel can operate at elevated temperatures, under the influence of microbubbles (>45°C), without demonstrating an increase in NH₃ losses, providing an opportunity for enhanced heat integrations, to lower the energy burden for solvent regeneration.

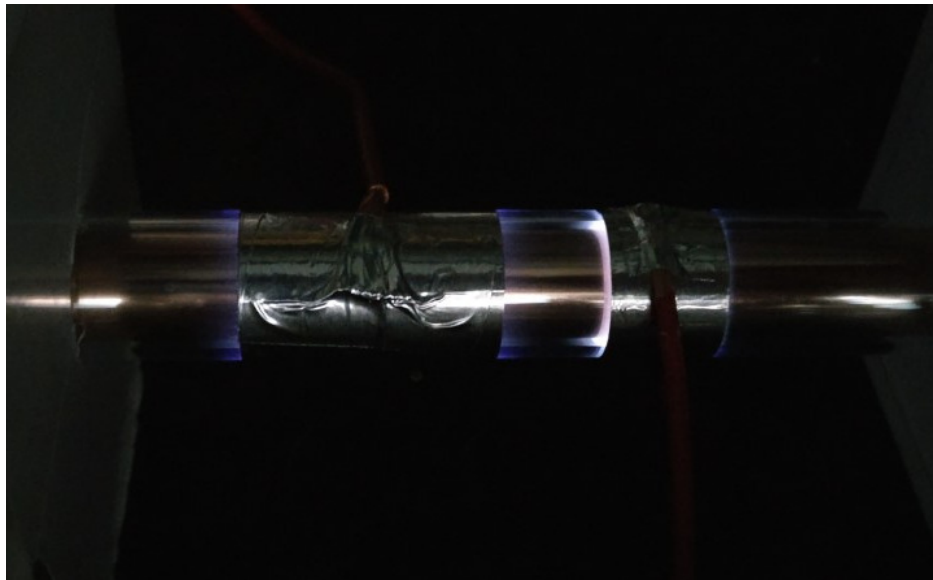
The plasma activation did not result in the predicted enhanced catalytic effect at the bubble surface. It was observed that the influence of the plasma reactor was a delay in the temperature peak, potentially favouring endothermic reaction pathways. Also, the plasma activation resulted in greater NH₃ loss from the system (an increase of ~20ppm), resulting in lower precipitate yields.

The application of these discoveries will be further assessed within chapter 6.

Chapter 4

The development of a breakthrough concept to high conversion efficiency plasma CO₂ dissociation

Figure 4.1: Operational, twin-plasma reactor design with visibly high and low SEI regions



4.1 Introduction to chapter 4

At the outset of this research it was not clear how the successful development and application of the micro-plasma design used for low energy production of ozone within The University of Sheffield could be applied to the dissociation of CO₂ (Lozano-Parada, & Zimmerman, 2010). It was evident that micro-plasma systems offered unique low-energy consumption and it was intriguing to find an application for these properties within the application of CCU. The research therefore set out to fully understand the process, consider the gaps in knowledge and how it could be applied to the steel sector and, finally, from this gap analysis, move this technology forward through an innovative new process.

Following extensive research from available texts on the theory of plasma CO₂ dissociation, it quickly became evident that the most effective mechanisms for ozone production, which lend themselves to micro-plasma systems, were quite different from those for efficient CO₂ dissociation. The properties of the micro-plasma system that yielded the efficiency improvements for ozone production may not be applicable to a CO₂ plasma reactor, due to the processes and reactions involved in CO₂ dissociation, and therefore a new approach to reactor design was needed. Even so, the presence of energetic electrons, which gain the most energy from a plasma's

electric field due to their smaller mass, creates an opportunity for efficient conversion of problematic and energetically stable CO₂. The CO₂ does not have to be heated to carry out the dissociation, indeed it can happen at ambient conditions, potentially using fossil-free electrical energy. To quote the work of Bogaerts et al., (2015);

“...plasma technology is quite promising for CO₂ conversion, but more research is needed to better understand the underlying mechanisms and to further improve the capabilities” (Bogaerts, et al., 2015)

As seen from the literature review, the focus for existing research within the field has been on understanding the details of CO₂ dissociation mechanisms, to achieve more accurate plasma modelling exploit catalyst or new method of excitation and quench. Whilst this has led to a greater understanding of the dissociation processes, it has not directly tackled the issues of increasing the relatively poor reactor efficiencies at the expense of higher conversion rates. Therefore, this study has aimed to move the field forward via a new reactor design concept, by focusing upon the known CO₂ dissociation deficiencies.

Within this research section, the barriers to highly efficient CO₂ dissociation are discussed further and evaluated. Following this evaluation, a new approach to reactor design is proposed, developed and tested. This development leads onto the breakthrough of a new CO₂ plasma reactor design and power system: a novel contribution, within this particular field.

I would like to recognise Mr Campbell’s contributions in assisting with the SEI measurements.

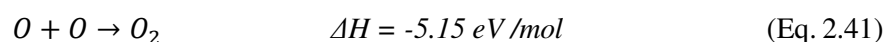
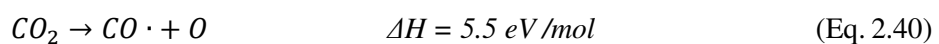
4.1.1 CO₂ plasma dissociation pathways

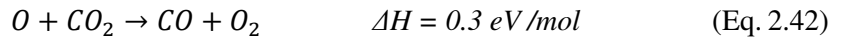
To recap, dissociation of CO₂ and the associated enthalpy can be demonstrated by the following formula 2.39.



$$(\Delta H = 279.8 \text{ kJ/mol} = 2.9 \text{ eV/mol at 300K})$$

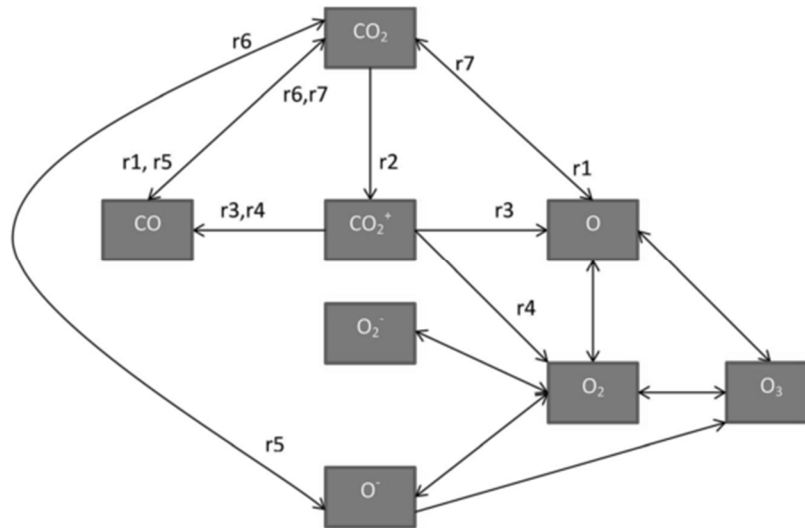
The enthalpy is shown in both kJ and eV. The use of eV is more applicable and regularly used to describe the plasma process. The enthalpy is high, yet this already highly endothermic process formula can be slightly misleading, as it does not provide a complete picture. The decomposition is in fact limited by the activation into CO· and molecular oxygen (Eq. 2.40). This dictates the minimum activation energy required to initiate the reaction. The following reaction, which lead to our final production of CO and O₂ are demonstrated in equations 2.41 and 2.42. The oxygen atom recombination or the detachment of an oxygen atom from CO₂ molecule once diatomic oxygen is available should not limit the process, if sufficient time and quantities are available.





A simplified overview, representing the most important pathways for CO₂ dissociation is demonstrated by Bogaerts et al., (2015) and are shown in the following figure 4.2 (Bogaerts, et al., 2015).

Figure 4.2: Chemical reactions within DBD plasma CO₂ dissociation



Source: (Bogaerts et al., 2015)

The reactions pathways which correspond to figure 4.2 are as follows:

| Reaction pathway | |
|------------------|---|
| r1 | Electron impact dissociation \rightarrow CO and O |
| r2 | Electron impact ionisation \rightarrow CO ₂ ⁺ |
| r3 | Recombination of CO ₂ ⁺ with electrons \rightarrow CO and O |
| r4 | Recombination of CO ₂ ⁺ with O ₂ ⁻ ions \rightarrow CO + O ₂ + O |
| r5 | Electron dissociative attachment \rightarrow CO and O ⁻ |
| r6 | Recombination of CO with O ⁻ to reform \rightarrow CO ₂ |
| r7 | Recombination of CO with O to reform \rightarrow CO ₂ |

Generation of atomic oxygen via r1 or r2 followed by r3 or r5 are the limiting reactions of the dissociation process within a DBD reactor and therefore the most important to initiate the dissociation processes. The dissociation of CO is not considered important, due to the very high energy requirement of 1069.2 kJ/mol. The generation of O₃ is possible following the availability of oxygen atoms from reactions r1, 2, 3, 4 and 5, but only in small amounts and with long residence times. Reactions r6 and r7 are to be avoided as they represent losses in the system (other system losses will be discussed later), however the CO molecule is relatively stable, unless excess energy is input into the system.

The reactions rates of the most dominant reaction of concern for a DBD are also represented in table 4-1 (Aerts, et al., 2015). The primary reaction pathways, r1, r2 and r5 are of a similar reaction rate, with r1 and r 2 quicker than r5. All pathways are likely to occur with sufficiently high electron densities within the reactor.

Table 4-1: Most relevant CO₂ dissociation pathways within atmospheric, non-thermal plasma regime

| | Reaction | Rate Coefficient |
|-----------|--|---|
| r1 | $e^- + \text{CO}_2 \rightarrow \text{CO} + \text{O} + e^-$ | $5.8 \times 10^{-11} \text{ cm}^3\text{s}^{-1}$ |
| r2 | $e^- + \text{CO}_2 \rightarrow \text{CO}_2^+ + 2e^-$ | $5.4 \times 10^{-11} \text{ cm}^3\text{s}^{-1}$ |
| r3 | $e^- + \text{CO}_2^+ \rightarrow \text{CO} + \text{O}$ | $6.5 \times 10^{-7} \text{ cm}^3\text{s}^{-1}$ |
| r4 | $\text{O}_2^- + \text{CO}_2^+ \rightarrow \text{CO} + \text{O}_2 + \text{O}$ | $6.6 \times 10^{-7} \text{ cm}^3\text{s}^{-1}$ |
| r5 | $e^- + \text{CO}_2 \rightarrow \text{CO} + \text{O}^-$ | $7.0 \times 10^{-12} \text{ cm}^3\text{s}^{-1}$ |
| r6 | $\text{O}^- + \text{CO} \rightarrow \text{CO}_2 + e^-$ | $5.5 \times 10^{-10} \text{ cm}^3\text{s}^{-1}$ |
| r7 | $\text{O} + \text{CO} + \text{M} \rightarrow \text{CO}_2 + \text{M}$ | $1.7 \times 10^{-33} \text{ cm}^6\text{s}^{-1}$ |

4.1.2 Most efficient mechanisms to CO₂ dissociation

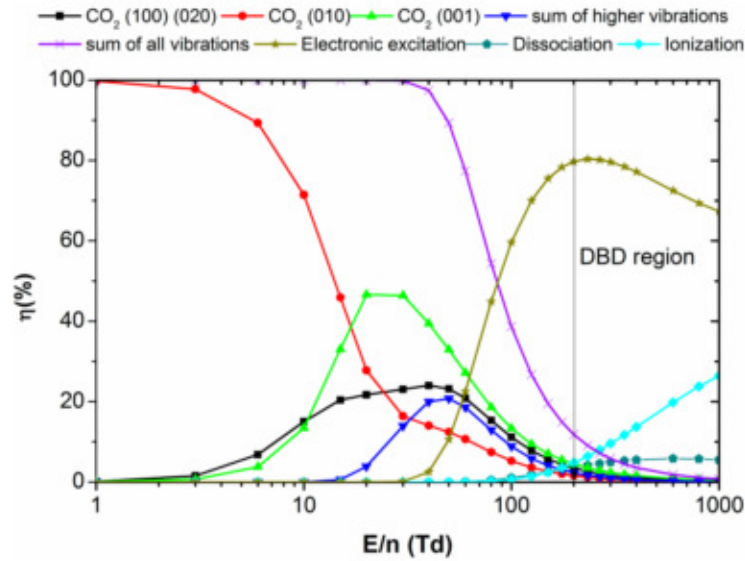
Within the non-thermal plasma region, the energy required to commence the dissociation reaction via a direct electron impact is at minimum 8 eV (Fridman, 2008), leading to an excess of 2.5 eV of energy into the system, which will generate unwanted heat. In contrast the energy required via vibrational excitation is only 5.5 eV and coincidentally equal to OC=O bond. Within a vibrational excitation occurrence, 95% of the discharge energy can be transferred from the plasma generated electrons to the CO₂ molecule, making this a highly efficient process (Rusanov, et al., 1981). Vibrational excitation, operates within an electron temperature (T_e) range of $T_e = 1\text{-}2$ eV, mostly in the asymmetric vibrational mode. Above this (>2 eV), electronic excitation will dominate.

The dissociation from a direct electron impact requires more than the 5.5 eV of the OC=O bond, leading to energy losses. Approximately 11.5 eV is required per CO molecule and an energy efficiency of only 25%. Clearly vibrational excitation is much more preferable to electronic excitation for high efficiency operation. For comparison, ozone generation can reach theoretical efficiencies of 85% energy transfer within a region of 4 to 8 eV, as the energy losses from vibrational relaxations and wall recombinations are not as influential.

At the lower 1-2 eV range elastic electron impact into the CO₂ molecule does not have sufficient energy to dissociate the molecule. Therefore, it is considered that an accumulation of impacts and energy that lead to a stepwise effect, ultimately leads to the dissociation once sufficient energy is gained. This can be displayed in figure 4.4 as proposed by (Bogaerts, et al., 2015). The study by Bogaerts et al., (2015), discussed a comparison between microwave and DBD reactors. Whereby microwave (MW) plasmas have significantly better energy efficiency as the stepwise vibrational excitation is more dominant than with a DBD (Bogaerts, et al., 2015). The diagram below (figure

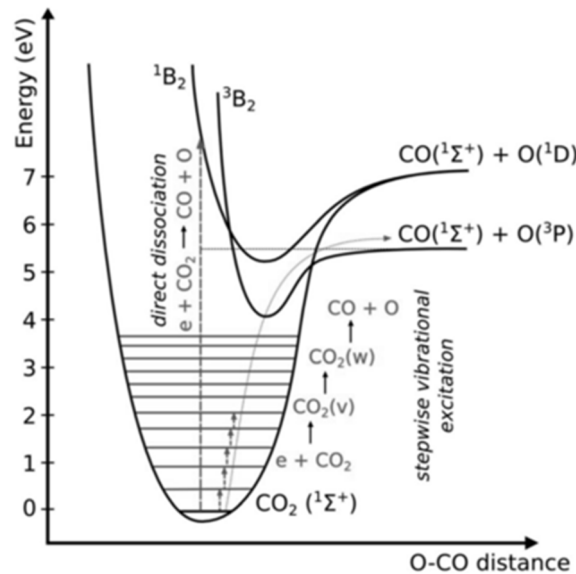
4.3) from Aerts et al. (2012) demonstrates that a DBD reactor operates beyond the region for vibrational excitation, typically above 200Td ($200 \times 10^{-21} \text{ V m}^2$ and electron energies of 2-3 eV) into the region where electronic excitation dominates (Aerts, et al., 2012). However, MW plasmas operate with a reducing electric field (E/n) lower than 200 Td, typically $E/n = 50\text{Td}$, suitable for effective vibrational excitation. Even so, MW plasma reactors still do not operate with very high efficiencies, which we will discuss later.

Figure 4.3: The fraction of electron energy transferred to different channels of excitation as well as ionization and dissociation of CO₂ for MW plasma and DBD plasma



Source: (Aerts, et al., 2012)

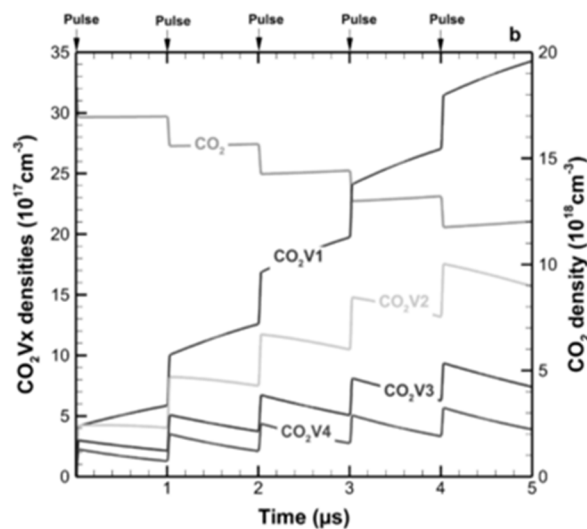
Figure 4.4: CO₂ electronic and vibrational levels for dissociation



Source: (Bogaerts, et al., 2015)

Stepwise vibrational excitation, also known as ladder climbing, ultimately leads to the dissociation of CO₂ once sufficient energies can be reached. With a pulsed energy input, typical of plasma reactor design, ladder climbing can be achieved, via interactions with the high temperature electrons, but not without energy losses and vibrational relaxation. VT relaxation gives rise to gas heating, which also ironically increases VT relaxation rates, so keeping gas temperature as low as possible leads to better efficiencies. Relaxation occurs at different speeds for the vibrational levels 1 to 4, also demonstrated by Aerts et al. (2012) and shown in figure 4.5. Sufficient pulses (interaction with an energetic electron) are needed to sustain the ladder climb all the way to dissociation. Pulse duration of less than 1μs allows for an increase in the vibrational energy needed to progress through the vibrational levels before decay occurs. Pulse duration of 1-10μs starts to see a fall in the vibrational excitation towards ground state and at pulse periods longer than 10ms, most have decayed back to ground level. Therefore, sufficient pulse periods and residence time is needed to gain sufficient energy before decay occurs. Under very short residence times, high efficiency can be achieved, but limited electron impacts occur to allow high conversion rates to be achieved. Indeed, with all types of plasma reactor, there is an inverse relationship between energy input and conversion rate.

Figure 4.5: Densities of vibrationally excited CO₂ species (left axis) and the ground state CO₂ (right axis) as a function of time



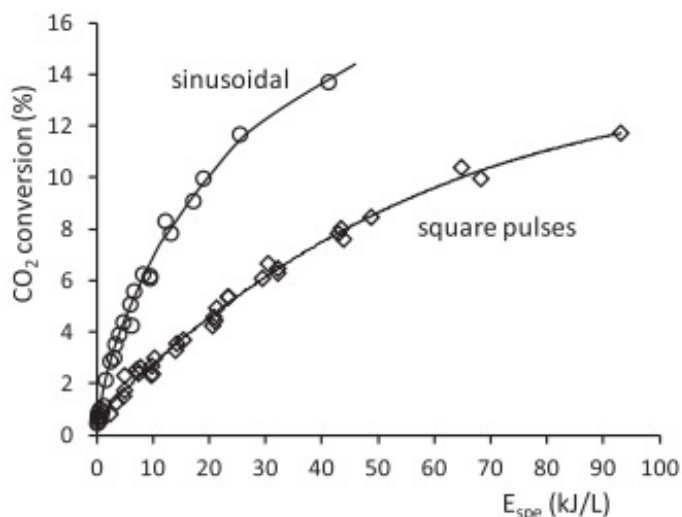
Source: (Aerts, et al., 2012)

Operating at DBD reduced electric field (E/n) above 200Td leads to 70-80% of the electron energy being attributed to the lower efficiency electronic excitation, with 20-30% attributed to ionisation and 5% dissociation. At 200Td only 12% of the energy is used in vibrational excitation, however this is expected to drop rapidly with an increase above 200Td (Bogaerts, et al., 2015).

Besides the dissociation mechanisms, other key parameters that influence a reactor's efficiency and conversion rate that should be taken into consideration when designing a reactor. These will be discussed next along with various reactor options and can be summarised as follows:

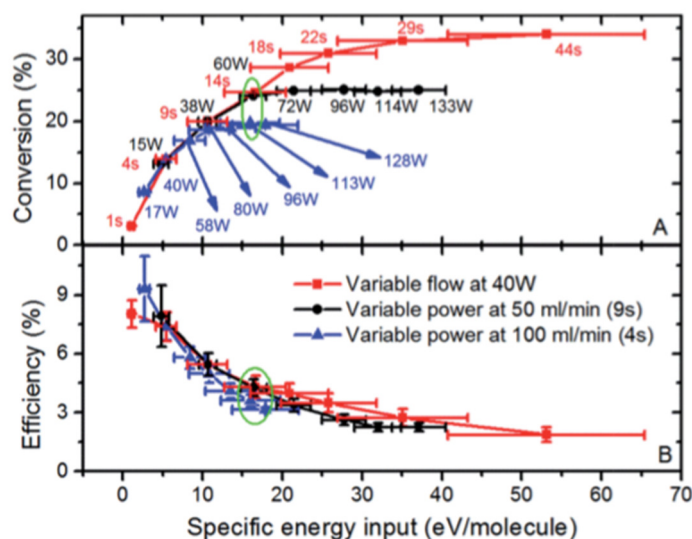
- a) Reactor Geometry – The length of the reactor (along with flow) will determine the residence time. This is a critical parameter for CO₂, as reverse reactions lead to high energy losses (see supersonic flow later). Reactor discharge gap and dielectric material and thickness will also play a part in determining the strength of the electric field, influence of the sheath and ultimately the electron density.
- b) Type and characteristics of energy input – The energy input is critical to determine the strength of the reduced electric field (E/n). High energy inputs generate greater electron densities, which lead to higher conversion, but greater losses. The shape of the power energy wave can also play a part in conversion rates, as demonstrated by Yap et al. (2015) in figure 4.6 (Yap, et al., 2015). Also, the amplitude of the power input is known to have a much greater influence than the frequency of the power supply (Aerts, et al., 2015). The choice of energy supply leads to a significant change in the dominating dissociation mechanisms, as we've just discussed. Microwave energy inputs lead to greater vibrational excitation, whereas thermal input would lead to high gas temperature plasma and greater energy losses.
- c) Specific Energy input (SEI) – Whilst the reactor geometry and flow determine the residence time of the gas, the power input and flow rate provide the specific energy input. This method allows the efficiency of the process to be determined. Greater SEI leads to higher electron densities, but electron densities are not independent of electrode surface area. The same power input, but a smaller electrode will lead to greater concentration of micro-discharge formation per m³ compared to the same power input, but over a much larger electrode area. High densities of electrons can be advantages for CO₂ dissociation. The inverse relationship of conversion vs efficiency at increasing SEI as examined by Bogaerts, et al.,(2105) is shown in figure 4.7.
- d) Catalytic material – A catalyst can be incorporated into the reactor design to promote conversion. Often the presence of the catalyst material, such as a bead packed bed, will lead to a change in the reactor's effective geometry. This leads to a change in gas flow path and electron distribution. Catalytic plasma reactors are certainly a promising area, if the design and incorporation of the catalyst is such that it can be easily replaced and does not inversely affect the performance.

Figure 4.6: CO₂ conversion as a function of input power: CO₂/He = 1/1 AC power supply



Source: (Yap, et al., 2015)

Figure 4.7: The Relationship between CO₂ Conversion and Efficiency



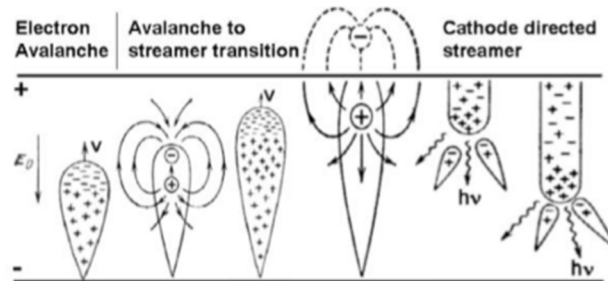
Source: (Bogaerts, et al., 2015)

4.1.3 A comparison of current reactor efficiencies

Dielectric barrier discharges are also known as a silent discharge as they lack the sparks, shock waves and noise of the corona discharges, jets and thermal plasmas. The absence of sparks and local overheating is preferable to the high energy efficiencies of low-temperature discharges. This allows the DBD reactor to operate within a strong non-equilibrate condition. The dielectric barrier blocks the increase in current that leads to spark formation. Instead we see that a primary avalanche formation leads to a subsequent streamer, which are collectively known as micro-discharges. The streamer is a thin ionised channel that stretches quickly between the electrodes, along the positive trail that is left by the primary avalanche. The primary avalanche generates

photons that initiate further avalanches that lead to a rapid chain of new micro-discharges that fill the electrode gap. The density of discharges is linked to the overall energy input into the system, with respect to electrode surface area. The evolution from avalanche to streamer is shown from left to right in figure 4.8.

Figure 4.8: Streamer evolution (left to right)



Source: (Fridman, 2008)

The presence of the streamer causes an effective short circuit between the electrodes and the current rises rapidly, the streamer is extinguished as the potential between the electrodes are reversed. The lifetime of the streamers is therefore directly linked to the frequency of the AC power supply.

Whilst the glow from the silent discharge may seem continuous, it is a collection of the micro-discharge channels. After a polarity reversal leads to the collapse of the micro-discharge channel, existing vibrational energies and electron excitation are still present and their influence on the dielectric remain until the streamer is reformed. The energy within the plasma system remaining once the energy pulse is terminated is known as the afterglow. It is believed that the new reformed streamer will form in the same place as the previous, known as the Memory Effect (Fridman, 2008). The memory effect is stronger in the use of electronegative gases, which can lead to the operations of an atmospheric pressure glow discharge, whereby the electric field is below the Meek criterion and operates in the Townsend ionisation regime. Streamers are easy to produce, but operation in the Townsend mode is not always possible. Townsend mode is dependent upon the secondary electron emission, unlike streamers.

The streamers are thought to repel each other, leading to a regular arrangement structure, which will be more evident at greater micro-discharge densities. The arrangement of such streamers in their spatial and temporal organisation is entirely a result of the voltage amplitude, not the frequency. We could conclude from this assessment that the greater amplitude resulted in higher densities of streamer formation. Similarly, Aerts, et al. (2015) noted that frequency has limited influence on dissociation efficiency. (Aerts, et al., 2015). The stepwise accumulation of vibrational energy is dependent upon collisions (pulse of energy) within less than 10 μ s. A greater density of streamers and energetic electrons, will provide the collisions with sufficient frequency

as the gas passes through the reactor, therefore E/n is apparently more important than power frequency. This principle is demonstrated in figures 4.9 and 4.10. With lower densities (a) there is a greater chance the CO_2 molecule can pass through the reactor without achieving sufficient energy for dissociation. This probability increases if the density is greater (b) and a route through the reactor without interaction with a streamer becomes more unlikely. Contradicting initial memory theory, the work of Akishev et al. (2011) concluded that the streamers do not have spatial memory and are chaotically organised (Akishev, et al., 2011). Further work from the team to monitor the formations showed that the streamers move rapidly at a speed of 0.1m/s , which can be considered fast for such a small micro-discharge of $100\mu\text{m}$ diameter. The organisation of the streamers is less critical than their density, but the rapidly moving streamers are more likely to obstruct the path of the incoming CO_2 .

Figure 4.9: Low streamer (Electron/plasma) density

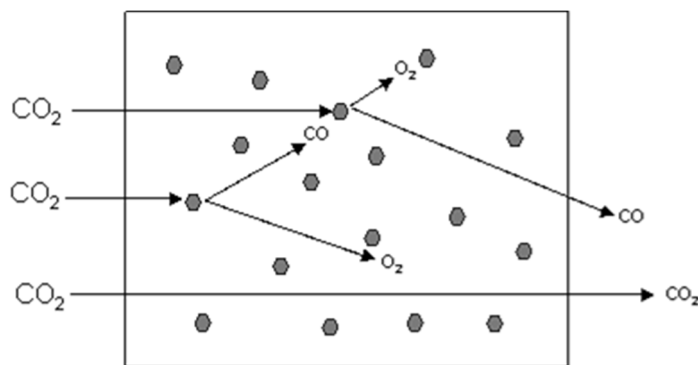
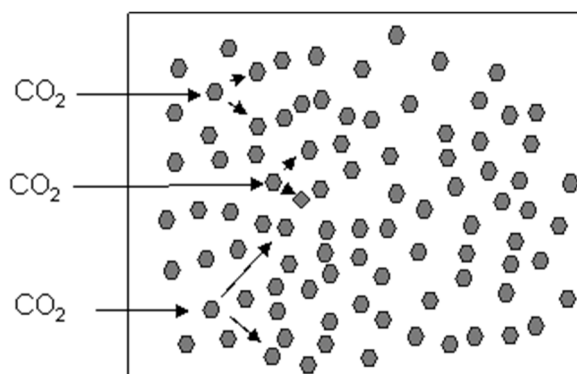


Figure 4.10: High streamer (Electron/plasma) density



There are a wide range of CO_2 dissociation efficiencies that have been achieved within various plasma reactor designs. Yet the high efficiencies come at a cost of low conversion rate. Within table 4-2 is a summary of the various reactor efficiencies along with their respective conversion and flow rate at atmospheric pressure. Whilst the DBD design yields some unique properties and low temperature operation, only low efficiencies have been achieved for the conversion of CO_2

as the inefficient electronic excitation dominates. Conversions of 35% and efficiencies of 8% have been achieved by Bogaerts et al., (2015).

Microwave plasmas have been shown to offer unique, high efficiency generation between 80%-90%, which have been reported under very specific conditions with supersonic flow (Fridman, 2008). The high (supersonic) flow rate means that the plasma is initiated and very soon after decays back to ground state. Under these conditions, there is no window for reverse reactions, energy loss from VT-relaxation and heat loss. Because the CO₂ passes through the reactor very quickly, there is also little time for the plasma reactor to transfer energy to the CO₂ molecules, leading to a very low conversion efficiency. These high efficiencies (80%-90%) have not been recreated and recent reports under similar conditions are at 45%, which is still very good (Van Rooij, et al., 2015). Bongers et al. (2017) reported a high efficiency between 35% and 50% with an inverse rate of conversion (11% to 23%) in a microwave vortex plasma system (Bongers, et al., 2017). The exit of the vortex, into a larger reactor volume leads to rapid pressure drop that aims to result in the limitation of vibrational-translational (VT) relaxation losses. Still, a 45% conversion at a 20% efficiency with microwave plasma has also been achieved, which is much better than those achieved via DBD conversion owing to the dominance of the vibrational excitation within the lower E/n that is achieved with a microwave plasma. At a pressure of 1 atm, Spencer and Gallimore (2013) achieved a conversion of 45% (at 1 l/min) and an energy efficiency of 20% (at 16 l/min) (Spencer & Gallimore, 2013). The low (<1 eV) energy density of a microwave plasma as modelled by Kozak et al. (2014), is ideal for high efficient vibrational CO₂ dissociation mechanisms (Kozák & Bogaerts, 2014).

The gliding arc concept is intriguing as high conversions have been reported. The plasma is initiated in the higher energy near thermal region, due to the narrow electrode gap.

Adding a packed bed of catalytic material in a DBD set-up can increase CO₂ dissociation, due to the influence of the catalytic material, helping the conversion. However, this set up produces uneven micro-discharge distributions following a change in the effective geometry by introducing catalytic material. Local hotspots of electron densities are formed where the catalytic materials touch and the gaps are smallest. This non-homogeneous distribution of electron densities could lead to the high electron densities and unnecessary heat in these regions, allowing a higher probability of lower efficiency electron excitation to occur as well as reverse reactions in these hot-spots. The presence of small packing material can also reduce the flow rate of the gases and increase the residence time as it finds its way amongst the packing material. Longer residence time gives a greater chance of reverse reactions and VT relaxation (Bogaerts, et al., 2015).

Table 4-2: A comparison of plasma reactors and their conversion and efficiency using pure CO₂ only

| Plasma Type | Max, Conversion | Flow Rate | Max. Efficiency | Flow Rate | Reference |
|--------------------|------------------------|------------------|------------------------|------------------|-----------------------------|
| | <i>%</i> | <i>l/min</i> | <i>%</i> | <i>l/min</i> | |
| Co-axial DBD | 35 | 0.01 | 8 | 0.5 | (Bogaerts, et al., 2015) |
| Co-axial DBD | 30 | 0.05 | - | - | (Paulussen, et al., 2010) |
| Co-axial DBD | 12.5 | 0.05 | 3.5 | 0.04 | (Yu, et al., 2012) |
| Gliding Arc | 9 | 14 | 43 | 27 | (Nunnally, et al., 2011) |
| Microwave Plasma | 45 | 1.0 | 20 | 16 | (Spencer & Gallimore, 2013) |
| Thermal Splitting | 22 | 0.02 | - | - | (Nigara & Cales, 1986) |

To summarise, the benefits and properties of a micro-plasma reactor that yield an exponential increase in electrical field strength with a decrease in the discharge gap are not recognised with CO₂ gas dissociation. This increase in electric field leads to the more inefficient electronic excitation of CO₂, rather than the preferential stepwise vibrational excitation. Therefore, the benefits of the micro-plasma design are not realised with CO₂ gas. A reduced electric field that promotes only the vibrational excitation, followed by fast quench with minimal reverse reactions and VT relaxations are the most desirable for this application.

Fast (supersonic) flow rates lead to a reduction in losses, however longer residence times are needed within the reactors to achieve complete dissociation and so only small conversion at high flow can be achieved. The benefits seen by Lozano-Parade and Zimmerman (2010) for the fast ozone reaction are not transferable to the CO₂ gas due to the slower speed of multi-staged dissociation reaction pathways and a need to maintain activation for the duration of the dissociating processes, to achieve high conversion rates (Lozano-Parada, & Zimmerman, 2010).

4.1.4 Invention of a new plasma reactor concept

Analysing the literature and experimental data for CO₂ plasma dissociation and the various conventional reactor designs, we are able to understand the most effective mechanism and dominant dissociation processes and also learn the shortcoming of conventional reactor design. We have seen from the previous research (Aerts, et al., 2012), (Bogaerts, et al., 2015) that the

more efficient stepwise vibrational excitation does not play a significant role in the DBD reactor at a predicted 12%. This is because the T_d is too high to prioritise these mechanisms, and so electronic excitation is dominating at the higher >2 eV energy level. This higher energy operation is needed within a DBD to activate the plasma, often >14 eV/mol (Fridman, 2008). This is much greater than the 2.9 eV/mol that is required for the dissociation of CO_2 , leading to unnecessary gas heating, losses and inefficiency.

Evidently what is needed is a plasma reactor with two properties. Firstly, a high micro-discharge density to initiate the reaction and ensure all incoming CO_2 gas does not pass without interaction with the energy source and produce the necessary molecular oxygen needed for the subsequent reaction. Secondly, a reactor design that also sustains and promotes the following reaction into CO and O_2 without overheating the gas, so that rapid quenching to eliminate reverse reaction, can be avoided. A 'two-in-one' reactor approach is proposed.

The gliding arc shows promise due its similar two-in-one approach, whereby the plasma is initiated at a narrow, near-thermal region and the converging plates sustain the plasma, but at a lower electric field due to the increase in electrode gap. This provides a high-energy start to the reaction, to overcome the high energy needed for dissociation (>5.52 eV/mol), but the latter stage of the reaction is uncontrolled and will extinguish itself and restart once the gap is too large to sustain the reaction. A continuous system would be more advantageous for the maximum benefit. This system does not lend itself to scale-up to commercial levels and tailoring the electrode lengths and residence time at the correct energy input is difficult as only one power source is used. The greater electrode gap in the latter stages needed to extinguish the plasma could limit power input below optimum levels, and whilst the plasma front is operating within the latter stage of the reactor, the new incoming CO_2 is not gaining the high energy densities needed to initiate the molecular O formation.

Therefore, it is proposed a two-staged, single reactor with continuous dual power input is the way forward. First, we will exploit the benefits of high energy input, greater than the 14 eV/mol needed to initiate the plasma. This high energy region within a DBD reactor, from thermal imaging in research chapter 3, has shown to generate considerable heat, whereby a cooling system was employed to manage the temperatures. This is a region of significant energy loss, but is absolutely necessary within a DBD to activate the plasma and generate the molecular ozone. We would not wish to continue operating in this high energy region (as all other DBD must do) as the following reactions do not need to sustain this energy input and result in excess heating of the gas and energy loss. This section of the reactor should be limited to the residence time needed only to initiate the process and provide sufficient yields of CO and O and ionic counterparts CO_2^+ and O^+ . Previous assessments suggest that there is no benefit from going beyond 20cm in reactor length as this leads to reverse reactions, with 9cm being optimal for the specific DBD-

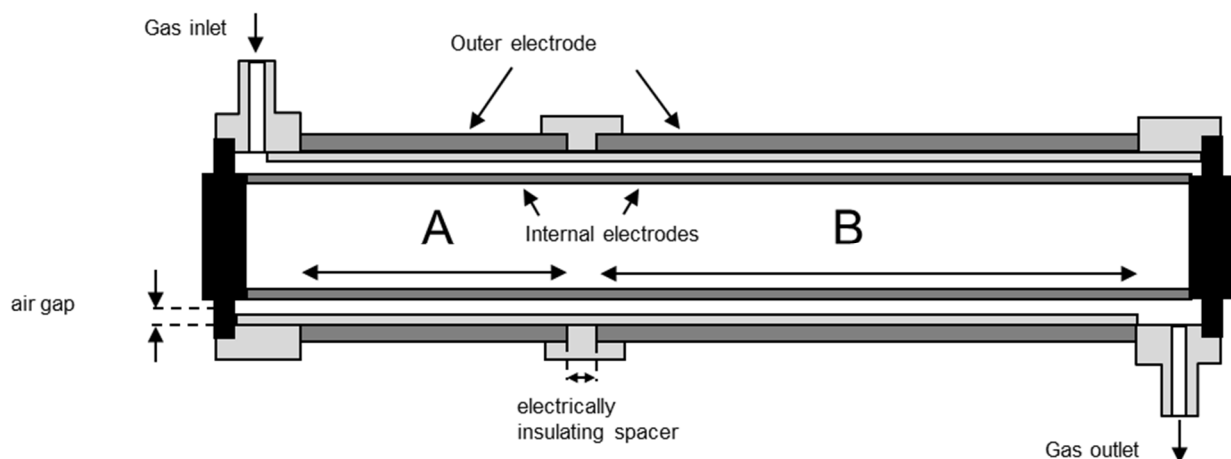
corona hybrid (Liu, et al., 2017). The first section is to be kept much shorter with high micro-discharge density and SEI.

The initial short high energetic stage has, by electron excitation, resulted in the production of CO and O that can pass into the second stage of the reactor. This second stage can now operate at a lower SEI, as the higher electron density is no longer needed for the plasma activation and generation of molecular oxygen. Within the second stage, only sufficient energy can be applied from a second power supply to counteract the reverse reaction and losses and to provide sufficient residence time for the formation of molecular oxygen. It is critical that the gas temperature is kept low, to prevent the heating the CO to lead towards recombination with the atomic O to reform CO₂.

It was determined that a three-stage process was not needed, as there was no apparent benefit from a third, lower energy plasma stage given the reaction processes. Further residence time could give rise to greater losses.

The proposed reactor design is demonstrated in figure 4.11.

Figure 4.11: Twin electrode DBD plasma concept



4.2 Experimental Design – A new plasma reactor invention

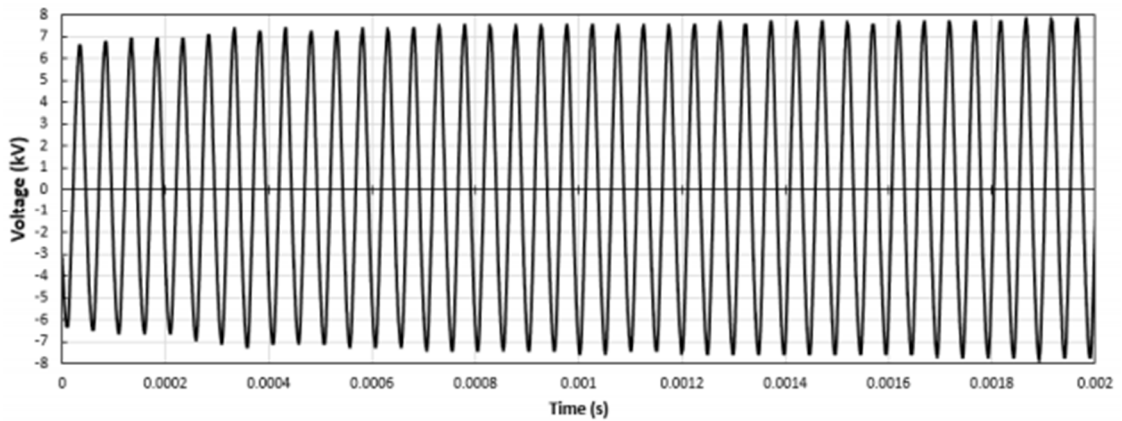
To test if the reactor theory is at all possible a two staged reactor is needed, along with two power supplies that can be adjusted for power input.

By adjusting the electrode length the effective SEI, a critical parameter, can also be adjusted for a given power input. To then adjust the residence time means the flow rate of gas can be varied. To alter the electrode length aluminium tape is used as this can be cut to length. Given previous experimental results (Liu, et al., 2017), we know there is no benefit to going beyond 200mm, with 90mm being optimal for the given conditions. However, the length of borosilicate glass and available power supply dictates that a total of 50mm electrode length is chosen. The operation of a two-stage system can be compared to a continuous 50mm electrode and against the twin

electrode, equalling the same total length. To develop the higher SEI and streamer density for the first stage, a shorter electrode is used; the power density will be higher for given energy input if the area is smaller. A 30 / 70% split was chosen, giving a 15mm first electrode followed by a second 35mm electrode.

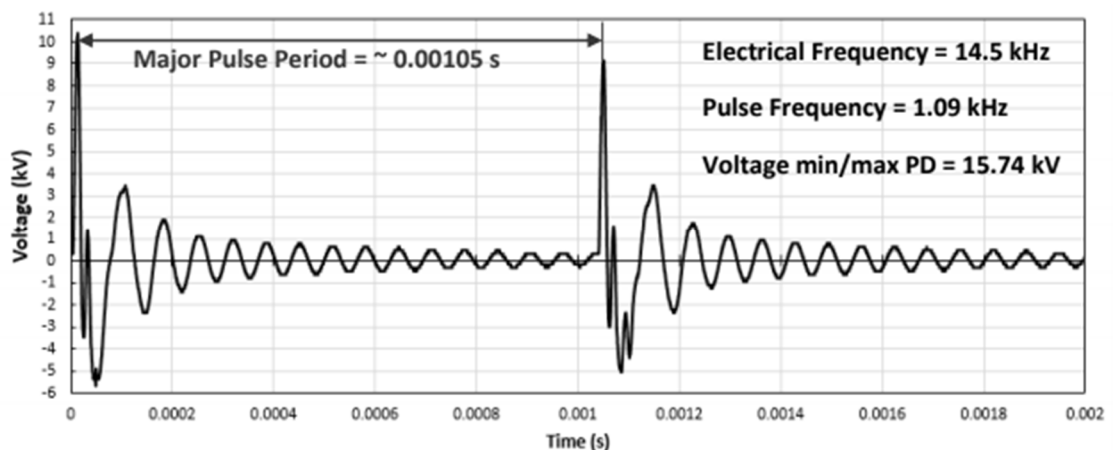
A variety of inexpensive power supplies used for ozone generation were obtained and tested. These power supplies chosen as they are easy to obtain, being imported into the UK from online retailers and easily dismantled and modified to suit this particular purpose. A trade-off is that they are limited by their fixed frequencies. Power supplies were obtained with a continuous sinusoidal output and a pulsed peak and decaying amplitude power signature, shown in figures 4.12 and 4.13.

Figure 4.12: Plasma power supply A continuous waveform



Pulse frequency for reactor A is 20 kHz at a total of 15.32 kW.

Figure 4.13: Plasma power supply B decaying waveform

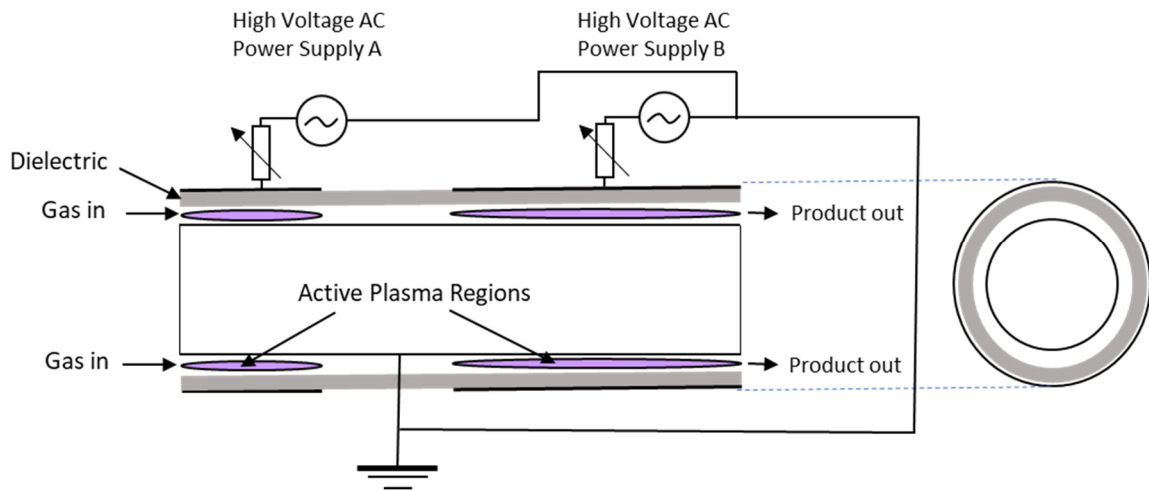


The characteristic waveform signature of plasma power supply B is quite different, with major pulse occurrences at 0.00105 seconds as shown in figure 4.13.

From the power supply testing experiments, it is necessary to modify the power input so that the second stage of the reactor SEI can be reduced, so to minimise any unwanted increase in gas temperature and loss. A pulse width modulation unit was first applied, but a simple variable resistor was ultimately chosen, as this reduces the amplitude of the input energy, rather than influence the signals wave profile and steamer formation.

The circuit is shown in the following figure 4.14.

Figure 4.14: Twin electrode DBD plasma circuit



A borosilicate glass tube is used for the dielectric layer and a single grounded electrode is constructed from standard 15mm copper tubing. A smaller diameter reactor system can result in damage to the dielectric surface due to arcing causing high temperatures often in resulting in a damaged dielectric. To avoid damages, the reactor was made from a larger diameter glass tube as this will dissipate the heat more effectively and spread the streamer formation over a greater area for a specified SEI. It is also critical to keep the plasma gap as constant as possible, so quality control is important to prevent single ‘hot spots’ at areas of uneven charge distribution. The electrode gap, due to the standard diameter materials chosen are not fully optimised, but well within an acceptable range and actually very close to the target 1mm gap at an average gap of 0.83mm (table 4-3).

Table 4-3: Reactor geometry

| Reactor Component | Size range | Average | Ovality |
|---|-------------------|---------------------------------|----------------|
| | <i>mm</i> | <i>mm</i> | <i>mm</i> |
| Glass dielectric OD | 20.05 – 20.14 | 20.10 | 0.09 |
| Glass dielectric ID | 16.64 – 16.67 | 16.66 | 0.02 |
| Dielectric thickness | 3.38 – 3.50 | 3.44 | 0.12 |
| Central Electrode | 14.96 – 15.02 | 14.99 | 0.06 |
| Dielectric to electrode gap | 0.81 – 0.85 | 0.83 | 0.04 |
| Effective reactor volume (total 50mm electrode length) | | 2.08 (<i>cm</i> ³) | |

Total power input is measured using an inline plug power measurement device, with gases measured using an ADC MGA 3000 series multi-gas analyser (table 4-4). With the following measurements:

Table 4-4: ADC MGA 3000 series, multi-gas analyser specification

| Component | Measurement range | Units | Detection method |
|-----------------------|--------------------------|--------------|-------------------------|
| CO₂ | 0-35 | % | Infrared |
| CO | 0-10 | % | Infrared |
| SO₂ | 0-1000 | ppm | Infrared |
| O₂ | 0-25 | % | Chemical |

This is not the first choice of analyser, due to its range and sensitivity, as will be discussed. However, due to Covid-19 restrictions, this was the one available. Gas composition options were again limited due to Covid-19 restrictions. A 5% CO₂, 2% O₂ with Ar mix is used, however this was not anticipated to cause a disadvantage and these are in line with the ranges of the analyser available.

4.3 Results & analysis

4.3.1 Power consumption and reactor operation results

For the following results and analysis, the standard formula are used:

To define the energy input to the system we use the following:

$$\text{Specific Energy Input (SEI), (kJ/l)} = \frac{\text{Plasma Power (kW)}}{\text{Gas Flow Rate (l/s)}} \times 60 \text{ (s/min)} \quad (\text{Eq. 4.1})$$

The % conversion rate of CO₂ is defined as:

$$x_{\text{CO}_2} (\%) = \frac{\text{CO}_{2,\text{inlet}} - \text{CO}_{2,\text{outlet}}}{\text{CO}_{2,\text{inlet}}} \times 100\% \quad (\text{Eq. 4.2})$$

The energy required to produce 1 mol of CO is defined as:

$$E_{\text{CO}} = \text{SEI} \times \frac{\text{molar volume, CO} \times 100\%}{x_{\text{CO}_2}} \quad (\text{Eq. 4.3})$$

The energy efficiency (η) is defined as:

$$\eta = \frac{\Delta H_R}{E_{\text{CO}}} \times 100\% \quad (\text{Eq. 4.4})$$

Where ΔH_R (kJ/mol) is the sepcific heat of the dissocation reaction of CO₂, equation 4.4.

For the first time, a twin-stage plasma reactor set-up was shown to be possible, utilising a single common earth electrode and two power supplies. The power consumption for the operational modes can be seen in table 4-5 below. Total power consumption is used, rather than Lissajous power consumption. Total power consumption also includes the system losses. For this application, total power consumption is appropriate as we aim to compare the two operational modes; single plasma power supply and twin plasma power supplies. This measurement is more applicable to real world application, such as deployment on steel plant gas conversion.

Table 4-5: Power consumption for the operation modes of the twin-plasma concept

| Mode | Power Consumption | Power/electrode area |
|---------------------------------|--------------------------|-----------------------------|
| | <i>W (J/s)</i> | <i>(J/cm²)</i> |
| 15mm plasma supply A | 24.6 | 3.48 |
| 35mm plasma supply B | 6.6 | 0.40 |
| Both plasma (50mm total) | 32.5 | 1.38 |
| Single 50mm electrode | 35.1 | 1.49 |

Power input for the first reactor stage was set at 24.6 W as shown above. This provided an optimised power setting, which did not transition to arcing, producing a very controlled and quite characteristic plasma glow. Whilst SEI is the standard measurement of power input, the power per area of electrode provides further insight into the energy density, and thus expected streamer density, irrespective of gas flow. The smaller electrode length combined with a higher power input generated a high SEI, compared the much lower respective SEI for the longer electrode and small power input. Although the power supplies for the single power set up and twin power set-up vary slightly, the energy density (power input / electrode area) is quite comparable, with 1.49 J/cm^2 and 1.38 J/cm^2 respectively. SEI at high and low flow rates are shown in table 4-6.

Table 4-6: SEI at 0.5 and 1 litres per minute (l/min)

| Mode | Power input | SEI at 0.5 l/min | SEI at 1 l/min |
|---|------------------------|-------------------------|-----------------------|
| | <i>W</i> | <i>(kJ/l)</i> | <i>(kJ/l)</i> |
| 15mm plasma supply A | 24.6 | 2.95 | 1.48 |
| 35mm plasma supply B | 6.6 | 0.79 | 0.40 |
| Both plasma (50mm total) | 32.5 | 3.90 | 1.95 |
| Single supply 50mm electrode | 35.1 | 4.21 | 2.11 |

The gap between the two electrodes was set at 13mm. This is because the electrodes could not be brought closer, due to jumping and arcing between the two power supplies. This is not ideal (zero gap would be optimal) however, some gap was anticipated. A variety of insulating materials was trialled, in an attempt to bring the electrodes closer. Surprisingly, none of the materials used has a discernible effect.

Reducing the power input to the second reactor stage caused the arcing to increase, leading to the 6.6 W and the 13mm as the optimum for this set up. Observations showed that it is clearly possible to prevent the plasma initiation when attempting to use only the low power (35mm) reactor under operation with air. Argon initiates much easier at lower SEI. Only upon the application of the 1st stage (15mm) reactor, can the second stage reactor be initiated, using air as the feed gas. With the set-up this cannot be replicated with the Ar mix, due to the lower initiation SEI of Ar.

The operation of the two-stage reactor can be seen in the image (figure 4.15) below.

Figure 4.15: First-of-a-kind two-stage plasma reactor concept in operation

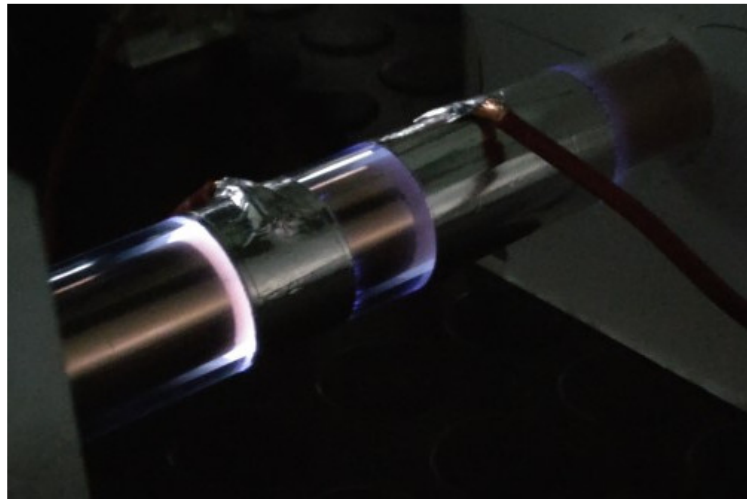


Figure 4.15 clearly shows the characteristic glow, with the first stage reactor (15mm) demonstrating a higher SEI (brighter discharge) than the latter (35mm) reactor. Flow of gas is from left to right.

Table 4-7: Gas residence time comparison at 0.5 to 2 litres per minute (l/min) for a 50mm electrode, plus 13mm electrode gap

| Flow rate | Residence time | Residence time |
|------------------|-----------------------|-----------------------|
| <i>l/min</i> | <i>minutes</i> | <i>seconds</i> |
| 1 | 0.00262 | 0.157 |
| 0.5 | 0.00523 | 0.314 |

The residence time of the gases within the reactor are shown in table 4-7. The residence times are potentially above optimal for maximum conversion but are limited by maintaining flow to the analyser and the dimensions of the system. The shorter electrodes have also reduced the residence time. A 9cm length electrode was previously shown to be optimal at 0.5 l/min by Liu et. al (2017). This 9cm electrode would provide a much longer residence time, especially as the volume of the reactor design used within this thesis is greater, due to increased diameter. Increased diameter is needed to obtain the low, second stage energy input (J/cm²) and reduce the occurrences of heat damage.

4.3.2 Conversion rate and efficiency results

Gas analysis is carried out using the ADC MGA 3000 series multi-gas analyser. Characteristic of most analyser designs, a minimum flow rate is required. Usually excess flow is delivered to prevent any air ingress. An error is demonstrated on the analyser if the flow rate falls too low, so a minimum flow of 0.5 l/min is required to satisfy the analyser.

The maximum conversion rate and maximum efficiency that was achieved for the twin stage plasma device can be seen in the table 4-8.

Table 4-8: Max conversion rate and max efficiency achieved

| Mode | Conversion rate at 0.5/min | Error estimate | % of CO₂ converted to CO | Efficiency | Error estimate |
|-------------------------------|-----------------------------------|-----------------------|--|-------------------|-----------------------|
| | % | +/- % | | % | +/- % |
| Single stage operation | 4.4 | 3.5 | 2.4 | 13 | 24.5 (+/- 3) |
| Twin stage operation | 11.1 | 3.5 | 6.8 | 36 | 24.5 (+/- 9) |

4.3.3 Analysis and discussion

The SEI of the first stage is in line with the literature (3.90-1.95 *J/l*) and, while maybe not optimal, due to the compromises made to enable this design, they are within range. The second stage, low-power plasma section (35mm) achieves a very low power density (0.79-0.40 *J/l*) not typical for a DBD CO₂ plasma reactor as this is too low to initiate the plasma.

Following the initial high plasma stage, where high excitation occurs, there is a period of afterglow, within the 13mm gap. Although this gap is not ideal and likely leads to some decay and loss of energy efficiency, it is sufficient to sustain the plasma energy going into the second stage. This theory was demonstrated using air (which does not initiate as easily as the CO₂ / Ar mixed gas), whereby the second stage will not ignite without operation of the first stage. The afterglow period could be reduced, minimising loss, if the gap can be decreased. To achieve this an exemplary insulation material is needed to prevent arcing between the reactor stages. To date, only a sufficiently large air gap has prevented arcing from occurring, with insulation showing minimal effect. A higher flow rate will reduce the residence time within this gap (reducing loss), but also limit the achievable conversion rate, which will compromise the detection limit. At a flow rate of 1 *l/min*, this afterglow period is only 0.032 seconds (32ms). Decomposition is expected to occur within the μs range.

After the trials, it became apparent that the power supplies could have been improved. The decaying pulsed power supply that proved adequate for the previous experiments in Research Chapter 3, caused a noisy and inhomogeneous plasma for the low power second stage. The more spaced, high amplitude current peaks cause flashes of plasma streamers and, if the two stages are too close, arcing between the two. This inefficiency is audible, with the second stage much noisier, than the almost silent first stage. Even with the compromises discussed, a new plasma concept was designed, built and demonstrated as part of this research, resulting in the successful operation

of a first-of-a-kind twin-stage, two power plasma reactor system. Within the same system an SEI is achieved that is comparable to a continuous electrode but demonstrating two distinct areas of plasma excitation. This is more aligned with the two stages of CO₂ excitation as demonstrated by the increase in both CO₂ conversion and efficiency. Conversion was increased from 4.4% up to 11.1%, a 40% increase. 6.8% of the CO₂ which was input into the reactor was detected as CO. This CO generation, combined with such a low SEI input, led to the efficiency of CO generated (kJ/mol) to increase from 13% (+/- 1.3) up to 36% (+/- 8). A 4.4% conversion at 13% efficiency seems correct given the inverse relationship to conversion vs efficiency. Note that Bogaerts et al. (2015) demonstrated an 8% efficiency with a DBD reactor at the same flow rate and is within our estimated error range, however a higher conversion was detected. For the twin-stage reactor the efficiency is surprisingly high, especially given the low SEI. However, if we look towards the gliding arc, which we hope to emulate in our two-stage approach, the maximum efficiency achieved here is ~ 40% (Sun, et al., 2017) implying the DBD can approach gliding arc levels of efficiency. Recall that the gliding arc has an initiation (high SEI) stage followed by a lower, decreasing SEI stage due to its geometry in much the same way as the new two-stage design, which could explain the higher energy efficiencies achieved. It is possible to conclude that allowing the very low SEI of the second stage to operate within the same reactor leads to an improved energy efficiency.

The conversion efficiencies are aligned to the literature, and due to the compromises made, as discussed to allow the operation of this first-of-a-kind concept, are not dissimilar to those of fully optimised systems, presented by Bogaerts et al. (2015). An 18% CO₂ conversion rate was achieved using the same, unrestricted power supply that was used for the second (low SEI) reactor stage, but with a different, longer reactor as used in chapter 3. This was confirmed using a Hiden HPR-20 Mass Spectrometer analyser. The reactor geometry and flow rate resulted in a longer residence time (4.95s at 0.5 l/min) and the higher power input (54.2W), which would account for the higher conversion that was achieved, compared to the 50mm system testing within this chapter.

Various methods have been employed by different researchers to calculate their efficiencies. The power efficiencies reported here are total efficiency, including energy losses due to power supplies and transmission. Whilst not directly comparable to some of the literature, which only calculate plasma efficiency, it does allow for satisfactory comparison between the various modes of operation. A standard and common method was used that provides data that is directly applicable to chapter 3: Application of plasma devices in real world situations; in this particular case, a steel plant.

4.3.4 Errors

The gas analyser, as the primary detection method, may be the greatest source of error in determining the conversion rate. A 5% CO₂ with Ar mix gas was used to bring the concentration within range of the analyser. Similar experiments have also used CO₂ and N₂ mixes for the same affect. A 100% CO₂ feed may yield greater total molecular mass of conversion due to higher CO₂ availability. This could potentially lead to greater CO availability for measurement. The analyser is span to the 5% mixture, but it is possible that there is some error between the stated and actual gas composition of the cylinder. One concern with such low concentrations is that of approaching the limits of analyser detection. Although the infrared analyser is very sensitive, it can be prone to drift within the measurement range and care must be taken to repeat and check the span and drift regularly. This adds some increased error within the measurement. A higher differential CO measurement will reduce this error. That said, CO₂ conversion is typically very low for plasma systems if high efficiencies are a target. Therefore, this problem is not uncommon to CO₂ plasma assessment, but the accuracy is not often discussed. Utilising a Mass Spectrometer may alleviate this issue and provide some greater accuracy. For this analysis, the current set-up proved adequate to demonstrate and test the concept. A single analyser was used, needing a pre and post-test span check. Duplicate analysers could alleviate this, and provide closer to real time analysis, but to fix two highly accurate measurement devices, side by side was not within scope of this research demonstration project.

The analyser measures to 2 decimal places ($\pm 0.01\%$ / 100ppm) for the compounds of interest. If we assume that in practice it can measure accurately to within 0.05 % and apply this to the CO₂ conversion, this produces a $\pm 1.8\%$ deviation on the best-case result. Whilst the analyser should be able to measure accurately within the 500ppm range, to include the error in the actual cylinder content vs displayed, ± 500 ppm, we gain a total of $\pm 0.1\%$ (1000ppm) combined error. At a total of $\pm 0.1\%$ (1000ppm) analyser accuracy, we gain an error in our conversion rate of $\pm 3.5\%$. It is unlikely that CO₂ and CO will be over-reported, rather that CO₂ and CO will be under-reported due to losses, leaks or air ingress. Therefore, any CO generated can be considered due to the plasma reaction process, increasing the confidence in this result. In the same respect, there is less confidence in the CO₂ conversion rate, as CO₂ can be under-reported in the exhaust gas, suggesting a higher conversion rate, when in reality CO₂ is lost somewhere within the system.

Whilst the conversion rate is dependent upon accurate gas measurement, efficiency is reliant upon gas composition, power input and flow rate, increasing the possible sources of error. The flow rotameter used can determine between 0.1 *l/min* increments. If the flow is miss-interoperated by 0.1 *l/min*, at such low flow rates (~ 0.5 *l/min*) this represents a significant error of $\pm 20\%$, which in turn would result in a 20% error in the efficiency calculation. Retrospectively a mass flow controller should be used to repeat the experiments.

The power input measurement device, measures to within 0.1W. The effect of +/-0.1W on the efficiency measurement yield is an error of 1 %. The compound error for efficiency, taking into account gas analyser, power and flow measurement error is 24.5%. Some caution should be applied to the efficiency calculation, not just of this study. As this is a first-of-a-kind, it would be necessary to validate these discoveries with replicable plasma systems.

4.3.5 Conclusions

After reviewing the CO₂ dissociation mechanisms it was hypothesised that the gliding arc system is able to reach higher efficiencies because the reaction is initiated in a high SEI region and subsequently sustained in a lower SEI region. This compliments the multiple stages of CO₂ dissociation, as described in equations 2.40-2.42, and results in few losses. Having to sustain the entire reaction at the level required to reach plasma initiation results in energy losses, as this continuous high level of power input across the entire reaction length is not required to sustain the reaction. As such, a DBD system that emulates this two-stage dissociation process was designed, built and successfully operated. Analysis of the system demonstrated that, compared to the conventional single power set up, much greater energy efficiencies can be achieved; from 13% up to 36% efficiency (energy per CO molecule produced).

This first-of-a-kind system will value from further validation and the use of more accurate flow and gas analysis equipment. However, the work to date has shown that a twin-stage two power supply system is possible and can be operated successfully within a single pass plasma reactor and that greater efficiencies can be achieved, approaching those of the best case gliding arc systems.

4.4 Areas for further investigation

Whilst the aim was achieve and a new reactor concept was shown to be achievable, the design did not set world leading conversion rates and efficiencies for a DBD reactor. Optimisation of the system is needed to achieve higher performance, in line with world leading DBD reactors. Future work should focus upon optimisation of the process parameters, in particular the geometry and residence times and power input to find the most optimum configuration...to improvement of the insulating barrier, between the two outer electrodes so that they can be closer, reducing the period of loss and VT relaxations between the two power phases. This became a material science issue beyond the scope of this work. Greater attention to more sophisticated power supplies, with greater control over the parameters (pulse frequency, shape, voltage and amplitude) would also be a useful, along with more accurate measurement, although access to not only one, but two sets of supplies and equipment is needed and was prohibited by availability and costs for this work. Varying the concentration of input gases into a wider range would be beneficial, to include some industrial gas compositions. More versatile gas analysis equipment, with greater operating range

will be required. Improvement upon the reactor design to be tested could include varying the geometry, electrode lengths and respective residence times. Replication and repeatability of these results with similar reactor design by others is needed to further validate the findings of this study. Also, the potential to include a gas permeable membrane that could remove the product O₂ and drive the reaction forwards without recombination. However, selectivity of removal could be an issue as the ionic species are beneficial and the atomic oxygen is essential for the complete dissociation process. Finally, a combination of this technology, with another complementary technology, such as a solid oxide electrolysis cell SOEC to produce a hybrid reactor, may yield greater conversion rates.

4.5 Chapter summary

Following an in-depth investigation into the methods and barriers to the efficient dissociation of CO₂, it was determined that a new reactor design was needed. Previous efforts primarily used the same, narrow range of reactors designs, especially in the field of DBD reactors. The proposed new reactor, was designed, built, tested and operated successfully.

The research aim, to conduct a *detailed review of CO₂ plasma dissociation mechanisms...to address the gap within low energy efficiencies and conversion rates along with the proposal of a new plasma reactor design*, has been successfully achieved. In achieving this aim, Hypothesis B has been confirmed.

The new design exploits a two-stage approach to split the high energy required to initiate the reaction from the lower energy input needed to sustain and complete the total dissociation pathways. The result is believed to minimise unnecessary further overheating that can lead to unwanted reverse reactions. This is more consistent with the two stages of CO₂ dissociation, requiring 5.52 eV/molecule and 0.34 eV/molecule.

It was therefore demonstrated, for the first time, that it is entirely plausible to conduct a single pass plasma reaction within two separate plasma stages, both operating with a different SEI. The developments in new plasma design and knowledge of achievable conversion efficiencies addressed within this research chapter, will be further evaluated in chapter 6.

Chapter 5

Detailed techno-economic simulation of a future low-carbon steel making facility for 2050

5.1 Introduction to research chapter 5

To establish a low-carbon solution for the steel sector by 2050, it became critical to understand the technology pathways that may be taken to achieve this vision. To evaluate the application of any new technology, one must understand how a future steel plant will operate and have answers to the following questions:

1. Will fossil energy still feature between now and 2050?
2. Will CO₂ still be emitted from our future steel plant, for how long and by how much?
3. What technologies are we likely to employ to significantly reduce the carbon emissions?

As part of a strategic planning process, it is necessary to consider what low-carbon technologies might be possible for the production of steel in 2050 and also, which ones are likely to be economically viable. To understand this in detail, a techno-economic model was developed and the model was then used to simulate possible future steelmaking pathways. The purpose of the model was to provide a comparison of various alternative technology pathways from a selected base case. The base case will be built using actual data obtained from a UK integrated steel plant. Without understanding the potential layout of a 2050 steel plant and the resulting transition, it became clear that it would not be possible to evaluate and adapt the plasma technology, microbubbles and ammonia capture, or any other technologies within a steel making site of the future. Whilst roadmaps for steel plant carbon reduction exist, their scope covers entire continents and multiple regions. A model for a single plant is needed to fill this knowledge gap and provide a tool for further analysis of the novel technology deployment recognised in chapters 3 and 4. The construction of this model and analysis of the data will now be discussed.

5.2 Technology Roadmapping

Roadmapping has become an important tool, to help visualise the options and actions needed to achieve future decarbonisation. These roadmaps are often produced to guide Governments, the energy sector and industry on what can be achieved by when and how much it may cost. The elements of the roadmap can vary, but usually consist of a timeline along which certain action is taken to achieve the end objective. In the first stage of road mapping it is therefore essential to set out the purpose (goal) and also the scope. From here different scenarios can be set, which achieve either the same or different outcomes. These scenarios dictate the pathway that is taken

to achieve the set goal. These pathways will include actions such as Government policy or new technology rollout that, at certain points in the timeline, will be deployed to help achieve the goal. What determines a successful roadmap is establishing pathways that under different scenarios provide the ability to avoid unacceptable risks (such as high CAPEX, regret capital or the inability to switch to a different pathway). These risks might also include missing carbon reduction targets or an unprofitable solution.

A barrier to technology deployment is often technological readiness (TRL). Successful roadmaps will incorporate some time for development and deployment of unproven technology and factor in time (and cost) required to reach commercial scale.

The exercise undertaken in this thesis was to produce a techno-economic analysis that can be used as an integral part of a technology roadmap. The objective: “*carbon reduction of steel plant operations, at least cost and minimal risk*”. Whilst many aspects of the roadmapping were addressed, some elements of a successful roadmap, such as identifying means of deployment and the implementation have not been addressed, so this should not be considered a complete roadmap.

The construction of the following techno-economic model would not have been achievable without the expertise of my Tata Steel colleagues. Where Mr Barnes provided expert assistance in identifying possible pathways and consideration on energy balance and performance. These considerations helped shape the assumptions used in the technical model. Mr Westerveld provided access to his vast knowledge surrounding economic modelling to help build this economic model, sharing his approaches and use of table function to manipulate the data within Excel.

5.3 Construction of the techno-economic model

5.3.1 Technology selection process

The first stage of developing a steel sector roadmap was to produce an accurate model, which will span the time period between now and 2050. For this purpose, the research uses an integrated steel production site typical of those found globally as the test case to provide the data and level of detail required to make accurate predictions on technology deployment. Having followed global research efforts in the steel sector, described in the literature review, it was concluded that the technologies would be one of a number of configurations that fall into the three basic categories:

1. Replacement of the current coal reductant with a low-carbon alternative
2. Electrification of the steel production process(es)
3. The application of Carbon Capture, Use and Storage (CCUS)

This provided a short list of potential technology outcomes. These were:

1. Increased utilisation of scrap and transition toward EAF, fed by iron supplied from a DRI facility, that will use hydrogen as the reductant (electrification / low-carbon reductant route)
2. Increased utilisation of scrap via existing route and transition toward EAF, and (where applicable) supplemented by BF iron (electrification route)
3. Deployment of CCUS on existing Blast Furnace technology (CCUS route)
4. Deployment of CCUS on the instillation of new state-of-the-art iron making technology (CCUS route / low-carbon reductant route)

Not all of these technologies are fully commercialised, with various TRL levels and require further developments. The point at which some of the technologies could be deployed in the model's timeline takes into consideration when each technology is likely to become available. The technologies short listed, however, could be deployed in full or in a combination with other technologies. Also described as partial deployment. This combination of factors led to a possible 20 technology outcomes for our chosen steel production site in 2050.

Of the 20 possible pathways, 18 are modelled. The decision on the 18 potential technology pathways, which were to be modelled, was influenced by geographical opportunities as well as current assets configuration. Within the literature study, global activity was investigated and a trend in technology pathways emerged, depending upon geographical location, availability to generate large quantities of renewable power, political intervention and public perceptions. None of these factors ruled out any of the technology options for our chosen base case site and so all technologies, with suitable TRL ($\geq 6/7$) were considered. The modelling process aimed to be technology agnostic, so not to purposely favour the two technologies that were developed within chapters 3 and 4. The 18 new asset configurations and their deployment were influenced by current assets, their existing lifetime and need for replacement and a product market analysis. Product market analysis was considered separately, but is not a focus of this research, only used to identify that delivery of a future product portfolio to potential emerging markets was a key consideration in asset configuration. Specifically, production capacity and the limitations on product quality caused by some production routes. It was decided that supplying a hot mill with 4mt of steel annually was the key objective, therefore only 'heavy end' production (this is the production of unfinished steel coil known as hot rolled coil (HRC) for the base case site) was considered and that downstream processes would remain unchanged to supply the future product markets.

5.3.2 Key asset replacement decision points

Primary iron production is a highly capital-intensive industry. Assets are often very large with long lifetimes, in the range of 25-30 years, but can be extended through partial rebuilds. Typical,

ongoing investment for a 4mt/yr integrated facility would be ~£200m per year, not including essential maintenance. For this reason, it is often quite a conservative industry as key investment decisions must be taken years in advance and preparations set in place. The transition period from now, 2020, up to 2050 is within only one investment cycle, so it is critical that investment decisions do not lead to regret capital and stranded assets. The average age of global steel assets is only ~13 years, and with such large CAPEX investments and long payback, transition to new technology before the end of asset life is very unlikely. Key investment decision points were mapped out along with the assistance of steelmaking expert, Mr Barnes, to determine when these investments should be made and how they would influence overall site configuration. It soon became evident that the transition phase between now and the future 2050 low-carbon vision would be challenging. Some assets would need to be replaced that could become redundant in certain scenarios, otherwise imports of materials would be needed to fill shortfalls in capacity. Profitability during this transition due to potential mismatch of assets and energy balance would lead to negative cash flow as well as logistical issues. A complete solution to overcoming all the transition phase technical issues is beyond the scope of this study, but the issue must be highlighted.

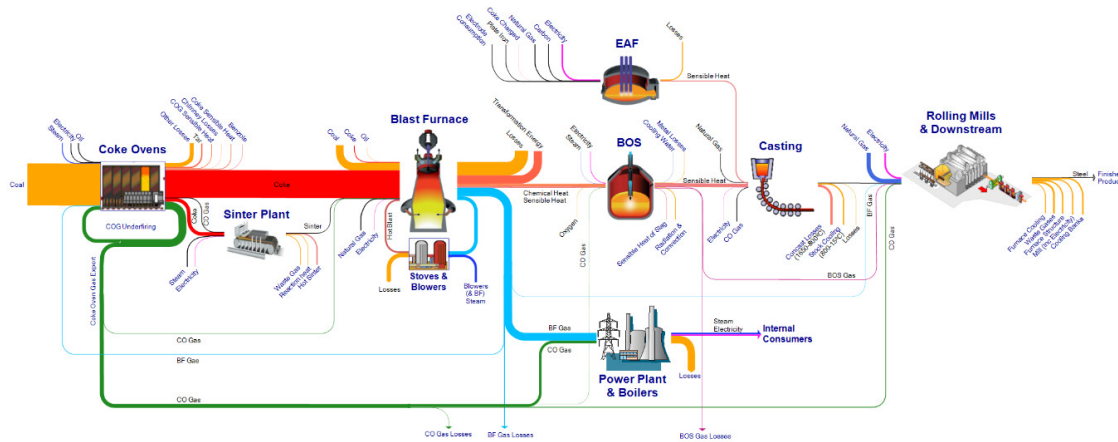
The key investment decisions led to a flow diagram of asset configuration, following rebuild or replacement of assets once they reach end of life.

Replacement of current assets with new technologies has to be taken into consideration with the current TRL of the alternative technologies. This would lead to a delay when some technologies could be deployed. For example, full replacement with hydrogen steel production is unlikely to be available before 2030, and more likely to become a reality post-2040. The transition to hydrogen is taken into consideration within the fuel mix.

5.3.3 Energy balance model

The energy balance provides the heart of the techno-economic model, from which the demands and costs can be calculated. Establishing a base-case site energy balance was one of the major challenges for the modelling process, followed by developing a highly flexible model that will reflect the energy use within the 20 scenarios. Accuracy here is critical and access to good data is not always possible, as the sites are very complex and the energy mix at all points is not always monitored and often estimated using process parameters. This may be where some other models fail to accurately assess the impact from changes in steelmaking technology, so great care was taken to produce the most sophisticated model possible. An example of this complex energy integration can be seen in the Sankey diagram below in figure 5.1. Raw materials, power, steam, water, heat and various gases are all used around the site, resulting in a total of 8 CO₂ emission releases (6 major emissions points at our test case site).

Figure 5.1: UK steel plant energy Sankey diagram



Source: Tata Steel UK

Multiple models that make up the complete, techno-economic assessment need to interact with one another and be sufficiently flexible to incorporate the changes in technology deployment (a user friendly interface). The energy balance and the raw material input models must both interact with the economic model. A base-case energy model was established that splits the energy production and consumption into the two areas of interest, heavy end and downstream processes. Heavy end refers to the point where steel is cast in the BOS plant from concast (continuous casting). Downstream is the further processing of the cast steel, into final strip product. This is described later within the construction of the base case. Downstream processing can vary depending upon the finished product and was less of a concern in the modelling processes.

After establishing an energy balance, the base case net energy flows can be determined as well as their impact on the processes and the cost. Because the heavy end processes produce gases, it is often the goal of many steel manufactures to be energy self-sufficient. The processes gases, as described in the literature study, are used within the site to generate heat and energy, often in the heavy end, but also in the downstream processes. Changes to the heavy end can result in a reduction of process gases available onsite. The need to import energy is avoided where possible by steel manufacturers due to the increased cost. However, the test site does not produce sufficient coke and the powerplant is slightly undersized, so there is a need to import gas (following limited availability of COG) and electricity. Power plants are often undersized due to the variability of the process and difficulty in storage of large volumes of process gases (large nitrogen volumes). Power station assets are much larger than those for natural gas, given the low calorific values of the process gases, therefore cost and payback times are long. A compromise in capacity is often made to ensure the power plants are able to utilise all available gases and are not sitting idle.

The model uses the energy balance to consider the impact on any modification to site and the influence on internal gas production: the possibility of importing more of our energy needs, increasing imported energy costs and the associated CO₂ emissions. The energy balance considers the gas balance and electricity demand only and does not include the steam generated and used onsite as this is thought to be incorporated as part of the gas usage. Future development of the model should consider steam use, however, there is an opportunity to electrify some of the steam demands or generate the steam from waste heat sources, which was not included. It is clear that there are opportunities for steam demand reduction, but given the current availability of steam on-site, there is no financial driver to achieve this.

The steel making process is naturally a high temperature operation and a considerable amount of power is used in cooling processes. Recovery of this heat or any reduction in energy used for cooling in a transition towards a different technology was not considered.

The blast furnace produces the greatest volumes of gas and energy proportion, but this gas has quite a low calorific value. Coke-oven gas, on the other hand, has a significantly higher CV and also a low carbon emission associated with combustion due to the hydrogen present, yet represents a smaller proportion of total energy. Abating coke-oven gas therefore produces minimal impact on carbon emissions compared to capturing BF gas, hence abatement of this process is not considered within the model. The process gases have a certain energy content, based upon their average composition (this varies depending upon site and operations), which is used to calculate energy production, per ton of HRC and balanced with energy use, per t/HRC. The shortfall (or surplus) would determine the amount of energy import needed. Electricity use will increase if more electrification of the processes is applied, resulting in an increased cost of electricity import, and accounts for the carbon emissions trajectory of the imported power.

5.3.4 Basic modelling principles

The model has been constructed utilising the commercial model approach described below as the foundation for the cost calculation supplied by Mr Westerveld, Tata Steel Europe (TSE), Group Strategy. Upon this, a technology appraisal was conducted for the chosen site, and the two are evaluated in order to simulate multiple possible future scenarios. The basic principles of this model are very similar to those used within the European 2050 steel making model developed by the Boston Consulting Group (BCG). That is, to provide a timeline from now until 2050 and to show how the site might change over this period using 1-year increments. Although this model is distinctly different in the analysis approach, as the BCG model represents a European-wide steel industry transition, rather than a specific single plant. The major assumption basis for the BCG assessment was that the transition for Europe, would be scrap limited. That is, once all scrap is used the demand must be met from primary iron ore routes, maximising EAF production.

Whilst this approach may work for a broad, European wide view, it does not consider the impact in product portfolio and site-specific factors, such as access to low carbon electricity and does not say which sites will convert to EAF. It also does not consider scrap flows in and out of the European boundary within this assumption, nor a pull in scrap demand from emerging markets. In the new model that has been developed, we are looking at an individual site and are not scrap limited, however in a European wide context, the scrap availability needs to be taken account of for the scrap price estimates. Equally, the BCG model assumes that a maximum roll out of DRI will be established, however, again the model does not say where this will occur and gas availability (and cost) is very location specific. The lifetime of the assets, and therefore new CAPEX, is really a critical factor in determining where plants will be built and when, as well as environmental factors and legal permits, that would most likely prohibit the construction of new greenfield steelmaking facilities in Europe.

Data tables are produced for the base cases and for the alternative technologies. These data tables include the essential data that would be needed, such as energy use, material inputs and outputs, including by-products and of course associated emissions factors. This data is typically set as a function of tonnes per crude steel output. The data tables display the various parameters for each scenario in either single, 5 or 10-year increments. Using look-up data tables, this data is called upon within the model in order to simulate possible future outcomes. Flexibility was considered key to the construction, to allow modification of the data. The data can be easily updated when more accurate data is obtained, which is vital for the lower TRL technologies this can be amended, without the need to reconstruct the model. It can also be changed to compare future simulations and determine the influence of certain sensitivities within future simulations.

The amount of new technology deployment, or % of production in tonnes of crude steel can be adjusted over the aforementioned yearly timeline. The model can then apply the associated values for that technology, per tonne of steel produced. For each of the 20 potential scenarios, there are 'volume scenarios' that will relate to the quantity of steel produced via each production method. There is some overlap between asset configuration and production process, meaning some of the 'volume scenarios' can be used more than once. The application of carbon capture is an add-on technology and therefore the volume of steel from the process will be the same.

Excel utilises a table look-up function, which is exploited throughout the model. `{=TABLE(,cell)}`. This is a powerful tool that will allow values in the data tables to be adjusted and recalculated, depending upon the chosen scenario. The scenario that the user wishes to analyse can be selected from a drop-down menu. From this the relevant data is obtained from the scenario matrix. A matrix was used to determine the data sources that will be used in each scenario, so that if the scenarios are adjusted, only the matrix content needs to be amended and

the source of the data can be easily adjusted. The model values for each of the 20 scenarios are then calculated and each are displayed within tables.

5.3.5 Limitations of the model

A limitation of the model is the ease at which sensitivity analysis can be carried out for multiple simulations. Because the data in the data tables are fixed values, and are a result of the best estimate, they are not presented in a range or potential minimum and maximum values. The extreme values have to be manually entered in order to see the impact of these variations and perform the simulation again. It was determined that the model was quite capable of delivering the results needed, and further investment to improve this limitation was not necessarily needed to provide the results within the timescales. A solution to the sensitivity would be to add upper and lower limits to the data, in both high and low scenarios. But this would create many more scenarios to analyse if each of the data inputs required three variations and the model is already limited by analysis time. Another limitation is the ability to compare each scenario with the next over the full lifetime of the study. Only key dates were chosen, in ten-year periods: 2020, 2030, 2040 and 2050. This shows sufficient resolution for investment cycles. Key milestone dates were chosen for the data output. Showing continual (annual) trends in the data needed further analysis for some for the key areas, such as annual cash flow, but individual parameters can easily be selected and analysed.

5.3.6 Commercial model

The steel industry can be simplified into a commodities business, purchasing materials and, through process chemistry, converting this to steel for sale to customers at an agreed price. Successful steel producers add value to these commodities through improved process chemistry knowledge, efficiency of processes and added product value (such as further processing, coating or specific metallurgical properties). But the fundamental raw material (coal, lime, iron ore, scrap) and energy inputs dictate revenues, due to their scale and influence.

The commercial calculations and assumptions used within this model are supplied from a commercial model used by Mr Westerveld, of the Tata Steel Europe Strategy department. This thesis' techno-economic model builds upon the commercial model assumptions for predicting profitability and cash flow that are set out within this model. However, by including process variation, due to the changes in each scenario as a result of new technology deployment, we are able to demine the financial impact of these variations on the economic models' predictions. These technologies could, for example, use a greater amount of electrical power, hence the cost of power use would increase, influencing the energy balance, but also cash flow. The day-to-day operational cost for each technology route are split into fixed and variable costs. The amount of steel that is produced will impact the variable cost, but the fixed cost will be a one-off cost

irrespective of crude steel output. The commercial model needed to be reconstructed to reflect, for example, the new site location, different configuration of assets, future investments, product portfolio etc., and to forecast this data up to 2050, for the new site.

Managing cash flow is critical to determining a successful technology transition up to 2050 and the model clearly shows some methods are much more expensive to implement than others. Not only is cost to operate important, product quality is critical to maintaining a successful business. Some assumptions on the necessary process steps have to be taken within the model that influence the volume scenarios, but the model is not capable of predicting product quality and relies upon the experience of the user. Expert advice was sought to ensure product quality was met, but even so some options are included that would not meet product quality, in order to see their impact on operational costs, so caution in interpreting the results is needed.

The amount of investment needed (CAPEX) within each scenario is also vital when comparing each scenario, alongside day to day operational cost (fixed and variable OPEX), in order to determine cash flow. The 'Investment scenarios' data tables are called upon to analyse the cost for each production route. Investments take into consideration the implementation of new technology, or the repair and replacement of existing technology as well as essential environmental improvements. It is expected that, as environmental performance for the sector in general must improve in order for technologies to achieve or exceed best available technology (BAT) level will be needed in the future. Some process routes would avoid the need to install BAT on assets that are eliminated. For example, a transition to a new process route could remove the need to maintain and invest in coke and sinter production.

Data tables relating to cash flow include:

1. Investment cost (CAPEX)
2. Emission trading cost associated with the Emissions Trading Scheme (ETS)
3. Tariffs or variable costs (Variable OPEX)
4. Fixed costs (Fixed OPEX)
5. Carbon capture and storage cost

Investment costs are those needed to either implement a new technology, or keep existing equipment operational and include one-off large scale investments for repair, replacement or environmental compliance. The timing of these investment points is critical, replacing equipment at the end of serviceable life. We have not considered the early investment in new technologies (prior to end-of-life) within the model, however that could be possible, if a new process route were to lead to significant cost savings from the base case.

The European steel sector, as well as other large emitters, are subject to carbon taxation in the form of the European ETS. To avoid carbon leakage (the off-shoring of carbon emissions by

relocation of industries outside of Europe and the import of goods) free allocations have been given to the ‘foundation industries’. The amount of free allocations per year will reduce over time and the sectors must purchase carbon credits to pay for the carbon emitted by the process. Within the model the amount of free allocation and also the price has been estimated. It is difficult to predict these two values, but they play an important part in the costs of carbon abatement. Those technologies that can reduce carbon emission at a cost less than the predicted ETS prices, and at a rate faster than the decline in free allocation, will result in a greater cash flow. The opposite is obviously true, resulting in a net loss if, for example, we continue with the base case scenario.

Variable costs will relate the purchase of energy, raw materials, consumables, by-products, labour and more. These will vary depending upon the quantity of steel produced, via each route and are hence considered variable. Most of the tariffs have been fixed for the duration of the model. This was to eliminate the uncertainty surrounding prices forecasting and allow a comparison between the 20 scenarios, based on current knowledge. Exploring the boundaries of cost predictions, will determine how robust (level of risk) each scenario is exposed to.

Fixed costs are operational costs, irrespective of steel output. For example, essential maintenance, lighting, cleaning, etc. The fixed costs for each facility are estimated and will vary from one scenario to the next if a plant or facility is no longer required.

Carbon capture is assumed to be an additional cost. The most effective method for this study was to use the predicted costs found with the literature for the application of CCS to Blast Furnace. An estimation of capture costs for a State-of-the-art (SofTA) unit was also obtained. Below we discuss CCS application in the model in more detail.

5.3.7 Establishing a base case model (Blast Furnace route)

Developing an accurate base case was a critical step in the modelling process. The data and model output needed to reflect the true nature of a typical steel production site, before modifications to this process can be made. The BF route was modelled using actual site data and process knowledge, collected for the reporting of CO₂ emissions for the ETS, and is considered accurate. An understanding of production yields, conversion rates and process gases is needed to develop and validate the model.

Below (table 5-1), we have the data input (Blast Furnace Process parameters) that will vary over time depending on scenario. 2016 data was used as the reference base case, since the plant has not changed since 2016, this data has been validated for the ETS, and is considered typical of current operations. Data post 2016 is interrupted by process upgrades and stoppages, hence it is important to understand if the data you have is representative of typical operations. Some elements are removed for confidentiality, and the economic model described above is not shown for this reason. Negative values represent energy production onsite, in the form of useful

processes gases. In contrast, positive values relate to consumption of materials or energy. Efficient and effective utilisation of these materials and gases within a conventional integrated steel plant leads to greater process efficiencies, reduced energy imports and costs.

Following the parameter inputs, which, as mentioned, will vary over time (yearly) due to changes in the individual production levels for each processes route within the scenarios, the CO₂ intensity per ton of crude steel is calculated, based on carbon inputs and site energy balance. Only the 2016 data is shown, but this data is calculated each year, up to 2050. The CO₂ emissions resulting from the site energy balance is a result of any additional energy import into the site in the form of electricity or natural gas, whereby the imported coal and resulting process gases are insufficient to meet the site energy demands.

Table 5-1: Inputs to the modelling base case calculations (values used with the model are deliberately hidden for confidentiality of processes conditions)

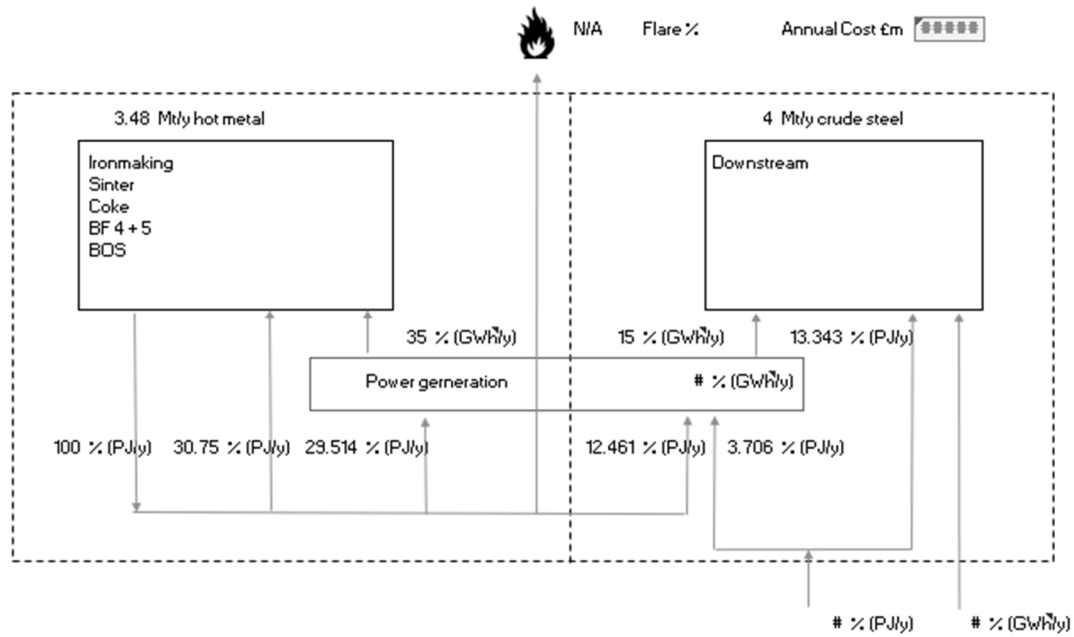
| Model Inputs | Units |
|---------------------------------------|-------------------------|
| Casting yield | kg / t Liquid Steel |
| Hot metal losses | kg / t Hot Metal |
| Hot metal ratio | kg hm / t Liquid Steel |
| Scrap ratio | kg hm / t Liquid Steel |
| Agglomerate Input | kg / t Iron |
| Sinter moisture content | % |
| Sinter ore yields | kg ores / t sinter |
| Blast furnace Scrap | kg / t Iron |
| Pulverised coal injection (PCI) yield | % |
| PCI moisture content | % |
| Coke consumption | kg coke / t Iron |
| Breeze production | kg breeze / t coke |
| Coking coal yields | kg coal / t coke |
| Coal input SRE | kg coal / t Iron |
| Oxygen demand | NM3 / t hm |
| Compressed air demand | NM3 / t hm |
| Energy demand down stream | GJ / t |
| Coke Oven Gas (COG) production | GJ / t coke |
| BF Gas (BFG) production | GJ / t HM |
| Coal Use BOS Vessel | kg / ton Iron |
| BOS Gas production | GJ / t ls |
| Oxygen demand BOS | Nm3 / tls |
| By-product generation | t By-products / t Cokes |
| Carbon content PCI | kg C / t PCIcoal |
| Carbon content coaking coal | kg C / t coaking coal |
| Carbon content Natural Gas | kg C / GJ |
| Carbon content imported coke | kg C / t Cokes |
| Carbon content by-products | kg C / t By-product |
| Energy content of steam | GJ / t |
| Steam consumption | kg / t Crude Steel |

| | |
|-----------------------|-----------------------|
| Energy loss flaring | GJ / t Crude Steel |
| Energy sintering | GJ / t |
| Energy CGP (Coke Gas) | GJ / t |
| Energy BF | GJ / t |
| Energy BOS | GJ / t |
| Power Other | kWhr / t Crude Steel |
| Power Sintering | kWh / t sinter |
| Power Pellets | kWh / t pellet |
| Power CGP | kWh / t coke |
| Power BF | kWh / thm |
| Power BOS | kWhr / t cs |
| Power O2 production | kWh / Nm ³ |
| Power down steam | kWh / t cs |
| Total energy input | GJ / t Crude Steel |

5.3.8 Base case energy balance model

To validate the model's energy balance, which will include only the upstream areas of interest to liquid hot metal (heavy end), first a more sophisticated site energy balance was needed. This site energy balance included all energy users and generators. Using gas and electrical consumption data for the site, the energy generations and consumptions were established. The data is represented in figure 5.2 in either % (PJ/y) for gas, and % (GWh/y) for the electrical generation and import. Percentages are used to hide the confidential nature of the site information. Steam generation and boiler efficiency are calculated based upon the calorific value of gases and steam production data. Turbine alternator (TA) efficiencies are determined to calculate the overall power generation capacity for the site. The shortfall in energy generation is met by gas import, which correlates well with the site consumption data, based upon the annual financial energy costs. This model is unique to this techno-economics assessment, as the processes are split between heavy end and downstream, so that we can establish the effect of changes to our heavy end production on site energy imports and costs for the whole site. With this approach it is possible to determine the impact of a reduction in WAG generation, use or power plant modifications on the site energy balance and costs.

Figure 5.2: Breakdown of site energy balance in to upstream (heavy end) and downstream processes



There is some simplification to the model’s energy balance (calorific values of gases for example), but the CO₂ emission correlates well with the actual emissions data for the site. A similar calculation is also conducted for each of the various technology options. The calculations are different, due to process changes, energy inputs and process gases generated. For example, EAF does not need such complex carbon input calculations and the off-gases are not used throughout the site for energy and reheating. The CO₂ intensity of each process is then cross-referenced to the volume of steel produced via each method (given in the volume scenario), which is then summed within the ‘Mass Energy Flow’ spreadsheet. Note that the results for alternative technologies within the 2016 base case are, of course, zero. No volume of steel is produced via these routes within the base case, therefore we do not expect any CO₂ associated with these methods. This provides a useful systems-check for the model.

Energy efficiency improvements are integrated into the model, buy reducing the amount of wasted processes gases (a reduction in flared gas). This assumes that, over a period of ten years improvements are implemented so that all process energy is used. Also, to reflect improvement elsewhere, the amount of imported energy is reduced over time. However, the carbon emissions gained here are offset by continuous decarbonisation of the grid decarbonisation, so this primarily benefits the cost performance.

5.3.9 EAF model

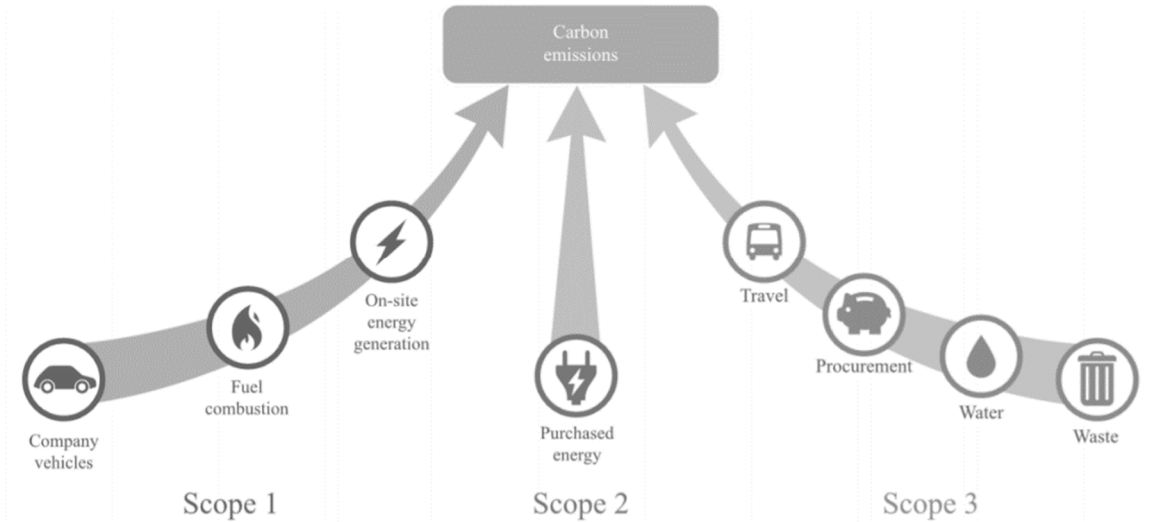
EAF data inputs were sourced from previous roadmapping data used for EUROFER's 2050 roadmap (Eurofer The European Steel Association, 2013) and cross-checked with online data from Steelonthenet.com's EAF cost model (Steeletonet, 2020). It is important to note the scope of CO₂ emissions. Different reporting methods for CO₂ process intensity include different emissions scopes. An example of emissions scopes is shown in figure 5.3. As we are considering EAF technology, which is powered primarily with purchased electricity, it is important that we also consider scope 2 emissions. The model does not include scope 3. An estimate for the CO₂ intensity of grid power has been made. It was not considered valid to assume we would gain access to 100% renewable power for the process from moment of installation, owing to the time taken to decarbonise the grid and a disinterest in investing in new power production from the perspective of a steel plant operator. However, we should not rule out a private wire arrangement if possible, but this would be on a case by case basis, and is not included in the model.

The CO₂ intensity of the grid 'CO₂ External Power' has been estimated for the UK based upon estimated carbon reduction trajectory (figure 5.4). This reduction may accelerate if net-zero targets are enforced and carbon budgets are re-assessed. Under the model's assumption, the grid will reach zero carbon intensity, reducing by 17 tCO₂/GWh each year, in 2046. A linear transition was assumed, given the difficulties in predicting the future trajectory. A sensitivity analysis on this was not carried out, due to the already high uncertainties in the grid carbon reduction trajectory, and except for full EAF (which as we will discuss has critical issues) this energy input plays a minor role in the carbon reduction, with either coal CCS or fuel switching to hydrogen being the significant factor.

The ability to utilise greater scrap content should be considered essential in any future configuration and it is a key enabler for a transition to DRI, but there are limits in a global context of its ability to solve the issue. There is no credible evidence to support that scrap availability will be able to meet global steel demands, even if steel is used more efficiently. Steel from primary iron will be needed well beyond 2050. More recently, the 'Steel Arising' report promoting the solution to the UK steel sector challenge, from a credible academic has emerged (Allwood, et al., 2019). Whilst using less, a key theme of the work, is a viable solution that should certainly be taken forward, this work exclusively identifies 'new' EAF technologies for the UK. Ironically EAF technology is not new and is around 100 years old. Metallurgical industry experts confirm that a 100% UK transition to EAF is currently not technically viable, due to restrictions on product quality, leading to a reliance upon steel imports. A globally co-operative approach would seem sensible, whereby those with the ability to decarbonise the primary route should take the opportunity, so that scrap is available for more difficult to decarbonise regions that are without access to alternative low-carbon fuels, carbon storage solutions and economic incentive. That is

to say, CO₂ is not patriotic and reducing CO₂ in one region does not correlate to the global reduction in carbon emissions if the CO₂ is later imported or outsourced to different regions of the globe.

Figure 5.3: Definition of emissions scope 1, 2 and 3



Source: (ARUP, 2018)

Figure 5.4: Forecast of CO₂ grid intensity

| Forecast1 | CO2S2 | 1 | 2 | 3 | 4 | 5 | 6 | 7 | 8 |
|-----------------------------|-------|-------|-------|-------|-------|-------|-------|-------|-------|
| | ktons | 2015 | 2016 | 2017 | 2018 | 2019 | 2020 | 2021 | 2022 |
| CO2 allowances (%) | 2 | 79% | 79% | 79% | 79% | 79% | 79% | 76% | 73% |
| Direct cost (€/tCO2) | 3 | 0 | 5 | 6 | 6 | 22 | 26 | 27 | 28 |
| Indirect cost (€/tCO2) | 4 | 0 | 0 | 0 | 0 | 0 | 0 | 0 | 0 |
| Market compensation (€/tCS) | 5 | 0 | 0 | 0 | 0 | 0 | 0 | 0 | 0 |
| CO2ExternalPower(tCO2/GWh) | 6 | 516 | 499 | 482 | 465 | 448 | 431 | 414 | 397 |
| Xrate (€/€) | 7 | 0.902 | 0.902 | 0.902 | 0.902 | 0.902 | 0.902 | 0.902 | 0.902 |
| Xrate (GBP/€) | 8 | 0.750 | 0.750 | 0.750 | 0.750 | 0.750 | 0.750 | 0.750 | 0.750 |
| EnergyUsePoP (MWh/TJ) | 9 | 39 | 39 | 39 | 39 | 39 | 39 | 39 | 39 |

5.3.10 DRI model

The significant model differences between the base case and a transition to a DRI installation are the switch in energy input from coal to gas. As NG contains almost an equal amount of hydrogen as well as carbon, the following reactions both take place. A transition to DRI with NG can lead to a ~50% carbon reduction compared to the BF due to the hydrogen content of NG. Equations 5.1 and 5.2.



The DRI process naturally has a lower carbon emission than BF-BOF, given the hydrogen within the input energy. Given the restrictions on available gas in the studied plant area, a Finex process was chosen as it is considered an advanced commercially available technology. Finex could also be operated with non-coking coals in the transition process, allowing for greater flexibility. The use of a DRI shaft furnace as a gas-based solution allows the transition, once available, to large volumes of hydrogen. Note that the BF is limited by the amount of gas that can be used due to the structural burden that is fed into the top of the furnace, hence is not a future solution in a hydrogen transition. To simulate the transition to hydrogen within the model, the natural gas energy input is reduced from baseline 10GJ/thm and replaced with the same hydrogen energy content in the quantities, 35%, 55% and 70%. The transition starts in 2042, as it is expected that large volumes of hydrogen will take time to be available for the steel plant.

At the time, no detailed TEAs exist of the Hydrogen process, with only one comprehensive academic study by Vogl et al, and even more recent modelling by Patisson & Mirgaux (2020) as part of the ULCOS program (Vogl, et al., 2018), (Patisson & Mirgaux, 2020). Hence some of the parameters are not fully known and estimations are made on the influence of hydrogen injection.

10GJ/thm is considered the energy requirement for the DRI process and is therefore the same energy used for a hydrogen substitution within the model. At 10GJ/thm this corresponds to 76.92 kg of H₂/thm. Yet some recent reviews state that stoichiometric consumption is 54kg of H₂ per ton of iron, which equates to only x 7.02 GJ. (Vogl, et al., 20), (Patisson & Mirgaux, 2020). A 3 GJ (30%) energy difference between the consensus from proven DRI operation and academic studies can lead to significant misinformation from future TEA assessments and analysis. Overall, the hydrogen reaction is endothermic, whereas CO is exothermic (Kato, 2012). Keeping the iron molten is therefore of some concern, not specifically raised within the literature. No information is available as to how a 100% H₂ furnace will perform at scale and following the lack of availability of surplus GJ quantities of H₂, many uncertainties exist. Low metallization is expected within the DRI furnace, leading to greater FeO reduction required within the following EAF stage. Common metallization within the DRI is close to 94%. The model does not take account of the influence of metallization degree, with the volume % split for DRI and EAF, leading to some degree of error. The metallization degree for a H₂ reductant is unknown as this is unproven (and could be higher), so no guesses have been made at this stage.

The details available for the Finex process suggests a 15-20% lower CAPEX and OPEX cost when compared to the BF route. If economic modelling analysis suggest that this process is feasible, a more detailed study (which would include logistics, plant locations and gas pipelines for example) would be needed. The reduction in carbon in the iron that is subsequently supplied to the EAF, following a transition to H₂, needs further investigation as to its impact. As no

detailed information exists for this region, it is not taken account of in the model analysis, so some care must be taken at this stage. Even so, if the technology seems equal to the BF route in costs, we could conclude that further work is need as this opens the door for a future transition to full hydrogen and zero emissions. For simplification in the modelling and because it shares the same parameters as the SoftA, the Finex process is built into the model as an alternate SoftA process. DRI model data example is shown in figure 5.5.

Figure 5.5: Example of DRI data input into the model

| DRI with H2 | | | 26 | 27 | 28 | 29 | 30 | 31 | 32 | 33 | 34 | 35 | 36 |
|--------------------|--------------------|----|--------|--------|--------|--------|--------|--------|--------|--------|--------|--------|--------|
| HISS7 | | | 2040 | 2041 | 2042 | 2043 | 2044 | 2045 | 2046 | 2047 | 2048 | 2049 | 2050 |
| ktons | | | | | | | | | | | | | |
| kg / t LS | LossPerTonHM | 2 | 80 | 80 | 80 | 80 | 80 | 80 | 80 | 80 | 80 | 80 | 80 |
| thmt-LS | HlsarnaHM-ratio | 3 | 0.960 | 0.960 | 0.960 | 0.960 | 0.960 | 0.960 | 0.960 | 0.960 | 0.960 | 0.960 | 0.960 |
| kg/t hm | Scrap-ratio | 4 | 169 | 169 | 169 | 169 | 169 | 169 | 169 | 169 | 169 | 169 | 169 |
| kg/t hm | IronOreNeed | 5 | 1,440 | 1,440 | 1,440 | 1,440 | 1,440 | 1,440 | 1,440 | 1,440 | 1,440 | 1,440 | 1,440 |
| 0 | MoistureInjectCoal | 6 | 6% | 6% | 6% | 6% | 6% | 6% | 6% | 6% | 6% | 6% | 6% |
| kg coal wet / t hm | CoalNeed | 7 | 0 | 0 | 0 | 0 | 0 | 0 | 0 | 0 | 0 | 0 | 0 |
| GJ / t hm | NGNeed | 8 | 10.00 | 10.00 | 6.50 | 6.50 | 6.50 | 4.50 | 4.50 | 4.50 | 4.50 | 3.00 | 3.00 |
| NM3 / t hm | OxygenNeed | 9 | 50 | 50 | 50 | 50 | 50 | 50 | 50 | 50 | 50 | 50 | 50 |
| kg C / t inj coal | CarbonCoal | 10 | 806 | 806 | 806 | 806 | 806 | 806 | 806 | 806 | 806 | 806 | 806 |
| kg C / GJ | CarbonNG | 11 | 15 | 15 | 15 | 15 | 15 | 15 | 15 | 15 | 15 | 15 | 15 |
| GJ / t | EnergyUseBOS | 12 | -0.847 | -0.847 | -0.847 | -0.847 | -0.847 | -0.847 | -0.847 | -0.847 | -0.847 | -0.847 | -0.847 |
| GJ / t | EnergyUseDS | 13 | 1.650 | 1.650 | 1.650 | 1.650 | 1.650 | 1.650 | 1.650 | 1.65 | 1.65 | 1.65 | 1.65 |
| MWh/TJ gas | PowerBoilHIS | 14 | 0 | 0 | 0 | 0 | 0 | 0 | 0 | 0 | 0 | 0 | 0 |
| kWh/t hm | PowerUseHIS | 15 | 100 | 100 | 100 | 100 | 100 | 100 | 100 | 100 | 100 | 100 | 100 |
| kWh/Nm3 | PowerUseOxP | 16 | 0.00 | 0.00 | 0.00 | 0.00 | 0.00 | 0.00 | 0.00 | 0.00 | 0.00 | 0.00 | 0.00 |
| kWh/t cs | PowerUseBOS | 17 | 18 | 18 | 18 | 18 | 18 | 18 | 18 | 18 | 18 | 18 | 18 |
| kWh/t cs | PowerUseDS | 18 | 121 | 121 | 121 | 121 | 121 | 121 | 121 | 121 | 121 | 121 | 121 |
| kg/t hm | Hydrogen | 19 | 0.00 | 0.00 | 26.92 | 26.92 | 26.92 | 42.31 | 42.31 | 42.31 | 42.31 | 53.85 | 53.85 |
| t output / t input | CastingYield | 20 | 0.966 | 0.966 | 0.966 | 0.966 | 0.966 | 0.966 | 0.966 | 0.966 | 0.966 | 0.966 | 0.966 |
| 0 | | 21 | | | | | | | | | | | |

5.3.11 State-of-the-art (SoftA) iron production model

The parameters and values to input into the model for the application of a State-of-the-art blast furnace technology were obtained from the R&D department. This technology is under development (demonstration stages) and the details are not publicly available. A consideration for full scale technology availability has to be made. Implementation pre-2028 is unlikely, which makes transition to this technology challenging, following lifetimes of existing assets, but it is possible, potentially in a phased approach. The basic modelling principle was to substitute, where applicable, the new values with those of the BF base case, with some consideration for changes in upstream processes, energy balance and imported energy requirements. Wider benefits from the improved circular-economy of materials and local air quality using this method have not been included as it was not possible to monetise their value, but they should be noted as additional benefits to this process route. A reduction in necessary investments to achieve future environmental compliance can and has been considered within the investment scenarios, improving the cost performance for this technology. Other cost benefits include the closure of sintering and coking capacity, lower cost of carbon capture implementation, and the ability to use lower-grade, thus cheaper iron ores. All of which are factored into the investment (CAPEX) and OPEX calculations.

5.3.12 CCS model

A detailed assessment of the overall energy impact as a result of the application of CCS to the reference integrated site was not fully known at the time of the model development. Therefore, a simplified methodology was adopted for the model. The CO₂ capture rate and the associated cost per ton of CO₂ captured has been applied. By altering the capture rate and adjusting the cost, the effect from these parameters can be clearly evaluated. The cost of capture is based on internal Tata Steel technical assessments and validated with assistance of partners. Various CO₂ separation methods and technologies could be adopted, and the choice will often depend upon the type of store and transport method (the specification of gas composition or pressure the CO₂ to be supplied), local opportunities and access to external, alternative energy sources. There is also currently no standardisation of CO₂ specification for storage. What was apparent from the literature and process modelling undertaken by the author are the typical costs for the implementation of CCS; both CAPEX and OPEX. The implementation of CCS on a site increases both the investment and operation costs for the ‘with CCS’ scenarios. An estimate of transport and storage (T&S) cost was made, given the geographical location of the CO₂ source and proximity to a potential storage site, utilising current internal cost estimates in collaboration with external consultants. A fixed cost for T&S was used, and shipping was the preferred option for the reference site. The T&S cost is likely to vary significantly between sites, due to a number of factors, such as store type, distances to store and number of store users. Without a pre-front end engineering design (FEED), or indeed a full FEED assessment, these costs are difficult to quantify with a high degree of certainty.

Both the BF (~71% of base case CO₂ emissions) and the sinter plant (~11%) emissions would need to be captured to reach >80% total capture for the base case. Although the aim for carbon reduction was $\geq 80\%$, a specific carbon reduction target was not set for the model, so additional CO₂ sources were dismissed for this exercise. It should be noted that greater capture rates are possible at additional cost. Capturing gases from other sources, for example reheat furnaces or coke production are possible, but would be more costly as the concentration of CO₂ within the exhaust gases are much lower than BF gas. It is anticipated that the application of low levels of CO₂ capture (~30-40%) can be conducted at the least cost, due to improvements in the effectiveness of onsite gas utilisation. The method for separation has not been specified as there are still many variables to assess, however IEA GHG assessment and internal analysis would place this in the range from £43 – £61 /tCO₂ captured (IEAGHG, 2014). Additional capture rates, due to the lower CO₂ concentrations as mentioned, will increase this cost, therefore an estimated capture cost of £40 per ton of CO₂ captured has been used for an 80% capture rate. This is considered toward the low end of the capture estimate, but it is believed that improvement in onsite energy efficiencies would be possible. Also, continuous improvement in capture

performance such as those demonstrated within the chapter 3 and demonstrated in the use of proprietary could be realistically achieved within the years to full deployment (Okon, et al., 2017), (Zacchello & Wang, 2018). A cost of £20 per ton of CO₂ stored has also been applied for the transport and storage, producing a total capture, transport and storage cost of £60 /tCO₂ for the BF-BOF route capture cost.

The impact of removing BFG from the energy mix was not assessed in detail. Although of low calorific value, the blast furnaces provide a valuable energy source for use onsite for heat (pre-heating blast air in the stoves), steam and power. The impact on the site's energy balance is a complex issue (and varies significantly from one steel plant to the next) that must be addressed. The impact is estimated and applied to the cost of applying CCS, where it is assumed the calorific content of the gases will not be lost and recovered via some means on-site. It is clear that this is an oversimplification of a rather complex matter that is site specific, but allows adequate comparison of the costs to apply the technology and the ability to compare the various technology pathways. Any shortfall in site energy balance is made up of NG import.

Application of CCS to a SoftA furnace has a significantly reduced cost following the nitrogen removal in an air separation unit, similar to oxy-fuel combustion processes. Whilst air separation has its own cost associated, the overall operational costs is lower than the conventional BF + CCS capture route. An estimated cost of £15 /tCO₂ captured has been estimated, with an equal £20 /tCO₂ for transport and storage. Total costs of capture, transport and storage for the SoftA route is estimated at £35 /tCO₂.

5.3.13 CCU model (the conversion of CO₂ into a product of greater value)

There are various projects exploring options for the steel sector to utilise the carbon within process gases (table 2-2). Within the model an estimate was made of the costs and impact, however, as these programmes are still in the low to mid TRL stages, with limited publicly available data, it is difficult to assess the overall impact. The model's outputs do provide the ability to assess and discuss within the results how the two technologies investigated within this study may be applied in a future steel making context. Without this assessment, it would not be clear what part they may play in a future asset configuration and it would be difficult to make a case for continued development. Further analysis and investigation into the deployment of CCU technologies is made outside of the model and discussed in the analysis and results.

Whilst some CCU methods, such as algae and carbonation, can utilise direct process streams, it can be assumed that the CO₂ needs to be supplied in a 'storage ready' composition for the CCU process. Within the model we can assume that the energy and cost needed for the CCS is also applicable to CCU. A crude, but effective, method has been used to then add the additional energy

and cost onto the CCS model, to generate a value for the CCU potential, offset by a nominal value of the product made.

It is generally understood that for large scale conversion of CO₂, hydrogen is required, with a few exceptions. There are 3 potential sources of hydrogen associated with steel production that can be considered for CO₂ conversion. The first is the hydrogen within coke oven gas (COG). Most European steel plants will have an onsite coking facility producing hydrogen rich gas, whereas in China these coke plants are often independent of the steel works, and given local Chinese energy policy, these gases are often transformed into methanol. In European plants these gases are used within the processes. Removing the hydrogen would impact upon the site energy balance, requiring an import of NG (or converting to electricity or hydrogen). Because the current, onsite use of the hydrogen produces low emissions, utilising this hydrogen is not considered in the modelling as it would likely result in high cost and an increase in emissions. The total volume of hydrogen available in COG would limit the quantity of sites CO₂ conversion to <5%, depending upon carbon content of product.

The second potential source of hydrogen could be either blue or green hydrogen. For this, a significant investment in infrastructure is required. Within the model we have assumed, as is the case for hydrogen based DRI, a cost to supply the hydrogen only and not the necessary investment in infrastructure, which would be outside of scope for the steel producer. For this exercise, only green hydrogen is considered as blue hydrogen would also require CCS unfractured, and greater import of NG. Within this context, although the LCA is incomplete, it was difficult to justify this approach when considering a reduction in total fossil carbon use.

A third and final source of hydrogen comes from utilising the site's CO contained within the WAGs using a water gas shift (WGS). Using CO onsite for power generation will ultimately result in a CO₂ emission. This method provides a way to utilise the energy content of CO in an effective way that simultaneously produces a high concentration of CO₂ and a hydrogen and nitrogen rich gas. The analysis of this process is still under development, but shows promise. Again, in the context of the modelling, a simpler approach has been taken; the purchase of green hydrogen into the process. A WGS approach, however, is a possible solution, supplemented by green hydrogen for a full-scale facility.

Given the consideration above, the model was used to evaluate CCU upon a BF case, with and without the application of CCU. There has been no modelling of CCU without the application of CCS as the capture element is still required. Instead of sending the CO₂ to store, the transport and storage cost has been set to zero. A cost for green hydrogen is included as offset by an estimate for the value of the product, minus the estimated cost of CAPEX and OPEX for the facility.

Whilst the model has the ability to evaluate CCU methods, given the uncertainties, many possible process options, various products, sources of energy, market condition and lack of real data, it was considered that it would need further development, once first the CCS technicalities and cost uncertainties are overcome. The data is likely to be misleading if a thorough assessment is not carried out, which will require considerable effort and development budget. Hence the model results for the CCU function are considered a useful feature, but still ‘under development’.

5.3.14 Risks

The model is unable to directly determine risks associated with technology choices, but the ability to assess risk is very important with any strategy development or roadmapping process. The ability to avoid ‘regret capital’ is essential, given the size and scale of typical of steel making operations. Those technology pathways that provide the greatest flexibility with minimal risk and investment are more likely to be considered (by corporations and their lenders) above those that lead to only one possible technology option. It is also not possible to determine if new technologies that are not yet commercially viable, or just concepts, will be successful. A decision on technology available is factored into the volume scenarios data (when the technology will be deployable), but it is not possible to precisely predict if these technologies will become commercially available within these timescales. Again, flexibility to change to a different technology pathway would be advantageous in any strategic decision making if these technologies prove unviable.

Most of the prices in the financial model are fixed and based upon current costs. It was chosen to fix these variables to today’s prices, to be able to compare the technologies using a common price. Predicting future prices was not within the scope of this study (and price forecasting is highly subjective), but would clearly have an impact upon chosen pathway, if say electricity prices were to suddenly increase due to policy and renewable deployment. Likewise, it was not possible to predict policy intervention to incentivise certain pathways, such as a tax incentive for a lower-carbon route, but it is clear that some policy intervention is needed to transition away from the well-established, higher carbon emitting processes. Some predictions have been made, such as the allocation of ETS credit and their associated cost to business, as well as the CO₂ intensity of grid electricity, otherwise fixed costs are used throughout the model. The current policy mechanisms in place are designed to deliberately push up the price of carbon credits, following limitation of free allowances (free allowance allocations are known) leading to increased demand, therefore some estimate of cost increase has been made for ETS credit price. It has been assumed that if the technology is cost effective with today’s prices, it should also be fit for the future. Predicting prices is quite challenging and risky given the uncertainty surrounding the energy transition and challenges in achieving net-zero emissions, but care should

be taken to the options sensitivity to cost fluctuations (such as a surge in scrap price if demand is to soar, following, for example, a policy intervention stipulating recycled content).

The timeline for key decision (investment) points aims to avoid regret capital. It is well in advance of these key decision points, that critical decisions to retain, or replace assets must be made, with a view on if these assets will be needed in the future.

5.4 Simulation results and discussion.

5.4.1 Introduction to section

For this section of the thesis, the results for the future scenario simulations will be presented, immediately accompanied by the discussion for each model output. This decision was taken so that the reader can follow the results and the meaning in a logical order, without skipping back and forth to the charts to visualise the output of the subsequent discussion. Results are displayed in, as far as possible, the order of importance.

5.4.2 Carbon reduction potential

The primary objective of the technology roadmapping exercise was ultimately to determine carbon reduction potential. An 80% carbon reduction target by 2050 is the benchmark, reflecting the previous emission target for the UK. This target has subsequently been extended to NetZero, however this ability to meet the final 20% has not been evaluated at this stage, and may be considered very challenging, as this represents the most difficult (often low concentration or dispersed) fraction of emissions. The ability to decarbonise the process is critical in determining the future pathways of steel making operations. However, given the requirement to remain competitive, the cost per-ton of CO₂ saved could equally be taken as the most significant output of the modelling exercise to steel plant operators. The carbon intensity of the process is determined by the summation of the carbon inputs into the production of crude steel as well as the energy balance and the carbon source intensity of the energy and any imports.

A BF example is presented below (table 5-2) to demonstrate the process. Numbers have been changed slightly from those used within the model (taken from actual site data) for confidentiality.

CO₂ = sum of carbon inputs multiplied by the molecular weight of carbon dioxide to that of carbon (*44/12).

Table 5-2: Carbon intensity of the blast furnace (base case) processes

| Model parameter | Units | Value |
|--|--------------|--------------|
| Carbon use from coal | <i>Kt</i> | 1,500 |
| Carbon use from Purchased Coke | <i>Kt</i> | # |
| Carbon by-products | <i>Kt</i> | - 50 |
| Carbon use from NG | <i>Kt</i> | # |
| Carbon use external gas powerplant | <i>Kt</i> | # |
| CO ₂ from electricity | <i>Kt</i> | # |
| CO ₂ from crude steel production | <i>Kt</i> | 5,800 |
| CO ₂ from external gas powerplant | <i>Kt</i> | # |
| CO ₂ from electricity | <i>Kt</i> | # |
| Total CO ₂ from BF steelmaking | <i>Kt</i> | 6,300 |

The robustness of the model stands up well to a comparison of the literature for the various technologies (taken from World's Steel data and displayed in the following table 5-3). The model produces a CO₂ intensity of 1.986 tCO₂/ton of crude steel (tcs) for the BF route and 0.38 tCO₂/tcs for and EAF. Utilising available EU ETS data, as well as site data, this shows the model produces data that is accurate for the purpose.

Table 5-3: Carbon intensity of processes, as determined by the model and World Steel data

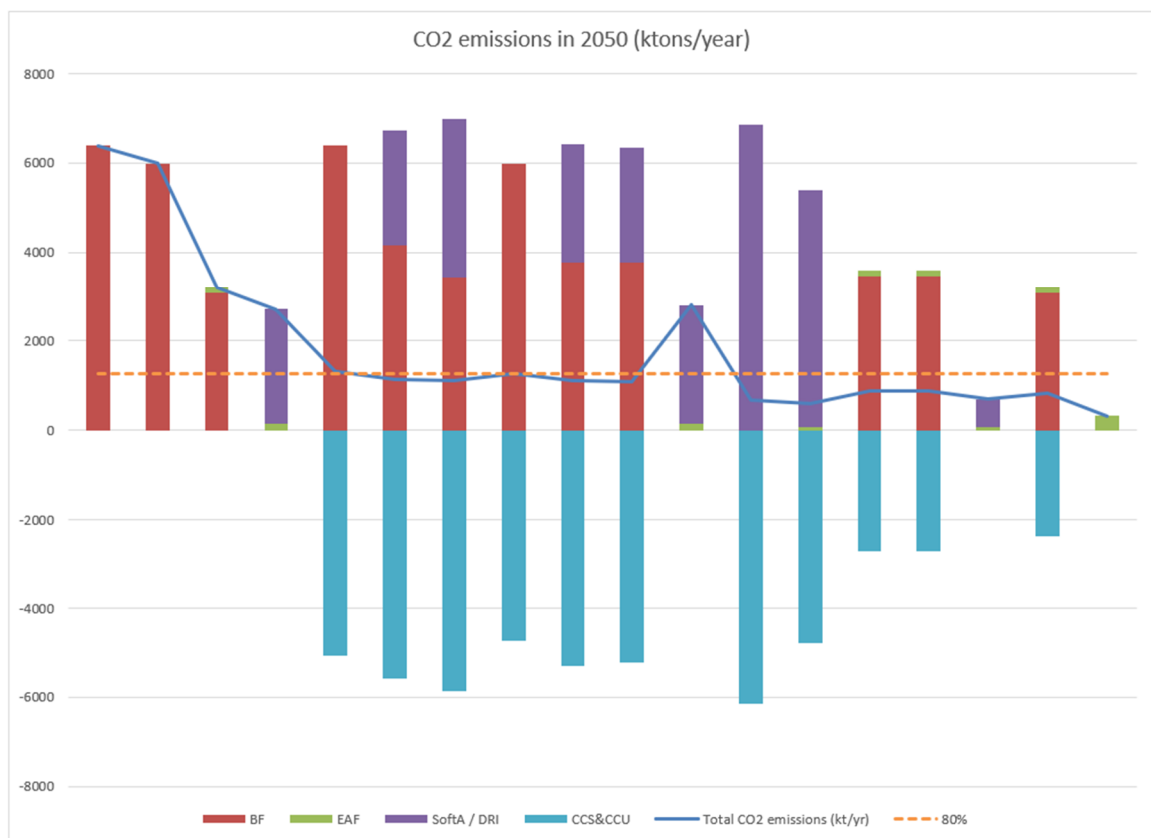
| tCO₂/tcs | Model | World Steel (top 15%) |
|----------------------------|----------------------|--|
| BF-BOF | 1.986 | 1.85 |
| EAF | 0.38 | 0.37 |
| DRI / Finex | 1.68 (Finex process) | 1.49 (15 site average DRI) |
| SoftA | Confidential | No comparison (constant with internal reported data) |

Table 5-3 shows the carbon intensity, calculated within the model compared to data table at today's (2019) electricity grid intensity.

Figure 5.6, shows the final carbon intensity (tCO₂/tcs) of the process by 2050, for each of the 18 modelled scenarios. The results are broken down into technology category, to show the contribution of each type of process towards the total emission reduction. In particular, the impact of CCS is clearly visible as a negative emissions contribution, as shown in light blue. For many of the technology scenarios (those that include in part of in full, BF or SofTA), significant carbon reduction cannot be achieved without the implementation of CCS, since they are primarily carbon based. The scenarios are kept confidential to maintain commercial sensitivity, but the analysis

demonstrates that significant carbon reduction (80%) can be achieved by 2050, with the anticipated technology roll-out and expected availability. The orange dashed line represents an 80% carbon reduction. Biomass has not been included within this analysis, but it could be used to add further carbon reduction, beyond the typical 80% reduction target, to reach more challenging net-zero target. Implementation of CCS onto other site processes, considered out of scope, would increase the cost, but would potentially allow an 80% site emissions reduction target to be achieved. Assessing the model results, achieving **net-zero** without the addition of some atmospheric carbon removal technology is **not possible**. This could be achieved by employing biomass into some of the CCS options or carbon offsetting, with air capture and CCS.

Figure 5.6: Site annual carbon intensity, as simulated in the year 2050, under the different technology scenarios



The following figure (figure 5.7) is presented with a 5 year resolution. Whilst the target set by Government determines the amount of CO₂ that could be emitted within a single year (or % reduction from a point in time), it does not provide an accurate representation of the impact upon total carbon reduction in the atmosphere. To address climate change, the total area under the curve, that is the cumulative emissions between now and 2050, is ultimately the most important output value. This value is the total carbon emitted into the atmosphere from this test case production site. The model has demonstrated that acting quickly will ultimately lead to a greater reduction in the total carbon emissions, and the greatest impact upon climate change. For this

reason, technologies with a higher TRL that are available today and that are also cost effective will lead to the best solution. Whilst a DRI-hydrogen furnace in theory produces the ultimate solution for the future, the low TRL and much later availability of the bulk, low-cost hydrogen that is anticipated within the model, results in no effective improvement within the pre-2050 emission reductions when compared to the readily available options, such as CCS. The choice to transition to hydrogen would need external incentives to accelerate the availability of hydrogen and be seen as a long-term strategy, considering the higher initial cost and being highly reliant upon future hydrogen prices; speculation into which, varies greatly.

The maximum cumulative emissions are 200,563 kt, for the base case, and the minimum is 73,526 kt, producing a range of ~127,000 kt. The average BF technology options with CCS produce a total carbon emission of 124,049 kt, whereas those that employ an EAF option, alongside a fossil CCS option, produce an average emission of 93,545 kt. Where possible, recycling more scrap proves to have the greatest impact on total emissions to atmosphere, assuming cautiously that access to zero-carbon electricity is possible. However, we should be very careful with this assumption. The scrap has high value, it is used throughout the world and unlikely to end its life in landfill. Hence, reduction at one site may lead to an increase in emissions elsewhere, if that scrap is diverted and those emissions are subsequently not captured or reduced by some other means (CCS, electrification or hydrogen). That means domestic emissions may appear to be reduced, but the overall global emissions may remain unchanged as a result. A domestic emissions approach should be treated with caution and is clearly not sufficient to estimate the global carbon impact. This model does not predict the global carbon emission, but it should be taken into account in any decision making, especially if off-shoring production is seen as an attractive solution. Estimates for steel recycling, as of 2018, are that 88% of all used steel is recycled, making it the most recycled material, per ton, in the world (American Iron and Steel Institute - Steel Recycling Institute, 2020).

Figure 5.7: The cumulative summation of all the carbon emitted between 2020 and 2050

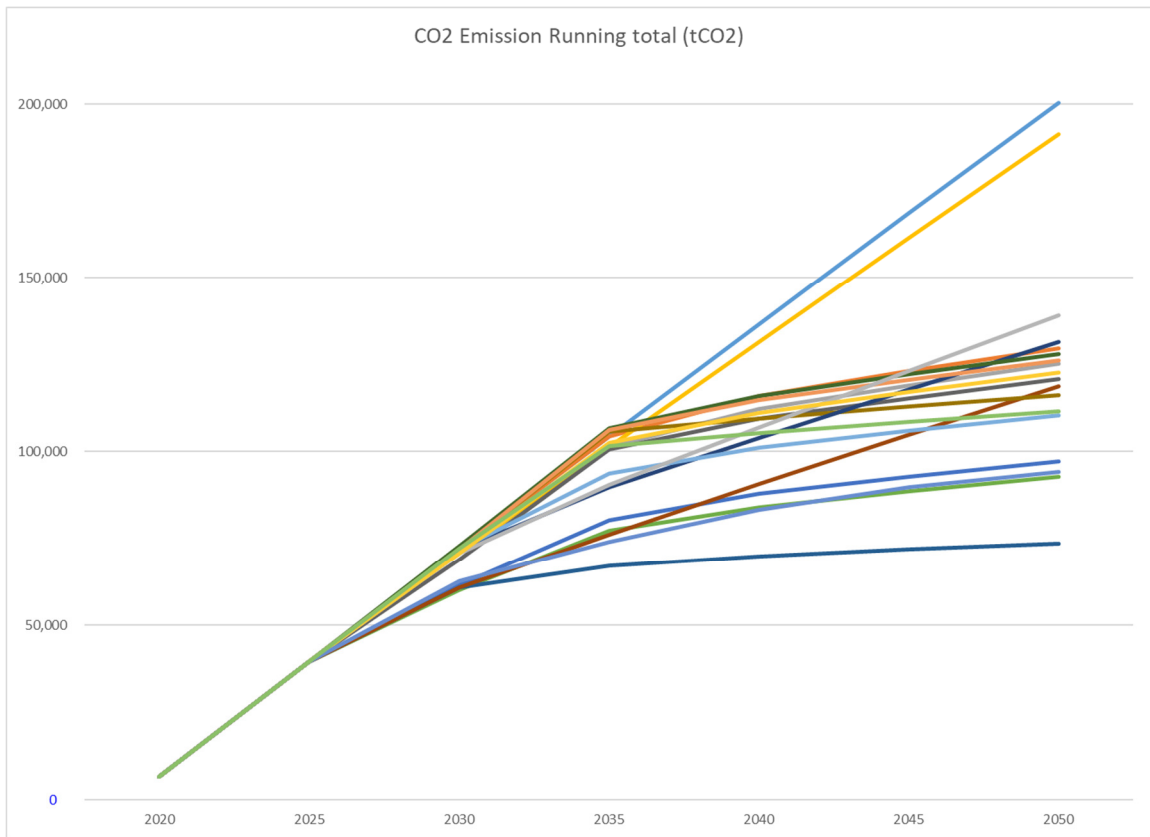


Figure 5.8: Annual carbon emission intensity of the chosen scenarios and contribution of technologies, within the year 2040

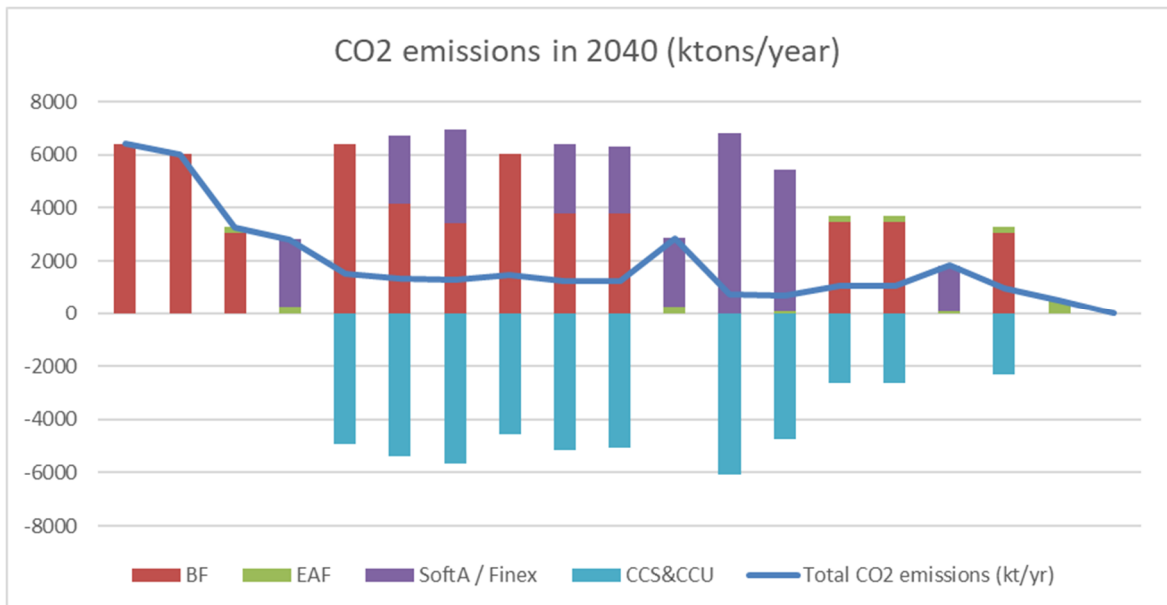


Figure 5.9: Annual carbon emission intensity of the chosen scenarios and contribution of technologies, within the year 2040

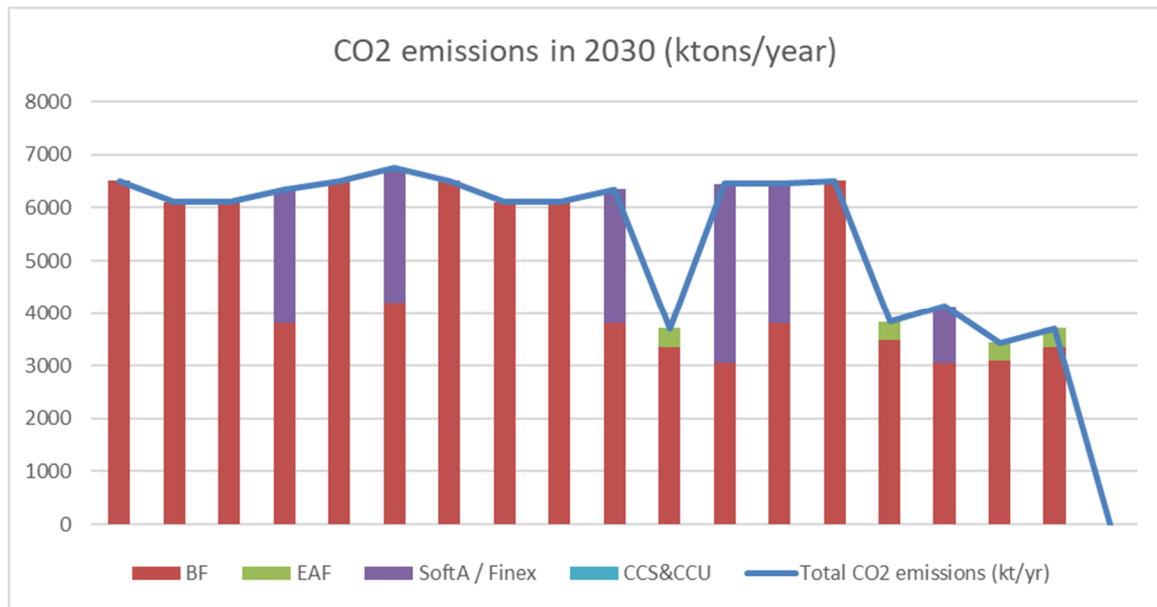


Figure 5.8 and 5.9. shows the carbon intensity of the process in 2040 and 2030 respectively.

The annual emission within 2030, as illustrated in the model output within figure 5.9, demonstrates little reduction in emissions and a clear contrast to the emissions in 2040. Before 2030, new technologies, especially CCS, are not fully implemented. Only the implementation of EAF shows significant reduction before 2030. However, as discussed above, this will not reduce overall global carbon emission to atmosphere due to already high 88% global steel recycling rate and will likely only influence domestic emissions.

Table 5-4: Cumulative emission of selected pathways

| Technology | 2020 | 2025 | 2030 | 2035 | 2040 | 2045 | 2050 |
|-----------------------------|-----------|-----------|-----------|-----------|-----------|-----------|-----------|
| | <i>kt</i> |
| Base-case (no abatement) | 6,601 | 39,409 | 72,018 | 104,427 | 136,637 | 168,647 | 200,563 |
| BF full CCS | 6,601 | 39,409 | 72,018 | 104,427 | 116,004 | 123,001 | 129,534 |
| BF CCS / EAF | 6,601 | 39,409 | 60,187 | 77,131 | 84,069 | 88,574 | 92,723 |
| DRI-H2/ EAF | 6,601 | 39,409 | 62,704 | 74,076 | 83,221 | 89,813 | 94,040 |

Table 5-5: % reduction of process compared to base case 2016 emissions

| Technology | 2020 | 2025 | 2030 | 2035 | 2040 | 2045 | 2050 |
|--------------------------|------|------|------|------|------|------|-----------|
| | % | % | % | % | % | % | % |
| Base-case (no abatement) | 0 | 1 | 2 | 2 | 3 | 3 | 4 |
| BF full CCS | 0 | 1 | 8 | 8 | 78 | 81 | 81 |
| BF CCS / EAF | 0 | 1 | 48 | 49 | 85 | 87 | 87 |
| DRI-H ₂ / EAF | 0 | 1 | 37 | 73 | 72 | 86 | 89 |

The two sets of data shown within tables 5-4 and 5-5 provide great insight into the actual climate impact. Whilst the 3 technology options, have been shown to all reach the 80% reduction target ahead of schedule, the outcome cannot be more different. Primarily due to the estimated TRL and ability to roll out the new technology, the dates at which carbon reduction accrues differ significantly. For the full CCS BF case, although the 80% reduction target can be met in 2045, the overall % reduction stalls at this value, because of the difficult and costly carbon point sources that are not included in this exercise. Due to the estimated availability of CCS in the test case region (2037), significant carbon reduction is not made prior to this date, whereas including an EAF demonstrates greater carbon reduction, but at the possible consequence of increased emissions outside of the UK, if this scrap demand is likely filled with iron from unabated processes. The difference in cumulative emissions by 2050 due to this delay in technology deployment is >30,800 tCO₂. This is a significant amount of carbon that must be captured from the air with ever increasing and costly technology, if a NetZero target is to be reached. The delayed availability of bulk low carbon hydrogen stalls the even greater potential for H₂ DRI to match the carbon reduction potential of BF CCS with additional CCS. Initial carbon reduction of this route is achieved if we assume a switch to the less carbon intensive NG fuel input, which can potentially come online long before a BF CCS facility. Yet the reduction from this pathway is stalled in the 2040s due to lack of bulk hydrogen, ultimately resulting in slightly greater emission to atmosphere over the period 2020-2050. It would appear that fast action within the 2030s might have the greatest impact in stalling dramatic climate change, so a switch to DRI with NG would seem a sensible approach to limit global climate change in the short term.

All technology routes can achieve an estimated >80% carbon reduction, however, fast action, regardless of technology option will make the greatest difference in overall carbon reduction. Whilst a >80% reduction can be achieved, neglecting impact on global emission displacement from scrap use, domestic emissions to atmosphere are still likely to greater than 90,000 tCO₂, between now and 2050.

5.4.3 Cash flow (profitability)

The cost per ton of CO₂ captured may be seen as the second most critical factor from the modelling exercise. Taken out of context the data can be misinterpreted, as the most cost-effective way forward is to continue to utilise unabated fossil fuels, or to import unabated steel from elsewhere, (with high-embedded carbon emissions), when only viewing the annual data. Figure 5.10 demonstrates that all cases modelled show an increase in operational cost from base case in 2050. This is because the move to decarbonise the current operation requires measures to remove the CO₂ or change the processes, which will add cost to current operations. In particular, the cost of hydrogen for a DRI hydrogen shift shows the greatest increase in operating costs. To keep costs for the hydrogen as low as possible, a blue hydrogen source and estimated cost has been used. For this purpose, it was fixed at a cost of £4 per kg. It is estimated that hydrogen can, by 2050, reach a cost comparable with unabated hydrogen at £2 per kg, but this was considered unlikely in the region due to gas prices, or a need to import low-carbon hydrogen. The error in estimating price reduction in low-carbon fuel prices is one of the greatest sources of error. Producing green hydrogen in the volumes required would increase the cost significantly and likely take longer for the conversion to hydrogen, resulting in a greater total of CO₂ emitted into atmosphere. Moving quickly with the transition to hydrogen will limit the emissions to atmosphere, but likely increase the cost (certainly if the cost has not yet come down to the estimated value) and will require more Government intervention. An estimate of the impact of moving quickly has not been made, but could be used to assess the impact of active Government intervention, if the hydrogen route was politically favoured over the abated fossil alternative. For now, we can conclude that the hydrogen options modelled result in greater cost of operation and possibly delayed roll out of decarbonisation technology. Again, it should be emphasised that the costs are based upon today's commodity prices, with some estimates on the cost trajectory for the ETS scheme carbon credits and a fixed cost of £4/kg hydrogen.

The aim was to determine if an $\geq 80\%$ carbon reduction target could be achieved, with some scenarios shown to exceed this value. In the interest of minimising cost, it could be that all the scenarios are set to a maximum carbon limit of 80%. However, with the NetZero target now applicable to the UK, any emissions that are not prevented, could suffer a cost for carbon offsetting. Therefore, no maximum carbon emission limit has been set.

Figure 5.10: The percentage shift (increase) in the sites operational costs as a results of decarbonisation methods in the year 2050

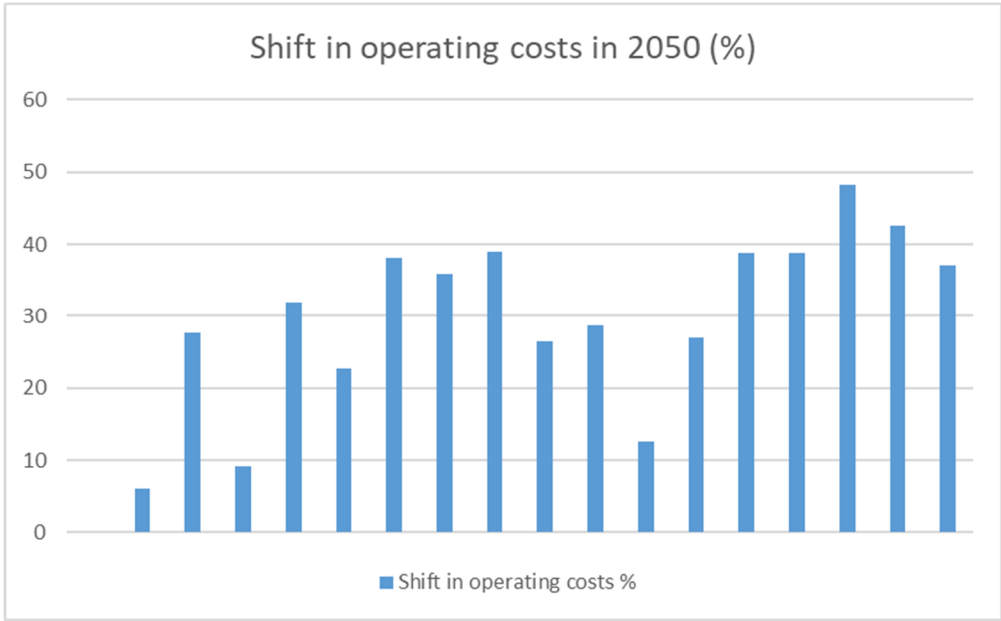
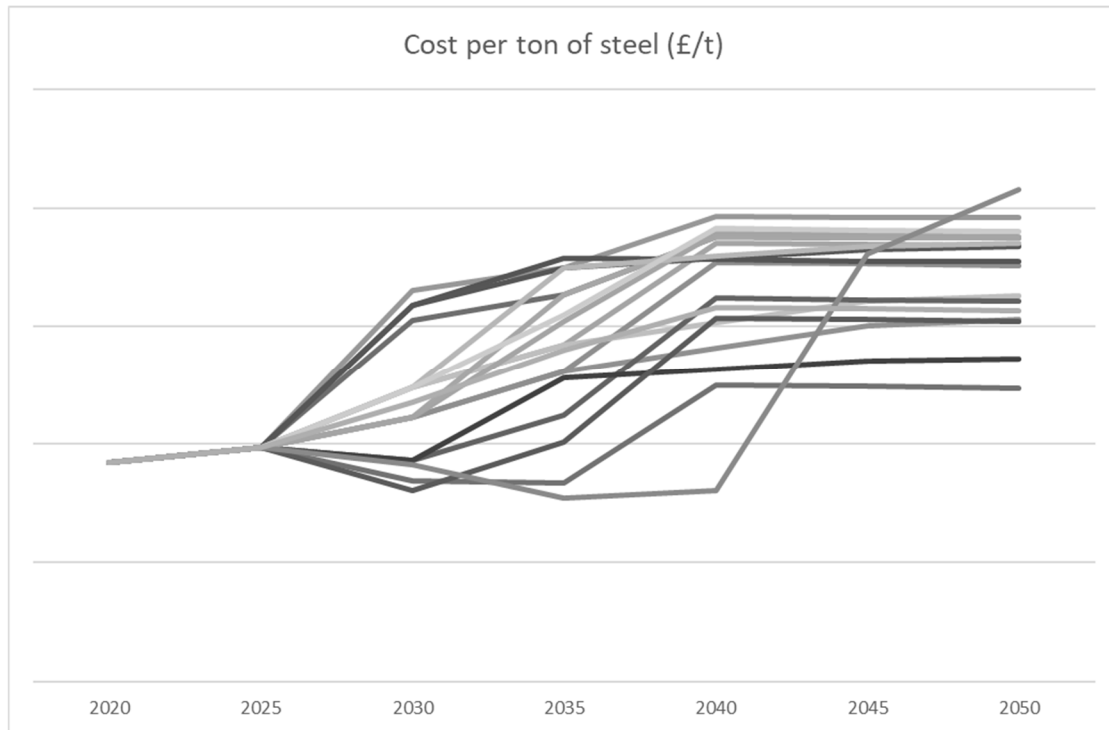


Figure 5.11 shows the cost per ton of steel over time. This is a summation of fixed and variable operational costs and does not factor in CAPEX requirements. The labels, quantities and the colours have been deliberately removed for commercial sensitivity, yet the variability and the changes can be clearly seen, showing some routes are highly sensitive to process (changes. The model does not feature a simple sensitivity analysis function due to its complexity. It is still advantageous to input high and low costs to the model to determine the impact on the cost trajectory shown. As fixed costs were chosen for this exercise (except for ETS price), no estimates of the parameters for high and low-cost forecasts have been displayed.

Analysis of the primary influences to cost increase showed that measures to reduce carbon, such as carbon capture or use of hydrogen have a clear impact on operating cost. Therefore, minimising these costs, whilst still achieving carbon reduction is critical. Within the base case, taking no action to minimise carbon emissions equally results in a greater operational cost, due to the estimated ETS price impact. The breakeven point whereby cost of decarbonisation is equal to the cost of the ETS is subjective due to the difficulties in estimating future ETS cost, but can be evaluated within the model. Obviously, taking no action will not reduce carbon emissions and will incur an ETS charge. Whilst this maybe more cost effective in some scenarios with a low future ETS price than taking positive action, this was not the objective. Including the ETS price was used to establish if moving quicker, by employing higher TRL technologies, could reduce the overall cost and improve cash flow. The effectiveness of an ETS scheme for the steel sector is questionable. Without supporting business models, to pass on the cost of decarbonisation or to protect from high-carbon embedded imports, this will mostly likely lead to further carbon

leaking. Whereby, heavy industry is located offshore (in locations with less stringent emission targets and no ETS) and the products are imported.

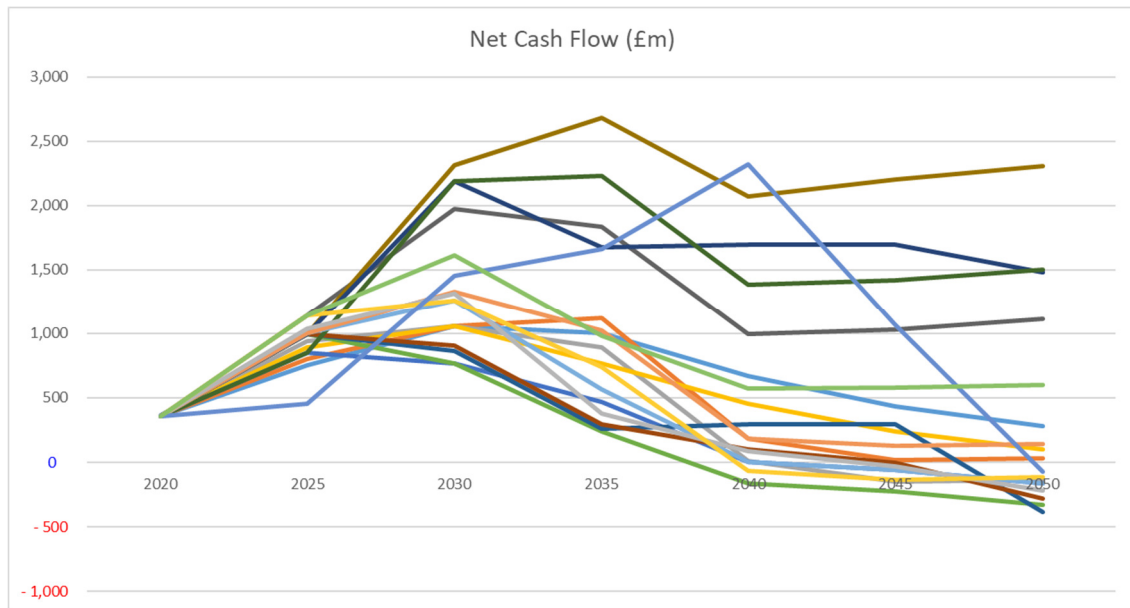
Figure 5.11: The cost per ton of steel from 2020, up to 2050 within each scenario. Actual values have been concealed, due to the commercial sensitivity of the scenario outputs



To establish the financial performance it is more relevant to look at the site's cash flow. Noticeably, long periods of negative cash flow would lead to bankruptcy, or continuous subsidies via respective Governments. Net cash flow is the total cost of operation, minus the necessary CAPEX investment. Greater CAPEX requirements must be met with an increase in profitability, if these are to be sustained. 2030 seems to be a critical year for cash flow, as a result of increased CAPEX needed for the technology transition, and few of the technologies can sustain an upward trend immediately thereafter, showing negative cash flow for at least a 10-year period or worse, perpetually. This means that some financial support mechanism or protection measure will be needed for at least a 10 year period between 2030 and 2040, to assist the steel sector. Ultimately an increase in the price of steel will be needed to allow the decarbonisation of the industry, but that must be within the global market context when competing with non-decarbonised steel.

The net cash flow, for the various configurations is shown within figure 5.12. Scenarios are concealed for commercial sensitivity.

Figure 5.12: The estimated net cash flow, between 2020 and 2050 for the chosen scenarios



Cash flow is calculated using the following formula, 5.3.

$$\text{Net Cash Flow} = \text{Operations before tax (EBITDA)} - \text{Capex Investments} \quad (\text{Eq. 5.3})$$

These trends need to be treated cautiously as they rely upon some future financial predictions, which is obviously difficult and risky. Sensitivity analysis of the data was carried out based upon the raw material and energy costs. This clearly showed that cost of energy and raw material inputs leads to the greatest variation in operation cost and profitability; a transition toward hydrogen is particularly sensitive. Using the cost ratios from steelonthenet.com as shown below, and converting the costs into % of total costs highlights the sensitivity to raw material prices and electrical energy costs (Steelonthenet, 2020). For the EAF route, raw materials account for 76% of overall cost, whereas for BF-BOS, they account for 79%. For BF-BOS, under these assumptions, coal is attributed to the raw materials total, even though it is also used as a high degree of the site's energy needs (table 5-6 and 5-7).

For those technology transitions showing significant ($\geq 80\%$) carbon reduction, an increase in operational cost between 20-40% is predicted. Little can be done within a fixed region to influence the labour costs greatly or increase efficiency beyond best practice. For example, if a 10% decrease in coal use could be achieved, this would only relate to a total of 2.5% decrease in total OPEX, which would not offset the increase due to decarbonisation measures.

Whilst a full EAF transition is included, due to the remaining difficulties in assessing the impact in product range and profitability, it has been assumed that a full orderbook can be maintained. This is incorrect. Therefore, this route was included, only to see the overall carbon impact and no reference to cost has been made in this assessment.

Table 5-6: The percentage of the total sites operational costs, per ton of steel for the EAF route

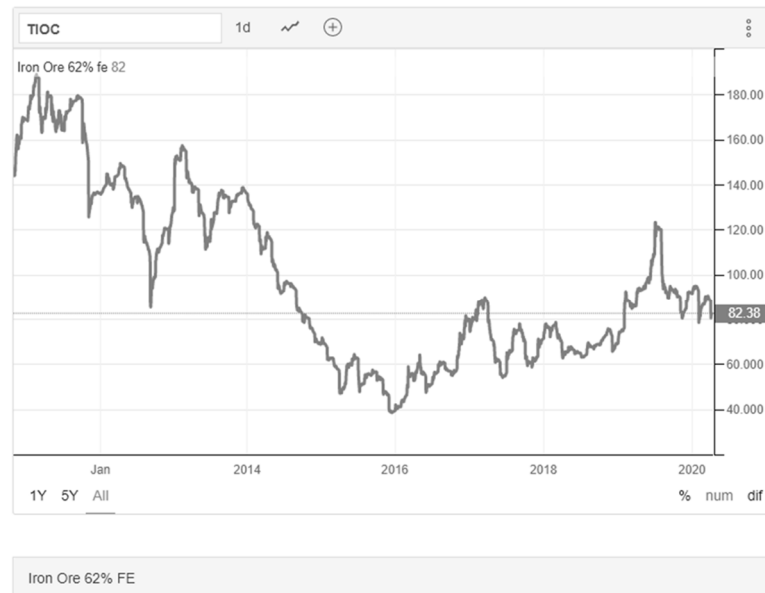
| EAF | % Cost per ton steel |
|-------------------------|----------------------|
| Steel Scrap | 65.5 |
| Electricity | 11.8 |
| Electrodes | 4.77 |
| Ferrous alloys | 4.27 |
| Capital Charges | 4.12 |
| Other | 3.20 |
| Labour | 3.03 |
| Steel Scrap Transport | 1.46 |
| Fluxes etc | 1.25 |
| Industrial Gases | 0.423 |
| Refractories | 0.260 |
| PIG Iron/ DRI | 0.00 |
| PIG Iron/ DRI Transport | 0.00 |
| Thermal Energy | -0.107 |
| Total | 100 |

Table 5-7: The percentage of the total sites operational costs, per ton of steel for the BF-BOS route

| BF – BOS | % Cost per ton steel |
|-----------------------|----------------------|
| Iron Ore | 35.3 |
| Coal | 25.4 |
| Capital Charges | 8.30 |
| Steel Scrap | 7.99 |
| Labour | 5.96 |
| Fluxes etc | 5.68 |
| Ferrous alloys | 4.73 |
| Other | 4.60 |
| Industrial Gases | 4.17 |
| Electricity | 3.21 |
| Iron Ore Transport | 2.33 |
| Coal Transport | 1.23 |
| Refractories | 0.976 |
| Steel Scrap Transport | 0.179 |
| By-Product Credits | -1.12 |
| Thermal Energy, Net | -8.90 |
| Total | 100 |

Figure 5.13 shows the variation in iron ore price (US \$/t) over recent years; a significant range of 40 to >180 US \$/t. A good performing, positive cash flow is needed to overcome these times of variability, which none of the trends show at current price estimates. It is not unusual for raw material prices to vary by more than 100%, which has a profound impact on operational cost. Iron ore seems particularly sensitive to supply and demand, due to global economic output.

Figure 5.13: The volatility of iron ore prices over time



Source: (Trade Economics, 2020)

5.4.4 Error analysis

Great care has been taken to produce as accurate a model as technically possible. Pivotal is an accurate energy and carbon balance, followed by a good cost estimate with an aim to reduce uncertainties. Limiting exposure to these uncertainties will reduce the overall risk of the low-carbon transitions, but it seems they are unavoidable. Two major sources of error exist, causing great uncertainty in the future technology selection for the steel plant operators. First are the cost estimates and second are the TRL or technology roll-out dates. Selecting the correct estimates is not always possible, as is evident from the wide fluctuations in iron ore price (figure 5.13). Energy and raw materials have been shown to provide the greatest source of variability in the operational costs, therefore accurate scrap price forecast, NG and H2 costing is necessary in any transition away from coal and iron ore. The best solution is one that can absorb this possible error and still remain profitable.

There is also a 30% discrepancy between the academic literature on hydrogen requirement needed for FeO reduction, and my estimate using known DRI energy requirements (7 GJ/thm vs 10 GJ/thm). Given the high cost of energy and the impact of hydrogen cost to the future viability of this pathway, this is a significant source of error, which the industry needs to address.

5.5 Conclusions from techno-economic simulation

The detailed simulation exercise has shown, using technologies with a TRL of 7 or higher, that an 80% carbon reduction from base-case is possible. Whilst these reductions are possible, most require CCS and where CCS is not applied, hydrogen-DRI, or a full shift to EAF (scrap based) will be needed, to reduce (domestic only) emissions.

The aim of this research chapter was to answer the following questions, so that we may evaluate the two technologies that have been developed in chapters 3 and 4:

1. Will fossil energy still feature between now and 2050?
2. Will CO₂ still be emitted from our future steel plant, for how long and by how much?
3. What technologies are we likely to employ to significantly reduce the carbon emissions?

From this evaluation we are able to conclude that due to cost and TRL, fossil energy is still likely to feature significantly either as coal input into the BF-BOS route with CCS, or as NG input into the blue hydrogen route to establish a hydrogen-DRI solution. It is highly probably that CO₂ will be emitted and this will need to be captured (and permanently stored) to reach significant carbon savings. A carbon reduction ($\geq 80\%$) would be possible, within the timescale up to 2050, using available technologies (currently at $\geq \text{TRL}7$). A technology agnostic approach was used, so not to purposely favour the two technologies that were developed within chapters 3 and 4. Only pathways considered close to commercialisation (currently at $\geq \text{TRL}7$) were chosen and no decarbonisation methods were deliberately rejected. Of the high TRL (≥ 7) technologies considered within the model, CCS is identified as a critical technology within most cases to achieve the significant ($\sim 80\%$) carbon reduction in the timescale, up to 2050. Those pathways that do not employ CCS (hydrogen-DRI and EAF) would likely be less economical and/or potentially unable to meet customer's product requirements, necessitating steel imports (when $\geq \text{TRL}7$ is considered an essential parameter). The greater the cost of operation, the higher the level of support mechanisms that will be needed to offset carbon leakage, due to unabated, high embedded CO₂ steel imports.

To achieve reasonable economic performance, it is assumed that the hydrogen will be Blue hydrogen from SMR or ATR with CCS. CCS is still required for the hydrogen-DRI option if blue hydrogen is the source, which is used in this model. Green hydrogen would produce a worse economic performance, following an expected higher hydrogen price and it is assumed that it would take longer to achieve the large volumes needed for steel production, needing first the role out of surplus renewable power and hydrogen storage. Imported H₂ in the form of shipped ammonia, produced in equatorial regions by solar energy, may prove cost effective if prices continue to decline, but this still proves more costly than a BF CCS route. Ultimately, the

transition to hydrogen and the associated longer lead times result in slightly greater CO₂ emissions into the atmosphere, following the delayed rollout of bulk hydrogen. The model has demonstrated that, moving quickly, independent upon low-carbon technology choice, ultimately leads to less net CO₂ emissions to atmosphere and the greatest positive impact in the mitigation of climate change. That is not to say that CCS is the only correct pathway, as this still locks in the use of carbon fuels. If hydrogen is seen as the way forward, in this analysis we have shown that much greater emphasis must be placed on making the volume of hydrogen that is needed available sooner. Regret capital may occur if a switch from a CCS BF to a hydrogen-DRI is needed, before the end of the asset lifetime, ultimately resulting in greater CAPEX spend overall.

A full transition towards EAF has major implications on product portfolio and due to the cruelly high (88%) global steel recycling rate. Viewing the global trends in steel carbon reduction and current asset lifetimes, it is thought that this will not have a global impact upon carbon reduction, only regional, domestic emissions. Predicted increase in scrap availability does not align with the carbon reduction goals and steel demands. Whilst an increase in scrap to align with availability is envisaged, a full transition to EAF to achieve decarbonisation does not correlate with the evidence that has been assessed.

Though converting to hydrogen would likely be the panacea for a future steel plant, the lower TRL, lack of high volume low-carbon hydrogen production, storage and distribution and therefore a longer duration of roll-out for the technology, would result in a slightly greater cumulative CO₂ emission to atmosphere, although some early gains in emissions can be made with an intermediate switch to natural gas. When the DRI-H₂ route is evaluated against alternative, lower-cost scenarios, especially over the early modelled period, whereby great reductions in carbon emissions are needed to slow climate change, higher TRL and quickly deployed solutions will lead to a reduction in CO₂ to atmosphere. The use of hydrogen from electrolysis (green hydrogen) has been found to be prohibitively expensive, compared to the alternative blue hydrogen sources (SMR with CCS) and likely require longer to implement, resulting in yet greater CO₂ emissions into the atmosphere. CCS is still required if utilising a blue hydrogen source. Ultimately, moving quickly, at the least-cost, has the greatest positive contribution towards climate change and possibly, the likelihood of remaining profitable. That is not to say a fossil-based CCS BF is preferential over a hydrogen solution, but if hydrogen is considered the preferred way forward for the industry, effort must be taken to accelerate its deployment and reduce the cost of hydrogen to align with that of fossil-based CCS. Swift action will be the greatest influence in overall carbon reduction. Although a >80% reduction can be achieved (neglecting impact on global emission displacement from scrap use), the domestic emissions to atmosphere are still likely to be greater than 90,000 tCO₂, between now and 2050, within the current technology roll out estimates. This is a significant amount of carbon, which

must be removed subsequently to reach NetZero. Therefore, from a cumulative emissions perspective, only a 55% reduction in total CO₂ emissions will be achievable at the current, best-case estimated pace of new technology deployment.

Economically, it was demonstrated that all of the scenarios modelled, generate a negative impact on the immediate cash flow, increasing the operational cost above the base-case. With all cases resulting in negative cash flow durations of ≥ 5 years, due to a combination of higher investment costs and increased operational costs. Limiting these costs will be critical to the future success and therefore form a foundation for future efforts. Whilst CAPEX requirements maybe reduced in some scenarios, this is offset by an increase in operational cost (and possible loss of market share due to steel/scrap quality, which has not been modelled) resulting in a negative cash flow in most cases, up to 2040. It is anticipated that some form of Government intervention would be required to support the steel sector financially during the transition period, especially to protect the sector from high-carbon embedded imports from inactive regions, so that the increase in cost can be passed onto the consumer. Ultimately, the cost of steel must increase for it to be made in a low-carbon way. This is echoed across the European steel industry, which supports this analysis. Evidently, the current, high-carbon emission steel production method proves to be the most cost-effective way of making primary iron, given that this is commercially proven and fully optimised over >100 years. Whilst some value may be raised from the use of CO₂, it does not look possible to fully offset the increased cost in production, within the scenarios that have been modelled. This function of the model requires further work, due to the many variables: access to actual data, market predictions and technical challenges.

Given the high contribution to operational cost (76% for EAF and 79% for BF- BOS), raw material costs have the greatest impact upon cost performance and sensitivity within the model. Access to cheap raw materials would be critical in cost reduction, however as a globally traded commodity, fluctuations will impact all steel makers, preventing cost differentiation. Pathways that lead to significant carbon emissions reduction ($\geq 80\%$) result in an OPEX increase of between 20-40%. Ultimately, access to cheaper alternative energy sources will drive the transition towards a low-carbon alternative. In the absence of these, CCS of fossil-based iron production is the cheapest option, whilst maintaining market share and avoiding de-industrialisation (reliance upon steel/iron imports).

5.6 Chapter summary

Whilst developing the technologies within chapters 3 and 4, it became critical to have access to the knowledge of what technologies are likely to be employed in a future low-carbon steel plant, so that the application of aqueous ammonia capture and CO₂ plasma conversion can be correctly evaluated. Reviewing the available literature, it was evident that a site-based investigation of steel

plant decarbonisation was needed to complement the regional approaches in identifying low carbon solutions. Therefore, to fully understand the potential pathways to a low-carbon, future steelworks and to envisage what technologies would exist in a likely future steel plant, a first-of-a-kind techno-economic model has been developed, using real data from a chosen test case site.

A model has been developed to simulate and then evaluated 18 potential new technology pathways and their deployment, in a yearly transition up to 2050, the carbon reduction potential of these new technologies and the asset configurations (utilising a detailed site energy and carbon balance), the cumulative carbon emission up to 2050, the shift in the operational costs and the impact of the technology transitions upon the cost per ton of steel and finally, the net cash flow.

From this detailed simulation exercise, we are now able to predict what a future steel plant may look like, what are the most likely technology pathways, raw material and fuel inputs and the operational costs. From here we have the ability to assess how new technologies and breakthroughs, such as those developed within chapters 3 and 4, (or indeed any other technology option) may be applicable to one of our future steel plant configurations, how they could be applied and also their relative cost implications.

It is highly likely that carbon capture, due to its TRL and cost will feature initially in either a BF-BOS route or a hydrogen-DRI solution. Especially if a 1.5 °C target is to be met and pace and scale of decarbonisation is prioritised. Given these technology pathways will increase the cost of steel manufacturing, cost reduction should feature prominently in the application of new technology or future research and development. Therefore, the improvements identified within chapters 3 and 4 seem, at first instinct, highly relevant.

In the following chapter, this knowledge of steel plant decarbonisation options will be applied to evaluate the application of the two technologies that have been progressed within this research.

Chapter 6

The application of novel ammonia-based CO₂ capture and micro-plasma systems to future steel plant operations

6.1 Introduction to chapter 6

Utilising the output from the simulation exercise and the further developments of the two technologies progressed within Chapters 3 and 4, we can now explore how these technologies may be applied in a steel making context, within a potential low-carbon future steel plant configuration. The modelling exercise has provided answers to the initial questions which we faced; will CO₂ still be emitted from our future steel plant, for how long and by how much? Will fossil energy still feature between now and 2050? What technologies are we likely to employ to significantly reduce the carbon emissions?

The modelling approach established within chapter 5 was necessary to establish if CO₂ as a result of fossil energy use, will still feature within a future steel plant scenario, between now and 2050. Or that the future is most likely carbon free, hydrogen or electrically powered. This is a critical question to answer, if it is possible to evaluate any CO₂ based technology solution within a steel plant scenario and it was believed has been neglected in current evaluations.

Next, we will evaluate how the two technologies could be applied within the possible new steel plant configurations evaluated in the model, followed by how they might perform economically.

6.2 Technology application of aqueous ammonia CO₂ capture

Using a technology agnostic approach and evaluating the most likely, cost effective pathways to achieve an $\geq 80\%$ carbon reduction, it would seem that fossil fuels (and hence CO₂ production) are likely prominent features within the steel production even up to 2050. Therefore, technologies that will capture or address the resulting CO₂ will be highly valuable, especially if they address the increase in cost that is incurred as a necessity to decarbonise.

For each ton of steel, about 1.8-2.0 tCO₂ is typically produced via the world dominating integrated BF-BOF route, therefore a use for the CO₂ would seem extremely desirable. We have seen from the model that, due to the lifetime of the existing assets and the availability of alternative new technologies, scrap or clean energy supplies, BF technology is likely to exist up to at least 2040 and quite possibly beyond 2050. Indeed, either the BF route or the DRI route, though the use of blue hydrogen is likely to continue to produce carbon emissions that need to be captured, used or stored to meet significant carbon savings.

Producing urea from the resulting CO₂, a common form of carbon utilisation, was envisaged within the early developments of the thesis, as a way of utilising some of the process CO₂. The use of CO₂ within urea fertilisers, currently represents the greatest commercial use of CO₂, if we exclude enhanced oil recovery (EOR). However, after assessing the composition of the current steelmaking gases, they would not be suitable for urea production in their present form. First the CO₂ needs to be captured and purified from the steel making process, adding significant cost. Yet, coincidentally, what we have established from the modelling is that the most economical pathways incorporate carbon capture (the process of CO₂ purification) especially in the early stages, if we wish to make quick gains in CO₂ reduction and reduce the overall cumulative emissions into the atmosphere. If we assume CCS will be applied with or without urea production, then this cost can be negated from the evaluation and saving may be realised on the transport and storage costs for the CO₂, which is alternatively recycled into the urea process.

Urea and nitrogen release fertiliser is currently a saturated market and therefore only growth in this market would see the need for more capacity (Yara, 2013). In the early stages of the decarbonisation trajectory, it is unclear when or where this market would appear. It is unlikely demand within the UK will be of sufficient size to warrant a commercial scale plant. We also find, from the literature review, that urea does not dominate as the preferred fertiliser option for European countries, due to high ammonia losses and slow release resulting from the low average temperatures, making the release process difficult to control. Nonetheless, the fertilisers produced could be transported outside of the UK and replace less efficient processes, or this concept applied to non-European sites. To improve production efficiencies and material costs due to corrosion, a low-temperature process was proposed and tested to generate the urea intermediate, carbamate.

What we find is that, if urea is the target product, whilst the process could be conducted at mild conditions, the current integrated commercial approach makes best use of the heat generated from the reaction of NH₃ with CO₂ to further drive the dehydration of ammonium carbamate to urea. The low-temperature approach would subsequently need a second stage heated reactor to convert carbamate to urea, alas the carbamate will decompose, over time once more back into CO₂ and NH₃. This energy could be met from waste heat utilisation from steel plants, but experience of this is very challenging, due to the intermittent nature of availability and the low exergy; requiring an upgrade of the heat to more useful temperatures, such as the use of an organic Rankine cycle. The cost and efficiencies of the Organic Rankine Cycle technology have led to slow adoptions of these processes. The urea process requires a source of NH₃, which itself is a highly carbon intensive process and accounts for >80% of the total energy requirement. The CO₂ that results from the ammonia production process is of high purity and does not require the use of costly CCS equipment, unlike the CO₂ separation from the steel processes gases. The urea production would be better suited to sites where ammonia is currently produced and therefore the CO₂ from the

ammonia process could be directly captured in an adjoining urea production plant. Continuous deliveries of ammonia would be needed otherwise to the point source of the CO₂. Around 80% of ammonia produced is used for the purpose of fertilisers, so it makes sense to locate and combine the ammonia production and the CO₂ source with urea production. (Yara, 2013).

A low carbon route to ammonia production was described by The Royal Society (2020), whereby hydrogen from electrolysis may be combined with nitrogen from air separation to yield carbon free ammonia (The Royal Society, 2020). Following the large volumes of oxygen required for the modelled SoftA iron making processes, an excess of nitrogen would become available from the air separation units, as would the nearly pure CO₂ (80%) source that is also required for the urea process. However, this steel making technology is not envisaged for deployment until post-2030 and also relies upon further roll out of bulk low-carbon hydrogen production. This could, though, yield a promising pathway to low-carbon ammonia, if the SoftA process is commercialised, in parallel to low-carbon hydrogen. Recovery of spent, low concentration ammonia from wastewater may also be an alternative ammonia source. A breakthrough at The University of Sheffield may make this possible, but further development is needed to increase the TRL and evaluate the cost (Desai, et al., 2020).

Nitrate fertilisers are preferred within Europe, as described, as their release of nitrogen is better controlled within the lower temperature climate. Much fewer nitrates can be added to the soil, compared to ammonia liquor or urea, resulting in reduced ammonia loss and lesser total carbon emission. While ammonia nitrate is preferred, ammonia bicarbonate (NH₄HCO₃) can also be used and is still common in some areas, such as China (8% fertiliser use). Therefore, the NH₄HCO₃ produced in the low-temperature, aqueous ammonia capture process (as described in Research Chapter 3), if the solvent is not regenerated, can be used directly as a low-cost nitrogen release fertiliser. NH₄HCO₃ is slightly hazardous and decomposes at an accelerated rate, at temperatures above 38°C. Yet it does not decompose below 27°C, which is fairly typical of UK weather conditions (Yeh & Bai, 1999). The nitrogen content of NH₄HCO₃ is only 18% N compared to the 45% N within urea. It is therefore less desirable for transport over longer distances, but would be perfectly adequate for localised use within UK climates. With the deployment of aqueous ammonia carbon capture, a low-cost fertiliser NH₄HCO₃ route, could become viable as a by-product, if the ammonia solvent loss is to be replaced with a low-carbon ammonia alternative.

It could be viable to use the NH₄HCO₃ within an ammonia capture system as a local fertiliser and to potentially source sustainable ammonia, for the capture process from waste waters. Within this context, it is unclear exactly how a future steelmaking facility equipped with CCS could make use of the mild-condition urea production process, without further developments and research to address access to carbon emission free ammonia (potentially from waste waters) and an expansion in the local or European fertiliser market. The unique composition of BF-BOF steel

plant gases provides access to large volumes of CO, and potentially hydrogen (if undertaking a WGS), that makes synthesis gas routes to chemicals and fuel attractive in assisting difficult to decarbonise sectors (aviation and shipping), as the steel plants sites energy requirements could then be met with electricity and/or hydrogen.

That is not to say that the developments within this study are not highly applicable to the steel sector. On the contrary, the breakthroughs discovered within this research lend themselves to the steel process gases and requirement for carbon dioxide capture, which, as mentioned, has been demonstrated as a key technology, established during the modelling exercise. The capture of CO₂ within aqueous ammonia has quickly become a very promising technology. Indeed, it has many beneficial properties over amine capture systems that lend themselves to the gas compositions typically found in steel making facilities, which are:

1. A higher CO₂ absorption capacity compared to conventional MEA technology
2. No degradation of the solvent from the presence of O₂
3. The removal of SO_x and NO_x from flue gases (typically present in steel plant gases)
4. Is non-toxic to the environment following solvent losses, compared to MEA (in the low volume anticipated)
5. Has a low regeneration energy

All of the above properties make aqueous ammonia highly appealing as a capture method to the steel sector. However, there are two major drawbacks to its use: the rate of CO₂ uptake into the solvent, and the NH₃ slip into the off-gas, which must be captured and recycled. These two critical restrictions mean a larger facility is needed per equivalent volume of gas, and a limit on the NH₃ concentration that can be used. Reducing the NH₃ concentration to avoid NH₃ slip will also restrict the rate of CO₂ uptake, thus increasing the solvent volume needed. To avoid NH₃ slip, GE employ a chilled ammonia process, which prevents NH₃ vaporisation. Whilst the chilling will consume energy, this is off-set by the reduction in the regeneration energy when compared to MEA systems. The GE process will also miss any benefit of heat integration by recovering heat generated during the capture process for the preheating of the regeneration stage.

There are 6 ways in which we can increase the reaction kinetics, to reduce the footprint of the capture facility. These are:

1. Increase the available surface area of the reactants
2. Vary the concentration of reactants and products to drive the reaction in the desired direction
3. Control the temperature and pressure to ideal conditions
4. Manage the pH concentration to the optimal conditions
5. Employ the use of a catalysis to lower the activation energy

6. Remove the presence of any inhibitors to the reaction

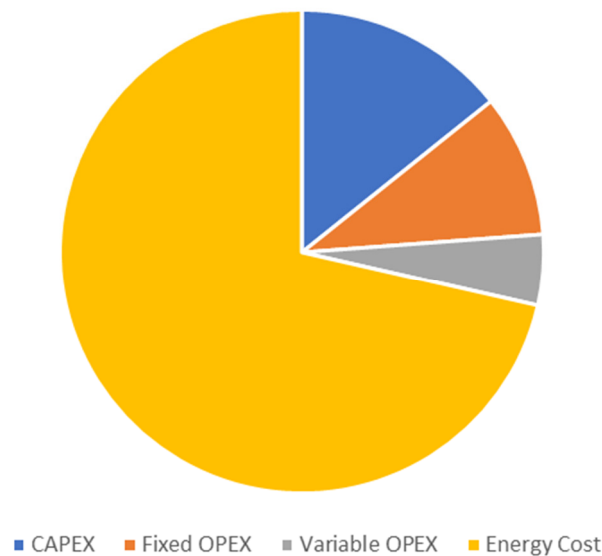
The system demonstrated within research chapter 3 directly addresses number 1. By incorporating microbubbles, the gas-liquid surface area is significantly increased. Also, the internal mixing of the bubbles gas is rapidly increased with reducing diameter, which will aid the reaction kinetic by ensuring the reactive component is near the surface of the bubble for the maximum time possible. The tests used a pure concentration of CO₂ gas delivered to the reactor, therefore the benefit of increased bubble mixing is not believed to be so applicable in this context as the pure gas bubble does not have competing components within. More rapid gas mixing does, however, become more relevant with gas compositions, typical of steel making process or combustion. Ensuring the CO₂ closest to the bubbles' surface is constantly replenished until it is depleted will rapidly improve the microbubbles' effectiveness. To test this hypothesis, a continuous capture system employing synthesised steel plant process gases is now needed. It is unclear if the remaining gas components, primarily nitrogen for steel and combustion processes, would cause the hot (>20°C) ammonia solution to vaporise and the escaping nitrogen to carry the vaporised NH₃ into the off-gases, causing greater NH₃ loss. Undertaking the process at low concentrations of NH₃ should prevent this, due to the high solubility of NH₃. What we do know is that the unique microbubble phenomenon, whereby microbubbles do not transfer heat energy either to or from the gas and liquid, would reduce the ammonia slip from temperature increase and vaporisation, as we have witnessed in the current experiments. Operating the system at an elevated pressure, in combination with microbubbles, would potentially prevent the vaporisation of NH₃ at high NH₃ concentrations.

The world's first application of microbubbles to a CO₂-NH₃-H₂O system resulted in some remarkable discoveries, which lend themselves well to a full-scale aqueous ammonia capture system. First, the low kinetics are overcome by the increase in gas bubble surface area, achieving high CO₂ to solvent loadings within 8 minutes. This allows low concentrations of NH₃ solvent to be used, which subsequently prevents the loss of NH₃ from the system, reducing NH₃ slip. The system is also able to operate at elevated temperatures, without an increase in NH₃ losses, due to the low kinetic environment, allowing for the possibility of heat integration within the solvent regeneration process.

Considering the economic performance of such a unique discovery, we can potentially re-evaluate the cost of CO₂ capture, to lower the total cost of capture. For a full chain CCS system, and a steel plant capture system is no exception, the capture element represents the most significant cost and energy requirement. For an MEA system, which is highly plausible for steel applications: experience from the vast commercial use of MEA has shown that these systems will tolerate gas compositions similar to those found in a steel plant. The estimated split between capture cost as transport and storage (T&S) is 70/30 (capture/T&S) (Roussanaly, et al., 2018).

Within a capture system, the regeneration of the capture medium is the greatest energy consumer, combined with alternative efforts made to reduce this energy demand, such a compression. A breakdown of the capture costs for a steel plant (blast furnace gas) are presented below, whereby energy cost represents ~70% of capture cost (Roussanaly, et al., 2018). This is mostly steam generation for the solvent reboiler, with a steam consumption of ~3.2 GJ per ton of CO₂ captured. These are estimated cost for an nth-of-a-kind CCS facility; to date a full chain (1st -of-a-kind) CCS plant has yet to be established on a BF-BOF steel making plant.

Figure 6.1: Breakdown of blast furnace MEA capture costs



The application of CCS using MEA would cost an estimated ~£60 per ton of CO₂ captured and stored from the blast furnace, following internal and external assessment (IEAGHG, 2014). Given an estimated finished steel coil price of £500 per ton and 1.8 ton of CO₂ per ton of steel, this corresponds to £608 per ton of steel; a 17.8% increase in the cost per ton of steel, if CCS is applied. If by employing microbubbles it is viable to control the size of the plant and the NH₃ loss, one can assume all other costs are the same as that of an established amine facility. Costs of amine facilities are well known, yet the cost of an ammonia-based capture system is still an estimate, so this approach was considered appropriate given the lack of cost data. Assuming all else remains equal, the major difference, and the greatest cost, is the reboiler energy use. If the temperature of the solvent regeneration is reduced from 120 to 80 (table 2-4), a 40°C drop in temperature, not knowing the volume of solvent to be heated to this temperature, we will cautiously assume 33.3% drop in steam demand and the energy cost. This would represent a reduction of 1.07 GJ steam per ton of CO₂ captured and roughly a 24% reduction in capture cost using the breakdown of capture costs represented in figure 6.1.

This would reduce the cost of capture and the total cost per ton of steel from £608 to £590 per ton for our low carbon steel offering, at a Blast Furnace capture rate of 80% CO₂. A 24%

reduction in capture cost results in an £18 reduction in total capture costs per ton of steel. With a 3.8 MT per year output of finished steel coil chosen for our test case steel plant (4MT of steel provided to the downstream processing), this equates to a £68.4 million cost saving per year.

This estimation compares well, if not slightly conservatively, to the cooled ammonia process, which was evaluated for Specific Primary Energy Consumption for Carbon Avoided (SPECCA), by Valenti et al. (2018), whose estimates are 4.16, 2.86 and 2.58 GJ/t CO₂ for MEA, chilled ammonia and cooled ammonia respectively (Valenti & Bonalumi, 2018). This represents a 1.58 GJ/t CO₂ energy reduction for the chilled process compared to MEA, against the assumed 1.07 GJ/t CO₂, utilising the 33.3% steam energy reduction method as described. The cost savings, estimated at £68.4 million, are therefore justified. Whilst newly emerging solvents may approach similar regeneration energy savings (Okon, et al., 2017), ammonia has the advantages of mild corrosivity, negligible thermal degradation, minimal environmental impact and cheap.

The size of a capture facility is also a significant barrier to the implementation of CCS at some steel making sites, with limited land availability. By increasing the kinetics, the size or number of absorption columns could be reduced. This will reduce footprint and also CAPEX. An estimate of this reduction has not been made but a full techno-economic assessment of aqueous ammonia based capture, enhanced with FO microbubbles and deployed on a steel plant should now be undertaken.

The ammonia capture system looks promising, as does the early developments of a mixed salts process, adding potassium carbonate (K₂CO₃) to the capture systems. This addition may yield an ever greater improvement in performance, although it is too early to say if these developments could lead to a commercialised system (Jayaweera, et al., 2017), (Han, et al., 2014).

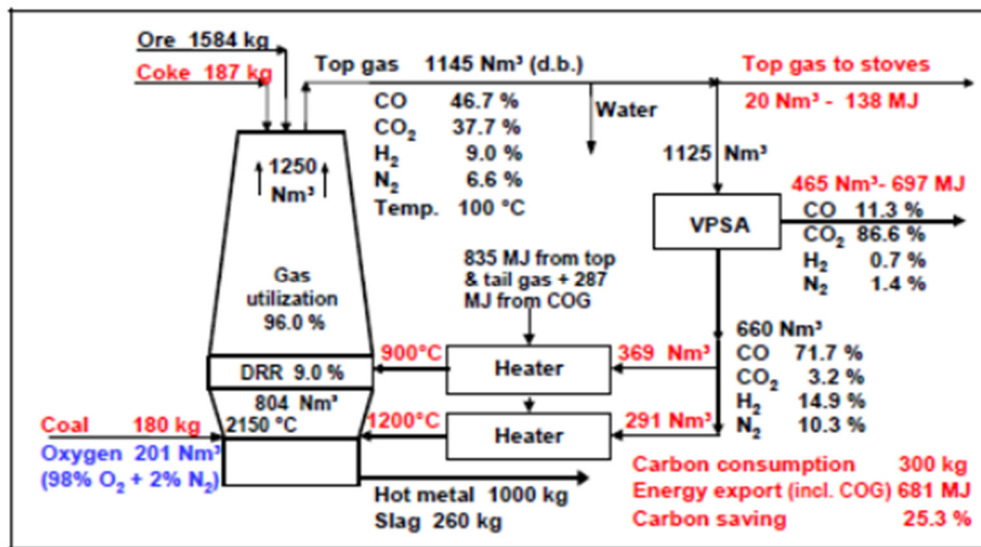
6.3 Technology application of CO₂ dissociation by DBD plasma

Within the steelmaking processes, equal proportions of CO and CO₂ gas are produced from the blast furnace. Whilst the CO has value as a fuel gas for the site, the CO₂ causes an immediate issue as it is vented, once cleaned of contaminants, to the atmosphere. The CO, however, once combusted also results in a significant and equal quantity of CO₂ emission to atmosphere.

CCS, as evaluated in the techno-economic model and enhanced within the work of Research Chapter A, is likely to be required in our future steel plant scenario, in the period up to 2050. With the application of CCS, high purity CO₂ could become available for dissociation within a plasma reactor. This could potentially lend itself to the top-gas-recycling concept (Directorate-General for Research and Innovation (European Commission), 2014), whereby CO₂ is separated from the processes gases of the blast furnace and a high concentration CO stream is recycled back to the furnace, to reduce overall carbon input (figure 6.2). If the CO₂ captured within this process is subsequently supplied to a plasma stage, the resultant CO and O₂ from plasma

dissociation could also be recycled back to the furnace, further reducing primary carbon input. The nitrogen content within the gas will be reduced (as the O₂ from the plasma reactor can replace a proportion of air) reducing the CCS cost, as less gas volume is generated and the CO₂ concentration of the gas is increased. One limiting factor in fossil-based steel production, is the ability to electrify this process by incorporating zero-carbon electricity. Using zero-carbon electricity to power the plasma reactors, we have in principle reduced the fossil carbon input (recycling the carbon back into the furnace in the dissociated form of CO) by the coveted substitution with zero-carbon electricity.

Figure 6.2: Configuration, energy balance and carbon savings of the top gas recycling blast furnace process



Source: (Directorate-General for Research and Innovation (European Commission), 2014)

If the electricity used is from a fossil free source, the total efficiency of the plasma process does not influence the carbon emissions, only the energy consumption of the process. This technology could be applied as a retrofit process to existing steel plant, reducing capex and disruption to operations from switching to new technology.

However, even when we consider the breakthrough in the new developments of the two-staged plasma reactor design that could potentially lead to world class CO₂ plasma dissociation, we still find that, due to the efficiency of the plasma dissociation mechanisms for CO₂, dominated via electronic excitation, the efficiency of the process is low and inversely proportional to CO₂ conversion. To achieve high conversions and high CO concentration that would warrant a return of the reactor gas back to the furnace, this would lead, under current operations, to low plasma efficiencies. The alternative, low conversion rates, would need subsequent CO₂ removal, which comes at a high energy penalty. The plasma dissociation of CO₂ at 100% efficiency, requires almost the same energy input as that for H₂O dissociation into H₂ and O₂, as set out in equations 2.39 and 6.1 (Fridman, 2008).



At 100% efficiency, a hydrogen electrolyser would consume 39.4 kWh per kg of H₂, where 1 kg of hydrogen has an energy content of 12.75 MJ/m³ at STP and 143 MJ/kg. A typical PEM electrolyser operates at an efficiency of 80%, which yields a total energy consumption of 47.3 kWh/kg H₂, or 0.33 kWh/MJ of H₂ (Bertuccioli, et al., 2014).

At 100% plasma conversion efficiency, the higher molecular weight of CO allows a lower energy requirement per kg of CO. Only 2.81 kWh/kg CO is required. The plasma CO₂ dissociation efficiency has a theoretical maximum of 43%, under quasi-equilibrium conditions. (Fridman, 2008). Whilst higher efficiencies may be possible under non-equilibrium conditions, the conversion rate is very low (Aerts, et al., 2015) (Bogaerts, et al., 2015). At an optimistic 50% efficiency, this would equate to a total energy consumption of 4.21 kWh per kg of CO. With an energy content of 10.1 MJ/kg CO, this equates to 0.41 kWh/MJ. Which, if the gases are both used as a fuel, at 100% efficiency, is slightly worse than the hydrogen example.

In a steel context, equal mols of H₂ and CO are required for the reduction of iron ore. The values are therefore presented in kWh per mol: 0.095 kWh/mol for hydrogen and 0.118 kWh/mol for CO. Hence, as an iron reductant, plasma conversion does not yield a promising result. A similar ~80% efficiency would be required to equal that of hydrogen conversion energy input, which appears unlikely with current technologies.

Under these assumptions the O₂ has been attributed no value, which is often quite mistakenly overlooked, yet this does not change the above comparison, as both dissociation pathways produce ½ O₂, with a similar energy input.

The generation of hydrogen rather than CO would also lead to no further carbon emission, if used to supplement coke or coal within the blast furnace, or indeed elsewhere with the steelmaking operation. Given the low conversion rates, it does not seem viable to use any surplus zero-carbon electrical energy to convert the CO₂ to an alternative carbon source, which would later require capture, when H₂ (and not excluding the valuable O₂) could be generated and supplied to the furnace resulting in no further carbon release at a higher electrical efficiency.

The scale-up of industrial hydrogen electrolyzers is also likely to occur before those of CO₂ dissociation plasma reactors. Given the results from the modelling exercise, we have learned that it is key to move quickly in technology deployment, to reduce the net CO₂ emitted to atmosphere, between now and 2050. Even so, the role out of industrial scale electrolyzers is limited by the availability of surplus renewable power and, of course, the cost.

It does not seem, given the mechanisms for CO₂ plasma dissociation and need to further address the carbon from the use of the resultant CO, that this technology could be applied to achieve a deep decarbonisation of the steel sector in the near to medium term. It is likely the hydrogen electrolyzers will dominate, if surplus renewable energy becomes available. From our techno-economic modelling within Research Section 5, we know that substitution of carbon with hydrogen, is more expensive than carbon capture, transport and storage. With hydrogen from SMR or ATR with CCS more cost effective than electrolyzers. A plasma system would only be applicable for smaller applications, where additional CO was needed, yet with the steel CCU applications being developed, the limiting component is hydrogen and not alternative forms of carbon. A WGS to turn the CO into hydrogen would in this case likely be considered an attractive alternative. The generation of hydrogen from CO and H₂O is demonstrated by equation 6.2.

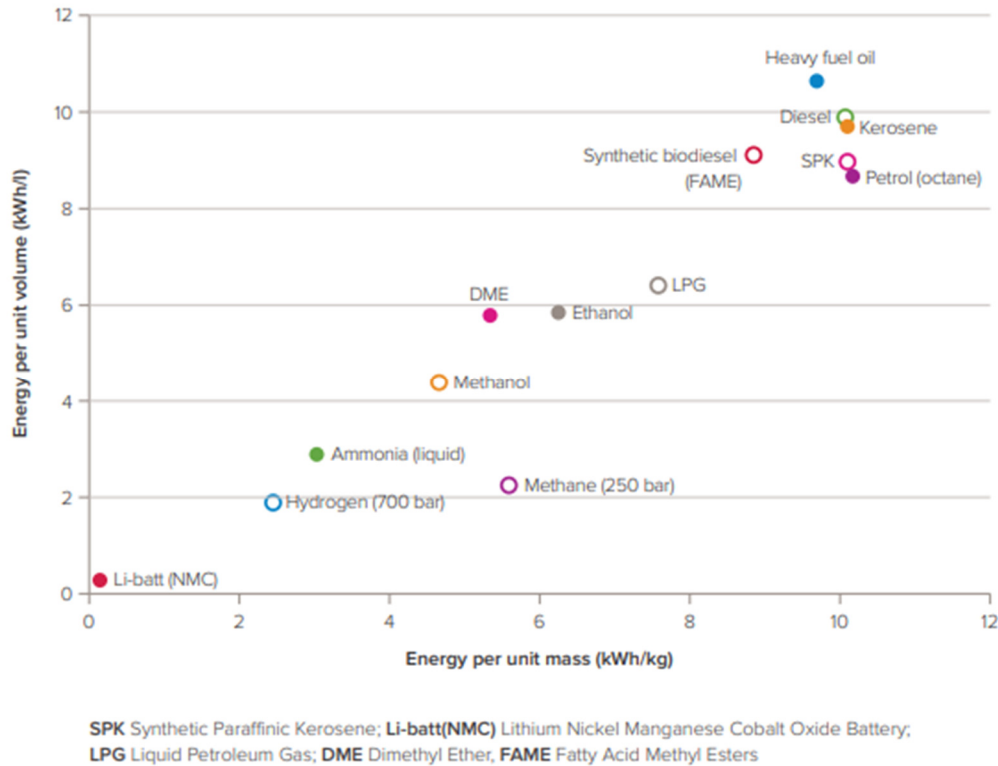


Where this technology is likely applicable to the steel sector, is utilising the industrial carbon emissions for the production of synthetic fuels to help the technically more difficult to decarbonised sectors, such as aviation. If renewable power is used in the process, CO can be generated from the CO₂, which can be used to produce methanol over a copper catalysis or using a fermentation process. Methanol synthesis from CO (typically from fossil based synthesis gas) is a proven technology and can be used to produce aviation fuels (The Royal Society, 2019). These processes require both a carbon source and hydrogen, eliminating the aforementioned requirement to compare the efficiencies between the two processes.

Given the challenges in decarbonising the aviation sector and the conflict with bio-energy sources, the use of industrially sourced carbon could be a viable pathway to lower carbon flight. Batteries, due to their very low energy density are not a viable solution to zero carbon flight in the medium term, so some carbon off-setting or carbon recycling to establish high density fuels is required (figure 6.3). Steel plant gas conversion (CO) via fermentation is becoming an established technology route for the production of synthetic fuels which responds favourably to high CO content, which can be enhanced via the plasma dissociation method (figure 6.4). This is effectively an indirect method of electrifying aviation. Whilst estimated current efficiencies are lower for a synthetic diesel fuel vehicle (13%), compared to using battery power (69%) it may be the only solution for long haul flights and so, any improvements in efficiency will be welcome. It's clear that transparent LCA, aligned to a consistent methodology is still required to assess the overall impact from this approach (Garcia-Garcia, et al., 2020). The LCA and techno-economic assessment for the application of CCU to synthetic fuel production to a steel plants has still to be performed, but will be assessed as part of the European Horizon 2020 project named COZMOS (COZMOS, 2019).

Evidently the improvement shown here within the CO conversion efficiency of 36% are a positive step for DBD plasma dissociation. However, they are of course no match for the record breaking 90% Faradaic efficiency achieved recently using an electrochemical method, over a copper–indium binary catalyst (Xiang, et al., 2020).

Figure 6.3: Energy density for fuel options including tank weight



Source: (The Royal Society, 2019)

Figure 6.4: Current examples of synthetic fuel production

| Facility/Operator name | Country | CO ₂ feedstock | Efuel output | Output quantity |
|--|---------|---------------------------|-----------------------------|--------------------------------------|
| Carbon Recycling International (Vulcanol) ¹¹¹ | Iceland | Geothermal plant flue gas | Methanol | 4000 tonnes/year |
| FReSME project (2020) ¹¹² | Sweden | Blast furnace gas | Methanol | 50 kg/hr |
| MefCO ₂ ¹¹³ (final phase construction) | Germany | Power plant flue gas | Methanol | 1 tonne/day (planned) |
| Soletair ¹¹⁴ | Finland | Direct Air Capture | Petrol, Kerosene and Diesel | 100 kg/hr |
| Sunfire ¹¹⁵ | Germany | Direct Air Capture | E-Crude (E-diesel) | Demonstration: 3 tonnes in 1500 hrs |
| Sunfire (2022) ¹¹⁶ | Norway | Direct Air Capture | E-Crude (E-diesel) | 8000 tonnes/year (planned 1st stage) |

Source: (The Royal Society, 2019)

6.4 Chapter Summary

The evaluation of the two developed and tested technologies within a future low-carbon steel plant have shown that the utilisation of steel plant carbon emission for the production of nitrogen release fertiliser is unlikely to lead to significant emission reduction. However, the capture of CO₂ using an aqueous ammonia system could become highly relevant. Following the detailed techno-economic modelling exercise, it is determined that the availability of CCS is a critical technology option, especially in the near term, and that a low-cost ammonia capture solution, would significantly improve economic performance. A conservative estimate of >£68m per annum could be recognised, for the test case steel plant following the successful deployment of this technology.

With respect to the application of plasma dissociation of CO₂, due to the mechanisms involved, achieving both high conversion yields and high efficiencies has not been possible, even when re-evaluating the plasma reactor design, with a breakthrough two-stage system. It is unlikely that the dissociation of CO₂ will lead to deep decarbonisation of the steel sector in the near to medium term, due to low conversion efficiency and current pace of technology development. Further assessment suggests substitution with hydrogen is more likely as the H₂O exhaust does not need further treatment. Given that equal mols of hydrogen and CO are required for iron ore reduction, hydrogen generation via electrolysis yields a better energy efficiency. The TRL of the hydrogen electrolyser is also much greater, and in the context of steel plant decarbonisation, moving quickly prevents a greater quantity of carbon entering the atmosphere. For these three reasons, it is likely that hydrogen electrolysers will dominate, if there is surplus renewable power, as a fossil fuel substitution within a steel plant.

Where this technology could be applicable is for the production of synthetic fuels or carbon-based products. As industry is likely to form an ongoing source of CO₂, being able to efficiently convert the CO₂ would seem highly desirable. It is likely that sourcing this carbon from industry will be more cost effective than direct air capture, due to the higher CO₂ concentration and also, possible necessity to separate the CO₂ for storage.

Chapter 7

Final summary and future recommendations,

7.1 Final summary

The steel industry today represents about 8% of anthropogenic CO₂ emissions, without obvious cost-effective solutions available to decarbonise this sector. This represents a major challenge to the industry and one which provided the focus and challenge for this research.

This research sought to first progress two technologies within the areas of aqueous ammonia CO₂ capture and CO₂ plasma dissociation, which were identified as promising solutions to reduce CO₂ emissions to atmosphere. Whilst aqueous ammonia capture systems had been applied to steel plants and show promise, it was believed that the fundamental issue of slow kinetics could be significantly improved. CO₂ plasma dissociation was believed to have been applicable to enhanced carbon recycling within the steel industry (such as to further enhance a TGRBF). However, low conversion efficiencies were seen as a significant barrier to address. The aim was to apply propriety knowledge to these issues to develop novel, state-of-the-art solutions. Whilst investigating the application of CO₂ based solutions to the steel sector, it was apparent that some fundamental questions needed to be answered. Will fossil energy (and CO₂) still feature prominently in the near, medium or long-term steel making future? Or will the current steelmaking solutions be replaced with electricity or hydrogen? To answer these questions and ultimately determine how the developments of the two technologies under development could be applied, a detail techno-economic model was produced. Multiple projects provided some insight into the possible future direction on a global, continental or regional level, but lack the detail needed to determine the possible pathways and the rate of deployment.

Three hypotheses were proposed. Each challenging and with the aim to advance the knowledge within their particular research field, to ultimately produce one significant contribution to the knowledge of steel plant decarbonation solutions.

The modelling methodology that was developed, showed that all available solutions (with a TRL today of ≥ 7) that could be applied to a typical steel plant to achieve significant (>80%) decarbonisation would increase operational cost. Therefore, cost reduction of the applied technologies, such as those demonstrated within this research would be highly advantageous to the industry. Equally the availability of hydrogen and its high cost is likely prohibited in the short to medium term and that if applied, blue hydrogen is the most likely source. This confirms that fossil energy and CO₂ would indeed feature prominently between now and 2050 within the industry. Therefore, methods to effectively reduce or recycle CO₂ would still feature in many

future steel making sites. It was also demonstrated that swift action would lead to the greatest reduction in cumulative emission to atmosphere, limiting catastrophic climate change, regardless of technology the solution. This is a unique discovery of this model and not previously demonstrated by other studies.

By applying FO microbubbles to the CO₂-NH₃-system for the first time, it was demonstrated that the much enhanced gas-to-liquid surface area and possible bubble surface pseudo-catalytic effect, overcame the slow kinetic problem for aqueous ammonia CO₂ capture. With this new discovery, it would be possible to apply this capture technology to a steel plant, so that the benefits of low solvent cost and low energy regeneration could be realised. It was estimated that, as removal of CO₂ is likely to feature in a future steel plant, either direct capture or from blue hydrogen, a significant cost saving could be recognised. Also, the size of the plant could be significantly reduced, limiting CAPEX and the plant footprint. Size of the capture facility is another major barrier to decarbonisation at many steel plant locations, not represented in this or indeed other modelling exercises.

The efficiency of plasma dissociation was further enhanced with the invention of a first-of-a-kind two stage DBD reactor. This reactor, with its high energy input and subsequent lower energy exit, reduced energy losses. A 40 % increase in plasma efficiency was gained over the single stage configuration. Whilst a significant step forward, this still represents a low overall efficiency, which still represents a barrier to full-scale deployment. Although it was determined that the application for deep decarbonisation of steel plant maybe limited, it could have significant application in the recycling of industrial CO₂ into synthetic fuels for difficult to decarbonised transport, such as aviation.

7.2 Recommendations for further work

As a first-of-a-kind demonstration of two new technological developments, there are limitations on what can be achieved within the timescale (and budget). Specifically, extra consideration must be given to identifying and overcoming new and unforeseen challenges as the new knowledge is generated. Naturally, there are recommendations for further work to take this knowledge forward and overcome existing barriers.

These can be categorised for the aqueous ammonia experiments as follows;

- Further back-to-back comparisons and optimisation of non-oscillatory bubbles with bubbles of various sizes to validate the results.
- Repeat of the aqueous ammonia experiments with different reactor set-ups and various levels of plasma power input, to determine the potentially competing influences of bubble surface charge (phantom catalyst) and the interference from the conversion of CO₂ into CO and O₂.

- Design and operation of a system for continuous operational modes to reflect a carbon capture system, with a greater focus on the accuracy of the CO₂ and NH₃ measurements.
- Review of the use of C-13 NMR for precipitate yield measurements, which may lead to carbamate losses in the analysis preparation process and replacement with a more suitable method.
- Identifying if ammonia can be efficiently recovered from wastewater, so that this may supply an aqueous ammonia capture unit and enable the ability to produce ammonia bicarbonate fertiliser, utilising an industrial CO₂ source.
- A full techno-economic analysis is aqueous ammonia based capture, with increased kinetics as a result of FO microbubble technology, is now needed to fully understand the potential.

Additional steps to the novel two-stage plasma reactor system should be taken to advance the knowledge. These are, to repeat the experiments to determine efficiency with greater accuracy by:

- Utilisation of a more accurate mass flow control.
- Continuous and accurate monitoring of the gases for both the reactor inlet and outlet, using either a twin Fourier-transform infrared spectroscopy (FTIR) or Mass Spectrometer Setup.
- Perform plasma gas measurement between the two electrodes within the intermediate 'after-glow' stage.
- Greater control in plasma power input, including wave formation, especially the decaying waveform of the second power supply input that may have caused arcing at smaller electrode gap distances.
- Review of insulating materials between the two plasma power stages, to reduce the gap beyond 13mm, to limit the after-glow period to within the μ s range.

To further improve the techno-economic model, the following could be implemented:

- Improvement in the detail and accuracy of the model data with pre-FEED assessment and full-FEED for the technology deployment, fuel switching and system abatement options.
- LCA assessment for the total impact of each technology option.
- Greater clarity on the global impact on emissions from changes to the UK scrap circulation.
- Expansion upon the CCU modelling capability with access to better data.

- Addressing of knowledge gaps in the local infrastructure requirements and lead times to access suitable quantities of low-carbon hydrogen (or ammonia), renewable power and CCS infrastructure.
- Until a DRI-H₂ furnace is operated at 100% H₂ the influences are still unknown. There is a 30% discrepancy in GJ/tm between some theoretical academic studies and the known energy input required for a DRI furnace, which needs to be rectified. Further knowledge is essential to full estimate the impact and cost of a transition to hydrogen-DRI.

References

- Abdulrazzaq, N., Al-Sabbagh, B., Rees, J. M. & Zimmerman, W. B., 2015. Separation of azeotropic mixtures using air microbubbles generated by fluidic oscillation. *American Institute of Chemical Engineers (AIChE) Journal*, Volume 62, pp. 1192-1199.
- Aerts, R., Martens, T. & Bogaerts, A., 2012. Influence of Vibrational States on CO₂ Splitting by Dielectric Barrier Discharges. *The Journal of Physical Chemistry*, Volume 116, p. 23257–23273.
- Aerts, R., Somers, W. & Bogaerts, A., 2015. Carbon Dioxide Splitting in a Dielectric Barrier Discharge Plasma: A Combined Experimental and Computational Study. *ChemSusChem*, 8(4), pp. 702-716.
- Agarwal, A., Ng, W. J. & Liu, Y., 2011. Principle and applications of microbubble and nanobubble technology for water treatment. *Chemosphere*, Volume 84, p. 1175–1180.
- Agarwal, S. K., Bhaskar, K. & Das, P. C., 2007. *Manufacture of Urea*, Rourkela: National Institute of Technology.
- Akishev, Y. S. et al., 2011. Role of the volume and surface breakdown in a formation of microdischarges in a steady-state DBD. *The European Physical Journal D*, Volume 61, p. 421–429.
- Alexander, L. et al., 2013. *Working Group I Contribution to the IPCC Fifth Assessment Report, Climate Change 2013: The Physical Science Basis Summary for Policy Makers*, s.l.: s.n.
- Allwood, J. & Cullen, J., 2012. *Sustainable Materials: with Both Eyes Open*. 1 ed. Cambridge, England: UIT Cambridge Ltd.
- Allwood, J. M., Dunant, C. F., Lupton, R. C. & Serrenho, A. C. H., 2019. *Steel Arising - Opportunities for the UK in a transforming global steel industry*, s.l.: ISBN 9780903428477.
- Al-Mashhadani, M. K. H., Wilkinson, S. J. & Zimmerman, W. B., 2015. Airlift bioreactor for biological applications with microbubble mediated transport processes. *Chemical Engineering Science*, Volume 137, p. 243–253.
- American Iron and Steel Institute - Steel Recycling Institute, 2020. *steelsustainability.org*. [Online]
Available at: <https://www.steelsustainability.org/recycling>
[Accessed 28 11 2020].
- ArcelorMittal, 2019. *Climate Action Report 1*, Luxembourg: ArcelorMittal.

Aresta, M., Dibenedetto, A. & Angelini, A., 2013. The changing paradigm in CO₂ utilization. *Journal of CO₂ Utilization*, Volume 3-4, pp. 65-73.

Aresta, M. & Dibenedetto, A., 2007. Utilisation of CO₂ as a chemical feedstock: opportunities and challenges. *Dalton Transactions: The Royal Society of Chemistry*, Issue 28, pp. 2975-2992.

Armstrong, K. & Styring, P., 2015. Assessing the potential of utilization and storage strategies for. *Frontiers in Energy Research*, Volume 3, pp. 1-9.

ARUP, 2018. *peopleandplanet.org*. [Online] Available at: https://peopleandplanet.org/system/files/resources/scope_3_methodology_guidance_0.pdf [Accessed 27 11 2020].

Attri, P., Arora, B. & Choi, E. H., 2013. Utility of plasma: a new road from physics to chemistry. *RSC Advances*, 3(31), pp. 12540-12567.

Bachu, S., 2015. Review of CO₂ storage efficiency in deep saline aquifers. *International Journal of Greenhouse Gas Control*, Volume 30, p. 188–202.

Badie, M. et al., 2012. Overview of Carbon Dioxide Separation Technology. *Proceedings of the IASTED International Conference on Power and Energy Systems and Applications, PESA 2012*, Volume 1, pp. 164-151.

Barzagli, F., Mani, F. & Peruzzini, M., 2011. From greenhouse gas to feedstock: formation of ammonium carbamate from CO₂ and NH₃ in organic solvents and its catalytic conversion into urea under mild conditions. *Green Chemistry*, Volume 3, pp. 1267 - 1274.

BASF, 1993. *Technical Leaflet - Ammonium Carbamate*, Ludwigshafen: BASF Aktiengesellschaft.

Bassarov, A. I., 1870. Bassarov Synthesis. *Prakt Chemistry*, 2(1), p. 283.

Bellan, P. M., 2006. *Fundamentals of Plasma Physics*. 1st ed. California: Cambridge University Press.

Bertuccioli, L. et al., 2014. *Development of Water Electrolysis in the European Union*, Lausanne (Switzerland) & Cambridge (United Kingdom): E4tech & Element Energy (on behalf of New Energy World Joint Undertaking Fuel Cells and Hydrogen).

Birat, J. P., 2010. *Steel sectoral report, contribution to the UNIDO roadmap on CCS (fifth draft)*. Amsterdam, s.n., pp. 24 September 2010,.

Bogaerts, A., Kozk, T., Van Laer, K. & Snoeckx, R., 2015. Plasma-based conversion of CO₂: current status and future challenges. *Faraday Discussions*, 183(1), p. 217–232.

- Bongers, W. et al., 2017. Plasma-driven dissociation of CO₂ for fuel synthesis. *Plasma Processes and Polymers*, 14(6), p. n/a.
- Bosch, C. & Meiser, W., 1922. *Process of Manufacturing Urea*. US, Patent No. 1,429,483.
- Bouaifi, M., Hébrard, G., Bastoul, D. & Roustan, M., 2001. A Comparative Study of Gas Hold-Up, Bubble Size, Interfacial Area and Mass Transfer Coefficients in Stirred Gas-Liquid Reactors and Bubble Columns. *Chemical Engineering and Processing*, 40(2), pp. 97-111.
- Cai, X., Yang, F. & Gu, N., 2012. Applications of Magnetic Microbubbles for Theranostics. *Theranostics*, 2(1), pp. 103-112.
- Campbell, L., 2016. *Micro-plasma activated urea synthesis from CO₂ and NH₃*, MEng Research Thesis, s.l.: .
- Carpenter, A., 2012. *CO₂ abatement in the iron and steel industry, report CCC/193*, London: IEA Clean Coal Centre.
- CCUS Cost Challenge Taskforce, 2019. *Delivering Clean Growth: CCUS Cost Challenge Taskforce Report*, s.l.: s.n.
- Committee on Climate Change, 2019a. *Net Zero: The UK's contribution to stopping global warming*, London (UK): Committee on Climate Change.
- Committee on Climate Change, 2019b. *Net Zero – Technical Report*, London (UK): Committee on Climate Change.
- COZMOS, 2019. *COZMOS Efficient CO₂ conversion over multisite Zeolite-Metal nanocatalysts to fuels and OlefinS*. [Online] Available at: <https://www.spire2030.eu/cozmos> [Accessed 09 12 2020].
- Cussler, E. L., 1997. *Diffusion: Mass transfer in fluid systems*. 2nd ed. s.l.:Cambridge University Press.
- Danloy, G. et al., 2009. ULCOS - Pilot testing of the Low-CO₂ Blast Furnace process at the experimental BF in Luleå. *Metallurgical Research & Technology*, 106(1), pp. 1-8.
- de Donder, T., 1936. *L'affinité*. Paris: Gauthier-Villars: Ed. Pierre Van Rysselberghe.
- Desai, P. D., Hines, M. J., Riaz, Y. & Zimmerman, W. B., 2018. Resonant Pulsing Frequency Effect for Much Smaller Bubble Formation with Fluidic Oscillation. *Energies*, 11(10), p. 2680.
- Desai, P. D. et al., 2019. Comparison of Bubble Size Distributions Inferred from Acoustic, Optical Visualisation, and Laser Diffraction. *Colloids and Interfaces*, 3(4), p. 65.

- Desai, P. D., Turley, M., Robinson, R. & Zimmerman, W. B., 2020. Hot microbubble injection in thin liquid film layers for ammonia separation from ammonia rich-wastewater. *Preprint*.
- Directorate-General for Research and Innovation (European Commission), 2014. *ULCOS top gas recycling blast furnace process (ULCOS TGRBF)*, Brussels: RFCS Publications.
- Ekins-Coward, T., Lee, J. & Caldwell, G., 2015. The effect of bubble size on the efficiency and economics of harvesting microalgae by foam flotation. *Journal of Applied Phycology*, 27(2), pp. 733-742.
- Erismann, J. W. et al., 2013. Consequences of human modification of the global nitrogen cycle. *Philosophical Transactions of The Royal Society B*, 368(1621).
- Estrada, F., Perron, P. & Martínez-López, B., 2013. Statistically derived contributions of diverse human influences to twentieth-century temperature changes. *Nature Geoscience*, 6(12), pp. 1050-1055.
- Eurofer The European Steel Association, 2013. *A Steel Roadmap for a Low Carbon Europe 2050*, Brussels: Eurofer.
- Fickling, D., 2020. *BHP's Road To Reduced Emissions Should Be Electric*. s.l.:Bloomberg.
- Fischedick, M., Marzinkowski, J., Winzer, P. & Weigel, M., 2014. Techno-economic evaluation of innovative steel production technologies. *Journal of Cleaner Production*, Volume 84, pp. 563-580.
- Fischedick, M. et al., 2014. *limate Change 2014: Mitigation of Climate Change. Contribution of Working Group III to the Fifth Assessment Report of the Intergovernmental Panel on Climate Change*, Cambridge, United Kingdom and New York, NY, USA: Cambridge University Press.
- Florin, N. et al., 2010. An overview of CO₂ Capture Technologies. *Energy & Environmental Science*, Volume 3, pp. 1645-1669.
- Fridman, A., 2008. *Plasma Chemistry*. 1st ed. Cambridge: Cambridge University Press.
- Friedlingstein, P., Andrew, R. M. & Rogelj, J., 2014. Persistent growth of CO₂ emissions and implications for reaching climate targets. *Nature Geoscience*, 7(10), pp. 709-715.
- Garcia-Garcia, G. et al., 2020. Analytical Review of Life-Cycle Environmental Impacts of Carbon Capture and Utilization Technologies. *Preprint*.
- Gilmour, D. & Zimmerman, W., 2020. Microbubble intensification of bioprocessing. *Preprint*.
- Goto, K., Yogo, K. & Higashii, T., 2013. A review of efficiency penalty in a coal-fired power plant with post-combustion CO₂ capture. *Applied Energy*, 111(1), pp. 710-720.

Han, K., Ahn, C. K. & Lee, M. S., 2014. Performance of an ammonia-based CO₂ capture pilot facility in iron and steel industry. *International Journal of Greenhouse Gas Control*, 27(1), pp. 239-246.

Hanotu, J., Bandulasena, H. C. H. & Zimmerman, W. B., 2012. Microflotation performance for algal separation. *Biotechnology & Bioengineering*, 109(7), pp. 1663-1673.

Hanotu, J., Zimmerman, W. B., Bandulasena, H. C. H. & Chiu, T. Y., 2013. Oil emulsion separation with fluidic oscillator generated microbubbles. *International Journal of Multiphase Flow*, Volume 56, pp. 119-125.

Hirsch, A. et al., 2013. *New blast furnace process (ULCOS)*, Brussels: Publications Office of the EU.

Hotten, R., 2018. *BBC News*. [Online] Available at: <https://www.bbc.co.uk/news/business-44613652> [Accessed 14 06 2020].

Hunt, A. J., Sin, E. H. K., Marriott, R. & Clark, J., 2010. Generation, Capture, and Utilization of Industrial Carbon Dioxide. *ChemSusChem*, Volume 3, p. 306 – 322.

IEA (International Energy Agency), 2013. *Technology Roadmap - Energy and GHG Reductions in the Chemical Industry via Catalytic Processes*, Paris: IEA.

IEAGHG, 2014. *Iron and Steel CCS Study (techno-economics of an integrated steel mill)*. [Online] Available at: <https://ieaghg.org/publications/technical-reports/reports-list/9-technical-reports/1001-2013-04-iron-and-steel-ccs-study-techno-economics-integrated-steel-mill> [Accessed 10 12 2020].

International Energy Agency, 2014. *CO₂ Emissions from Combustion Sources - 2014 Highlights*, Paris: IEA Publications.

IPCC, 2005. *Intergovernmental Panel on Climate Change: Special Report on Carbon Dioxide Capture and Storage*, New York: Cambridge University Press.

Jayaweera, I. et al., 2017. Results from Process Modeling of the Mixed-salt Technology for CO₂ Capture from Post-combustion-related Applications. *Energy Procedia*, Volume 114, pp. 771-780.

Kantarci, N., Borak, F. & Ulgen, K. O., 2005. Bubble column reactors. *Process Biochemistry*, 33(5), p. 883–894.

Kato, Y., 2012. Hydrogen Utilization for Carbon Recycling Iron Making System. *ISIJ International*, 52(8), p. 1433–1438.

- Kogelschatz, U., 2003. Dielectric-barrier discharges: Their History, Discharge Physics, and Industrial Applications. *Plasma Chemistry and Plasma Processing*, 23(1), pp. 1-46.
- Kohl, A. & Nielsen, R., 1997. *Gas Purification*. 5th ed. Houston: Gulf Publishing Company.
- Kozák, T. & Bogaerts, A., 2014. Splitting of CO₂ by vibrational excitation in non-equilibrium plasmas: a reaction kinetics model. *Plasma Sources Science and Technology*, 23(4).
- Kulkarni, A. A. & Joshi, J. B., 2005. Bubble Formation and Bubble Rise Velocity in Gas - Liquid Systems: A Review. *Industrial & Engineering Chemistry Research*, 44(16), p. 5873–5931.
- Leach, A. M. et al., 2012. A nitrogen footprint model to help consumers understand their role in nitrogen losses to the environment. *Environmental Development*, 1(1), pp. 40-66.
- Lillia, S., Bonalumi, D. & Valenti, G., 2016. Rate-based approaches for the carbon capture. *Energy Procedia*, Volume 101, pp. 400-407.
- Liu, J. et al., 2011. Kinetics and mass transfer of carbon dioxide absorption into aqueous. *Energy Procedia - GHGT-10*, Volume 4, pp. 525-532.
- Liu, J. et al., 2009. Absorption of carbon dioxide in aqueous ammonia. *Energy Procedia*, 1(1), pp. 933-940.
- Liu, Y., Rehman, F. & Zimmerman, W. B., 2017. Reaction engineering of carbon monoxide generation by treatment with atmospheric pressure, low power CO₂ DBD plasma. *Fuel*, 209(1), pp. 117-126.
- Lou, X. K., Yang, G. Q., Lee, D. J. & Fan, L. S., 1998. Single bubble formation in high pressure liquid-solid suspensions. *Powder Technology*, 100(2-3), pp. 103-112.
- Lozano-Parada, J. H. & Zimmerman, W. B., 2010. The role of kinetics in the design of plasma microreactors. *Chemical Engineering Science*, 65(17), pp. 4925-4930.
- MacDowell, N. & Fajardyab, M., 2017. Can BECCS deliver sustainable and resource efficient negative emissions?. *Energy & Environmental Science*, 10(6), pp. 1389-1426.
- Mandová, H. et al., 2019. Achieving carbon-neutral iron and steelmaking in Europe through the deployment of bioenergy with carbon capture and storage. *Journal of Cleaner Production*, 218(1), pp. 118-129.
- Mani, F., Peruzzinib, M. & Stoppionia, P., 2006. CO₂ absorption by aqueous NH₃ solutions: speciation of ammonium carbamate, bicarbonate and carbonate by a ¹³C NMR study. *Green Chemistry*, 8(11), pp. 995-1000.
- McGinty, R. et al., 2017. Techno-economic survey and design of a pilot test rig for a trilateral flash cycle system in a steel production plant. *Energy Procedia*, Volume 123, pp. 281-288.

McKinsey & Company, 2018. *Decarbonization of industrial sectors: the next frontier, June*, Amsterdam: McKinsey & Company.

McKinsey and Company, 2017. *Metals Model*, s.l.: McKinsey and Company.

Meesen, J. H., 2012. Urea. *Ullmanns Encyclopedia of Industrial Chemistry*, 37(2), pp. 657-695.

Merchant Research, 2015. *Urea: 2015 World Market Outlook and Forecast up to 2019*. [Online] Available at: <http://mcgroup.co.uk/researches/urea> [Accessed 27 October 2015].

Mergel, J., Fritz, M. & Carmo, D., 2013. Status on technologies for hydrogen production by water electrolysis. *Transition to Renewable Energy*, 1(1), pp. 424-450.

METABOLIC, 2017. *Carbon-monoxide re-use through industrial Symbiosis between steel and chemical industries (CORESYM)*, Amsterdam (Netherlands): METABOLIC.

Metabolic, 2017. *CORESYM - CarbOn-monoxide RE-use through industrial SYMBiosis' between chemical and steel industries*, Amsterdam: Metabolic.

Mikkelsen, M., Jorgensen, M. & Krebs, F., 2010. The teraton challenge. A review of fixation and transformation of carbon dioxide. *Energy & Environmental Science*, Issue 3, pp. 43-81.

Mulvana, H. et al., 2012. Theoretical and experimental characterisation of magnetic microbubbles. *Ultrasound in Medicine & Biology*, 38(5), pp. 864-875.

NASA, 2012. NASA. [Online] Available at: https://www.nasa.gov/directorates/heo/scan/engineering/technology/txt_accordion1.html [Accessed 11 November 2015].

National Statistics, 2015. *Energy Trends section 6: renewables*. [Online] Available at: <https://www.gov.uk/government/statistics/energy-trends-section-6-renewables> [Accessed 2015 October 2015].

Nigara, Y. & Cales, B., 1986. Production of carbon-monoxide by direct thermal splitting of carbon-dioxide at high-temperature. *Bulletin of the Chemical Society of Japan*, 59(6), pp. 1997-2002.

Novek, E. et al., 2016. Low-Temperature Carbon Capture Using Aqueous Ammonia and Organic Solvents. *Environmental Science & Technology Letters*.

Nunnally, T. et al., 2011. Dissociation of CO₂ in a low current gliding arc plasmatron. *Journal of Physics D: Applied Physics*, 44(27), p. 274009.

Office for National Statistics, 2019. *The decoupling of economic growth from carbon emissions: UK evidence.* [Online]

Available at:

<https://www.ons.gov.uk/economy/nationalaccounts/uksectoraccounts/compendium/economicreview/october2019/thedecouplingofeconomicgrowthfromcarbonemissionsukevidence>

[Accessed 13 08 2020].

Oko, E., Wang, M. & Joel, A., 2017. Current status and future development of solvent-based carbon capture. *International Journal of Coal Science & Technology*, Volume 4, pp. 5-14.

Patisson, F. & Mirgaux, O., 2020. Hydrogen Ironmaking: How It Works. *Metals Online MDPI*, 10(7), p. 922.

Pauliuk, S., Milford, R. L., Müller, D. B. & Allwood, J. M., 2013. The Steel Scrap Age. *Environmental Science & Technology*, 47(7), pp. 3448-3454.

Paulussen, S. et al., 2010. Conversion of carbon dioxide to value-added chemicals in atmospheric pressure dielectric barrier discharges. *Plasma Sources Science and Technology*, 19(3).

Prigogine, I., 1980. *From being to becoming. Time and Complexity in the Physical Sciences.* s.l.:W.H.Freeman, 1980.

Pycroft, J., Vergano, L. & Hope, C., 2014. The economic impact of extreme sea-level rise: Ice sheet vulnerability and the social cost of carbon dioxide. *Global Environmental Change*, 24(3), pp. 99-107.

Qin, F. et al., 2011. Heat of absorption of CO₂ in aqueous ammonia and ammonium carbonate/carbamate solutions. *International Journal of Greenhouse Gas Control*, 5(3), pp. 405-412.

Quader, M., Ahmed, S., Raja Ghazilla, R. A. & Ahmed, S. & D. M., 2015. A comprehensive review on energy efficient CO₂ breakthrough technologies for sustainable green iron and steel manufacturing. *Renewable and Sustainable Energy Reviews*, Volume 50, pp. 594-641.

Rehman, F., Medley, G. J., Bandulasena, H. & Zimmerman, W. B., 2014. Fluidic oscillator-mediated microbubble generation to provide cost effective mass transfer and mixing efficiency to the wastewater treatment plants. *Environmental Research*, Volume 137, pp. 32-39.

Rhee, A. I. O. C. H. et al., 2011. Process analysis for ammonia-based CO₂ capture in ironmaking industry. *Energy Procedia*, Volume 4, pp. 1486-1493.

Roussanaly, S., Anantharaman, R., Lindqvist, K. & Hagen, B. .. 2., 2018. A new approach to the identification of high-potential materials for cost-efficient membrane-based post-combustion CO₂ capture. *Sustainable Energy & Fuels*, 2(6).

Rusanov, V. D., Fridman, A. A. & Sholin, G. V., 1981. The physics of a chemically active plasma with nonequilibrium vibrational excitation of molecules. *Soviet Physics Uspekhi*, 24(6), p. 447.

Schuler, F. et al., 2013. *Steel's Contribution to a Low-Carbon Europe 2050*, https://www.stahl-online.de/wp-content/uploads/2013/09/Schlussbericht-Studie-Low-carbon-Europe-2050_-Mai-20131.pdf: Stahl und Eisen.

Schutze, A. et al., 1998. The atmospheric-pressure plasma jet: a review and comparison to other plasma sources. *IEEE Transactions on Plasma Science*, 26(6), p. 1685–1694.

Scopus, 2015. *Scopus - Plasma Analysis*. [Online] Available at: <http://www.scopus.com/term/analyzer> [Accessed 11 December 2015].

Seo, . Y. et al., 2015. Evaluation of CO₂ liquefaction processes for ship-based carbon capture and storage (CCS) in terms of life cycle cost (LCC) considering availability. *International Journal of Greenhouse Gas Control*, Volume 35, pp. 1-12.

Shuangchen, M. et al., 2015. Experimental study on the effect of Ni(II) additive on ammonia escape in CO₂ capture using ammonia solution. *International Journal of Greenhouse Gas Control*, Volume 37, pp. 249-255.

Smil, V., 2000. *Enriching the Earth - Fritz Haber, Carl Bosch, and the Transformation of World Food Production*. ISBN 9780262194495 ed. Cambridge, Massachusetts: The MIT Press.

Solomon, S. et al., 2007. *Climate Change 2007: The Physical Science Basis. Contribution of Working Group I to the Fourth Assessment Report of the Intergovernmental Panel on Climate Change*. Cambridge, United Kingdom: Cambridge University Press.

Spencer, L. F. & Gallimore, A. D., 2013. CO₂ dissociation in an atmospheric pressure plasma/catalyst system: a study of efficiency. *Plasma Sources Science and Technology*, 22(1).

Steelanol Project,, n.d. *Steelanol.eu*. [Online] Available at: <http://www.steelanol.eu/en> [Accessed 15 06 2020].

Steelonthenet, 2020. *www.steelonthenet.com*. [Online] Available at: <https://www.steelonthenet.com/cost-eaf.html> [Accessed 27 07 2020].

Styring, P. & Jansen, D., 2011. *Carbon Capture and Utilisation in the green economy*. Sheffield, The Centre for Low Carbon Futures.

Sun, S. R. et al., 2017. CO₂ conversion in a gliding arc plasma: performance improvement based on chemical reaction modeling. *Journal of CO₂ Utilization*, Volume 17, pp. 220-234.

Sutter, D., Gazzani, M. & Mazzotti, M., 2015. Formation of solids in ammonia-based CO₂ capture processes — Identification of criticalities through thermodynamic analysis of the CO₂–NH₃–H₂O system. *Chemical Engineering Science*, Volume 133, pp. 170-180.

Tata Steel Europe, 2019. *tatasteeleurope.com*. [Online] Available at: https://www.tatasteeleurope.com/static_files/Downloads/Corporate/About%20us/hisarna%20factsheet.pdf [Accessed 14 06 2020].

Tesař, V., 2014. Shape oscillation of microbubbles. *Chemical Engineering Journal*, Volume 235, pp. 368-378.

Tesař, V. & Bandalusena, H. C. H., 2011. Bistable diverter valve in microfluidics. *Experiments in Fluids*, Volume 50, p. 1225–1233.

Tesař, V., Hung, C.-H. & Zimmerman, W. B., 2006. No moving part hybrid synthetic jet mixer. *Sensors and Actuators a-Physical*, 125(2), pp. 159-169.

The CCUS Advisory Group (CAG), 2019. *Investment Frameworks for Development of CCUS in the UK*, London: CCUS Advisory Group.

The Institute of Materials, Minerals and Mining (IOM3), 2014. *European Steel Environment & Energy Congress (ESEC)*. Teesside, IOM3.

The Royal Society, 2019. *Sustainable synthetic carbon based fuels for transport*. [Online] Available at: <https://royalsociety.org/-/media/policy/projects/synthetic-fuels/synthetic-fuels-briefing.pdf> [Accessed 09 12 2020].

The Royal Society, 2020. *Ammonia: zero-carbon fertiliser, fuel and energy store*, London: The Royal Society.

Thomsen, K. & Rasmussen, P., 1999. Modeling of vapor—liquid—solid equilibrium in gas—aqueous. *Chemical Engineering Science*, 54(1), p. 1787—1802.

ThyssenKrupp Steel, n.d. *ThyssenKrupp newsroom*. [Online] Available at: <https://www.thyssenkrupp.com/en/newsroom/content-page-162.html>. [Accessed 15 06 2020].

Trade Economics, 2020. *Trade Economics.com*. [Online] Available at: <https://tradingeconomics.com/commodity/ironore62> [Accessed 28 11 2020].

UK Government, Department for Business, Energy & Industrial Strategy, 2019. *UK becomes first major economy to pass net zero emissions law*. [Online] Available at: <https://www.gov.uk/government/news/uk-becomes-first-major-economy-to-pass-net-zero-emissions-law>

[Accessed 05 12 2020].

UNCED, 1992. *Agenda 21*. [Online] Available at: <http://sustainabledevelopment.un.org/content/documents/Agenda21.pdf>

[Accessed 20 02 2014].

UNFCCC, 2015. *The Paris Agreement*. [Online] Available at: <https://unfccc.int/process-and-meetings/the-paris-agreement/the-paris-agreement>

[Accessed 30 11 2020].

UNFCCC, 2015. *The Paris Agreement*. [Online] Available at: <https://unfccc.int/process-and-meetings/the-paris-agreement/the-paris-agreement>

[Accessed 05 12 2020].

UNFCCC, 1997. *Kyoto Protocol*. [Online] Available at: <http://unfccc.int/resource/docs/convkp/kpeng.pdf>

[Accessed 20 02 2014].

Valenti, G. & Bonalumi, D., 2018. Chemical Absorption by Aqueous Solution of Ammonia. In: R. K. Agarwal, ed. *Carbon Capture, Utilization and Sequestration*. s.l.:IntechOpen, pp. <https://www.intechopen.com/books/carbon-capture-utilization-and-sequestration/chemical-absorption-by-aqueous-solution-of-ammonia>.

Van Rooij, G. J. et al., 2015. Taming microwave plasma to beat thermodynamics in CO₂ dissociation. *Faraday Discussions*, 183(1), p. 233–248.

Vesel, A., Mozetic, M., Drenik, A. & Balat-Pichelin, M., 2011. Dissociation of CO₂ molecules in microwave plasma. *Chemical Physics*, 382(1-3), pp. 127-131.

Vogl, V., Åhman, M. & J.Nilsson, L., 2018. Assessment of hydrogen direct reduction for fossil-free steelmaking. *Journal of Cleaner Production*, 203(1), pp. 736-745.

Wesley, D. J. et al., 2016. Development of an optical microscopy system for automated bubble cloud analysis. *Applied Optics*, 55(22), pp. 6102-6107.

Wood, D. A., 2015. Carbon dioxide (CO₂) handling and carbon capture utilization and sequestration (CCUS) research relevant to natural gas: A collection of. *Journal of Natural Gas Science and Engineering*, 25(July 2015), pp. A1-A9.

- World Energy Council, 2013. *"Time to get real – the case for sustainable energy investment,"* in *World Energy Trilemma*. 0, ISBN: 978 0 946121 22 9 ed. London: Wyman .
- World Steel Association , 2019. *World Steel in figures 2019*, Brussels: World Steel Association.
- World Steel Association, 2015. *Steel in the Circular Economy - A life cycle perspective*, Brussels: World Steel Association.
- World Steel Association, 2019. *Fact Sheet - Steel and Raw Materials*, Brussels: World Steel Association.
- Wortler, M. et al., 2013. www.bcg.de. [Online] Available at: www.bcg.de [Accessed 15 04 2020].
- WSP, Parsons Brinckerhoff & DNV.GL (On behalf of DECC & BIS), 2015. *Industrial Decarbonisation & Energy Efficiency Roadmaps to 2050*, s.l.: s.n.
- Xiang, H. et al., 2020. Copper–Indium Binary Catalyst on a Gas Diffusion Electrode for High-Performance CO₂ Electrochemical Reduction with Record CO Production Efficiency. *ACS Applied Materials and Interfaces*, 12(1), pp. 601-608.
- Xiang, X. et al., 2012. Urea formation from carbon dioxide and ammonia at atmospheric pressure. *Environ Chem Lett*, Volume 10, p. 295–300.
- Yap, D., Tatibouët, J. & Batiot-Dupeyrat, C., 2015. Carbon dioxide dissociation to carbon monoxide by non-thermal plasma. *Journal of CO₂ Utilization*, Volume 12, pp. 54-61.
- Yara, 2013. *Yara Fertilizer Industry Handbook, October*, Oslo, Norway: Yara.
- Yeh, A. C. & Bai, H., 1999. Comparison of ammonia and monoethanolamine solvents to reduce CO₂ greenhouse gas emissions. *Science of The Total Environment*, 228(2-3), pp. 121-133.
- Ying, K. et al., 2013. Enhanced Mass Transfer in Microbubble Driven Airlift Bioreactor for Microalgal Culture. *Engineering*, 5(9), pp. 1947-3931.
- Yu, H., 2018. Recent developments in aqueous ammonia-based post-combustion CO₂. *Chinese Journal of Chemical Engineering*, 26(11), pp. 2255-2265.
- Yu, Q. et al., 2012. Characteristics of the Decomposition of CO₂ in a Dielectric Packed-Bed Plasma Reactor. *Plasma Chemistry and Plasma Processing*, 32(1), pp. 153-163.
- Zacchello, B. & Wang, M., 2018. Process analysis and economic evaluation of mixed aqueous ionic liquid and monoethanolamine (MEA) solvent for CO₂ capture from a coke oven plant. *Greenhouse Gases: Science and Technology*, 8(4), pp. 686-700.

- Zhuang, Q., Pomalis, R., Zheng, L. & Clements, B., 2011. Ammonia-based carbon dioxide capture technology: Issues and solutions. *Energy Procedia*, Volume 4(1), pp. Pages 1459-1470.
- Zimmerman, W., 2015. *ERC Advanced Grant 2015 - Research proposal - Heterogeneous catalysis on microbubble gas-liquid interfaces Part B1 & B2*, Sheffield: BubbleCat.
- Zimmerman, W. B., Al-Mashhadani, M. K. H. & Bandulasena, H. C. H., 2013. Evaporation dynamics of microbubbles. *Chemical Engineering Science*, Volume 101, pp. 865-877.
- Zimmerman, W. B. & Kokoo, R., 2018. Esterification for biodiesel production with a phantom. *Applied Energy*, Volume 221, pp. 28-40.
- Zimmerman, W. B. et al., 2011. Design of an airlift loop bioreactor and pilot scales studies with fluidic oscillator induced. *Applied Energy*, Volume 88, pp. 3357-3369.
- Zimmerman, W., Tesa, V., Butler, S. & Bandulasen, H., 2008. Microbubble Generation. *Recent patents in Engineering*, 2(1), pp. 1-7.
- Zolotajkin, M., Szarawara, J. & Pietrowski, J., 1984. Chemical Kinetics of the Urea-Synthesis Process. *Chemia Stosowana*, Volume 1, pp. 85-99.
- Zutphen, H. v., 2018. *co2-cato.org*. [Online] Available at: https://www.co2-cato.org/cato-download/5541/20181213_122245_15_2018.12.04_CATO-meets-the-projects_Zutphen-pu [Accessed 14 06 2020].

